

1983

ITERATIVE NONLINEAR MODELING OF EXHAUST PRESSURE PULSES FROM A SMALL ROTARY ENGINE.

ROBERT G. S. GASPAR
University of Windsor

Follow this and additional works at: <http://scholar.uwindsor.ca/etd>

Recommended Citation

GASPAR, ROBERT G. S., "ITERATIVE NONLINEAR MODELING OF EXHAUST PRESSURE PULSES FROM A SMALL ROTARY ENGINE." (1983). *Electronic Theses and Dissertations*. Paper 2529.

This online database contains the full-text of PhD dissertations and Masters' theses of University of Windsor students from 1954 forward. These documents are made available for personal study and research purposes only, in accordance with the Canadian Copyright Act and the Creative Commons license—CC BY-NC-ND (Attribution, Non-Commercial, No Derivative Works). Under this license, works must always be attributed to the copyright holder (original author), cannot be used for any commercial purposes, and may not be altered. Any other use would require the permission of the copyright holder. Students may inquire about withdrawing their dissertation and/or thesis from this database. For additional inquiries, please contact the repository administrator via email (scholarship@uwindsor.ca) or by telephone at 519-253-3000ext. 3208.

CANADIAN THESES ON MICROFICHE

I.S.B.N.

THESES CANADIENNES SUR MICROFICHE



National Library of Canada
Collections Development Branch

Canadian Theses on
Microfiche Service

Ottawa, Canada
K1A 0N4

Bibliothèque nationale du Canada
Direction du développement des collections

Service des thèses canadiennes
sur microfiche

NOTICE

The quality of this microfiche is heavily dependent upon the quality of the original thesis submitted for microfilming. Every effort has been made to ensure the highest quality of reproduction possible.

If pages are missing, contact the university which granted the degree.

Some pages may have indistinct print especially if the original pages were typed with a poor typewriter ribbon or if the university sent us a poor photocopy.

Previously copyrighted materials (journal articles, published tests, etc.) are not filmed.

Reproduction in full or in part of this film is governed by the Canadian Copyright Act, R.S.C. 1970, c. C-30. Please read the authorization forms which accompany this thesis.

THIS DISSERTATION
HAS BEEN MICROFILMED
EXACTLY AS RECEIVED

AVIS

La qualité de cette microfiche dépend grandement de la qualité de la thèse soumise au microfilmage. Nous avons tout fait pour assurer une qualité supérieure de reproduction.

S'il manque des pages, veuillez communiquer avec l'université qui a conféré le grade.

La qualité d'impression de certaines pages peut laisser à désirer, surtout si les pages originales ont été dactylographiées à l'aide d'un ruban usé ou si l'université nous a fait parvenir une photocopie de mauvaise qualité.

Les documents qui font déjà l'objet d'un droit d'auteur (articles de revue, examens publiés, etc.) ne sont pas microfilmés.

La reproduction, même partielle, de ce microfilm est soumise à la Loi canadienne sur le droit d'auteur, SRC 1970, c. C-30. Veuillez prendre connaissance des formules d'autorisation qui accompagnent cette thèse.

LA THÈSE A ÉTÉ
MICROFILMÉE TELLE QUE
NOUS L'AVONS REÇUE

ITERATIVE NONLINEAR MODELING
OF EXHAUST PRESSURE PULSES
FROM A SMALL ROTARY ENGINE

A Dissertation

Submitted to the Faculty of Graduate Studies through the
Department of Mechanical Engineering in Partial Fulfilment
of the Requirements for the Degree of
Doctor of Philosophy at the
University of Windsor

by

© Robert G.S. Gaspar

Windsor, Ontario
1983

© ROBERT G.S. GASPAR 1983

793700

ABSTRACT

An experimental study was undertaken to investigate some of the factors affecting the behaviour of pressure variations in a straight exhaust pipe attached to a rotary engine. The investigation involved the measurement of engine load, speed, fuel consumption, combustion air properties and flow rate, mean static pressure near the exhaust port, mean temperatures at two locations in the exhaust pipe and transient gas pressures at two locations in the exhaust pipe. A theoretical, nonlinear model of the particle velocity of a gas excited by an acoustic wave propagation was modified to model the transient pressure behaviour of an acoustic wave. The model was correlated with the transient pressure measurements with the aid of an iterative correlation technique and digital signal processing. Standard curve fitting procedures were used to relate the various measurements as functions of engine speed.

The iterative procedure outlined has been found to be a good method for the treatment of data which cannot be correlated by standard linearization and regression techniques. Further, the analysis indicates that the model correlates very well with the pressure pulse created by the rotor chamber blow-down. It is also possible to predict the length through which the pressure pulse must travel before the leading portion of the pulse distorts into a shock wave.

DEDICATION

This work is dedicated to my wife Heather on our thirteenth anniversary. Thank you for taking care of all the things that I didn't have time for while I was busy writing. I also want to thank our daughter Jennifer for understanding why I couldn't always play with her.

ACKNOWLEDGEMENTS

The author would like to express his appreciation to Dr. K. Sridhar for his abundant patience and understanding and to Dr. Z. Reif for his guidance and good humour. The author would also like to thank Mr. Werner Beck and Mr. Robert Tattersall for their technical assistance, Dr. William Miller for his encouragement and interest in a Mechanical Engineer's problems, Dr. D.J.L. Kennedy for additional financial support when it was needed, the members of the Department of Mechanical Engineering, Mr. Johann Wagner, whose best acknowledgement is the line at the bottom of this page, and the National Sciences and Engineering Research Council for its financial assistance through grant numbers A2190 and A7439.

CONTENTS

	<u>Page</u>
ABSTRACT	iii
DEDICATION	iv
ACKNOWLEDGEMENTS	v
TABLE OF CONTENTS	vi
LIST OF FIGURES	ix
I. INTRODUCTION	1
II. LITERATURE SURVEY	7
2.1 Empirical Methods	8
2.2 Acoustic Wave Propagation	13
2.3 Acoustic Theory with Gas Flow	17
2.3.1 Work of Blair and Associates	18
2.3.2 Work of Davies and Associates	22
2.3.3 Other Contributors	25
2.4 Nonlinear Effects	34
2.5 Summary	36
III. MODEL	38
IV. EXPERIMENTAL DETAILS	52
4.1 Construction of the Test Facility	52
4.2 Equipment Selection	60

CONTENTS CONTINUED

	<u>Page</u>
4.2.1 Engine and Dynamometer	60
4.2.2 Exhaust Pipe	61
4.2.3 Pressure Transducers	62
4.2.4 Exhaust Gas Back Pressure Measurement	63
4.2.5 Exhaust Gas Temperature Measurements	64
4.2.6 Engine Speed Measurement	64
4.2.7 Combustion Air Flow Measurements	65
4.2.8 Fuel Flow Measurements	65
4.2.9 Electronic Processing and Recording Equipment	66
4.2.10 Signal Analysis Equipment	67
4.2.10.1 System 1	67
4.2.10.2 System 2	67
4.2.10.3 System 3	69
4.2.10.4 System 4	69
4.3 Experimental Procedure to Run a Test	70
V. DATA PROCESSING	73
5.1 The Sampling Program	73
5.2 The Configuration Program	76
5.3 The Concatenation Program	78
5.4 The Correlation Program	80
VI. RESULTS	91
6.1 Room Acoustic Tests	91

CONTENTS CONTINUED

	<u>Page</u>
6.2 Engine Performance Tests	93
6.3 Tests Related to Exhaust Gas Behaviour	99
6.4 The Pressure Pulse Correlation	124
6.5 Predicting the Discontinuity Distance	145
VII. CONCLUSIONS	150
VIII. RECOMMENDATIONS	151
APPENDIX I — The Sampling Program	152
APPENDIX II — The Configuration Program	172
APPENDIX III — The Concatenation Program	177
APPENDIX IV — The Correlation Program	186
APPENDIX V — Sample Results from the Correlation Program	195
APPENDIX VI — Results of Engine Testing and Error Analysis	203
APPENDIX VII — Engine Data Sheet	249
REFERENCES	251
VITA AUCTORIS	264

FIGURES

<u>Figure</u>		<u>Page</u>
1	Plane Wave Motion in a Wave Guide	38
2	Progressive Distortion of a Finite Amplitude Wave	45
3	Sketch of Engine Laboratory Layout	56
4	Location of Engine Laboratory, West Elevation View of Building	57
5	Location of Engine Laboratory, North Elevation View of Building	58
6	Sketch of Low Noise Transmission, Ventilation Ducting	59
7	Schematic Diagram of Primary Data Acquisition System	68
8	Graph of Engine Room, Ambient, Interior Sound Level Versus Frequency	92
9	Graph of Engine Room, Wall Transmission Loss Versus Frequency	94
10	Graph of Engine Shaft Power Output, At Constant Torque, Versus Engine Speed	95
11	Graph of Engine Fuel Consumption; At Constant Torque, Versus Engine Speed	97
12	Graph of Engine Brake Specific Fuel Consumption, At Constant Torque, Versus Engine Speed	98
13	Graph of Volumetric Flow Rate of Combustion Air Versus Engine Speed, At Constant Torque	100
14	Graph of Mean Static Gauge Exhaust Gas Pressure Versus Engine Speed, Measured at Location 1 Near the Exhaust Port	101

4

FIGURES CONTINUED

<u>Figure</u>		<u>Page</u>
15	Graph of Mean Exhaust Gas Temperature Versus Engine Speed, Measured at Two Locations in the Exhaust Pipe	103
16	Graph of the Exhaust Gas Pressure Level Spectrum, Near the Exhaust Port, at an Engine Speed of 2000 RPM	104
17	Graph of the Exhaust Gas Pressure Level Spectrum, Near the Exhaust Port, at an Engine Speed of 3000 RPM	106
18	Graph of the Exhaust Gas Pressure Level Spectrum, Near the Exhaust Port, at an Engine Speed of 3000 RPM	107
19	Graph of the Exhaust Gas Pressure Level Spectrum, Near the Exhaust Port, at an Engine Speed of 4000 RPM	108
20	Graph of the Exhaust Gas Pressure Level Spectra for Engine Speeds Ranging from 1750 to 5250 RPM in 250 RPM Increments, Measured Near the Exhaust Port	110
21	Graph of Exhaust Gas Pressure Versus Time with a One Metre Separation Distance Between Measuring Locations, at an Engine Speed of 2000 RPM	111
22	Graph of Exhaust Gas Pressure Versus Time with a One Metre Separation Distance Between Measuring Locations, at an Engine Speed of 3000 RPM	113
23	Graph of Exhaust Gas Pressure Versus Time with a One Metre Separation Distance Between Measuring Locations, at an Engine Speed of 4000 RPM	114
24	Graph of Exhaust Gas Pressure Level Spectra at a Location Near the Exhaust Port and at Another Location One Metre Downstream, for an Engine Speed of 4000 RPM	117
25	Graph of One Cycle of the Exhaust Pressure Signals Near the Exhaust Port, for Engine Speeds Ranging from 1750 to 5250 RPM in Increments of 250 RPM	118
26	Graph of One Cycle of the Exhaust Pressure Signals, One Metre Downstream of the First Measuring Location, for Engine Speeds Ranging from 1750 to 5250 RPM in Increments of 250 RPM	119

FIGURES CONTINUED

<u>Figure</u>		<u>Page</u>
27	Graph of Maximum Amplitude of the Exhaust Gas Pressure Pulse Versus Engine Speed	121
28	Graph of the Relative, Maximum Pressure Pulse Amplitude Versus Engine Speed	122
29	Graph of the Relative, Average Pressure Pulse Amplitude Versus Engine Speed	123
30	Graph of Dimensionless Acoustic Pressure Versus Time, Sampled at Location 1 Near the Exhaust Port for an Engine Speed of 2000 RPM, Tape Section 1.1	125
31	Graph of Dimensionless Acoustic Pressure Versus Time, Sampled at Location 1 Near the Exhaust Port for an Engine Speed of 2000 RPM, Tape Section 1.2	126
32	Graph of Dimensionless Acoustic Pressure Versus Time, Sampled at Location 1 Near the Exhaust Port for an Engine Speed of 2000 RPM, Tape Section 1.3	127
33	Graph of Dimensionless Acoustic Pressure Versus Time, Sampled at Location 1 Near the Exhaust Port for an Engine Speed of 2000 RPM, Tape Section 1.4	128
34	Graph of Dimensionless Acoustic Pressure Versus Time, Sampled at Location 1 Near the Exhaust Port for an Engine Speed of 2250 RPM, Tape Section 2.1	131
35	Graph of Dimensionless Acoustic Pressure Versus Time, Sampled at Location 1 Near the Exhaust Port for an Engine Speed of 2250 RPM, Tape Section 2.2	132
36	Graph of Dimensionless Acoustic Pressure Versus Time, Sampled at Location 1 Near the Exhaust Port for an Engine Speed of 2250 RPM, Tape Section 2.3	133
37	Graph of Dimensionless Acoustic Pressure Versus Time, Sampled at Location 1 Near the Exhaust Port for an Engine Speed of 2510 RPM, Tape Section 3.1	135
38	Graph of Dimensionless Acoustic Pressure Versus Time, Sampled at Location 1 Near the Exhaust Port for an Engine Speed of 2510 RPM, Tape Section 3.2	136

FIGURES CONTINUED

<u>Figure</u>		<u>Page</u>
39	Graph of Dimensionless Acoustic Pressure Versus Time, Sampled at Location 1 Near the Exhaust Port for an Engine Speed of 2730 RPM	137
40	Graph of Dimensionless Acoustic Pressure Versus Time, Sampled at Location 1 Near the Exhaust Port for an Engine Speed of 2980 RPM	138
41	Graph of Dimensionless Acoustic Pressure Versus Time, Sampled at Location 1 Near the Exhaust Port for an Engine Speed of 4020 RPM	139
42	Graph of Dimensionless Acoustic Pressure Versus Time, Sampled at Location 1 Near the Exhaust Port for an Engine Speed of 4250 RPM	140
43	Graph of Dimensionless Acoustic Pressure Versus Time, Sampled at Location 1 Near the Exhaust Port for an Engine Speed of 4760 RPM	142
44	Graph of Pressure Pulse Pseudofrequency Versus Engine Speed	143
45	Graph of Distortion Coefficient Versus Engine Speed	144
46	Graph of Predicted Discontinuity Length Versus Engine Speed, Using Average Pressure Pulse Amplitude	147
47	Graph of Predicted Discontinuity Length Versus Engine Speed, Using a Peak Pressure Pulse Correction	148
48	Graph of Predicted Discontinuity Length Versus Engine Speed, When Corrected for Initial Pressure Pulse Distortion and Peak Pulse Pressure	149

I. INTRODUCTION

The fact that, in recent years, noise control legislation covering recreational vehicles and general noise nuisance situations of other machines has been suggested or enacted, in the United States [57] and Canada [1,86,126], serves to remind us that a continuing effort in noise abatement is required. The advancement of noise control measures for small power plants, which until recently have been all but ignored, has significant technological and sociological importance. The advent of the energy crisis has compounded the situation. Although the peak of the energy crisis may have passed, its momentum has fostered the redesign of small internal combustion engines of various types. The goals to be attained are focussed on the need for quieter, more fuel efficient engines. The two goals are not separable as noise control can degrade fuel efficiency efforts [2]. The need to continue with research in engine related noise control will be of importance for a long time to come.

The original intent of this study was to develop a testing methodology which could be used to quickly indicate the type of exhaust system required by any small engine. This is of particular importance as most small engines have very little in the way of effective exhaust muffling systems. There were several reasons for choosing a rotary engine as the subject for the experimental testing. One of the most important of those reasons was that the rotary engine has characteristics of both a two-stroke and a four-stroke engine. The fact that the opening of its exhaust port is circular and that the operating characteristics are similar to most two-stroke engines was a very good design feature for experimental purposes. Other reasons

were its availability, novelty, and that it could be considered to represent a related class of similarly sized engines. Although the novelty of using rotary engines as power plants in automobiles has worn off considerably, it still has potential for this [9,66] and other uses [61]. The rotary engine cannot be written into history as just another 'flash in the pan' [128]. Small rotary engines can be used in recreational vehicles as well as other applications [92] where the smoother power output and the smaller number of moving parts is advantageous. It is also important to note that, in the interest of fuel economy, the specific fuel consumption of a rotary engine does not differ greatly from that of an equivalent four-stroke engine and it is better than that of an equivalent two-stroke engine [6,7]. Indeed, recent work in the areas of light-load performance [93] and fuel efficiency [9,10,11] have demonstrated that improvements are possible when compared to results of earlier years [58,65,76,78,119,125].

With regard to noise related problems, a number of manufacturers and research groups have demonstrated that significant advances are possible [44,79,82,116]. Although it is a fact that engine emitted noise can be as great as or greater than muffled exhaust noise [91], it is still desirable to improve the techniques of controlling exhaust noise. This does not mean that engine noise can be ignored. Control of engine noise is important but the nature of the control generally does not significantly affect fuel economy.

After the initial experimental testing of the rotary engine was performed, it became evident that the exhaust gas behaviour was far more complicated than was originally expected [69]. The nature of that complication being the presence of nonlinear pressure wave propagation effects. As this phenomenon appears to be present in other engine testing [25] and could easily be present in other engines of this size and class, it was decided that a study of the wave behaviour would

be worthwhile. As well, the possibility of applying nonlinear acoustic wave theory to the problem was of interest since it was apparent that linear acoustic theory would not adequately handle the problem.

There are many factors which may influence acoustic wave propagation, such as:

1. Variation of exhaust gas properties
2. Acoustic pressure in the exhaust pipe
3. Exhaust pipe geometry
4. Engine type
5. Engine operating conditions
6. Engine performance

Manufacturers [118] have used approximations with respect to exhaust gas properties in the evaluation of muffler design parameters. These procedures have also been found to be reasonable when used in the research project. It also aided in the conclusion that additional instrumentation and data reduction facilities would be required for future work in the more extensive analysis of acoustic pressure wave propagation in exhaust pipes.

The acoustic pressure in the exhaust pipe has a significant effect on the acoustic wave propagation [54]. One dimensional, low amplitude acoustic waves propagate in a linear manner. That is, the relative particle velocity on each part of the wave remains constant with respect to the wave as it propagates. Beyond a particular acoustic pressure condition dictated by the local property values, the acoustic wave will no longer propagate in a linear manner. The speed of sound (the limiting velocity of the acoustic wave in medium) is significantly affected by the

acoustic pressure. As the acoustic pressure increases, the acoustic wave velocity increases. The phenomenon that occurs is the development of a shock wave as the acoustic wave propagates. The shock is initiated at a low pressure condition and it grows in intensity as the higher pressure, higher velocity portions of the wave catch up with the lower pressure, lower velocity components.

There are a wide variety of engine exhaust port configurations which have been used by manufacturers [17]. Many variations of square, rectangular, T-shaped, oval, single or multiple circular exhaust port openings have been used to control and direct exhaust gas egress from the engine combustion chamber. The port design will have some effect on the acoustic pressure wave formation because of cylinder blow-down time. This can be affected by port opening area, rate of change of port opening area and transition section to the exhaust pipe.

The exhaust pipe geometry has a significant effect on the acoustic pressure wave [55,59,129]. An increase or decrease in the diameter of the exhaust pipe section can cause reflected expansion or compression waves, respectively. These reflected waves in combination with the primary exhaust wave cause considerable complication of the pressure-time signature. In addition, the changes in section can affect the amplitude of the acoustic wave. Frictional effects can also cause decreases in the amplitude of the wave; even for the case of a constant diameter exhaust pipe [93].

Engine type can have a considerable effect on the exhaust gas pressure wave propagation [8]. Some of the factors involved are: compression ratio; air to fuel ratio, spark timing, exhaust port location in the cylinder, piston motion during cylinder blow-down, piston position in the cylinder when the exhaust port is opened, etc. The engine operating conditions also affect exhaust gas behaviour. This is primarily due to the fact that higher engine speeds and loads produce higher peak acoustical

pressures in the exhaust pipe. This condition is to be expected since the higher engine loads require higher mean effective pressures in the cylinder to provide the driving power. Consequently, the exhaust gas pressures will also be higher.

An increase in engine operating speed will likewise have a similar effect but for a different reason. In this case the time between successive cylinder blow-downs will decrease due to the increased rotating speed. Therefore, although the mean effective cylinder pressure may be moderate, the duration in which the volume of gas is expelled from the cylinder will be shorter. This means that the peak pressure of the exhaust wave may be higher. The maximum peak pressure will occur at the engine speed corresponding to the maximum power output. Finally, the engine performance also has an effect on the exhaust gas pressure wave. If the engine is not tuned properly, that is: run with an incorrect spark timing, run with an incorrect spark plug, or any of a number of other improper conditions; there will be some effect on the peak acoustic pressure of the exhaust wave.

This work deals with the analysis of the experimental results obtained from a small rotary engine which has a displacement of 108 cubic centimeters per shaft revolution and is rated at 4.8 kW at an engine speed of 5500 rpm [48]. The exhaust gas has been evaluated with respect to ideal gas property values required in the nonlinear acoustic theory. Acoustic pressure has been measured in terms of its variation about the local mean static pressure at each measuring location. The inside diameter of the exhaust pipe used was the same diameter as that of the circular engine exhaust port. The exhaust pipe terminated flush with an exterior building wall to simulate a hemispherical radiation of noise from the exhaust port opening.

This configuration was also chosen because the geometric configuration is simpler for future analysis of reflected waves caused by the exhaust pipe termination. The engine tuning was maintained according to the manufacturers manual provided with

the engine. The engine performance was recorded for all engine speeds ranging from idle to full speed, full load conditions.

The engine data and analog recordings of the exhaust pressure measurements were analysed with the assistance of an Apple II+ computer. Analyses of the exhaust spectra were carried out with the use of a spectrum analyser and the pressure time histories were recorded from a digital storage oscilloscope. The pressure pulse model was correlated with data processed by an analog to digital conversion board in conjunction with an Apple II+ computer.

II. LITERATURE SURVEY

The history of the internal combustion engine has been a long and eventful one. According to Friede [104], the first atmospheric internal combustion engines were manufactured in 1810. The first recorded instance of a noise related problem with the engine was in Vienna, Austria in 1875. This occurred when the Viennese police barred Marcus from operating his primitive, atmospheric internal combustion engine driven car on the streets of Vienna. Also, the historical perspective of the time of the development of the first internal combustion engines would not be complete without mentioning Otto or Daimler. Otto built an engine which operated on what is now called the Otto Cycle in 1876 and Daimler introduced the four-stroke engine design in 1877 [104].

Clearly, the problem of engine related noise has been around since the inception of the internal combustion engine. It is somehow, not surprising that two of the founding fathers of acoustics lived during that same period. Helmholtz first turned his attention to acoustics in 1852 [71] and Rayleigh published "The Theory Of Sound" [105] in 1877. Acoustic theory has had almost the same amount of time to develop as the internal combustion engine.

The literature dealing with acoustic waves in engine exhaust systems can be divided into four relatively distinct groups; those that:

1. Have used empirical methods to attenuate exhaust noise or have developed experimental techniques to measure

conditions relating to the combustion gas such as flow rate or thermodynamic properties.

2. Have assumed zero exhaust gas velocity and have predicted gas pressures and acoustic plane wave propagation by employing linear acoustic theory. This has generally been used in conjunction with mathematical analysis or computer aided calculation procedures. The results have been presented with or without experimental verification.
3. Have used one dimensional linear acoustic theory with the condition of either a mean or unsteady gas flow. Experimental results are usually presented to demonstrate the validity of the procedure.
4. Have recognized that, quite frequently, nonlinear effects are present in the exhaust system.

Each of these groups will be discussed in turn as each has information to offer with regard to exhaust gas pressure wave behaviour.

2.1 Empirical Methods

The work performed by Mucklow and Wilson [93] provides a good illustration of an experimental approach to the analysis of the attenuation of compression waves in gases. The authors used three different diameters of pipe (approximately 3.8 cm, 5.1 cm and 10.9 cm), each of which was approximately 24 m long, to perform their experiments. From the measurements, the authors were able to determine an empirical equation of the form:

$$(1/P_H)^b = (1/P_i)^b + C(x_H/d)^{1.25} \quad \text{Eqn. 1}$$

where P_H is the gauge pressure after the wave peak has traversed a distance x_H , P_i is the incident gauge pressure of the wave peak, d is the pipe diameter, b is

a dimensionless exponent and C is a dimensionally consistent constant. The authors have claimed good agreement between the experimental results and the empirical formula; however, no theoretical analysis was attempted.

In his discussion of exhaust system design, Shepherd [113] concluded that:

"Although there does not appear to be a substitute for design and development experience with exhaust systems, instrumentation and computerization offer many aids to final product design and fabrication."

This observation was made by an automotive engineer who was discussing the transition of exhaust system design from 'art' to science. The art being alluded to was the exhaust system designer performing in situ testing of his design to determine if any objectionable frequencies were present. In the event that such frequencies were present, the designer then tuned his system to eliminate them. This 'cut and try' approach has been and continues to be used by exhaust system designers such as Roe [106,107] who has made use of annular cavity exhaust silencers. He has indicated that these silencers can be used to meet noise limitations required in competitive racing while not affecting engine performance. This design approach has been used irrespective of the size of the engine being silenced.

The transition to 'science' occurred in the 1960's as more advanced electronic equipment made automatic frequency tracking of engine speed possible. The result was the ability of the designer to more easily determine the noise attenuation effects of an exhaust system. This has led to use of increasingly complex exhaust system designs employing quarter wave resonators, co-axial resonators, or a combination of a resonator used in conjunction with a reactive or a dissipative muffler.

Some useful information has been derived from experimental testing associated with the empirical method. In his paper concerning exhaust system design, Thomas [118] has discussed some methods used to assist in the creation of a quiet exhaust system. The factors mentioned include: gas flow, muffler shell design and acoustics. Of the important details associated with these factors, those which are related to gas flow are the most useful. Part of the general approach to exhaust system design has included the knowledge of the basic engine data and the average values of intake and exhaust gas temperatures. The approximate exhaust gas flow rate can then be determined from the product of the engine displacement per shaft revolution, the compression efficiency of the engine and the absolute temperature ratio of the exhaust gas to the intake gas.

Thomas has pointed out that the gas volume could be corrected for the fuel consumed but that this is a negligible quantity. In addition, there should be a slight change in gas volume due to the replacement of oxygen by combustion products; however, since the air is 78% nitrogen, the molecular volume of the exhaust gas would not change significantly. Another useful treatment of the exhaust gas behaviour which has been implied by this approximation is that the gas properties can be approximated by using the properties associated with air. It has been pointed out that the most critical factor associated with the calculation of the exhaust gas flow rate is the compression efficiency of the engine.

Thomas has indicated that another important design criterion is the maximum back pressure which should be allowed at the exhaust port. In the case of chain saw and other engines having a high power to weight ratio, this pressure should be less than approximately $\frac{1}{2}$ inch Hg (1.7 kPa) [12]. It has also recommended that the maximum exhaust gas velocity be limited to approximately 130 m/s. One of the other general design criteria which was mentioned was the fact that the volume

of the muffler cavity should be at least 28 times the engine displacement of a single cylinder (or rotor displacement). Geometric considerations which have been mentioned include the length of the tailpipe and the exhaust pipe. It has been suggested that the ratio of exhaust pipe length to tailpipe length be 2. In the event that this is not possible, the next best ratio is $\frac{1}{2}$ and the worst ratio is 1. As well, it has been suggested that exhaust pipe diameter be progressively reduced until the muffler is reached and gas expansion takes place.

The importance of measuring flow rates and exhaust gas velocities as a function of time has been recognized because of its relevance to scavenging. One method of exhaust gas mass flow rate measurement from a Wankel engine has been demonstrated by Ferguson et al. [65]. Their method involved the use of an orifice of suitable size inserted into the exhaust pipe. The purpose of the orifice was to create a quasi-steady flow condition such that the mass flow rate could be predicted from the general equation for the mass flow rate of a compressible gas through an orifice [75]. Unfortunately, the area ratio correction term has not been included; therefore, the equation given in the paper is not correct. In their study, the authors have used the mass flow rate to aid in the evaluation of the time resolved exhaust gas composition. They have also demonstrated that orifice plates could be used to predict mass flow rates in unsteady flow situations by showing good agreement between the measured flow rate and that predicted by the orifice plate equation. Ferguson's associates have continued to work on Wankel engines. Their later work [49] was directed toward the prediction of Wankel engine performance.

A different method of measuring the exhaust gas velocity has been demonstrated by Gajendra Babu et al. [68]. The engine that they were using was a four-stroke engine. Their method involved ionizing the gas at a particular location by applying a high-voltage pulse across two electrodes. A detector, sensitive to the

ionized gas was positioned at a known distance downstream of this location. From the measured time delay between the ionizing pulse and its detection, the authors have demonstrated that it was possible to accurately measure the exhaust gas velocity. The authors have also made several observations associated with the exhaust gas behaviour. The most important of these was that the longer the exhaust pipe, the fewer the number of reflected wave interactions from each pressure pulse leaving the exhaust port. Also, they observed that the higher the engine speed, the greater the uncertainty in the exhaust gas velocity measurement. The one phenomenon that neither of these two groups commented on was the pulse shape for both mass flow rate and velocity. The figures provided in both publications show that the majority of the gas motion occurs during a very small portion (approximately one tenth) of a complete exhaust cycle.

Although Malchow et al. [87] were interested in heat transfer at the exhaust port of a four-stroke engine, they did use pressure measurements and an orifice meter to measure the unsteady mass flow rate as a function of crank angle. In this case, the demonstrated cylinder blow down compared favourably, during the period of rising pressure in the exhaust pipe, with that shown by the authors in the previously cited references. There were differences exhibited in the fall-off from the peak pressure for both mass flow rate and velocity. The reason for some of these differences was due to the presence of exhaust port valving.

It has become evident from the preceding discussion that although the empirical testing of exhaust systems may lack a strong theoretical background; the contributions made by these investigators play an important role in the commercial design of exhaust systems because of their simplicity. In addition, the use of such simplifications as modeling the exhaust gas as high temperature air should be noted. None of the authors commented on the absence or presence of terminal combustion

in the exhaust pipe nor did they mention the presence of shock waves created when the exhaust port opened. The contrast between the empirical evaluations of exhaust systems and the theoretical analysis of wave behaviour can be shown to be considerable.

2.2 Acoustic Wave Propagation

One of the most frequently cited papers on plane wave propagation is that of Levine and Schwinger [83]. The authors developed an expression for calculating the end correction of a pipe from which sound was radiating. The length correction l' given was equal to 0.6133 times the inside pipe radius. This length correction was then shown to be a controlling factor in the reflection coefficient of the pipe. The reflection coefficient has been defined as the ratio of the peak amplitude of the reflected pressure wave relative to the incident pressure wave due to a change in cross-sectional area of the pipe. The reflection coefficient has been given for two cases: (1) the product of wave number and pipe radius greater than 1 but less than 4 and (2) the product of wave number and pipe radius less than 1. There has been experimental verification of some of these results which will be discussed later.

The solutions to problems involving linear wave propagation with no flow in ducts have been presented by Davis [54] and Embleton [60]. It must be noted that Davis has pointed out that linear acoustic theory will not accurately predict acoustic behaviour in the exhaust pipe of an internal combustion engine. He has noted that peak sound pressures can be as high as one-third to one-half of the static pressure measured. Embleton has noted that some experiments have indicated that there is a linear relationship between acoustic pressure and particle velocity up to about 100 Pa. Beyond that point, the acoustic pressure is proportional to the square of particle velocity. The constant of proportionality that has been used is the mean

gas density.

A very good discussion of modeling low-frequency sound transmission in ducts, associated with no flow linear wave propagation, has been presented by Pierce [102]. The lumped-parameter modeling procedure has been used in this treatment. The major benefit derived from the use of this method is that it allows the interpretation of the acoustic problem in terms of either an analogous mechanical or electrical system. The limitation stated for this method is that it can be used only when the frequency is such that the product of wave number k and a characteristic dimension a of the duct is much, much less than unity ($ka \ll 1$). The two most commonly mentioned variables used in the lumped-parameter treatment are the volume velocity and the average pressure.

The property relationships involved with these quantities are associated with the Reynolds Transport Theorem [103]. The volume velocity used in the development has been related to the instantaneous volumetric rate of flow across a surface (the surface integral of velocity), created by the instantaneous particle velocity of the fluid rather than any gross motion of the fluid, when it was assumed that the fluid density was not a function of the space co-ordinates. The restriction on density used in this case was the result of assuming ambient density. The definition given for the average acoustic pressure was to divide the surface integral of the power per unit area by the volume velocity. The term 'average' has been dropped from the lumped-parameter model by assuming that the acoustic behaviour is one-dimensional. The derived characteristic from these two variables is the acoustic impedance which is a frequency dependent quantity. The impedance has been defined as the acoustic pressure per volume velocity.

With these definitions, it has been shown that it is possible to evaluate an acoustic wave guide (duct) in terms of its inlet, outlet and interior impedance. The similarity to electrical impedance concepts allows complex systems to be evaluated by methods analogous to those of electrical circuit analysis. Two limiting cases of consequence which are frequently used in linear acoustic analysis have been presented. The first of these was that of infinite inlet and outlet impedances. The implied consequence of this limiting case results in treating the flow as being incompressible. This could be translated into the fluid mechanics case of one dimensional, incompressible, unsteady flow.

The second case was that of the fluid impedance being zero. This case could be translated into the fluid mechanics situation of one dimensional, compressible, unsteady flow. This would be analogous to a mass storage having taken place. The concept in the electrical analog would be that of capacitance (acoustic compliance). This concept has been shown to be particularly useful in the evaluation of Helmholtz resonator behaviour. Finally, since the density of the fluid medium is a distributed quantity, an inertial effect can be associated with its motion. This inertial effect has been defined as the acoustic inertance. The major concern in the modeling of acoustic systems has been the choice of appropriate values of impedance, compliance and inertance of the system components.

Sreenath and Munjal [114] have demonstrated the application of linear acoustic theory in the evaluation of mufflers. Although their paper was primarily directed at the evaluation of tubular type mufflers, they have included corrections for the tail pipe termination and effects of the exhaust pipe. The major assumption which allows the development of the attenuation equation for the exhaust system is that the muffler cross-section diameter is of the same or lower order of magnitude than that of the wavelengths present in the exhaust system. Their limitation is stated

that $D \leq (3.832/\pi)\lambda$ where D is the muffler diameter and λ is the wavelength of the low frequency exhaust noise. Additionally, the authors have stated that they assumed that the frequencies of the exhaust noise were of the order of the firing frequency. The experimental verification of two mufflers, designed using their method of evaluation, shows remarkably good results. In one case the muffler performed to within 2 to 3 decibels of its design attenuation over a broad range of engine speed. However, it has been noted that their design technique relies on a 'design, calculate and evaluate the results' approach.

Another example of the application of linear acoustic theory has been illustrated by Lykkeberg [85]. The assertion of the author was that ignoring the steady flow component of the gas in an exhaust system was not detrimental to the predictive power of the theory. The author used the results of organ pipe investigations which indicated that the radiation impedance of an open ended tube must be corrected by adding 70% of the pipe radius to the length of the pipe. This compensates for the radiation of sound to the surroundings and compares favourably with the value calculated by Levine and Schwinger [83]. Additionally, he has presented relationships for the lower cut-off frequency of a simple, one chamber filter and the half wave resonances of an exhaust system. The author's comments include the observation that quite frequently these relationships are ignored in favour of more sophisticated system analyses.

Finite element methods have also been proposed to evaluate the acoustic field for a number of boundary conditions. James [73] has discussed the situation of an acoustic field between two finite length, concentric cylinders. He also has suggested that the technique can be applied to the radiation of sound from the opening of a circular duct. This application has not been demonstrated nor has any comparison with experimental results been shown. Both Craggs [46] and Crocker [47] have used

this technique in the prediction of insertion losses for mufflers. The authors have indicated that mean gas flow should be included in the procedure; however, Crocker has suggested that this is not a critical concern unless the gas velocities exceed 32 feet per second (9.75 m/s) [13]. Work in the area of finite differences [15] and more broadly, finite element computational methods [14] has increased due to the availability of computers with adequate memory. Other work in this area will be presented in the following section.

It should be noted that, in the preceding discussion, no mention has been made concerning the actual pressure and gas velocity fluctuations in an exhaust system. The reason is that the linear acoustic wave theory assumes a sinusoidal varying waveform. This does not mean that the theory cannot handle a complex waveform. What is required is a Fourier Series representation of the waveform such that the analysis can take place. An additional problem is the assumption of either no flow or the use of a mean flow approximation. Other researchers have recognized this problem and have applied various analysis techniques in an attempt to handle the problem of pulsating flow.

2.3 Acoustic Theory with Gas Flow

The material to be covered in this section can best be presented by dividing it into three sub-sections:

1. The work of Blair and his associates
2. The work of Davies, his associates and those who have been influenced by his work
3. Others who have contributed to this area

Of the three groupings, the work of Blair and his associates is the most prolific. The advances accomplished by Blair and his associates, have probably been the most useful. Nowak [99] has indicated that the computer programs, created by Blair and his associates for the analysis of exhaust systems, are very useful engineering tools for the designer intent on evaluating an exhaust system design.

2.3.1 Work of Blair and Associates

When Blair turned his research efforts away from valve timing [23] and turbine related studies [3,122,123], he started a methodical investigation into the unsteady flow of exhaust gases [24]. One of Blair's first comments has set the tone for the remainder of his work. He observed that the use of the method of characteristics is a labour intensive technique which does not take into account frictional losses. Also, in the case of linear acoustic theory, the approach is good only for pressure wave amplitudes up to $\frac{1}{2}$ lb/in² gauge (3.447 kPa) [12]. He also discards the possibility of using shock tube results as they do not provide interaction of successive pressure pulses.

The method of approach chosen by Blair is one suggested by Benson et al. [18]. The procedure uses the method of characteristics as the foundation of the analysis. The relationships between the local speed of sound and the local particle velocity are converted to a non-dimensional form. The two relationships for the two wave propagation directions are replaced by their corresponding Riemann variables λ and β . A rectangular mesh is set up and a digital computer is then used to iterate the related equations to a solution. The assumptions used in Blair's investigation are for the case of one-dimensional, unsteady, non-homentropic flow. The theory was compared with experimental result obtained using room temperature compressed air which was passed through a rotary valve. It was his opinion that the determination

of a suitable pipe friction factor was accomplished and that the method of approach had potential.

In a subsequent analysis [25], Blair extended the theoretical side of his work to include diffusers. The diffuser problem was studied because it assists in the scavenging process. The complicating factor which had to be overcome was the mathematical treatment of the normal shock in the diffuser section. This condition was assumed to occur rather than that of supersonic flow. Rankine-Hugoniot type relationships were used to handle the property relationships across the shock. The experimental testing included both the rotary air valve mentioned previously and a 250 cm³ motor cycle engine. Good agreement between the theory and experimental results for both cases was demonstrated. However, subsequent application of the mathematical analysis to the exhaust system of a Lotus-Cortina engine [26] was not as fruitful. Blair observed that the simulation of the exhaust pressure pulse was very important factor in achieving good computational agreement.

At the same time as Blair and Arbuckle were investigating intake system design [27], Blair and Johnston presented a simplified design criteria for expansion chamber exhaust systems for small two-stroke engines [28]. The important procedure noted in setting up the criteria is that of the assumption of the amplitude of the blowdown pressure pulse. This is matched to the experimental amplitude by varying the discharge coefficient C_d which is used to control the Reimann variable λ . The design criteria presented by Blair and Johnston are as follows:

1. The area ratio of the exhaust pipe to the tailpipe should be greater than 2.65 but less than 4.7.
2. The area ratio of the exhaust pipe to the exhaust port should be greater than 1.3 but less than 1.75. The proviso is that the area ratio must be large enough that the

exhaust pulse amplitude is limited to a peak pressure of 1.9 atmospheres.

3. The 'stuffing' or 'plugging' pulse should arrive approximately 40 crank angle degrees before the exhaust port closure. This is dependent on the distance from the exhaust port to the tailpipe. The empirical relationship must be established for each engine type. However, the distance is directly proportional to the product of the mean speed of sound and the degrees of crankshaft rotation during which the exhaust port is open, divided by the design engine speed for peak torque. The constant of proportionality must be determined by experimentation or by making a judicious assumption.
4. The ratio of the length of the conical diffuser of the expansion chamber to the distance from the exhaust port to the tailpipe must be less than 0.4 but greater than 0.25. Additionally, the ratio of the length of the contraction cone, connecting with the tailpipe, to distance from the exhaust port to the tailpipe must be less than 0.25 but greater than 0.125.
5. Since the scavenging pulse is created by the expansion cone of the diffuser, its position must be located by assuming that the pulse originates at midlength of the cone. The total length for the returning scavenging pulse is assumed to be proportional to the product of the mean speed of sound and the degrees of crank rotation from exhaust port opening to bottom dead centre, divided by the design engine speed for maximum torque. Again the constant of proportionality must be experimentally determined or a judicious value must be assumed. The tailpipe length is then determined by subtracting half the length of the expansion cone from this value.

6. The tailpipe length should be equal to the length of the contraction cone at the end of the expansion chamber.
7. The area ratio of the centre section of the expansion chamber should be greater than 3.4 but less than 4.5. The length of this section is controlled by the previously calculated component lengths.

In the discussion of this paper, Nowak [98] pointed out that most exhaust system designs for competition snowmobiles fall outside the criteria presented by Blair. In addition, it was pointed out that the length of the tailpipe is more important than Blair had assumed. It was indicated that the tailpipe controls the blow down characteristics of the expansion chamber and therefore, non-standard lengths might improve the engine performance. Blair responded by pointing out that Nowak's requirements necessitated a broad engine speed band with the engine providing good torque characteristics; whereas, Blair's goal was to provide the best torque possible over a limited range of engine speed.

Blair has continued in subsequent research to improve the analysis of unsteady gas by applying its results to the design and development of racing motorcycle engines [29,30,33,34]; as well as, the prediction of exhaust system generated sound pressure levels [31,32,45]. In the cases of the unsteady gas flow, the results of the induction system analysis [27] were coupled with the unsteady exhaust system analysis and a model of the gas exchange was developed. The results of these procedures were good. Blair indicated that the procedures coupled with practical experience would be very useful to a design engineer. The procedures allowed variation of inlet and outlet system design as well as bore, stroke, valve sizes and valve timing for single or multicylinder engines. The studies on the prediction of the noise levels produced by engine exhaust systems has likewise yielded good results. The comparison between the predicted noise levels and those measured for the same engine operating

conditions showed good agreement for frequencies below 1 kHz.

Further investigations were carried out to study scavenge flow [35] by using a procedure suggested by Jante [74]. The results of this study were applied to the development of a theoretical model for the scavenge process. The model was compared with experimental results for a two stroke engine [36]. The results of this and later studies [39,40,41,112] show remarkable agreement between theoretical and predicted inlet, crankcase, cylinder and exhaust pressures as well as the delivery ratio of fresh air. Improvements have also been presented in the area of modeling the combustion process [37]. The results of this modeling have also been successful.

Finally, Blair and Fleck have studied unsteady gas flow in a rotary engine [38]. The engine which the authors used for the testing was a Fichtel and Sachs Model 914A Wankel engine with a maximum output, according to the manufacturer, of 13.5 kW at 5500 rpm. The unsteady gas flow analysis used by Blair and his associates again proved to accurately predict the engine behaviour. The minor differences between the predicted and experimental values of the exhaust pressure wave, at the exhaust port, could probably be explained by the lack of information concerning friction losses in the engine. In addition, the numerical procedures presented included several approximations. The most notable of these was the calculation of the charging volume of the engine by a volume approximation rather than by using elliptical integrals.

2.3.2 Davies and Associates

Davies has approached the problem of pressure pulses in exhaust systems from a slightly different direction than that of Blair. Davies felt that the assumptions of one-dimensional, unsteady flow in a shock tube could be applied to

exhaust systems including silencers [50]. Thus he thought that an exhaust system could be analysed by using simple charts. The intended results would be the realistic prediction of exhaust system performance. Davies and Dwyer used this approach in conjunction with the governing equations for shock tubes. They reasoned that a shock condition would be present in any exhaust system because of the large peak pressures created when the exhaust port opened. In their justification, they used the example of a pressure pulse with a steady rise of half an atmosphere taking place in a period of 1 millisecond. They stated that this condition would form a shock front after it had travelled in air at standard temperature and pressure for approximately 2 milliseconds (the pulse will have travelled approximately 69 cm). Also, since exhaust gas temperatures are higher than temperature used in the example, the required time before a shock would be created would be much shorter. They also used the condition of an isentropic expansion occurring behind the normal shock so that the gas velocity behind the shock could be calculated.

The authors also reasoned that travelling shock waves would remain normal and would be stationary at any area expansion. The process involved tends to become very complicated. There are cases where the assumption of either the Mach number, just before an incident shock front at an area change, or the degree of expansion, just before it occurs, must be made. In addition, there is the necessity of determining whether shock tube relationships between the pressure ratio across the shock and the shock Mach number are used rather than normal shock table relationships. It is also necessary to construct time versus distance diagrams for the shock waves which are similar to those produced by the method of characteristics. In reply to this work, Blair pointed out that there are cases in which the entire pressure-time history would be necessary and that the procedure presented would not supply that information.

Alfredson and Davies [4] performed an experimental investigation of silencer components coupled with a theoretical analysis based on property perturbations and the method of characteristics. The analytical approach used was that of a linearized one-dimensional theory with mean flow. They found that the best method of analysis for sudden area changes was to assume that pressures were conserved. That is, the sum of the incident and reflected pressures on each side of the area change were equal. This method was not as accurate as that of assuming adiabatic behaviour but they found that the complexity of calculations was reduced by this assumption. Davies and Alfredson then went on to develop a computer program for expansion chamber silencers [51]. The key feature of this method was the assumption that the stagnation enthalpy was constant along a streamline crossing a change in section. This involved the optimization of the silencer component design using the previously developed theoretical approach. The authors claimed good performance of the silencers designed when they were fitted to their intended engines.

Davies has also discussed the problems of silencing associated with large engines [52]. Essentially he has reiterated the findings of his previous work with Alfredson. The important observation that he makes is that concerning gas flow in exhaust systems. Davies has shown, by mathematical analysis and comparison with experimental results, that the assumption of zero flow in an exhaust system can be detrimental to the correct calculation of silencer performance. In a later publication [53], he concluded that both flow conditions and temperature gradients should be included in any modeling study of an exhaust system. This would, as a consequence, improve the prediction of silencer performance considerably.

Later, Alfredson continued the discussion to include Helmholtz resonators in the theoretical treatment [5]. This also included the effects of yielding walls in the silencer. He has pointed out that the biggest problem in predicting

silencer performance has been with its resonance frequencies. The author states that in general the prediction of silencer performance is very good everywhere but at the resonant frequencies. Here the variation may be as much as 3 to 5 decibels. Since this variation occurs at the resonance frequencies, the quality of the overall design is lessened.

The work by Davies has influenced at least one muffler manufacturer as indicated by Eriksson [62,63]. Nelson Industries has modified the technique of Alfredson and Davies. The modification was in the nature of the analysis of each section of the exhaust system. The modification allowed the inclusion of temperature gradients in the general calculation procedure. Eriksson has indicated that the modeling procedure correlates well with experimental measurements.

2.3.3 Other Contributors

Wallace and Nassif [121] have also investigated the problem of predicting scavenging in a two-stroke engine. The authors broke the problem down into two related parts. Their method involved the use of finite wave theory, while maintaining conditions for dynamic similarity. The first part of the analysis breaks the problem of quasi-steady flow through the exhaust and intake ports into the following subsections:

1. Outflow (particle velocity outwards through the ports).†
2. Inflow (particle velocity inwards through ports).†

† These include conditions for subsonic and sonic flow, as well as a criterion for mass flow.

3. Limiting conditions which include flow reversal and port reflection criterion.

4. Changes of state in the engine cylinder. This included the general state relationships governed by the laws of Thermodynamics, the changes in state due to blow-down and the exhaust lead (the duration of port opening required to achieve the same mean pressure in the cylinder as that existing in the exhaust pipe).
5. Maximum exhaust pulse pressure.

The second part of the analysis was concerned with unsteady gas flow in the external pipe system. This included:

1. Progressive distortion of the wave profile and shock formation.
2. Superimposition effects.
3. Effect of temperature discontinuities.
4. Effect of friction.

This detail of coverage resulted in an excellent presentation of the problems associated with two-stroke engines. The experimental testing agreed well with the theoretical treatment. The authors observed that the design of both the intake and exhaust systems was very important. The intake and exhaust systems were found to be the controlling factors in the scavenging process. Another important factor was that of the rate of exhaust port opening.

Lambert [81] has also performed an analysis of side branch filtering of sound in a moving medium. He used the linearized equations of sound propagation in a dissipationless, homogeneous, progressively moving, isentropic gas. The author makes use of impedance relationships to determine the insertion loss of the side branch. He also showed that the performance of the filter was a function of the flow Mach number and the pipe geometry. It was also concluded that the viscous

dissipation was also an important factor.

A numerical method of calculating the unsteady flow in both intake and exhaust systems has been presented by Goyal et al. [70]. The standard assumptions of one-dimensional, unsteady flow have been used. The analysis was applied to a straight pipe of constant area with both heat transfer and friction. The method of characteristics was then applied to develop the governing equations. Empirically derived heat transfer coefficients were also used. The flow calculations were performed using a finite difference method. Exhaust pipe length was found to be an important factor. The comparison between the calculated and experimental results were deemed to be inconclusive by the authors. The inference being that the theoretical treatment did not adequately handle the problem.

Exhaust systems employing conical diffusers have been tested by Nassif [97]. The experimental results were compared with a theoretical analysis based on acoustic impedance. The conclusions reached were that:

1. The difference between measured and predicted flow behaviour was the greatest for small conical diffusers.
2. Longer diffusers were found to provide better delivery of fresh air due to scavenging.
3. Cone angles between 1 and 4 degrees did not seem to affect the delivery.

An additional observation was that the exhaust port acted as a partially closed end rather than the fully closed end condition which has been the commonly assumed condition.

A completely theoretical analysis of acoustic wave propagation has been carried out by Mungur and Gladwell [94]. The authors used the exact two-dimensional

Navier-Stokes equation in their analysis. The pressure, density and viscosity were assumed to be composed of a mean and fluctuating component. The gas velocity was also assumed to be composed of a mean and fluctuating component with the exception that there was no mean component orthogonal to the flow direction. The complexity of the equation was reduced by subtracting the time averaged equations from the x and y components. This process was also applied to the law of conservation of mass. The substitution was continued after assuming that the wave propagation was adiabatic and isentropic. A final substitution of a relationship between the fluctuating viscosity, mean viscosity, fluctuating to mean pressure ratio and fluctuating to mean density ratio yielded a final equation amenable to numerical solution. The numerical solution was by means of the fourth-order Runge-Kutta method applied to the inviscid case. A power law relationship was assumed for the velocity profile. No details were provided for the pressure variations in the direction of mean flow; however, since the solution involves an assumed function for pressure of the form:

$$P = F(y) e^{-\alpha x} e^{j(\omega t - k_x x)} \quad \text{Eqn. 2}$$

It may be possible to employ a different functional relationship such as the one to be discussed in the next chapter. In this equation, $F(y)$ is the amplitude of the pressure wave and α, k_x are respectively the attenuation and wave number in the x direction.

Hirata and Itow [72] have reinforced the arguments of other researchers that gas flow has a significant influence on exhaust system behaviour. In this case the authors extended the work of Lambert [81] by means of a very straightforward method of analysis. In their evaluation of side branch resonators, they assumed additional hemispherical masses at each end to the resonator neck. This additional mass was assumed to be proportional to $\frac{1}{2}$ of the product of the gas density and

the neck diameter. This was then used to correct the kinetic energy term for the neck. The gas flow in the main duct was assumed to be turbulent and to have a power-law velocity profile. Subsequent analysis of the displacement of the hemispherical end correction by the gas flow in the main duct yielded a energy dissipation relationship which could be expressed in the impedance form. The experimental results compared favourably with the theoretical predictions. However, the testing was conducted only for a steady flow of air in the test section. No results were presented for the muffler installed in an engine exhaust system.

In a survey of exhaust system evaluation techniques, Bender [16] has presented an alternative technique. He has suggested that it is possible to evaluate the effects of an orifice on sound by using the Bernoulli equation for unsteady incompressible flow. He has also noted that there are several nonlinear effects in exhaust systems. These are generally associated with vortices generated by orifices. The author concluded by suggesting that the following elements of the problem should be characterized:

1. Attenuation of perforated tubing with flow in the nonlinear pressure range.
2. Evaluation of the source impedance of internal combustion engines.
3. Generation of sound waves by unsteady flow through exhaust ports.
4. Effects of exhaust turbines on noise generation and propagation.
5. The effects of reflected pressure waves on engine performance.

He has also observed that insertion losses of mufflers cannot be predicted with a good degree of accuracy.

A comparison of experimentally determined exhaust gas velocity with a theoretical model has been presented by Yun and Mirsky [131]. One of the unique features of this evaluation was the comparison of instantaneous gas velocity measurements by a hot-wire anemometer and schlieren-streak photography. The two methods show good agreement over the range of engine crank angle presented. In the simulation, one-dimensional, unsteady gas flow was assumed. The conservation laws for mass, momentum and energy were combined with the ideal gas equation of state, the isentropic speed of sound equation, the Darcy-Weisbach equation for wall shear stress and the general form of the convective heat transfer equation. No indication is given of how the substitution and solution process is performed; however, the boundary and initial conditions were presented. The comparison between the calculated and measured gas velocity was excellent over the range of engine crank angle presented. No simulation of the exhaust gas pressure pulse was presented.

Munjal [95] advanced the use of the impedance method by first separating the mean and fluctuating components of velocity, density and pressure. The convective terms of pressure and velocity (those associated with the gross gas motion) were then written in terms of the incident and reflected acoustic pressures and the Mach number of the flow. Impedance relationships were then determined for exhaust system elements such as a uniform tube, a sudden contraction, an extended outlet, an extended inlet, a sudden expansion and a branch resonator. Unfortunately, no presentation of a comparison between a theoretical model and experimental result was made.

A novel approach to two-stroke engine modeling has been presented by Mutyla and Soedel [196]. Their assumption was that the expansion chamber muffler, cylinder and crankcase of the engine could be modeled by Helmholtz resonators. The exhaust gas was treated as though it was incompressible and exhibited inertia only in the exhaust port and tailpipe. The gas volumes in the crankcase, cylinder and expansion chamber were assumed to be compressible. Additionally, the gas pressures were separated into their mean and acoustic components. A thermodynamic modeling of the combustion process was also employed. The mathematical model included linear algebraic equations, seven first order differential equations describing the thermodynamic model and three second order differential equations for the Helmholtz resonators. The second order equations were converted into first order equations by the Runge-Kutta method. The theoretical calculations performed by the authors compared favourably with the experimentally determined pressures.

Kelsay and Margolis [197] performed experimental testing on a two-stroke engine to determine if a relationship existed between the exhaust gas pressure-time history and engine power. The authors found that the timing of the reflected exhaust pressure pulse was critical and had to reach the exhaust port just before it closed. They determined that the timing of this 'stuffing' pulse was the most important phenomenon in the development of engine torque. The exhaust pipe length was found to be the most important design consideration in the control of this timing. In addition, it was determined that the size and shape of the pulse itself was not important. An observation associated with this pulse was that the engine appeared to perform the best when the pulse had the largest amplitude. It was also found that longer exhaust pipes produced higher maximum torques at lower engine speeds. The result of this was a loss in engine power. They observed that the exhaust pipe length must be optimized for maximum power and not necessarily

for torque. This was because both engine speed (frequency of exhaust port opening) and the length of the exhaust pipe were important.

Margolis [88] and his associates [89,111] have also been working on the application of the Bond Graph technique [90,108] to the complete modeling of a two-stroke engine. Work similar to that of Blair was carried out. The authors produced a computer programme for the analysis based on this technique. Equations were written for mass, momentum and energy and frictional losses were included in the momentum equation to improve the accuracy of the model. The authors have stated that they used a one-dimensional, nonlinear gas dynamic model.

The Bond Graph technique assumes that there is a linear relationship between various elements (ports). These elements are composed of sources (effort or flow), storages (capacitance or inertance), dissipation (resistance), 2-port junctions (transformer or gyrator) and 3-port junctions (common effort junction). The application of this technique results in a matrix presentation of the governing state equations. These equations may then be solved by means of a computer. In the aforementioned case of the two-stroke engine, the results were used to evaluate the engine performance when various subsystems were changed. For example, changes in the loss coefficient of the tailpipe indicated situations of decreased engine performance. The difficulty with this analysis is that each of the port variables must be expressed in terms of its mathematical model. Considerable knowledge is necessary to select the appropriate form of the model and much 'fine tuning' of that model is required. This is usually accomplished by resorting to experimental testing.

As mentioned previously, numerical simulations have been gaining favour among researchers. Walter and Chapman [124] have made use of the work of Blair and his associates and also, indirectly, Davies, his associates and those who

have been influenced by his work. Walter and Chapman have used a finite difference scheme employed in a computer programme developed by Chapman. The GODEL programme (Generalized One-Dimensional Eulerian Lagrangian) was applied to the inviscid differential conservation equations of mass, momentum and internal energy. The ideal gas equation of state was also used. The polytropic exponent of 1.35 was used in the cylinder blow-down. The conclusions reached by the authors were that truncation errors adversely affected the results. In addition, they felt that the number of mesh points used in the calculations should be increased; however, they also observed that the cost of computer time would increase. The authors have suggested that further refinements in the modeling and the computational methods should be investigated.

The method of characteristics has been successfully employed by Jones [77] in the determination of two-stroke engine exhaust noise. The method used by the author permits the calculation of the actual wave diagram. The author has claimed that his method is more precise than that of Benson or Blair. He has made use of comparisons of his method with that of Benson to prove his point. Not only was the computer programme capable of accurately predicting the pressures and velocities in the exhaust system but it also demonstrated good agreement between the calculated and measured radiated sound pressure. With this paper, the author has shown that the method of characteristics can be applied to the acoustic problems in an exhaust system.

Recent work by Thawani and Doige [117] has presented an informative impedance based treatment of the acoustic problems in an exhaust system. They have broken the problem into four parts. These are the no flow case, the mean or moving flow case, the mean flow case with damping due to friction and the case of mean flow with damping due to shear viscosity. Their results for mean flow with damping

compare favourably with their experimental results; however, it should be pointed out that these experiments were not conducted in conjunction with an internal combustion engine. The conclusions expressed by the authors concerning exhaust system design agree with those of other researchers. That is, flow reversal elements in mufflers tend to increase back pressure, muffler elements which do not experience flow can be modeled as no flow elements, the inclusion of damping is necessary for good modeling and that knowledge of the source impedance is not necessary.

As can be seen from this section, there are many ways of treating the problems associated with the exhaust system. However, it should be noted that, in most cases, the methods of analysis are involved with linear acoustic systems with an assumed mean flow. A few researchers such as Blair, Jones and Davies have used methods which take into account the nonlinear gas behaviour.

2.4 Nonlinear Effects

Nonlinear effects in small engine exhaust systems have been recognized by Brammer et al [42,43] to be an important area of study. This phenomenon was first encountered when small Helmholtz resonator mufflers were tested on a small chain saw engine. It was found that there was a considerable difference in the exhaust noise spectrum between the muffler case of essentially a straight through exhaust when compared with a side outlet on the same muffler configuration. The authors reasoned that vortex 'jetting' which they observed was carrying most of the acoustic energy straight through the muffler without any dissipation. In their conclusions, they stated that any realistic description of the acoustical performance of mufflers for small two-stroke engines should recognize the nonlinear effects created by the pulsating gas pressure. In addition, they felt that the back pressure effect created by the muffler on the performance of the engine should specify the linear response

of the muffler at the firing frequency of the engine.

Although Donaldson Company, Inc. has been concerned with the manufacture of induction and exhaust systems for medium and heavy duty trucks, it also provides similar products for recreational vehicles. With such a vantage point, Rowley [109], who works for Donaldson Company, Inc., has been able to make some comments concerning exhaust system design. He has concluded that:

1. If the engine is not available, the actual engine exhaust system conditions must be somehow simulated
2. All conditions such as gas flow, temperature and temperature gradient down the exhaust system should be present.
3. The total exhaust system must be used. For example, one should not simply measure the insertion loss characteristics of a particular muffler by means of some test without having the rest of the intended exhaust system connected to it. Even the engine impedance must be simulated.
4. If the testing is of the off-engine variety, noise must be generated with a spectral content similar to that of the intended engine. In addition, the amplitude must also be high enough (140 - 170 dBA) "such that nonlinear acoustic conditions exist."

Rowley has observed that:

"Nonlinearity cannot be ignored since it can significantly affect acoustic velocity, especially in a naturally aspirated engine"

The author has indicated that he is a strong advocate of on-engine testing of exhaust systems as opposed to acoustic bench testing of an exhaust system.

Sturtevant and Craig [115] have indicated that they consider nonlinear effects to be important. The authors have concluded that this is one of the most important features of small engines operating at high speeds. They have also observed that the exhaust pressure pulses, generated by the opening of an exhaust valve or port, tend to be of large amplitude and steep fronted. Thus, the authors have advocated the use of shock tubes for simulating exhaust pressure pulses from small engines in contradiction to the beliefs of Blair. The authors have reasoned that the effects of nonlinear steepening of the exhaust pressure pulse must be investigated to better predict exhaust system performance.

Eriksson [64] has presented a brief survey of nonlinear acoustics. Unlike Rowley, Sturtevant and Craig, he has concluded that linear acoustics can be used in simple expansion chamber mufflers up to 160 dB. He has indicated that this level is also the linear 'limit' for resonator design except at the resonant frequencies. The author also indicated that the exception to the use of linear theory occurs for tuned exhaust systems which are used on high-performance two-stroke and four-stroke engines. He has noted that internal sound levels can be as high as 190 dB.

2.5 Summary

In this survey of examples of literature available on the topic of exhaust system design and associated problems, the intent was to show the diversity of experimental and theoretical treatment. It is evident that the majority of authors in this field are aware of the need for some kind of exhaust gas flow assumption. On the other hand, others have studiously ignored both the necessity of some sort

of a flow condition but have also persisted in performing acoustical tests on exhaust systems without ever attaching the system to a running engine. It is admittedly true that one must proceed gradually in developing a theoretical treatment of the problem which can stand up to the rigours of increasingly complex flow situations. Blair is an example of a researcher who has followed this methodical developmental procedure. Finally, it must be pointed out that no one has started by assuming a pressure wave shape at the exhaust port, nor do they have a method of anticipating its behaviour, as it progresses through the exhaust pipe, which does not require a large computer to perform the calculations.

III. MODEL

Nonlinear acoustics is the middle ground between linear acoustics and shock waves. To some extent, it is a transitory phase through which a so-called 'linear' acoustic wave passes while on its way to becoming a shock wave. According to Beyer [21], Poisson developed a relationship for finite amplitude waves of the form:

$$u = f[x - (c_0 + u)t] \quad \text{Eqn. 3}$$

which describes the relationship between a finite displacement (the product of u and t) on the propagation speed for a given value of that velocity. The equation shows that the propagation velocity of a wave increases as the velocity increases. What follows in this chapter is the development of an explicit relation for this equation.

The assumptions used in this development are:

1. One dimensional (plane) waves
2. Isentropic speed of sound in the medium
3. No viscous dissipation
4. Confined motion in a wave guide
5. Ideal gas behaviour

for the section of duct shown in Figure 1,

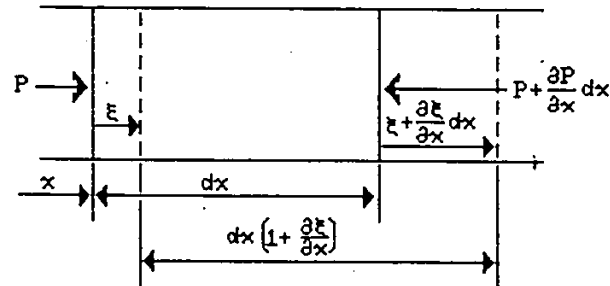


FIGURE 1. PLANE WAVE MOTION IN A WAVE GUIDE

where:

- A is the cross sectional area of the wave guide,
- P is the instantaneous pressure acting over an area,
- P_0 is the equilibrium pressure when there is no disturbance,
- ρ is the instantaneous density of the medium,
- ρ_0 is the equilibrium density when there is no disturbance,
- x is the coordinate measured along the axis of the wave guide which defines the location of the fluid element,
- dx is an incremental distance along the wave guide,
- ϵ is the displacement of the particles in a plane from their rest position due to the propagation of a disturbance.
- $\frac{\partial \epsilon}{\partial t}$ is the instantaneous particle velocity which can also be designated by u .

The original volume of the element is Adx at a density ρ_0 . The instantaneous volume when a disturbance is present is $Adx(1 + \frac{\partial \epsilon}{\partial x})$. Applying the law of conservation of mass to the undisturbed and disturbed condition:

$$\rho_0 Adx = \rho Adx(1 + \frac{\partial \epsilon}{\partial x})$$

Eqn. 4

Rearranging and eliminating common terms:

$$\rho/\rho_0 = 1/(1 + \partial\xi/\partial x) \quad \text{Eqn. 5}$$

For a reversible process:

$$P/\rho_0 = (\rho/\rho_0)^\gamma \quad \text{Eqn. 6}$$

Substituting Eqn. 5 into Eqn. 6 and rearranging:

$$P = \rho_0(1 + \partial\xi/\partial x)^{-\gamma} \quad \text{Eqn. 7}$$

Taking the partial derivative of P with respect to x:

$$\partial P/\partial x = \rho_0(-\gamma) * [(1 + \partial\xi/\partial x)^{-(\gamma+1)}] \partial^2\xi/\partial x^2 \quad \text{Eqn. 8}$$

Applying Newton's Second Law ($\Sigma F = \text{mass} \times \text{acceleration}$):

$$PA - [P + (\partial P/\partial x)dx]A = \rho_0(\partial^2\xi/\partial t^2)dxA \quad \text{Eqn. 9}$$

Eliminating common terms:

$$\partial P/\partial x = -\rho_0 \partial^2\xi/\partial t^2 \quad \text{Eqn. 10}$$

Equating Eqn. 8 and Eqn. 10 yields:

$$-\rho_0(\partial^2\xi/\partial t^2) = \rho_0(-\gamma)[1/(1 + (\partial\xi/\partial x)^{\gamma+1})] * \partial^2\xi/\partial x^2 \quad \text{Eqn. 11}$$

Since $c_0^2 = \gamma P_0/\rho_0$, then Eqn. 11 becomes:

$$\partial^2\xi/\partial t^2 = c_0^2[1/(1 + (\partial\xi/\partial x)^{\gamma+1})] * \partial^2\xi/\partial x^2 \quad \text{Eqn. 12}$$

Equation 12 can be simplified to the linear wave equation if it is assumed that

$$(\partial\xi/\partial x) \ll 1.$$

However, if it is assumed that:

$$\partial\xi/\partial t = f(\partial\xi/\partial x) \quad \text{Eqn. 13}$$

Then if f' is the derivative of the function with respect to its argument :

$$\partial^2 \xi / \partial t^2 = f'(\partial \xi / \partial x) * \partial^2 \xi / \partial t \partial x \quad \text{Eqn. 14}$$

But:

$$\partial / \partial x (\partial \xi / \partial t) = \partial^2 \xi / \partial x \partial t = f'(\partial \xi / \partial x) * \partial^2 \xi / \partial x^2 \quad \text{Eqn. 15}$$

Then:

$$\partial^2 \xi / \partial t^2 = f'(\partial \xi / \partial x) * f'(\partial \xi / \partial x) * \partial^2 \xi / \partial x^2 \quad \text{Eqn. 16}$$

And:

$$\partial^2 \xi / \partial t^2 = [f'(\partial \xi / \partial x)]^2 * \partial^2 \xi / \partial x^2 \quad \text{Eqn. 17}$$

Comparing the results of Eqn. 17 with Eqn. 12:

$$[f'(\partial \xi / \partial x)]^2 = c_0^2 / (1 + \partial \xi / \partial x)^{\gamma+1} \quad \text{Eqn. 18}$$

Therefore:

$$f'(\partial \xi / \partial x) = \pm c_0 (1 + \partial \xi / \partial x)^{-(\gamma+1)/2} \quad \text{Eqn. 19}$$

Integrating and using C as a constant:

$$\int f'(\partial \xi / \partial x) d(\partial \xi / \partial x) = f(\partial \xi / \partial x) \\ = \pm c_0 \int [(1 + \partial \xi / \partial x)^{-(\gamma+1)/2}] d(\partial \xi / \partial x) + C \quad \text{Eqn. 20}$$

$$= \pm c_0 (2/1 - \gamma) * (1 + \partial \xi / \partial x)^{(1-\gamma)/2} + C \quad \text{Eqn. 21}$$

For no wave disturbance $\partial \xi / \partial t = 0$ and $\partial \xi / \partial x = 0$, since $\xi = 0$

$$C = -[\pm 2c_0 / (1 - \gamma)] \quad \text{Eqn. 22}$$

Substitution of the value for C and using the relationship of Eqn. 13:

$$\partial \xi / \partial t = \pm \{ [2c_0 / (\gamma - 1)] - [2c_0 / (\gamma - 1)] \\ * [1 / (1 + \partial \xi / \partial x)^{(\gamma-1)/2}] \} \quad \text{Eqn. 23}$$

For a non-dissipating medium, the total energy content of the wave must remain constant. In this case, the kinetic energy is conserved. Therefore:

$$d[\rho(\partial\xi/\partial t)^2] = 0 \quad \text{Eqn. 24}$$

But:

$$d[\rho(\partial\xi/\partial t)^2] = \rho d(\partial\xi/\partial t)^2 + (\partial\xi/\partial t)^2 d\rho \quad \text{Eqn. 25}$$

Substituting for the property ρ from Eqn. 5 and eliminating common non-zero terms:

$$[2 * (1 + \partial\xi/\partial x) f'(\partial\xi/\partial x) - f(\partial\xi/\partial x)] d(\partial\xi/\partial x) = 0 \quad \text{Eqn. 26}$$

It can be shown that the terms inside the square brackets are non-zero by using the relationship of Eqn. 13 and substituting the results of equations 19 and 23 into Eqn. 26. Then:

$$d(\partial\xi/\partial x) = 0 \quad \text{Eqn. 27}$$

But:

$$d(\partial\xi/\partial x) = \partial/\partial x (\partial\xi/\partial x) dx + \partial/\partial t (\partial\xi/\partial x) dt \quad \text{Eqn. 28}$$

Therefore:

$$(\partial^2\xi/\partial x^2) dx = -(\partial^2\xi/\partial t \partial x) dt \quad \text{Eqn. 29}$$

Using the second relationship of Eqn. 15 and eliminating the common factor $\partial^2\xi/\partial x^2$ from the equation yields:

$$dx = -f'(\partial\xi/\partial x) dt \quad \text{Eqn. 30}$$

This can be rearranged as:

$$dx/dt = -f'(\partial\xi/\partial x) \quad \text{Eqn. 31}$$

Equation 31 is an expression for the propagation velocity v of the perturbation.

The use of Eqn. 19 yields:

$$v = -[\pm c_0 / (1 + \partial \xi / \partial x)]^{(\gamma+1)/2} \quad \text{Eqn. 32}$$

Or:

$$(\mp v / c_0)^{2/(\gamma+1)} = 1 / (1 + \partial \xi / \partial x) \quad \text{Eqn. 33}$$

From the definition that $u = \partial \xi / \partial t$ and rewriting Eqn. 23 in terms of $1 / (1 + \partial \xi / \partial x)$, the result is:

$$1 / (1 + \partial \xi / \partial x) = (1 \mp [(\gamma-1)/2] * u / c_0)^{2/(\gamma-1)} \quad \text{Eqn. 34}$$

Equating Eqn. 33 and Eqn. 34, and rearranging to solve for v yields:

$$v = \mp c_0 (1 \mp [(\gamma-1)/2] * u / c_0)^{(\gamma+1)/(\gamma-1)} \quad \text{Eqn. 35}$$

The lower positive sign corresponds to a perturbation moving with a velocity v in the positive x direction. It also shows that as the particle velocity increases, its propagation velocity also increases.

Beyer [20] has suggested that the general form of a positive going wave can be expressed as:

$$\xi = (1/\omega) F(\omega t - \omega x/v) \quad \text{Eqn. 36}$$

Then:

$$\partial \xi / \partial t = F'(\omega t - \omega x/v) \quad \text{Eqn. 37}$$

And:

$$\partial^2 \xi / \partial t^2 = F''(\omega t - \omega x/v) \omega \quad \text{Eqn. 38}$$

Also:

$$\partial \xi / \partial x = F'(\omega t - \omega x/v) * (-1/v) \quad \text{Eqn. 39}$$

And:

$$\partial^2 \xi / \partial x^2 = F''(\omega t - \omega x/v) * (\omega/v^2) \quad \text{Eqn. 40}$$

If Equations 38 and 40 are rearranged, equating of the second derivative of the arbitrary function F yields:

$$\partial^2 \xi / \partial t^2 = v^2 \partial^2 \xi / \partial x^2 \quad \text{Eqn. 41}$$

Equation 41 is similar to equation 12. Then:

$$u = G(\omega t - \omega x/v) \quad \text{Eqn. 42}$$

is a solution as well.

For the case of a wave which is sinusoidal in form at $x = 0$ and time t , the expression for the particle velocity would be:

$$u(0,t) = u_p \sin \omega t \quad \text{Eqn. 43}$$

where u_p is the peak particle velocity. Then:

$$u(x,t) = u_p \sin(\omega t - \omega x/v) \quad \text{Eqn. 44}$$

Substitution for v in equation 44 using the positive going wave results from equation 35 yields:

$$u(x,t) = u_p \sin\{\omega t - (\omega x/c_0) * [1 + (\gamma-1/2) * u/c_0]^{-(\gamma+1)/(\gamma-1)}\} \quad \text{Eqn. 45}$$

If this equation is plotted as a function of x for increasing values of u , it is found that the slope of the wave increases as x increases. Further, the slope increases more rapidly near $u(x,t) = 0$ as illustrated in Figure 2. Discussion of this distortion has been presented by Liepmann and Puckett [84]. Fox and Wallace [67] have made use of this discussion to illustrate the distortion of an originally sinusoidal wave into a shock wave.

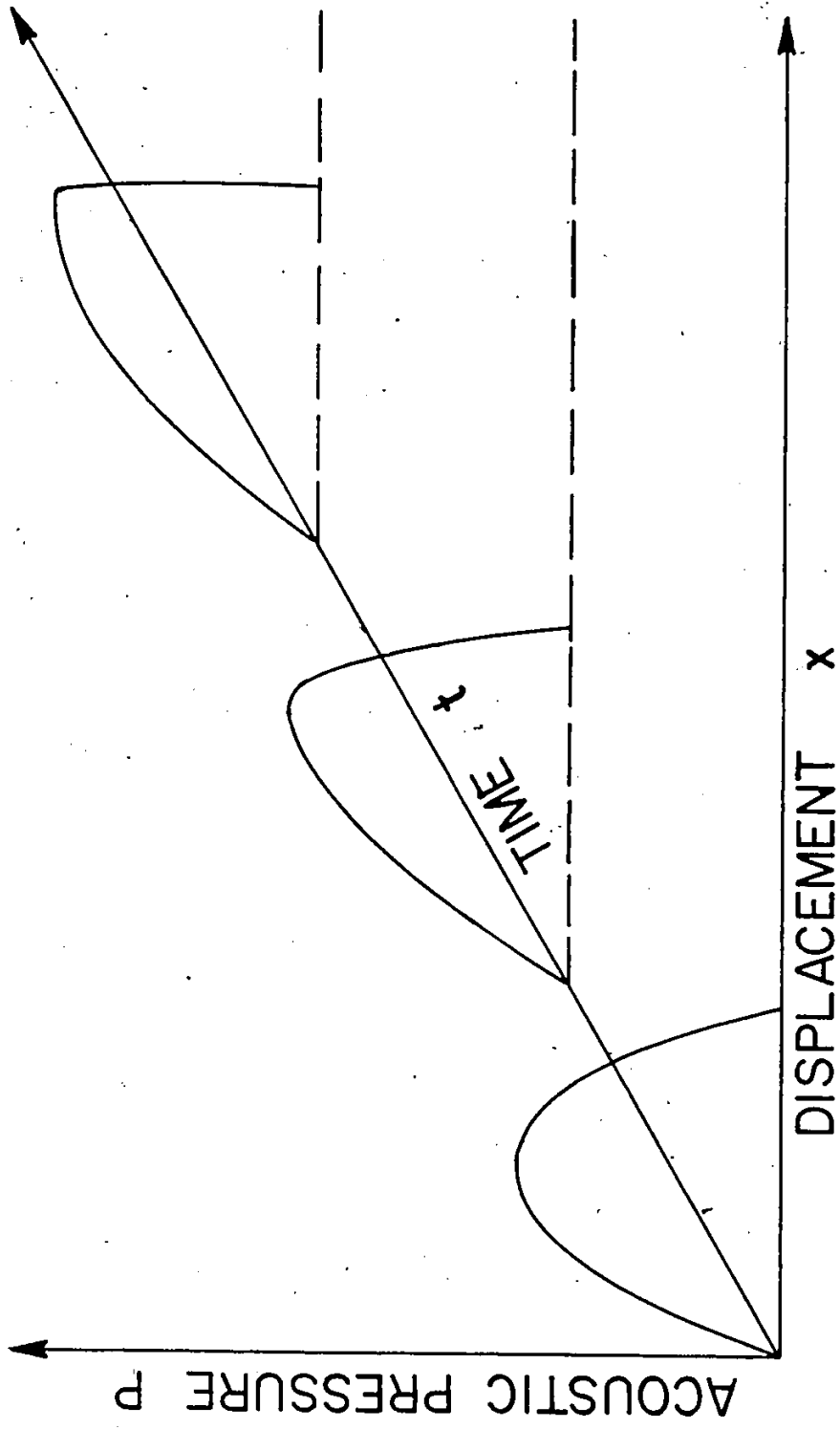


FIGURE 2. PROGRESSIVE DISTORTION OF A FINITE AMPLITUDE WAVE

Fox and Wallace have noted that the quantity $\partial u / \partial x$ will become negatively infinite at some distance $x = l$.

Taking the partial derivative of u with respect to x of the function $u(x,t)$ yields:

$$\begin{aligned} \partial u / \partial x = & u_p \cos(\omega t - (\omega x / c_0)) * [1 + (\gamma - 1/2) * u / c_0]^{-(\gamma + 1) / (\gamma - 1)} \\ & * \{ [1 + (\gamma - 1/2) * u / c_0]^{-(\gamma + 1) / (\gamma - 1)} * (-\omega / c_0) \\ & - (\omega x / c_0) * [1 + (\gamma - 1/2) * u / c_0]^{-1 - (\gamma + 1) / (\gamma - 1)} \\ & * \{ [(1 / c_0) * [-(\gamma + 1) / (\gamma - 1)] * [(\gamma - 1) / 2] \} \end{aligned} \quad \text{Eqn. 46}$$

if this is evaluated at $u = 0$, then:

$$\begin{aligned} \partial u / \partial x = & u_p \cos(\omega t - \omega x / c_0) * \{ -(\omega / c_0) + (\omega x / c_0^2) \\ & * [(\gamma + 1) / 2] * (\partial u / \partial x) \} \end{aligned} \quad \text{Eqn. 47}$$

This equation can be rearranged such that:

$$\begin{aligned} \partial u / \partial x = & -(\omega u_p / c_0) \cos(\omega t - \omega x / c_0) / \{ 1 - u_p \cos(\omega t - \omega x / c_0) \\ & * [(\omega x / c_0^2) * (\gamma + 1) / 2] \} \end{aligned} \quad \text{Eqn. 48}$$

This quantity should be negatively infinite at $x = l$ and therefore the denominator must be zero. This will occur first when $u(l,t) = 0$, since this occurs when the sine of the argument is equal to zero; the cosine of the argument will be unity.

Then:

$$1 - u_p (\omega l / c_0^2) * (\gamma + 1) / 2 = 0 \quad \text{Eqn. 49}$$

Then:

$$l = [2 / (\gamma + 1)] * c_0^2 / u_p \omega \quad \text{Eqn. 50}$$

If u_p/c_0 is the acoustic Mach number M and ω/c_0 is the wave number k , then:

$$1/l = [(\gamma+1)/2]Mk \quad \text{Eqn. 51}$$

This equation shows that if either the acoustic Mach number or the wave number increases; the distance l , that the wave must travel before a shock occurs, will decrease proportionally. The quantity l is usually called the discontinuity distance.

According to Beyer [21], the first explicit solution to the function of the function was carried out by Fubini-Ghiron in 1935. To do this, it is necessary to expand the term $\{1 + [(\gamma-1)/2] * u/c_0\}^{-(\gamma+1)/(\gamma-1)}$ by means of the Binomial Series expansion:

$$y^n = 1 + n * (y-a) + n(n-1) * (y-a)^2/2! \\ + n(n-1)(n-2) * (y-a)^3/3! + \dots, \quad \text{Eqn. 52}$$

Where:

$$y = 1 + [(\gamma-1)/2] * u/c_0$$

$$a = 1$$

$$n = -(\gamma+1)/(\gamma-1)$$

If it is assumed that term 3 and all subsequent terms are negligible, then:

$$\{1 + [(\gamma-1)/2] * u/c_0\}^{-(\gamma+1)/(\gamma-1)} \\ \approx 1 - [(\gamma-1)/2] * u/c_0 \quad \text{Eqn. 53}$$

Then:

$$u(x,t) \approx u_p \sin(\omega t - (\omega x/c_0) * (1 - [(\gamma+1)/2] * u/c_0)) \quad \text{Eqn. 54}$$

Or:

$$u/u_p = \sin(\omega t - kx + [(\gamma+1) * [\omega x u]/[2c_0^2]]) \quad \text{Eqn. 55}$$

Using the relationship for the discontinuity distance l , then:

$$u/u_p = \sin[\omega t - kx + (x/l) * (u/u_p)] \quad \text{Eqn. 56}$$

This is an implicit relation for the non-dimensional particle velocity as a function of the sine of an argument which includes the non-dimensional particle velocity.

Since the wave form is of a sinusoidal nature, one possible expansion of the function u/u_p is a Fourier Series, which is represented by:

$$u/u_p = \sum_{n=1}^{\infty} B_n \sin n(\omega t - kx) \quad \text{Eqn. 57}$$

Where:

$$B_n = 1/\pi \int_0^{2\pi} (u/u_p) \sin n(\omega t - kx) d(\omega t - kx) \quad \text{Eqn. 58}$$

Let $u/u_p = \sin \zeta$ and $z = x/l$, then:

$$\sin \zeta = \sin (\omega t - kx + z \sin \zeta) \quad \text{Eqn. 59}$$

Then:

$$B_n = 1/\pi \int_0^{2\pi} \sin \zeta \sin n(\omega t - kx) d(\omega t - kx) \quad \text{Eqn. 60}$$

Letting $\zeta = (\omega t - kx) + z \sin \zeta$, then:

$$(\omega t - kx) = \zeta - z \sin \zeta \quad \text{Eqn. 61}$$

It can be seen that if $(\omega t - kx) = 0$, then:

$$\zeta = 0 \text{ and } \sin \zeta = 0$$

and if $(\omega t - kx) = 2\pi$, then:

$$\zeta = 2\pi \text{ and } \sin \zeta = 0$$

Using the relationship:

$$\int u dv = uv - \int v du$$

where:

$$u = \sin \zeta$$

$$dv = \sin n(\omega t - kx) d(\omega t - kx)$$

Then:

$$du = \cos \zeta d\zeta$$

$$v = -(1/n) \cos n(\omega t - kx)$$

Then:

$$B_n = (1/n\pi) \left(\left[-\cos n(\omega t - kx) \sin \zeta \right]_0^{2\pi} + \int_0^{2\pi} \cos n(\omega t - kx) \cos \zeta d\zeta \right) \quad \text{Eqn. 62}$$

The term in the square brackets is zero for the limits used and it also must be noted that:

$$d\zeta = d(\omega t - kx) + z \cos \zeta d\zeta \quad \text{Eqn. 63}$$

Rearrangement yields:

$$z \cos \zeta d\zeta = d\zeta - d(\omega t - kx) \quad \text{Eqn. 64}$$

Since:

$$B_n = (1/n\pi) \int_0^{2\pi} \cos n(\omega t - kx) \cos \zeta d\zeta \quad \text{Eqn. 65}$$

$$= (1/nz\pi) \int_0^{2\pi} \cos n(\omega t - kx) (d\zeta - d(\omega t - kx)) \quad \text{Eqn. 66}$$

$$= (1/nz\pi) \left(\int_0^{2\pi} \cos n(\omega t - kx) d\zeta - \int_0^{2\pi} \cos n(\omega t - kx) d(\omega t - kx) \right) \quad \text{Eqn. 67}$$

$$B_n = (1/nz\pi) \left(\int_0^{2\pi} \cos n(\omega t - kx) d\xi - \left[(1/n) \sin n(\omega t - kx) \right]_0^{2\pi} \right) \quad \text{Eqn. 68}$$

The term in the square brackets is zero and therefore:

$$B_n = (1/nz\pi) \int_0^{2\pi} \cos (n\xi - nz \sin \xi) d\xi \quad \text{Eqn. 69}$$

By definition the integral:

$$(1/2\pi) \int_0^{2\pi} \cos (n\xi - nz \sin \xi) d\xi = J_n(nz) \quad \text{Eqn. 70}$$

is a Bessel function of the first kind of order n . Therefore:

$$B_n = (2/nz) J_n(nz) \quad \text{Eqn. 71}$$

and:

$$u/u_p = 2 \sum_{n=1}^{\infty} \left(J_n(nz)/(nz) \right) \sin n(\omega t - kx) \quad \text{Eqn. 72}$$

with the condition that $x < l$ or that $z < 1$ since the function:

$$u/u_p = \sin (\omega t - kx + zu/u_p)$$

becomes multivalued for $z > 1$. The final step in the development is to employ the fact that the change in pressure δP , which is associated with the wave propagation, is related to the particle velocity by the expression:

$$\delta P = \rho_0 c_0 u \quad \text{Eqn. 73}$$

Then:

$$P_{ac}/P_p = 2 \sum_{n=1}^{\infty} \left(J_n(nz)/(nz) \right) \sin n(\omega t - kx) \quad \text{Eqn. 74}$$

Where P_{ac} is the instantaneous acoustic pressure of the wave and P_p is the peak acoustic pressure which corresponds to the peak particle velocity of the wave.

For values of $z > 1$, one method of continuing the solution is by the use of Blackstock's bridging function [22]. However, for the purposes of this discussion, it will not be necessary to go beyond the Fubini-Ghiron solution. It should be noted that a graphical approach has been presented by Rudenko and Soluyan [110]. Their discussion of the wave behaviour has made use of this graphical method to explain the propagation velocity differences in terms of the isentropic process path. That is, a compression wave has a greater effect on the increase of propagation velocity than the effect that an expansion wave of equal amplitude would have on the decrease in propagation velocity.

There are several methods available with which to calculate the value of any Bessel function of the first kind. One possible method is to use tabulated values for higher order terms, such as those provided by Olver [100] in the handbook edited by Abramowitz and Stegun. Lower terms can then be calculated from recurrence relations. However, a simpler method is possible if a programmable computer is available. Olver has also provided an ascending series expression for a Bessel function of the first kind and integer order as:

$$J_\nu(vx) = (vx/2)^\nu \sum_{n=0}^{\infty} \frac{(-vx)^2/4)^n}{[n! \Gamma(\nu+n+1)]} \quad \text{Eqn. 75}$$

where $\Gamma(\nu+n+1) = (\nu+n)!$ if ν and n are integers. Since this is the case, a Bessel function of the first kind and any order can be calculated. In fact, the summation in the series need not proceed to infinity. To achieve eight significant digit results in the calculation, it is only necessary sum to the thirty-third term. This is sufficiently accurate for the purposes of this discussion.

IV. EXPERIMENTAL DETAILS

In order to observe and measure the operating characteristics necessary for the study of the exhaust gas behaviour of the rotary engine, it was decided that the construction of a suitable engine room was necessary. This was primarily because of the fact that a suitable location did not exist in the standard engine laboratory. The laboratory did not have an exterior building wall such that the exhaust pipe could be terminated in a suitable environment exterior to the laboratory space. Therefore, the immediate objective of this research project was to provide an economical test facility. To this end, an existing laboratory space was selected in which to construct an engine testing facility. One prime concern was that the engine performance tests and noise study could be conducted without unduly disturbing other people who might be in close proximity to the test area. The engine and the ancillary equipment were then incorporated into the overall design of the testing room.

4.1 Construction of The Test Facility

The general requirements of an engine testing facility can be subdivided into two parts. The first requirement is that the two main noise contributors of the engine, namely the engine noise and the exhaust noise, must be isolated from each other. Secondly, both noise sources must be isolated from the operator and others while providing acceptable ventilation for the engine room. Both requirements have been met by mounting the engine inside an acoustical enclosure which employed an exterior building wall and provided an acoustically isolating ventilation system.

In the case of the exhaust noise, there should be no obstacles near the egress of the exhaust pipe to avoid noise reflections back towards the exhaust area. The wall surrounding the exhaust pipe should be flat with no nearby windows or other projections. If exterior exhaust noise measurements are to be made, the area should be accessible from the ground; however, it should not be closer to the ground than twice the distance from the location where the exhaust noise measuring microphone is to be situated and the end of the exhaust pipe [32,53]. To negate wall reflection phasing and near field nonlinearities, the minimum distance from the microphone to the end of the exhaust pipe should be one meter although Blair and Coates [32] have suggested an alternative criterion of a separation distance of 40 pipe diameters. In addition, if obstacles such as plane walls facing the exhaust area are present, their proximity should be such that any reflected noise effects should be at least 10 dB less than the directly radiated noise to be measured. To avoid standing waves, the distance should not be a whole number multiple of the wavelength of the lowest frequency to be monitored.

The quality of the walls and ceiling of the acoustic enclosure must be as good as possible. The transmission loss of the construction must be a minimum of 10 dB in any of the spectrum levels which would be of interest or would be of annoyance to others. As well, the loss must be increased if the wall is expected to isolate a very loud noise source from a quieter, surrounding area. If the anticipated noise levels are high, a simple transmission loss test can be conducted [13]. This testing should be conducted as soon as the wall is constructed so that suitable modifications can be made immediately if they are required. A point which should be noted is that the lowest frequency of concern will either be the rotating frequency of the engine or its firing frequency. In the case of a rotary engine, the rotating frequency of the engine is the lowest frequency of concern.

Another consideration of a testing room is the ventilation system. There must not only be adequate fresh air for the engine combustion process but there must also be adequate air to maintain a reasonable room temperature for an air-cooled engine. An additional condition of concern is the fact that the ventilation ducting can transmit sound from the test facility to the surroundings. Finally, the test facility must be provided with adequate electrical power to run equipment in the engine testing room and the control room. Water must be provided for heat sink purposes as well as for loading a hydraulic dynamometer. With the water requirement is the attendant problem of drainage.

The production of a high transmission loss barrier [120] is dictated by three factors, the stiffness of the material, the mass of the material and the degree of damping that the material possesses or which has been added to it. It is not unusual to reduce the effect of the noise transmission through a wall by using a combination of materials to act as a barrier to the noise. The normally suggested construction method makes use of a high density support structure which is covered with an acoustic material of high porosity [19]. This procedure was used to construct the interior walls of the engine test facility. Polyurethane foam 'skins' were attached to high density chip board panels. The foam 'skins' were the by-product of the production of polyurethane 'buns'. The 'skins' had a relatively non-porous film covering due to the production method of the 'bun'. However, the remainder of the 'skin' was quite porous as smoke could be blown through it. These 'skins' ranged from 2 to 5 centimeters in thickness and measured roughly 1.5 m by 2.2 m.

The selection of the room size was based on practical considerations which happened to coincide with the recommended proportions for acoustical testing rooms [127]. The most frequently used proportions, relative to the smallest of the three dimensions, are $1: 2^{1/3}: 4^{1/3}$ or $1: 1.26: 1.59$. The proportions of the three dimensions,

relative to the smallest dimension, of the room constructed were: 1: 1.27: 1.37. The dimensions involved in this choice stemmed from the standard building panels being 2.44 m long and the slotted steel angle construction material selected for the framing being 3.05 m long. These factors led to the chosen outside dimensions of the room of 4.57 m long, 3.05 m wide and 2.44 m high. Figure 3, the floor plan of the room indicates how well the length and width fit in with the general building construction. The control room was an area 1.22 m by 2.44 m situated inside the main boundary of the testing facility. Figures 4 and 5 show two views of the exterior building layout and general location of the room relative to the rest of the building. The height was convenient as well because the suspended ceiling lights and ventilating ducts cleared the top of the testing room by a minimum distance of 45 cm.

The slotted steel angle was chosen rather than wood studding because of the ease of erection. The use of bolting techniques permitted the non-destructive removal of part or all of the structure. This allowed the general layout to be changed if necessary. Undersized bolts were used so that the panels could be set into place after the joints were caulked. This allowed final adjustments to each panel to yield the smallest gap between panel boundaries while the bolts were being tightened.

The ventilation inlet and exhaust ducts were constructed such that they yielded as high a transmission loss as possible. This was done without resorting to elaborate construction techniques or expensive acoustic control materials. The design shown in Figure 6 was a variation on a design for a high transmission loss plenum [56]. The difference in design was that the flow entered the control chamber on the side rather than the in-line entrance and exit configuration of the original design. The inside of the rectangular duct and all other interior surfaces were covered with a 1 cm thick layer of polyurethane foam. This was the major noise control component which attenuated noise carried into the room through the ventilation system. A similar

Figure #1 Gaspar, Reif, Sridhar MHD 5. 5%

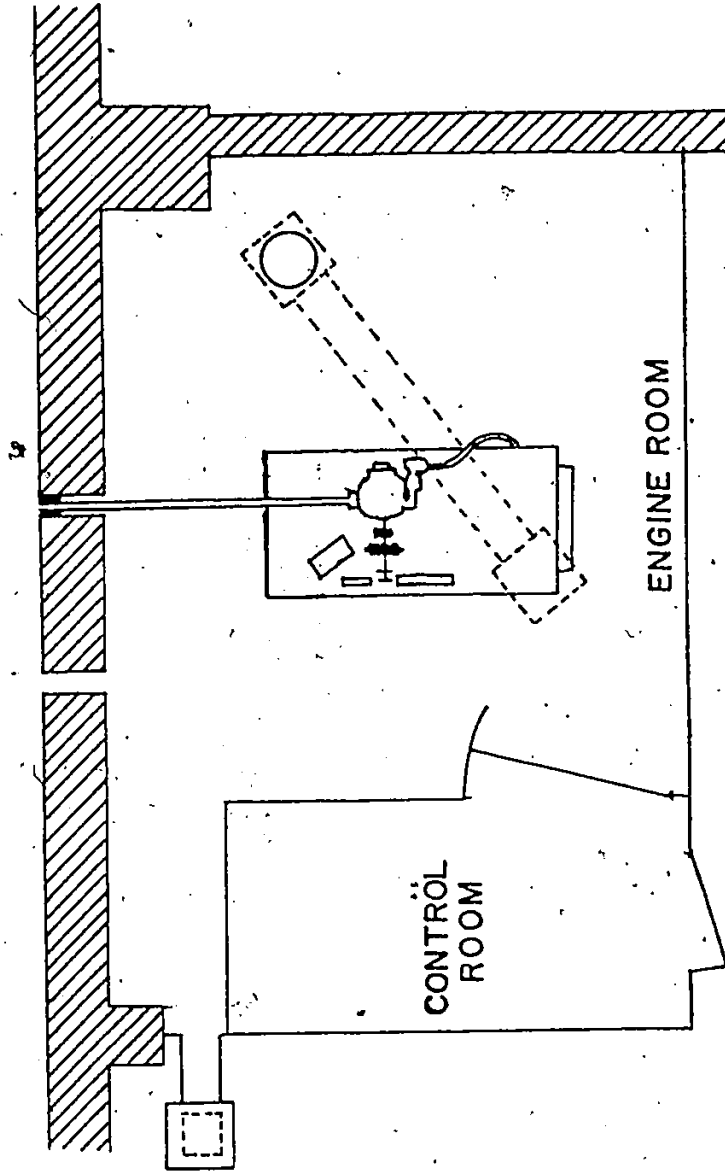


FIGURE 3. SKETCH OF ENGINE LABORATORY LAYOUT

Figure 4. Gaspar, Keith, and ...

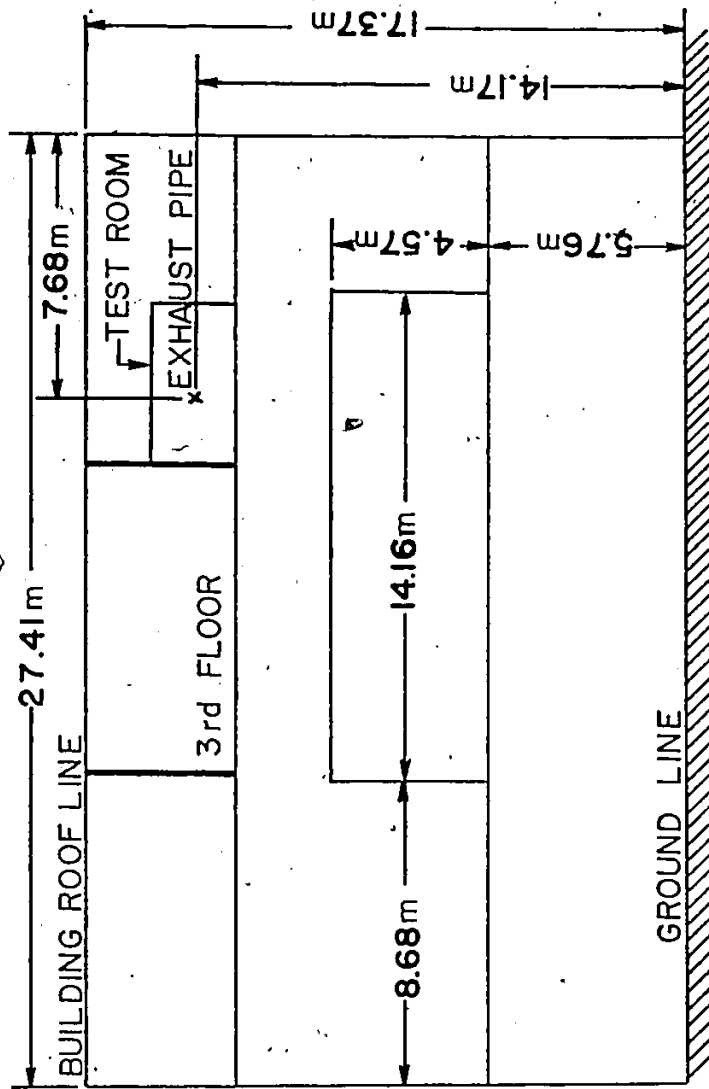


FIGURE 4. LOCATION OF ENGINE LABORATORY, WEST ELEVATION VIEW OF BUILDING

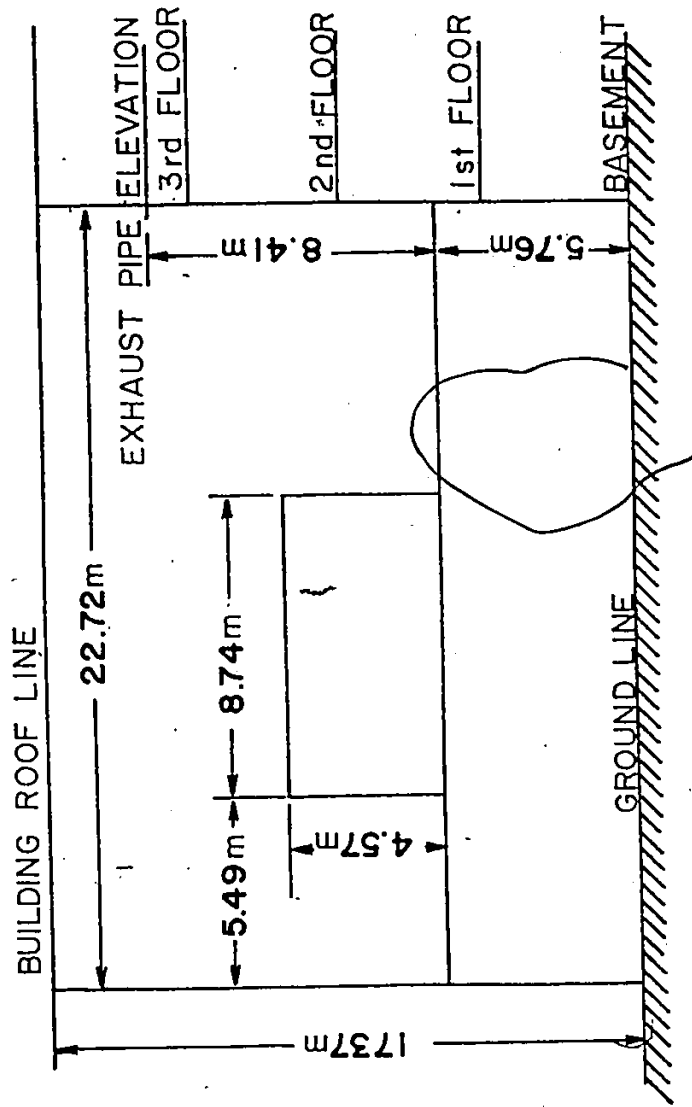


FIGURE 5. LOCATION OF ENGINE LABORATORY, NORTH ELEVATION VIEW OF BUILDING

Figure 6 - VASPI, VEIT, VIMMAR 11.00 57

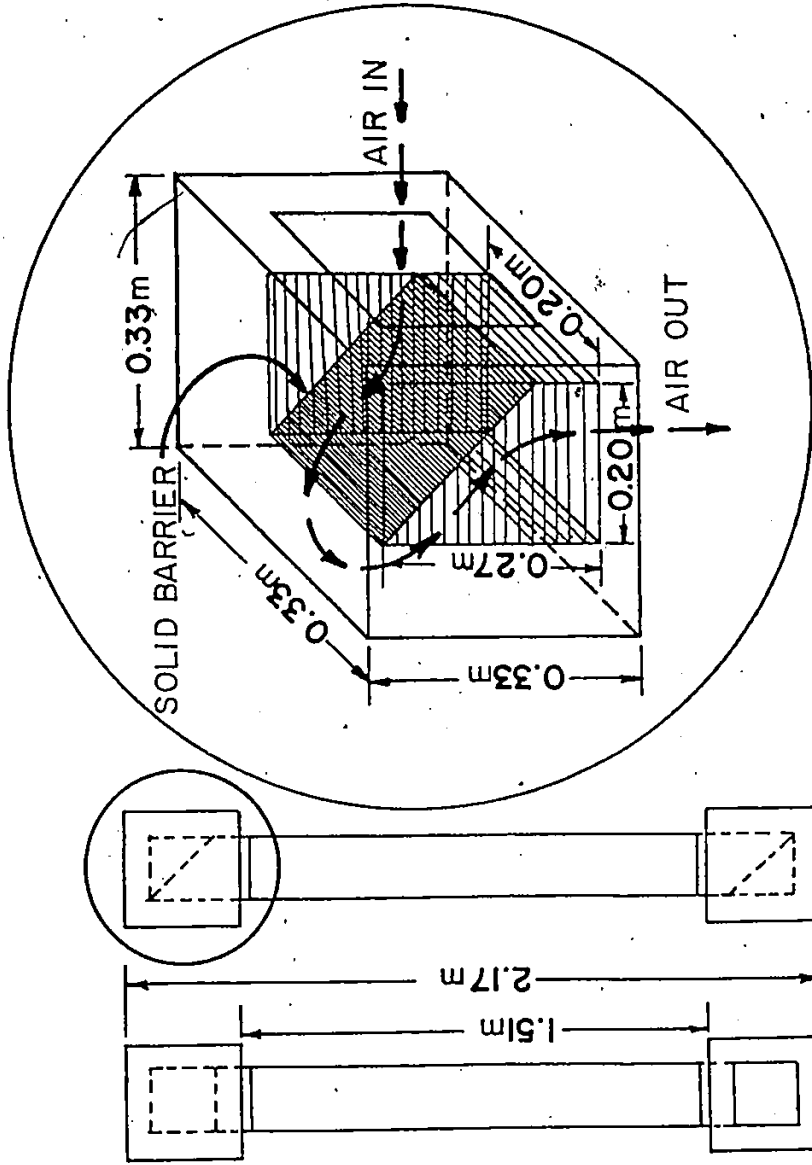


FIGURE 6. SKETCH OF LOW NOISE TRANSMISSION, VENTILATION DUCTING

arrangement was used to attenuate the engine noise transmitted to the surrounding area from the engine room through the outlet ventilation duct.

Random shaped panels of pressed fiber board were hung at various locations in the room to reduce the possibility of standing waves occurring. These panels were hung in corners to reduce directivity effects and at oblique angles to large wall surfaces. Additionally, an oval-shaped doorway was constructed in the wall separating the control room from the engine room. Weather stripping was used to seal the edge of the door against noise leakage. This was easier to do since the door had no corners.

4.2 Equipment Selection

4.2.1 Engine and Dynamometer

The engine chosen for the testing program was a Sachs-Wankel Engine, model number KM 37, manufactured by Fichtel & Sachs A.G. in the Federal Republic of Germany [111]. The specifications given for the engine were as follows:

- a. Piston displacement: 108 cc per chamber.
- b. Compression ratio: 8.5 to 1
- c. Output: 4.0 SAE HP at 3300 r.p.m.
7.6 SAE HP at 5500 r.p.m.*

* The value quoted here differs from that formerly quoted in the Introduction because the former was taken from the literature provided by Curtiss-Wright Corporation [48] who have distribution rights to the engine in North America. The value of 6.55 SAE HP quoted by Curtiss-Wright was found to be a better indication of the actual engine power rating. The engine and the dynamometer which was coupled to it had been used previously as part of an undergraduate Thermodynamics Laboratory. At the time that it was selected for the exhaust noise experiments, it was estimated

that the engine had been run for no more than forty hours. This was well short of the time limit of 1000 hours at which the manufacturer recommends that the rotor seals be replaced and the engine be given a complete overhaul.

The hydraulic dynamometer which was coupled to the engine was a Model DY-7D which was manufactured by Go-Power Systems of Palo Alto, California. The dynamometer has a maximum rating of 30 SAE HP. The dynamometer was calibrated after installation in the engine room. The calibration was performed according to the instructions supplied by the manufacturer using a calibration arm purchased for that purpose. The read-out of the load on the dynamometer was by means of a Bourdon type gauge which was liquid coupled with a load cell mounted on the dynamometer. A special silicon fluid was used to completely fill the load cell, connecting tubing and the gauge. The yoke on the load cell was clamped to a lever arm on the dynamometer such that, during a test, the product of engine speed and gauge reading when divided by 10,000 yielded the SAE HP being produced by the engine.

4.2.2 Exhaust Pipe

The standard oval muffler, supplied by the manufacturer, was removed to allow the attachment of a straight exhaust pipe. The depth of the engine casting at the exhaust port was 53.34 mm. The exhaust port on the engine was oval in shape, having a major diameter in the vertical plane of 18.16 mm and a minor diameter in the horizontal plane of 16.94 mm, at a distance of 1 cm from the outside face of the exhaust port. At its outside lip, the exhaust port was circular and had a diameter of 19 mm. Commercially available tubing was sought which had a similar inside diameter. It was felt that if any differences were present, it would be best if the inside diameter of the tubing was larger than that of the engine exhaust

port with the exception of its lip. The tubing chosen was a type 304 stainless steel with an inside diameter of 19 mm. An aluminum coupling was manufactured which would allow the exhaust pipe to be butted flush with the high temperature gasket from the original muffler installation. Thus a reasonably smooth transition from the engine to the exhaust pipe was achieved.

The exhaust pipe length was selected to provide acceptable conditions for measuring the exhaust gas behaviour while allowing the discharge of the exhaust gases through the building wall. The total length of the exhaust pipe was 157.6 cm. Provision was made for the measurement of various exhaust gas properties. This was accomplished by providing five locations where the transient exhaust gas pressure could be measured. The first such location was at a distance of 12.6 cm from the exhaust port opening. Each subsequent measuring location was 25 cm further downstream with the last measuring location being 112.6 cm from the exhaust port opening. At the closest and farthest measuring locations, provision was also made for the measurement of the mean exhaust gas temperature with the aid of shielded thermocouples. The mean exhaust gas pressure could also be measured at these two locations. The temperature measurements were made 1.8 cm downstream of the dynamic pressure measuring location. The mean exhaust gas pressure measuring location was 1.8 cm upstream of the transient exhaust gas pressure measuring location.

4.2.3 Pressure Transducers

The measurements of the transient exhaust gas pressure were made using two Model 112A23 quartz pressure transducers manufactured and calibrated by PCB Piezotronics, Inc. of Buffalo, New York. The transducers were protected from the high exhaust gas temperatures by means of two Model 64A watercooled adaptors. The transducers were powered by two Model 480A battery driven power supplies. The

power supplies were used to condition the output signal from the pressure transducers. The power supplies were passive devices. This meant that they did not affect the high frequency response of the transducers. Each transducer had an input time constant of 0.15 seconds, a rise time of 2 microseconds and a natural frequency of 250 kHz. The transducer closest to the engine (Serial No. 1080) had a calibrated average sensitivity of 53.4 mV/psi or 7.75 mV/kPa. The transducer which was mounted 1 m further downstream (Serial No. 1079) had a calibrated average sensitivity of 46.6 mV/psi or 6.76 mV/kPa.

4.2.4 Exhaust Gas Back Pressure Measurement

The exhaust gas back pressure was measured by a dual volume, capacitance coupled, liquid-in-glass, U-tube manometer. The connection to the exhaust pipe was made 1.8 cm upstream of the pressure transducer closest to the engine. As problems were encountered in the trial runs, a small heat exchanger which surrounded the copper tubing of the pressure take off was installed. This allowed the use of polyvinyl tubing for connection of the take off tubing and the primary chamber for smoothing the pressure pulse created by each chamber blow-down of the engine. A small capillary tube heat exchanger was installed inside the primary smoothing chamber. This was intended to condense the water vapour in the exhaust gas before it reached the long, polyvinyl tubing connecting the primary smoothing chamber to the secondary smoothing chamber. The secondary smoothing chamber was direct coupled to a vertical manometer (ME C26) manufactured by The Meriam Instrument Co. and containing a fluid of specific gravity 1.00. The primary smoothing chamber had a drain at the bottom through which the condensate could be removed. By using the two smoothing chambers, no oscillations of the fluid column due to exhaust pressure pulsations were ever observed.

4.2.5 Exhaust Gas Temperature Measurements

Two thermocouples were used to measure the exhaust gas temperature. These were Thermo-Electric type K, Nickel-Chromium (Cromel) versus Nickel-Aluminum (Alumel) thermocouples. The thermocouples were ungrounded, 1 mm in diameter and Inconel sheathed. The reference temperature used was a continuously stirred, distilled, ice-water bath. The stirring was provided by a Sargent Welch (S-76490) magnetic stirrer. The ice-water bath was held in a large, plastic lined, vacuum bottle, Thermos brand container. For voltage measurements, the thermocouples were connected to a Leeds & Northrup potentiometer (ME C356, Cat No. 8686) by means of a Thermovolt Instruments Ltd., thermocouple selector switch (ME C143).

4.2.6 Engine Speed Measurement

Two different methods were used to measure the engine speed. The primary method of measurement was by means of a digital tachometer constructed by the departmental electronics technician. The signal for the tachometer was generated by photosensitive transistor. The light source used was a low power laser. The laser beam was projected through four holes drilled in a small rotating drum connected to the dynamometer shaft. The four holes were equally spaced on a circumferential line such that each complete engine rotation transmitted four signal pulses to the tachometer. The time base for the tachometer was one minute. That is, the tachometer counted that number of pulses in a period of one minute and then converted that count into a corresponding rpm readout.

The secondary method used for checking the engine speed was by means of a type SA3/C, remote control, Briggs Stroboscope (ME C58). The stroboscope was

directed toward the engine flywheel. This allowed a visual check of the engine speed variations. By setting the stroboscope at a particular pulse rate consistent with the engine rpm, and noting the location of a reference notch on the flywheel, it was possible to check for large speed variations.

4.2.7 Combustion Air Flow Measurements

The combustion air flow rate was measured by means of an air intake tank. The tank had a sufficiently large volume such that pulsations of the air flow into the engine did not affect the measurement. The air flow was determined by measuring the pressure difference across a thin, square edged orifice plate mounted on one end of the intake drum. The hole in the orifice was measured to be 25.35 mm. The pressure inside the tank was measured relative to the surrounding ambient pressure by means of a T.E.M. Instruments tilting bank manometer (ME C154, No. 9645) which was set at an inclination of 12 degrees relative to the horizontal plane.

4.2.8 Fuel Flow Measurements

Fuel flow to the carburetor was measured by means of a Plint gauge. The volume indicators of the Plint gauge were calibrated for mass measurements by carefully extracting the volume samples and weighing them on a precision beam balance. The time required for a particular calibrated volume of the mixture of gasoline and oil, required by the engine, to be consumed was measured by a Model 1401 Lab Chron timer manufactured by Labline Inc.

4.2.9 Electronic Processing and Recording Equipment

The data acquisition and processing equipment was composed of a number of interconnected discrete components. The signal output from each of the pressure transducer amplifiers was simultaneously coupled to one input of a Model 1201A, Hewlett-Packard, 100 μ Volt, Dual Trace Oscilloscope and a Model 2607, Brüel & Kjær Measuring Amplifier. The dual trace oscilloscope was used for visually checking the output from each of the pressure transducers. In addition, the oscilloscope allowed photographic recording of the pressure transducer traces. Each measuring amplifier was used to condition the pressure transducer signal to a voltage high enough for suitable recording purposes. In addition, each measuring amplifier was used to provide a 50 mV r.m.s. calibration signal. This allowed the amplitudes of the pressure transducer signals to be compared with a calibrated standard amplitude.

Two Brüel & Kjær Model 4145 Microphones, each connected to a Brüel & Kjær Model 2619 Microphone Preamplifier, were used for all noise testing. This included the wall transmission loss testing as well as all engine/exhaust noise monitoring. The two microphones were connected to a Brüel & Kjær Model 2606 Measuring Amplifier by means of a Brüel & Kjær Model 4408 Microphone Selector Switch. For the wall transmission loss tests, the measuring amplifier was connected to a Brüel & Kjær Model 2307 Graphic Level Recorder.

All amplified pressure transducer signals and noise measurements were recorded on the three F.M. channels of an S.E. Labs (Eng.) Ltd., Model SE-8/4 tape recorder. The A.M. channel of the tape recorder was used for voice recording of engine operating conditions. All recordings were made on BASF low-noise recording tape. An external tape recorder monitor, constructed by the departmental electronics

technician, was used to ensure that all signals were being recorded.

4.2.10 Signal Analysis Equipment

Several different systems were used for various portions of the data processing.

4.2.10.1 System 1

The initial signal analysis was performed using a Spectral Dynamics Corporation Model SD305A Octave Converter, a Model 13116 X-Y Display, a Model SD301C Real Time Analyser and a Model SD309 Ensemble Averager. Graphical output from the system was recorded on a Hewlett-Packard Model 7054A X-Y Recorder. This analysis system was used to perform the initial Fourier analysis of the pressure transducer signals as well as the engine/exhaust noise recordings. All recordings were replayed through the tape recorder on which they were originally recorded.

4.2.10.2 System 2

As the original real time analyser system had been and was continuing to be used extensively, a point was reached at which time it could no longer be maintained in good operating condition. Therefore, it was replaced by a Scientific Atlanta, Spectral Dynamics Division Model SD375 Dynamic Analyser II. This system provided only narrow band analysis of the noise or pressure transducer signals; however, it has met the requirements for rechecking the original recorded information. The same X-Y plotter was used with this analyser. A schematic of the data acquisition system compatible with that described in sections a and b is shown in Figure 7.

Figures 4 Gaspar, Keik, Sridhar. PWD 7 68

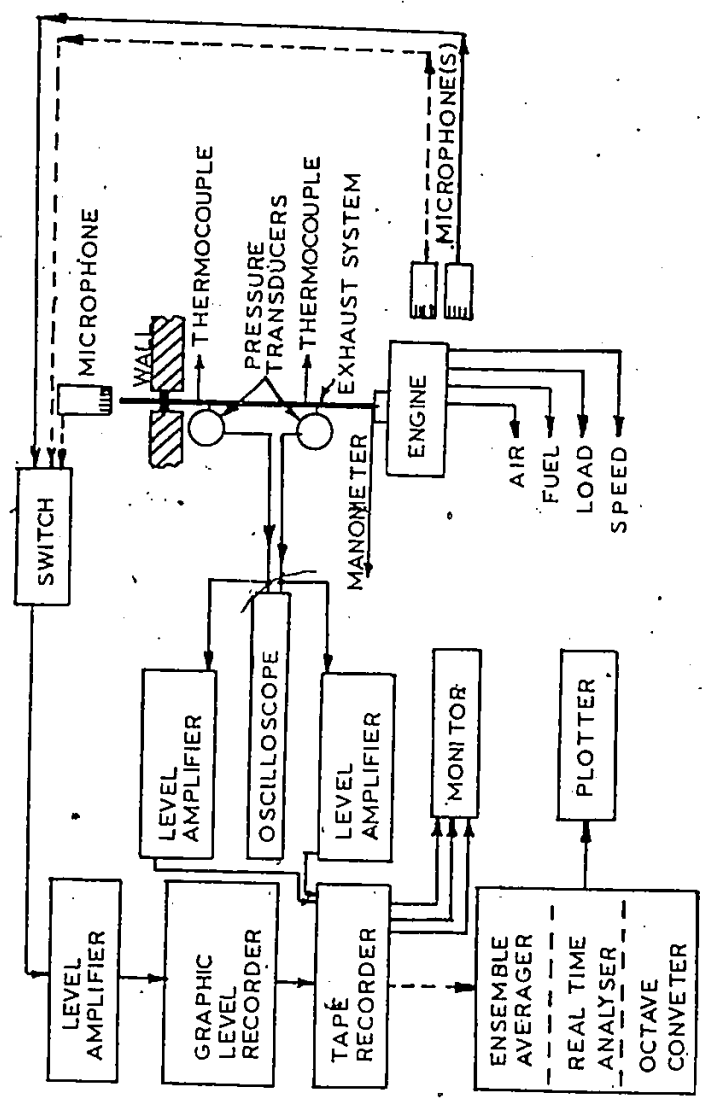


FIGURE 7. SCHEMATIC DIAGRAM OF PRIMARY DATA ACQUISITION SYSTEM

4.2.10.3 System 3

This analysis system was used to provide the first analog to digital conversion of the pressure transducer signals for comparison with the theoretical wave shape. This system consisted of a Gould Advance Model 054000/4001 Digital Storage Oscilloscope and a Fluke Model 2240B Data Logger. The pressure transducer recordings were played back into the digital storage oscilloscope. The wave pulse was stored in the oscilloscope memory. The information was then transmitted at a slow memory scanning speed through a digital to analog interface on the oscilloscope. The voltage signal output was recorded at a scanning rate of 3 samples per second by the data logger. The numerical information was printed out on a paper tape.

4.2.10.4 System 4

This system was used for all subsequent time domain analysis of the exhaust pressure pulses. The system consisted of the four channel tape recorder which was used to play back the original pressure transducer recordings into a Brüel and Kjaer Model 2607 Measuring Amplifier. The measuring amplifier was used for two different purposes depending on the desired information to be analysed. In the first case, the measuring amplifier was used to scale the peak voltage output to a value less than 5 volts peak. The signal was fed into an eight bit analog to digital conversion peripheral board of an Apple II+ computer. The computer was used for processing and analysing the waveform data. In the second case, the measuring amplifier was operated in its peak measuring mode. The output of the amplifier was directly proportional to the peak amplitude of the input signal. The calibration signal originally recorded was used to calibrate the system for the peak amplitude

measurements.

4.3 Experimental Procedure to Run a Test

The procedure for a testing sequence is:

1. Turn on all electronic equipment to allow the components to warm up for at least one hour.
2. Crush distilled water ice cubes for the thermocouple reference junction.
3. Mix the crushed ice with distilled water and place the mixture in the thermos. Turn on the stirrer and insert the thermocouple reference junction.
4. Top off the fuel tank and, if necessary, mix an additional quantity of the gasoline/oil mixture required by the engine.
5. Turn on the cooling water to all heat exchangers and make sure that the water is flowing to all equipment that is temperature critical.
6. Set the instruments for calibration and adjust all zero reference or voltage reference levels.
7. Record calibration signals on all four channels of the tape recorder.
8. Reset all instruments for general data recording.
9. Record the room temperature, barometric pressure, tape number and all instrument settings.
10. Turn on the water supply to the hydraulic dynamometer and adjust the flow to a low flow rate.

11. Fill the Plint gauge with fuel and set it for straight through flow.
12. Set the engine throttle to fast idle.
13. Purge the fuel line to the carburetor of all air and prime the carburetor before attempting to start the engine.
14. Pull start the engine and allow it to idle until it has warmed up.
15. Set the engine speed and torque applied by the dynamometer by adjusting the throttle and flow control valve to the dynamometer.
16. Wait for the engine conditions to stabilize. Check this by monitoring the exhaust gas thermocouple readouts and the engine speed tachometer.
17. Switch the Plint gauge to its flow measuring setting and start the fuel flow timer when the fuel level in the gauge passes the appropriate level marker.
18. Start the tape recorder and check the monitor output for an indication that the tape recorder is operating correctly. Record the test number and engine information on the voice channel. Check the Plint gauge condition and halt the fuel flow timer when the fuel level passes an appropriate level marker. When this happens, switch the Plint gauge back to the through flow setting.
19. Record the manometer differential pressure for the air flow, the initial and final tape count, the exhaust pipe thermocouple readings, the engine speed from the tachometer, the dynamometer torque, the amount of fuel consumed and the time required for its consumption.

- 20a. If testing is to continue, refill the Flint gauge, change the engine speed and the dynamometer torque for another test or:
- 20b. If the test sequence is completed, halt the fuel flow to the Flint gauge, idle the engine back to consume the fuel remaining in the Flint gauge while lowering the water flow to the dynamometer to unload the engine. Then shut down all the instrumentation.

V. DATA PROCESSING

The advent of the 'mini-computer' or personal computer has had considerable influence on the acquisition and analysis of experimental data. The procedures which were previously available either made use of expensive, very specialized equipment, if they were financially allowable, or were slow and cumbersome such as the data acquisition method described in Section 4.2.10.3, System 3. Both of these have been somewhat supplanted by computers such as the Apple II+. This class of computers has the capability of being specially configured by the addition of plug in peripheral boards. This was the situation as previously described in Section 4.2.10.4, System 4; however, the procedure was not simply composed of making a few electrical connections and then pushing a button on the computer keyboard. Four major programs were written to provide the data for correlation with the mathematical model described in Chapter III.

5.1 The Sampling Program

The first of the programs in the data processing sequence was the one used for converting the analog pressure signal into discrete time based digital measurements. The sampling program made use of three machine language routines to perform the analog to digital sampling and the preliminary analysis of the digital data. These programs have been listed in Appendix I. The main sampling program has been identified by the name KLAATU; while the three machine language routines have been identified by the names BIGSAMPLE, MAXGR and ADD7\$345.

When the program was run, the following sequence of events occurred:

1. The machine language routines were loaded into a memory area which was not used by Applesoft.
2. The upper limit of Applesoft memory was set below the first page of high resolution graphics so that this area could be used for viewing the waveform which had been sampled. This severely limited the length of the main program and was the reason that two other programs were required to preprocess the data.
3. The 22,016 bytes of computer memory above the first page of high resolution graphics were set aside for the storage of data output from the analog to digital converter.
4. Information and control was transferred to the sampling routine BIGSAMPLE which controlled the operation of the analog to digital converter.
5. The routine MAXGR was used to check that the greatest wave amplitude present did not occur so close to either end of memory such that the entire pressure pulse was not present. If there was such a problem, the sampling was automatically repeated.
6. The routine ADD7\$345 was used to find the average of all values sampled. This was to insure that a significant voltage offset was not present in the original analog signal.
7. The program then displayed the waveform of the maximum pressure pulse and subsequently, each pressure pulse waveform available in memory. These waveforms were saved as numerical data for reprocessing in the subsequent program.

As the analog to digital conversion was an important portion of the operation, its details should be discussed.

As mentioned previously, the machine language routine BIGSAMPLE was responsible for the analog to digital conversion. To perform this function, it made use of the Mountain Computer Inc. 8 bit analog to digital/digital to analog peripheral board. The procedure that the board employed for the analog to digital conversion process was the method of successive approximations. That is, the analog signal voltage is compared with a digitally created voltage signal which is proportional to the number of bits turned on in the binary signal. If all 8 bits of the signal are turned off (zero), the digital voltage signal which would be generated would be -5.0 volts. If all 8 bits are turned on, (representative of the decimal value 255) the digital voltage signal which would be generated would be +5.0 volts.

The voltage range between -5.0 and +5.0 volts can be divided into 256 incremental values. This corresponds to voltage steps of approximately 39 millivolts. The analog to digital conversion is started by the converter turning on the high order bit (bit 7, representing $1 \times 2^7 = 128$). This produced a comparison voltage of zero volts. The analog signal was compared with this voltage and if the analog voltage was higher than this value the comparison continued by turning on bit 6. If the analog voltage was less than the generated value, bit 7 was turned off and the comparison continued by turning on bit 6. This procedure continued until all 8 bits had been switched on or off. The analog to digital conversion board then outputted this 8 bit approximation of the analog voltage onto the data bus where it was transmitted to the microprocessor chip or CPU of the computer. The CPU was instructed by the machine language routine as to where this data was to be stored. It should be noted that the conversion and transmission process occurs in approximately 9 microseconds. However, approximately 10 microseconds were required

by the machine language routine to run the CPU through the complete sampling instruction set.

The second version of the sampling program which has been identified by the name KLAATU.DC is similar in performance to KLAATU. The difference between the two programs is that KLAATU.DC was used to determine the maximum and average values of the peak acoustic pressure. These values were computed relative to a measurement made from a calibration signal of known amplitude. As the values being sampled were all direct current voltages, the processing of the data was greatly simplified.

5.2 The Configuration Program

The second program which was used in the data processing has been listed in Appendix II. This program has been identified by the name BARADA and it was used to select the portion of the waveform data, associated with the pressure pulse, which was equal to or greater than the average of all the data in the sample. This criterion was used because of the mode of operation of the piezoelectric pressure transducers used for the analog sampling. These transducers were designed for the purpose of transient pressure measurement. As such, they can not be used for static pressure measurements. This limitation occurs because any static load applied to the transducer would cause the piezoelectric crystal to be deformed by a fixed amount which, in turn, would cause a proportional instantaneous voltage to appear across the loaded faces of the crystal. The presence of the circuit which monitors this voltage also allows the charge equalization between the two loaded faces of the crystal. Therefore, after a period of time which is dependent on the circuit design, there would no longer be a voltage difference across the loaded faces. The circuitry has been set up such that the time constant for this discharge is long with respect

to the time in which the transient pressure changes would occur. The consequence of this design is the fact that, during the initial application of the pressure signal to the transducers, there is a signal drift until the transducer output is operating about a mean reference zero. This reference zero for the transducer is equivalent to the mean of the dynamic pressure measured. Consequently, the average digital value represents the mean or reference zero gauge value of the exhaust pressure.

When the program was run, the following sequence of events occurred:

1. The program called for information concerning the data stored on the data diskette by the previous program KLAATU.
2. The program then read in each data file on an individual waveform basis. The first data read was concerned with the location in the data array of the maximum value, the first positive value and the position of the minimum value. In addition, the magnitude of the maximum of all amplitudes measured, the local maximum in the present data, the data average and the local minimum were input. This data was saved originally for scaling purposes.
3. The waveform data was read into the computer and plotted on page one of the high resolution graphics screen.
4. Starting at the first zero reference crossing, a search was conducted along the positive portion of the waveform to determine the point at which the waveform again crossed the reference zero value. This identified the extent of the positive portion of the exhaust pressure pulse.
5. A linear interpolation was performed to calculate a time delay correction factor for the first positive data point

in the pulse waveform. That is, a straight line was drawn between the last negative data point and the first positive data point. By knowing the magnitude of the data average, it was possible to calculate a sampling time correction factor between when the analog wave was equal to the mean or local static pressure and when the first positive digital data point was measured.

6. All negative data points were discarded and the positive waveform was saved under a numerically indexed work file on another data diskette.

It must be noted that this program could not be incorporated into the first program KLAATU as there was insufficient memory available for the program allocation as well as the necessary data arrays. The program BARADA could not be incorporated into the next program for similar reasons.

5.3 The Concatenation Program

This program which has been identified by the name NICTO was used to rearrange the data from the work files created by the previous program. To accomplish this as quickly as possible, a machine language program identified by the name MERGE was implemented. These programs have been listed in Appendix III. This auxiliary program was necessary as it reduced the complexity of the final program which was used for the correlation of the data. The present program accomplished this reduction in complexity by reorganizing the waveform data from separate waveforms into a single waveform. This waveform had all the original data points but they were assembled against increasing time. That is, the first cluster of data points would contain the first positive data point from each of the individual waveforms. The next cluster of data points would contain the second positive data point from each of the individual waveforms, etc. When the program was run, the following sequence of events occurred:

1. Applesoft high memory was set to the bottom of the first page of the high resolution graphics memory.
2. The initial data in each of the files was read into the computer. This included the sampling time correction factor and the length of each waveform data set.
3. The values of the sampling time correction factor were organized in ascending magnitude and the data set that each occurred in was recorded in a new data pointer array.
4. The length of the shortest data file was determined. This was done to simplify the concatenation. If it had not been done, the last positive data points would have caused problems during the merging operation.
5. The machine language program MERGE was loaded into a portion of computer memory which would not interfere with the main program or the memory set aside for data storage.
6. Each data file was read into a single page of 256 bytes of computer memory (each byte holds 8 bits of binary information) according to the new array file pointer. That is, although the original data files were stored in sequential order, they were now read into the computer according to their ascending magnitude of sampling time correction factor.
7. After the data storage was completed, the above mentioned machine language program was called. The function of this program was the sequential transfer of data from a specified location on each page of memory to a single page of memory, elsewhere in the computer memory, in an ascending order.

8. After the transfer was completed, the data was read from the new location in memory. It was then converted to a floating point value between zero and one by nondimensionalizing the data. Finally, the data was stored on a data diskette. The first value stored in each data file was the length of the file.
9. The final function of the program was to store the sampling time correction factors in ascending order of magnitude in a final diskette file.

It should be noted that, with this procedure, it would be possible to process a maximum of 59 individual waveforms with the available computer memory.

5.4 The Correlation Program

The final program in the series has been listed in Appendix IV. This correlation program has two components which are identified by the names BARANGA1 and BARANGA2. In actual fact, they are the first and second sections of a single program which, because of its length, can not be loaded into the computer at the same time. The program incorporates the generation of the factors for the theoretical waveform as well as a special method of correlating the data with the model. The program incorporates a number of features which include:

1. A fast correlation format which allows a quick calculation of trial values of the correlation variables.
2. The choice of the number of correlation variables to be used.
3. The storage of the complete data on which the correlation is based.
4. The storage of the data set describing the correlation line after the processing has been completed.

The correlation procedure that was used is based on an approximate solution suggested by Wylie [130]. He recognized the fact that it is not possible to linearize some general systems of nonlinear equations. Wylie suggested that one alternative would be to proceed as follows:

Let the equations to be approximately satisfied be:

$$g_1(z, f) = 0, g_2(z, f) = 0, \dots, g_n(z, f) = 0 \quad \text{Eqn. 76}$$

If the correlation is near perfect, then an approximate solution to the system of equations would be (z_0, f_0) . Then each function $g_i(z, f)$ can be expanded in a generalized Taylor's series about the point (z_0, f_0) . Then, if the series is truncated at the first order term, the result is:

$$g_i(z, f) = g_i(z_0, f_0) + \left. \frac{\partial g_i}{\partial z} \right|_{z_0, f_0} (z - z_0) + \left. \frac{\partial g_i}{\partial f} \right|_{z_0, f_0} (f - f_0) \quad \text{Eqn. 77}$$

as long as the differences $(z - z_0)$ and $(f - f_0)$ are small. If this is the case, then Equation 77 is linear in the unknown conditions $(z - z_0)$ and $(f - f_0)$. The application of this result can be appreciated by considering the procedure for curve fitting.

To obtain the curve of best fit, it is necessary to minimize the variance between the value measured and the value which is predicted by the correlation equation. If x_i is the i th measured and μ_i is the i th value predicted by the correlation equation, then:

$$\text{variance} = (1/N) \sum_{i=0}^N (x_i - \mu_i)^2$$

where N is the number of measurements performed. To find the minimum variance, it is necessary to take the derivative of the variance with respect to the value predicted by the correlation equation. Thus:

$$d(\text{variance})/d\mu_i = (1/N) \sum_{i=0}^N d(x_i - \mu_i)^2/d\mu_i \quad \text{Eqn. 78}$$

and

$$(1/N) \sum_{i=0}^N d(x_i - \mu_i)^2/d\mu_i = 0 \quad \text{Eqn. 79}$$

or

$$\sum_{i=0}^N d(x_i - \mu_i) = 0 \quad \text{Eqn. 80}$$

To minimize the variance, it is necessary to select the correlation equation such that the sum of the differences between the actual readings and the model, which is the correlation equation, are zero (the line of best fit). If $g_i(z, f)$ is the value of the i th term of the function which minimizes the variance, then all that is necessary is to determine the differences of $(z - z_0)$ and $(f - f_0)$ to achieve a solution. If $\partial g_i/\partial z$ is represented by z_i' and $\partial g_i/\partial f$ is represented by f_i' , then the i th term could be written as:

$$x_i - g_i(z, f) - z_i'(z - z_0) - f_i'(f - f_0) = 0 \quad \text{Eqn. 81}$$

or

$$x_i - \mu_i - z_i'(z - z_0) - f_i'(f - f_0) = 0 \quad \text{Eqn. 82}$$

for a perfect correlation:

What is required is the knowledge of the values of z and f which will make this true for the summation. To do this, an approximation must be used since, in the real case, it would not be likely that the variance could be minimized to zero. One method of solving this problem is to multiply the above equation separately by z_i' and f_i' to produce two equations. These can be written as:

$$(z_i')^2(z - z_0) + z_i'f_i'(f - f_0) = z_i'(x_i - g_i(z, f)) \quad \text{Eqn. 83}$$

and

$$z_i' f_i' (z - z_0) + (f_i')^2 (f - f_0) = f_i' (x_i - g_i(z, f)) \quad \text{Eqn. 84}$$

Summing for all N data points yields:

$$\begin{aligned} (z - z_0) \sum_{i=0}^N (z_i')^2 + (f - f_0) \sum_{i=0}^N (z_i' f_i') \\ = \sum_{i=0}^N [z_i' (x_i - g_i(z, f))] \end{aligned} \quad \text{Eqn. 85}$$

and

$$\begin{aligned} (z - z_0) \sum_{i=0}^N (z_i' f_i') + (f - f_0) \sum_{i=0}^N (f_i')^2 \\ = \sum_{i=0}^N [f_i' (x_i - g_i(z, f))] \end{aligned} \quad \text{Eqn. 86}$$

Let

$$A11 = \sum_{i=0}^N (z_i')^2 \quad \text{Eqn. 87}$$

$$A12 = A21 = \sum_{i=0}^N (z_i' f_i') \quad \text{Eqn. 88}$$

$$A22 = \sum_{i=0}^N (f_i')^2 \quad \text{Eqn. 89}$$

$$B1 = \sum_{i=0}^N [z_i' (x_i - g_i(z, f))] \quad \text{Eqn. 90}$$

$$B2 = \sum_{i=0}^N [f_i' (x_i - g_i(z, f))] \quad \text{Eqn. 91}$$

Then

$$A11 * (z - z_0) + A12 * (f - f_0) = B1 \quad \text{Eqn. 92}$$

and

$$A21 * (z - z_0) + A22 * (f - f_0) = B2 \quad \text{Eqn. 93}$$

Finally, the unknown differences can be solved for by using the method of determinants for two equations in two unknowns:

$$(z - z_0) = (B1*A22 - B2*A12)/(A11*A22 - A21*A12) \quad \text{Eqn. 94}$$

and

$$(f - f_0) = (B1*A12 - B2*A11)/(A11*A22 - A21*A12) \quad \text{Eqn. 95}$$

Because the choice of z_0 and f_0 is somewhat arbitrary and the summations do not exactly go to zero, it is necessary to iterate the differences to a solution. That is, the differences $(z - z_0)$ and $(f - f_0)$ are solved for and since both z_0 and f_0 are known, the values of z and f can be determined. These values may then be substituted for the original values of z_0 and f_0 and the process can then be repeated with the new values being substituted into the function $g_1(z_0, f_0)_{\text{new}}$. Several methods are possible for determining when the curve of best fit has been reached. One possibility would be to monitor the sum of the squared error to see how fast it is decreasing since the amount of reduction from one iteration to the next would decrease as the correlation approached its best fit. The drawback to this method is the fact that, for a large number of data points, the decrease may not be smoothly continuous. It has been observed that minor increases in the sum of the squared error occasionally occur from one iteration to the next.

Another method that can be used is to observe the relative change of the variables. That is, if $(z - z_0)/z_0$ and $(f - f_0)/f_0$ are less than a specified value, the iteration is stopped. As there is a possibility of selecting starting values of z_0 and f_0 which would cause divergence, a check on a rapidly increasing sum of the squared error or increasing variance should be made. In addition, there is the previously mentioned possibility of a temporary increase in error from one iteration to the next which must be accommodated. This can be handled by allowing a 5 percent

increase in the sum of the squared error or a similar increase in the variance. A comparison of values from one iteration to the next can be made and if the increase is greater than 5 percent, divergence can be assumed to have started.

In the case of the program BARANGA, the second procedure was used. Additionally, three variables were set up for the iterative correlation. They were the peak acoustic pressure P_D , the distortion coefficient z and the pseudofrequency of the wave f . The only complication that this made was the necessity of generating three equations for the three differences. This necessitated the calculation of 12 coefficients which were similar to the six coefficients shown in Equations 87 to 91. As certain factors were common in each linear equation, the equation was simplified before its conversion into Applesoft Basic program lines. This assisted in the reduction of the calculation time. Since P_{AC} of Equation 74 was being correlated with the experimental data, it was necessary to take the derivative of this function with respect to P_D , z and f , noting that $\omega = 2\pi f$. In the case of the z derivative, this produced Bessel functions of order $n+1$, n and $n-1$. This would have required the generation of three different sets of Bessel function coefficients; however, this was simplified by making use of recurrence relations presented by Olver [100]. As a result, only two sets of Bessel function coefficients had to be calculated.

Another special feature of the program was concerned with the limitation of the available data storage. The largest set of values for data from the sampled waveform and its corresponding sample time was limited to 2501 pairs of values. This was not only dependent on the available computer memory but also the fact that the program was excessively slow when it was run in the Applesoft Basic Language. The time required for one iteration of calculations on 2501 pairs of data was approximately 5 hours. When this was discovered, a search was undertaken to improve the calculation speed. This included rewriting the Bessel function generator routine

as well as reducing the number of program lines as much as possible. This had little effect on the computation time. Discussion with others [59] who were aware of what was available in computer software resulted in the purchase of The Applesoft Compiler (TASC).

TASC is a software routine which is capable of converting an Applesoft Basic program into pseudomachine language which is then run on the computer in conjunction with a library program which acts as a program manager. The library occupies approximately 2048 bytes of computer memory which was another memory limit imposed on the amount of memory available for experimental data. In fact, it was necessary to break the correlation program into the two components mentioned previously. This allowed the maintenance of a reasonably sized memory area for data. By using TASC, the execution time for one iteration of the data was reduced to 2½ hours. The time usually required to obtain coefficients from one experimental data set was from 7½ to 10 hours.

One final speedup was accomplished with the program. In March of 1983, a peripheral board was purchased which improved the processing speed by approximately a factor of 5. The board is made by ALF Products Inc. of Denver Colorado. The board utilizes an 8088 microprocessor for high speed calculations and it can be run in conjunction with TASC. The only additional requirement of this board is that a 16k memory expansion card must be available in peripheral slot 0 of the computer. When the card is addressed, it transfers the Applesoft Basic Language instruction set from the computer's Read Only Memory (ROM) to the memory card. The vectors which point to each of the arithmetic operations such as addition, subtraction, multiplication and division are altered so that they point to a faster instruction set co-resident with the 8088. Since the 8088 is a 16 bit processor and since it runs approximately 5 times faster than the Apple 8 bit, 6502 CPU, there is a considerable

increase in computation speed. The 16 bit operation is significant because an arithmetic operation involving 16 bit numbers requires less execution time than that of an equivalent 8 bit arithmetic operation which performs the same function.

The final feature of the program was required because of the amount of experimental data available. When data from the high speed engine tests was processed, it was found that more data points existed in the concatenated waveform than that which could be stored in the data arrays. If the entire waveform was not sampled, it was anticipated that erroneous coefficients could be calculated. The procedure which was implemented to circumvent this made use of the computers resident random number generator function. As the program could calculate the total number of data points available from the data diskette by reading the first data file; it could determine if a random data selection routine should be implemented. If this was the case, the program calculated the percentage of data points which should be rejected to achieve a representative sample from the entire waveform. This was made quite easy as the random number function returned decimal values equal to or greater than zero but less than one. As the percentage rejection could be converted to a decimal value, each data point could be considered for acceptance or rejection on the basis of the magnitude of the random number generated for that set of data. Since there were a large number of data files present, a check was made on the cumulative percentage rejection. This allowed the program to correct for previously rejecting too many data points or conversely not rejecting enough by altering the rejection criteria. The efficacy of this procedure was checked by determining the percentage of data points at the end of the waveform which were not considered for rejection because all 2501 array elements had already been filled.

When the program was run, the following sequence of events occurred.

1. The 8088 processor card was activated.
2. The TASC RUNTIME library was BLOADED into the computer.
3. The compiled version of BARANGA1 was BRUN. The operation caused the program to be loaded as well as automatically starting it.
4. The program called for instructions on which processing style was to be conducted. That is, whether the processing was done quickly on a very small sample of the data to generate a rough set of trial coefficients, or whether the complete data set was to be used.
5. The seed number for the random number process was extracted.
6. The program called for instructions as to how many coefficients were to be computed. The initial values for the appropriate variables were requested as well as the relative error for determining the end of the iterative process.
7. The name and number of data files was called for.
8. The data file containing the sampling time correction factors was read.
9. The remaining data files were read into memory. When the first file was read, the program automatically checked to see if more data was available than that which could be stored. If this was the case, the random rejection routine was implemented, otherwise the program ignored these steps.
10. The corresponding sample times were calculated.

11. The data set to be used for the correlation was transferred to a data diskette in a format compatible with a curve plotting program.
12. The TASC chaining utility was primed which saved the common variables to be transferred from BARANGA1 to BARANGA2.
13. BARANGA2 was BRUN. This caused the program to be loaded and to automatically start execution.
14. The Bessel function coefficients were calculated and the Bessel function of order n and $n+1$ were calculated for the trial value of the distortion coefficient. A check was also made on the limit of the value of the distortion coefficient.
15. All storage variables were initialized to zero and the special conditions were implemented if the distortion coefficient happened to be zero.
16. The general function and its derivatives were calculated for a particular sampling time. The correlation and matrix coefficients were accumulated in their respective variables. The program then looped back to perform the calculations on the next data pair until all the data had been processed.
17. The coefficient differences and the variance were calculated. If there was an unacceptable increase in the variance, the process was stopped; otherwise, checks were made on the relative change in each of the difference coefficients.
18. If the relative change was too large, the new values of the coefficients were substituted and the calculation procedure was repeated. If the changes were small enough, the correlation coefficient and other statistical data was

calculated and recorded.

19. When the correlation was completed, a flag was set and the program looped back to calculate data pairs which defined the curve of best fit. This data was then recorded in a format consistent with that required by a curve plotting program.
20. BARANGA1 was reloaded after all common variables were cleared. This readied the program to receive the next data for correlation.

This represents the completion of the data processing sequence. Samples of the output from this program have been included in Appendix V.

VI. RESULTS

All of the information gathered from the tests conducted with the rotary engine have been collected and organized for presentation in this chapter. The information presented covers the acoustic tests of the engine room, the engine performance tests, the measurements of properties relevant to the testing of the nonlinear pressure pulse model, the results of the pressure pulse correlation and the conditions predicted by the application of that model. The raw data, for the engine tests, and an uncertainty analysis has been included in Appendix VI.

6.1 Room Acoustic Tests

When the construction of the engine laboratory was completed, testing was performed to determine the wall transmission loss according procedures suggested by Brüel & Kjær [13]. Measurements were made of the ambient, interior, engine room noise level at the standard, $\frac{1}{3}$ octave centre frequencies as shown in Figure 8. It is apparent from an inspection of the information provided by Figure 8 that the noise spectrum has higher levels at the very low frequencies but that the background level drops quickly to a much lower level at frequencies above 200 Hz. As the ambient levels in the range above 200 Hz were in the 20–30 dB range, higher sound pressure levels were not expected to exist above 1 kHz. This is because the effect of energy dissipation at higher frequencies begins to predominate and the background levels are further reduced.

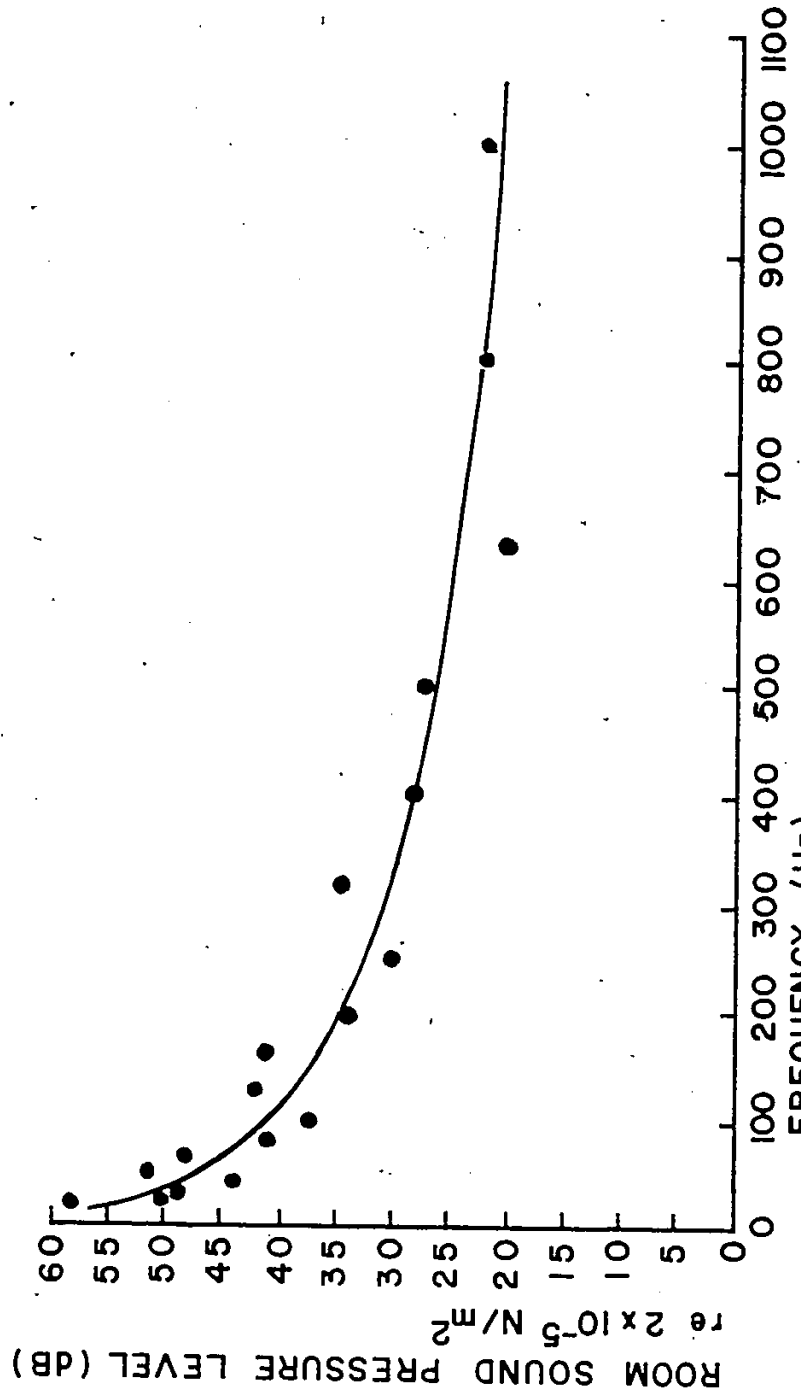


FIGURE 8. GRAPH OF ENGINE ROOM, AMBIENT, INTERIOR SOUND LEVEL VERSUS FREQUENCY

The results of the ambient level testing were used to determine the minimum sound pressure levels required for a meaningful test of the wall transmission loss. Since the transmission losses for a simple wall construction are bidirectional, the engine room was used as the receiving room for the transmission loss testing. The exterior laboratory space was used as the site of the noise source for the testing procedure. During the transmission loss testing, the exterior sound pressure levels used were high enough to ensure that the sound pressure level, measured in the engine room, was at least 10 dB higher than the previously measured ambient level. The measured wall transmission loss for the engine room is presented in Figure 9. It can be seen that, at frequencies above 250 Hz, the wall transmission loss exceeds 25 dB. Although the transmission loss was small in the frequency range below 250 Hz, there was no need to be worried about possible noise complaints from persons using the remainder of the laboratory space. This is because of the decreased sensitivity to noise of the human ear at frequencies below 250 Hz.

6.2 Engine Performance Tests

During the engine testing, all critical operating conditions such as engine speed, load and exhaust gas temperature were monitored. These conditions were used to determine when the engine had reached a steady state operating condition after the engine speed and load had been changed. At that time all operating conditions were recorded. This included the measurements which were required to test the nonlinear pressure pulse model. The information pertaining to the engine load, speed and fuel consumption was processed and plotted to determine the engine power, fuel consumption and brake specific fuel consumption as a function of engine speed.

The results of the engine power versus speed tests, shown in Figure 10, exhibits a performance trend similar to that quoted by Curtiss-Wright Corporation [48]; a

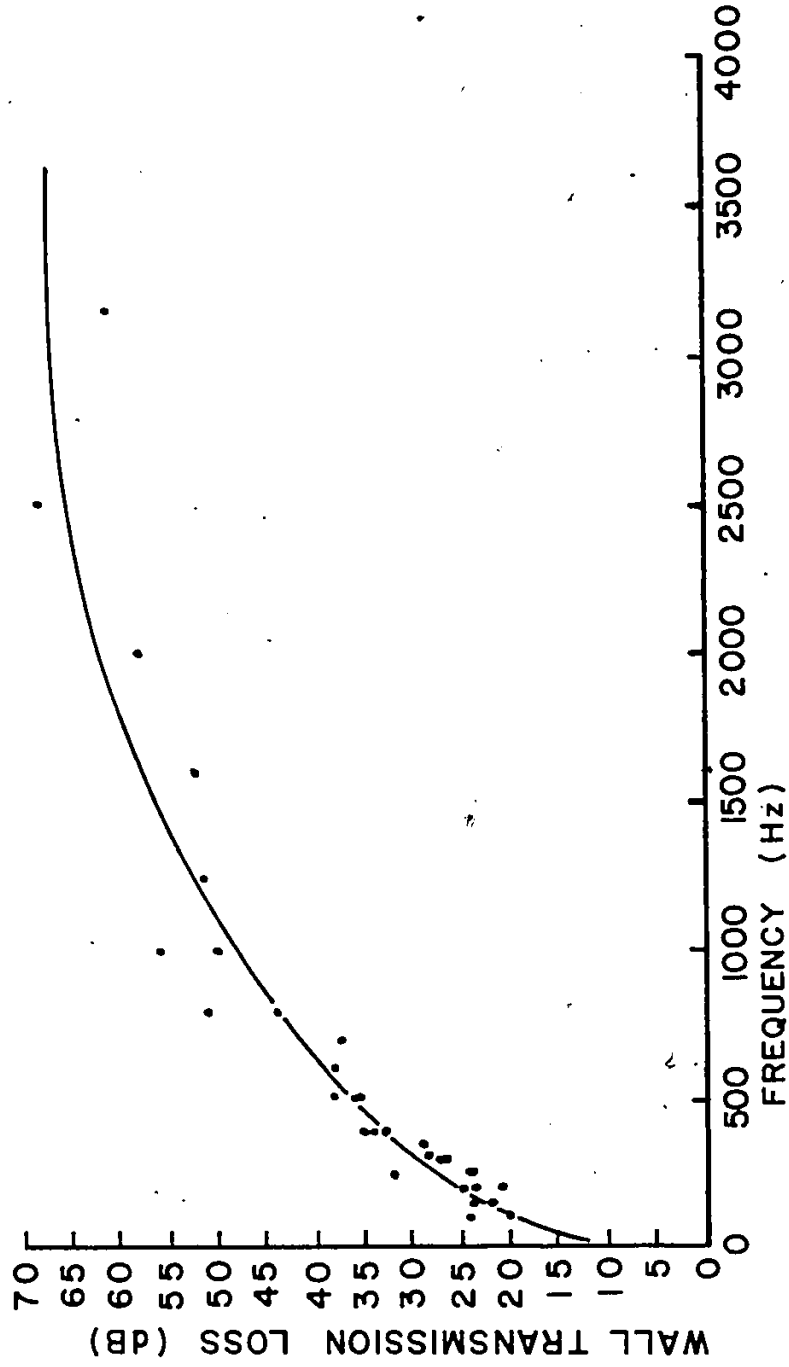


FIGURE 9. GRAPH OF ENGINE ROOM, WALL TRANSMISSION LOSS VERSUS FREQUENCY

1-1

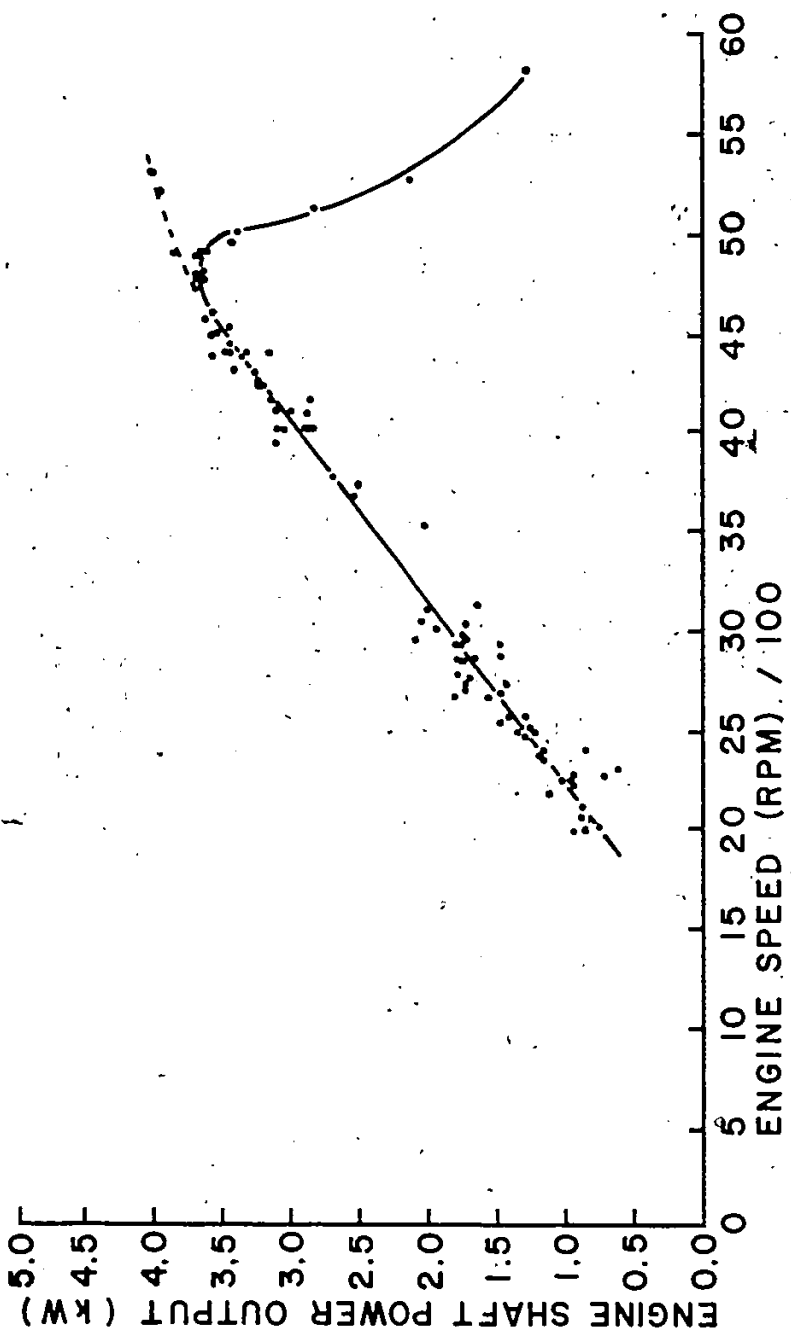


FIGURE 10. GRAPH OF ENGINE SHAFT POWER OUTPUT, AT CONSTANT TORQUE, VERSUS ENGINE SPEED

copy of this information has been provided in Appendix VII. The solid curve in Figure 10 follows the measured engine performance whereas the dashed curve, at the upper right of the figure, illustrates the expected performance if the trend predicted by Curtiss-Wright is included. A possible explanation of the differences is that the predicted trend is for an engine with a stock muffler attached and the results shown in Figure 10 are for the 157.6 cm, straight exhaust pipe attached to the engine. It is also important to note that the power output measured during testing was much less than the power output quoted by Curtiss-Wright Corporation. The variation can only be measured approximately because of the coarse scale of power versus engine speed used by Curtiss-Wright; however, the estimated percent reduction in the measured engine power output ranges from 62% at 2000 rpm to 83% at 4500 rpm. Other probable causes of the deviation of the engine performance, at high speeds, will be discussed when the information on the exhaust gas behaviour is presented.

The measured fuel consumption versus engine speed, shown in Figure 11, is a linear function of the engine speed as shown by the correlation line. Figure 12 illustrates the trend in the data associated with the brake specific fuel consumption when plotted against engine speed. The trend in the data appears to be linear but it is also evident that there is much more scatter present in this figure when it is compared to the previous two figures. This is due to the fact that this figure is the result of dividing the fuel consumption by the engine power at each engine speed. Since there is some scatter in the original data, it is magnified when the information is combined. Another notable feature of this graph is the actual trend in the data itself.

The trend for brake specific fuel consumption shown on the Curtiss-Wright Corporation data sheet (see Appendix VII) bears little similarity to the brake specific fuel consumption measured. However, this difference does not mean that any error

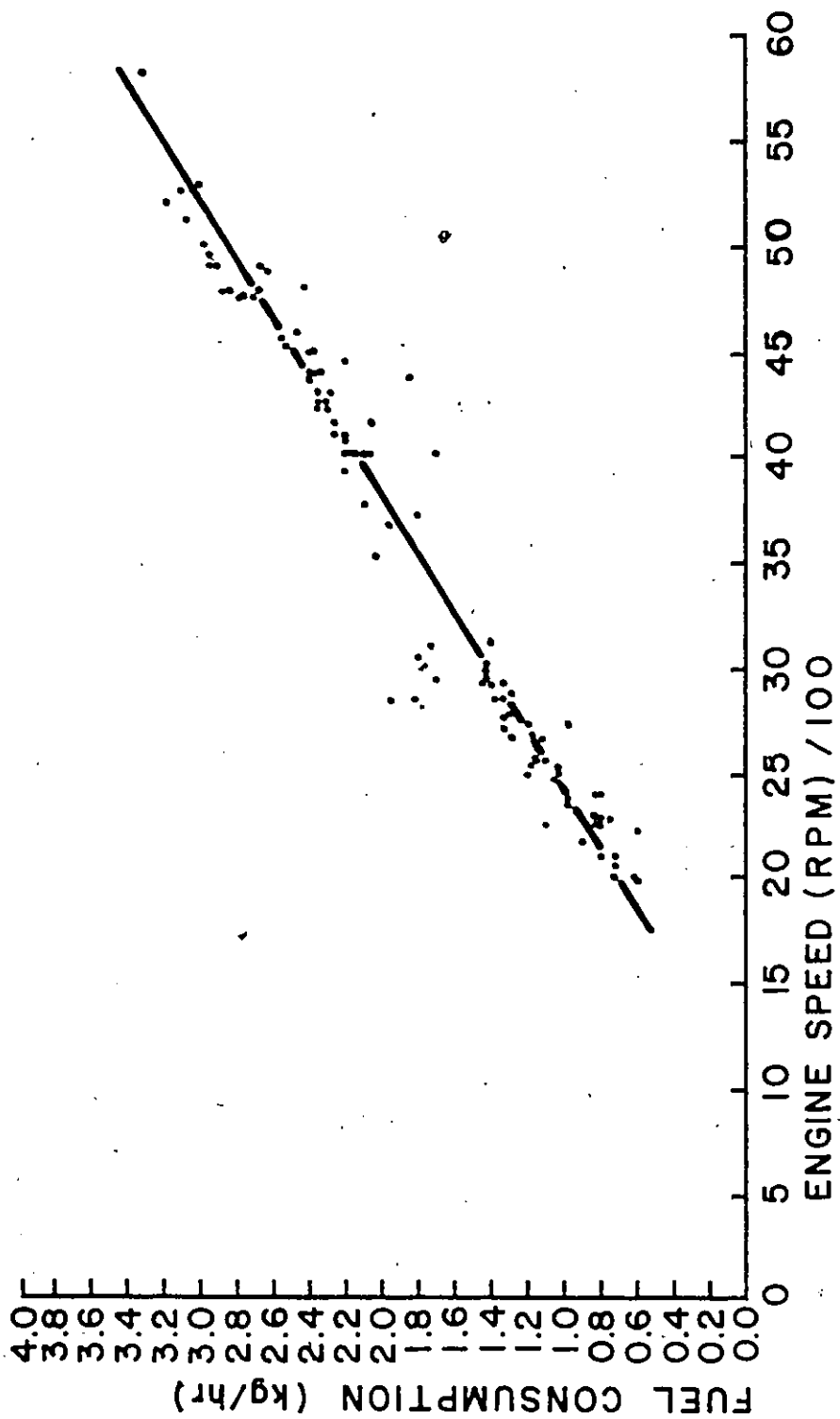


FIGURE 11. GRAPH OF ENGINE FUEL CONSUMPTION, AT CONSTANT TORQUE, VERSUS ENGINE SPEED

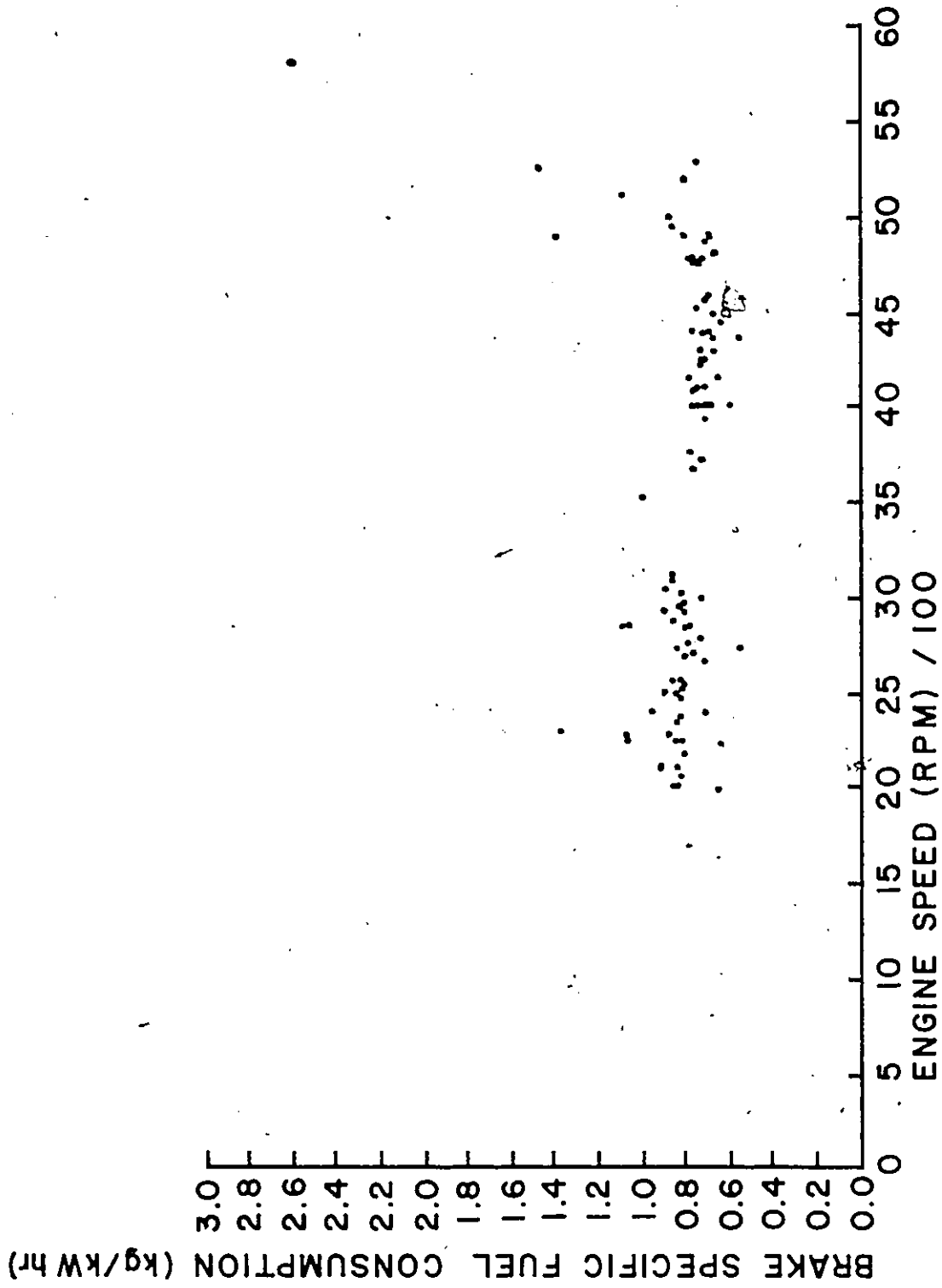


FIGURE 12. GRAPH OF ENGINE BRAKE SPECIFIC FUEL CONSUMPTION, AT CONSTANT TORQUE, VERSUS ENGINE SPEED

was made in the experiments conducted for the present investigation. If Figure 9 of the paper by Blair and Fleck [38] is consulted, it can be seen that their measurements of brake specific fuel consumption illustrate the same trend. This is a very important observation as their measurements were made on a Fichtel and Sachs, Model 914A, Wankel Engine with a 195 cm, straight exhaust pipe attached to it. It is apparent from this comparison that the straight exhaust pipe may have a considerable effect on the engine performance. The authors did not compare their measurements of engine performance to that predicted by the manufacturer and therefore, no further inferences can be gained.

The results of the volumetric air flow measurements are presented in Figure 13. The curve illustrating the theoretical flow rate was calculated using the quoted engine displacement per shaft revolution. It can be seen that the measured flow rate exhibits a linear behaviour with respect to engine speed and exceeds the predicted flow rate for engine speeds above approximately 4500 rpm. This behaviour will be related to the exhaust gas behaviour when that information is presented.

6.3 Tests Related to Exhaust Gas Behaviour

As was mentioned in Sections 4.2.3, 4.2.4 and 4.2.5 of Chapter IV, mean static and transient exhaust gas pressures were measured at locations very close to where the mean exhaust gas temperatures were measured. In this case, a single location for the measurement of the mean exhaust gas pressure was used. The measurements were made in the exhaust pipe 10.8 cm from the engine exhaust port. The change in mean static pressure as a function of engine speed has been presented in Figure 14. It can be seen that, for engine speeds beyond approximately 2500 rpm, the mean, static, gauge pressure exceeds the 1.7 kPa limitation suggested by Thomas [118]. The existence of this condition must be considered to be at least partly responsible for

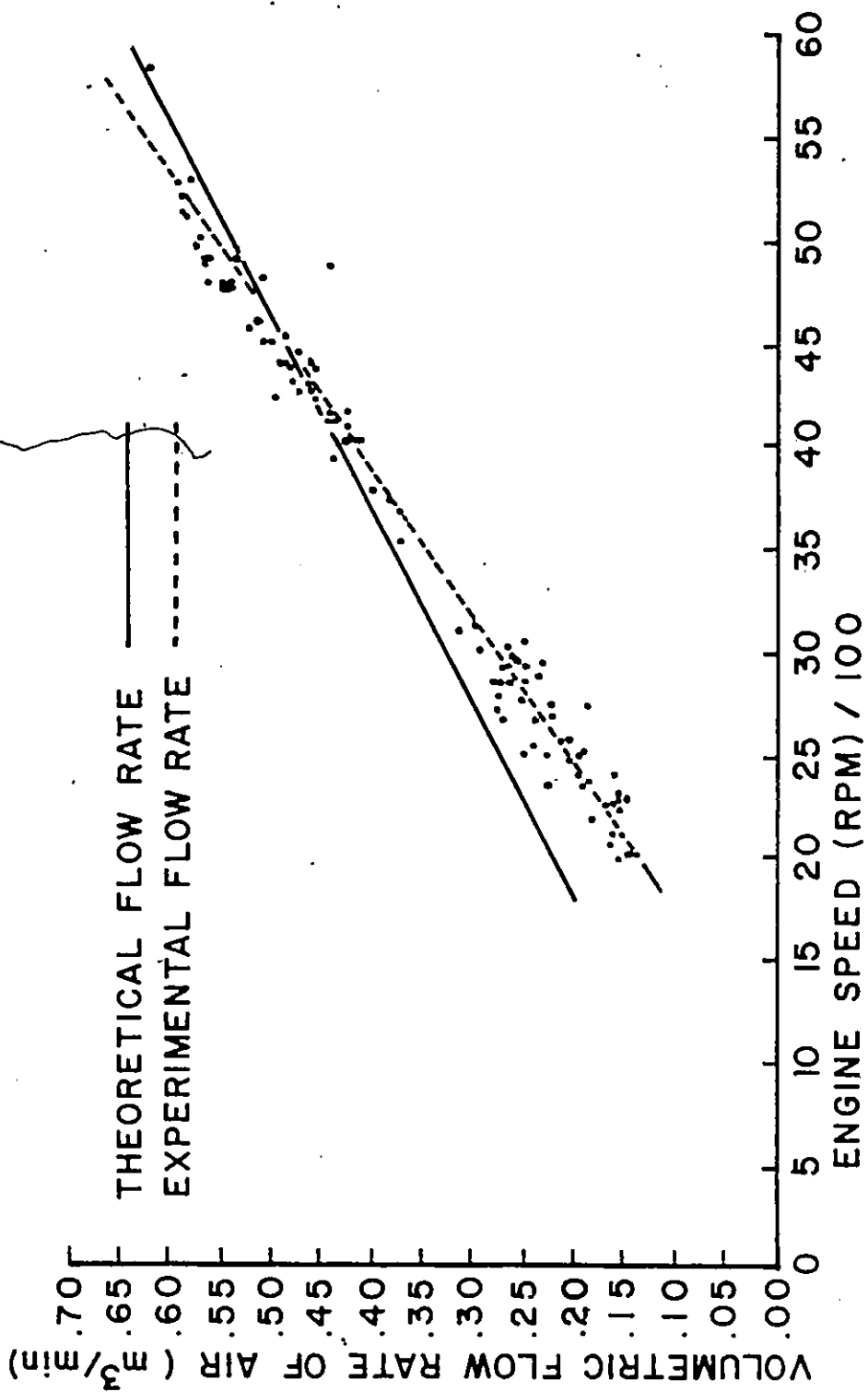


FIGURE 13. GRAPH OF VOLUMETRIC FLOW RATE OF COMBUSTION AIR VERSUS ENGINE SPEED, AT CONSTANT TORQUE

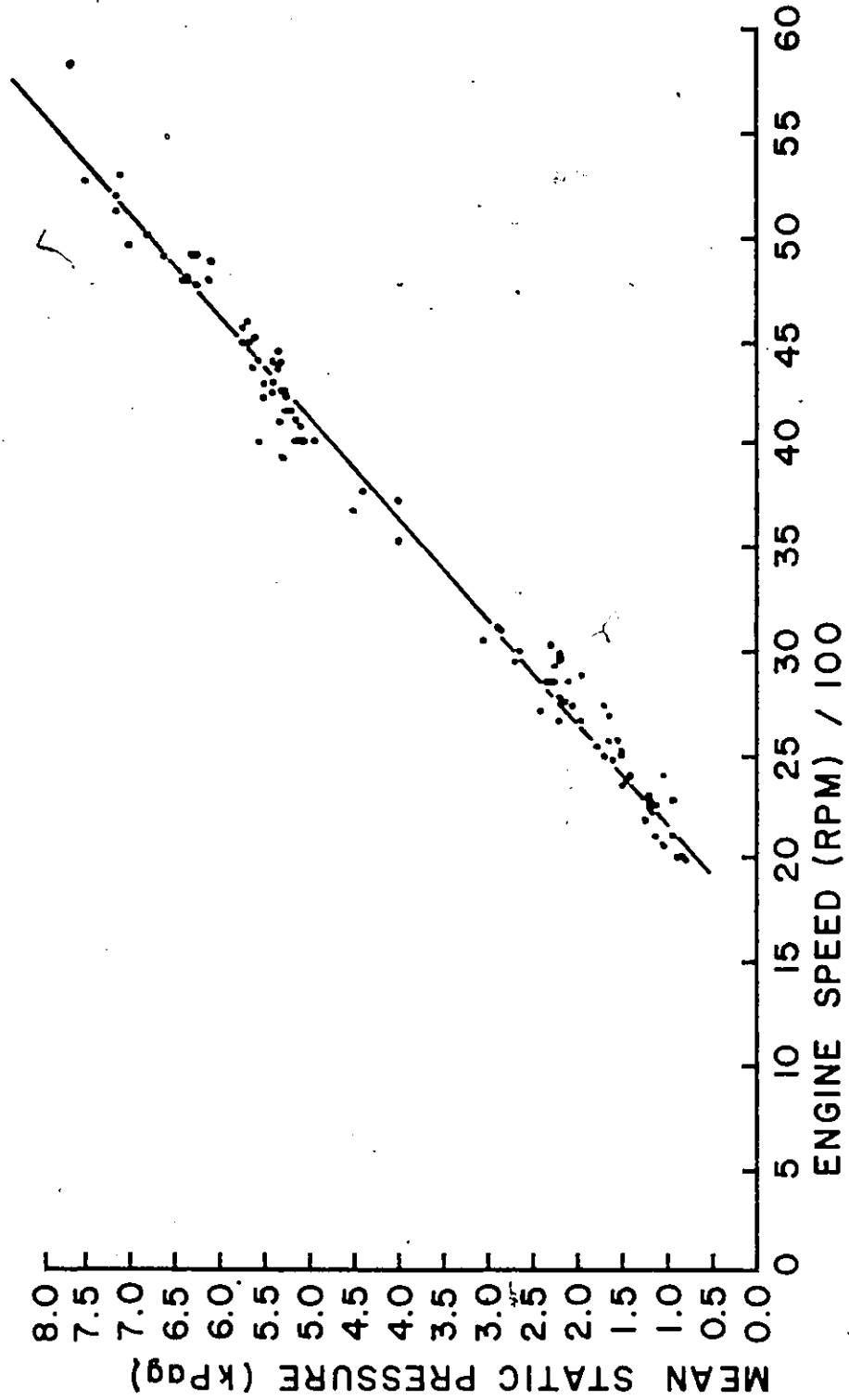


FIGURE 14. GRAPH OF MEAN STATIC GAUGE EXHAUST GAS PRESSURE VERSUS ENGINE SPEED, MEASURED AT LOCATION 1 NEAR THE EXHAUST PORT

the decrease in engine performance. The quoted values are for the engine with a stock muffler close-mounted to the engine. The exhaust pipe inside the muffler was very short and thus the back pressure, that the engine would have normally experienced, would be much less.

The results of the exhaust gas temperature measurements have been presented in Figure 15. As was mentioned previously, the temperature measurements were made at two locations in the exhaust pipe. The first location was 14.4 cm from the engine exhaust port and the second location was one metre further along the exhaust pipe. Inspection of Figure 15 reveals that the trends of temperature versus speed, at both locations, were similar. However, there is a noticeable variation in temperature difference, between the two measuring locations, over the range of engine speeds shown. It can be seen that gas temperatures exceeded 600 °C. The high gas temperatures experienced did create some problems because of the method used to mount the access blocks onto the exhaust pipe. Several of the intermediate access blocks originally had no cooling, as a result, the high gas temperatures caused the silver solder, used to bond the access blocks to the exhaust pipe, to melt. It must also be noted that the temperature measurements, at the engine speed near 6000 rpm, were not used in the computation of the curve of best fit for the two measuring locations.

During the early data processing of the analog record of the transient pressure signals, a number of spectrum analyses were performed. Examples of this procedure are presented for measurements made at the pressure transducer location closest to the exhaust port. The Fourier analysis, at an engine speed of 2000 rpm, shown in Figure 16 indicates that the fundamental frequency corresponds very closely with the firing frequency of the engine. In this case, a 1.3 Hz difference may be due to a slight variation in the engine speed or just as easily, it may be due to a slight drift or offset of the calibration of the measuring instrument. It can also

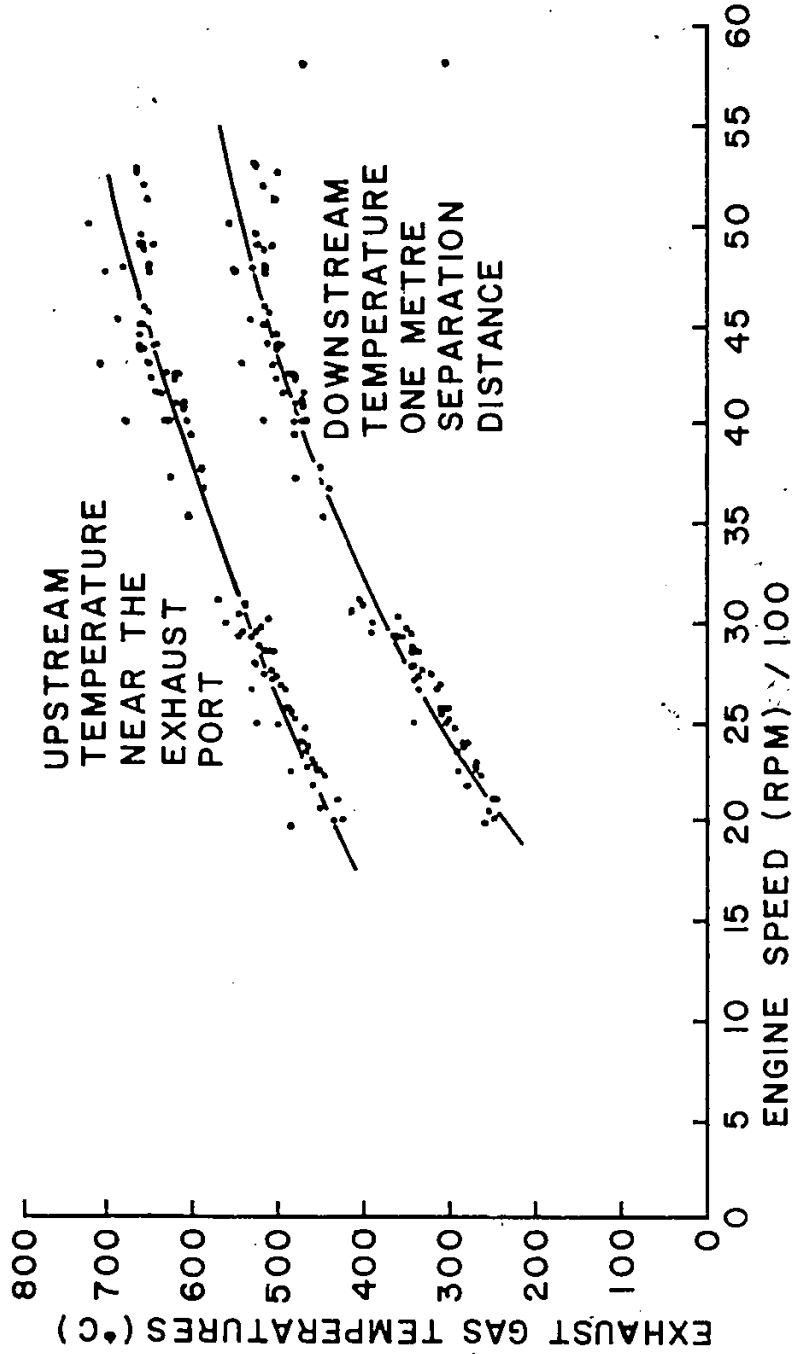


FIGURE 15. GRAPH OF MEAN EXHAUST GAS TEMPERATURE VERSUS ENGINE SPEED, MEASURED AT TWO LOCATIONS IN THE EXHAUST PIPE

NEAR EXHAUST 5000 RPM 104

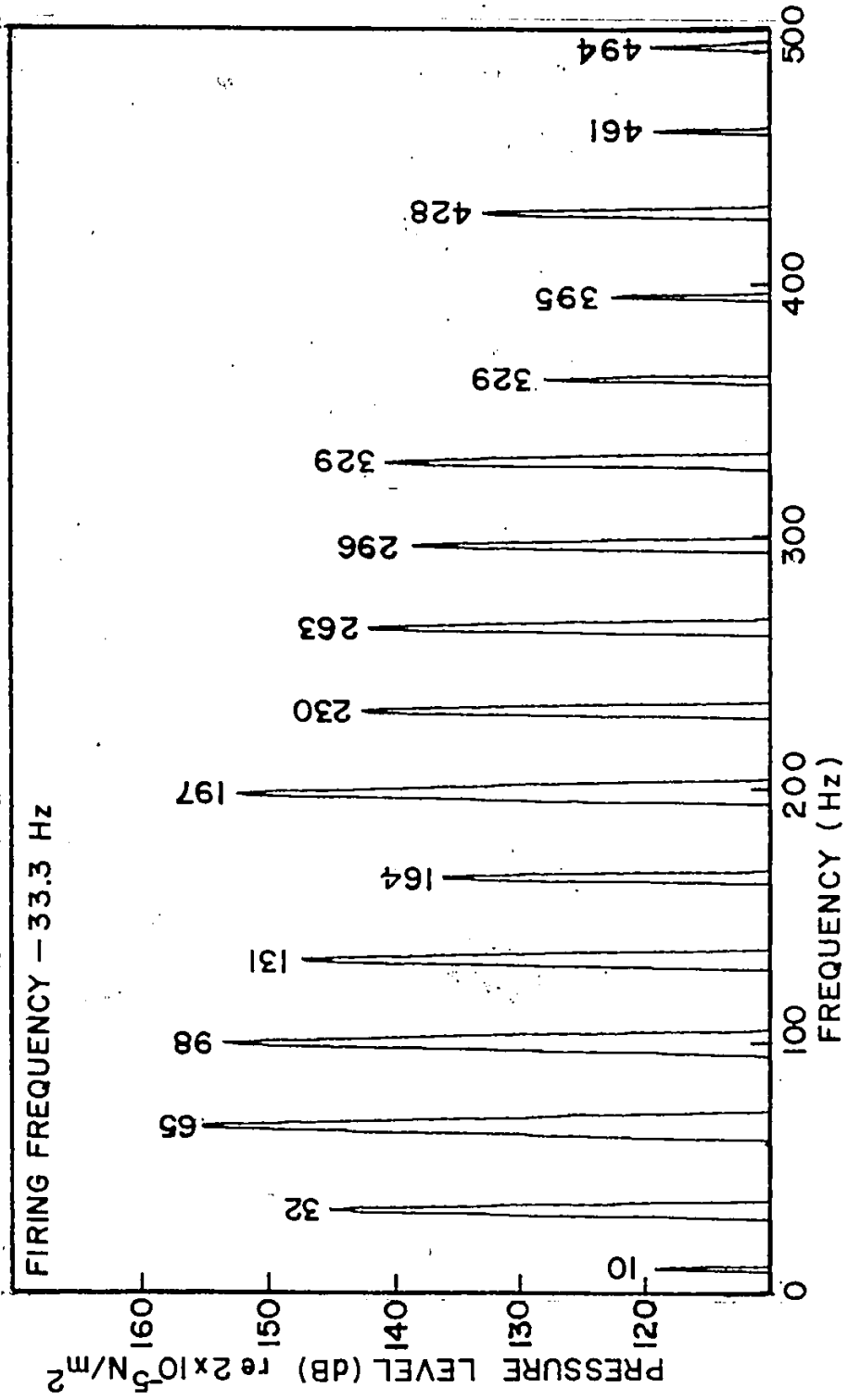


FIGURE 16. GRAPH OF THE EXHAUST GAS PRESSURE LEVEL SPECTRUM, NEAR THE EXHAUST PORT, AT AN ENGINE SPEED OF 2000 RPM

be seen that the frequencies of the other components, present in the spectrum, are all harmonics of the firing frequency. Additionally, it must be pointed out that the fundamental does not have the highest amplitude. It is the second, third and sixth harmonics which have the highest amplitudes and even the fourth harmonic has a higher amplitude than the fundamental. A similar pattern can be seen in Figure 17 which is the spectrum of the exhaust pressure pulses when the engine was operating at 3000 rpm. The same frequency range has been used for purposes of comparison. Again, it can be observed that the spikes in the spectrum all occur at higher harmonics of the fundamental. The only major difference is that it is not the sixth harmonic but rather the fifth which has an amplitude comparable to the second and third harmonics.

Figure 18 is also the spectrum of the exhaust pressure when the engine was operating at 3000 rpm. The frequency range of 0 to 1 kHz has been used for two reasons. First, it provides a good coverage of the most important portion of the spectrum and second, it can be also used for comparing the spectrum of the exhaust pressure shown in Figure 19 when the engine was operating at 4000 rpm. It can be seen that the most significant amplitudes, in both spectra, occur below 500 Hz. Also, there is a further shift in the importance of the high amplitude harmonics. For the case of the engine operating at 4000 rpm, one no longer sees the predominance of the second and third harmonics. In this instance it is the second and fourth harmonics which have the highest amplitudes. Indeed, there does not seem to be a significant trend which would be indicative of what pressure variations are occurring in the exhaust gas. The only information which would be of value to the exhaust system designer is that it is important to attenuate the first six harmonics if one is to reduce exhaust system noise.

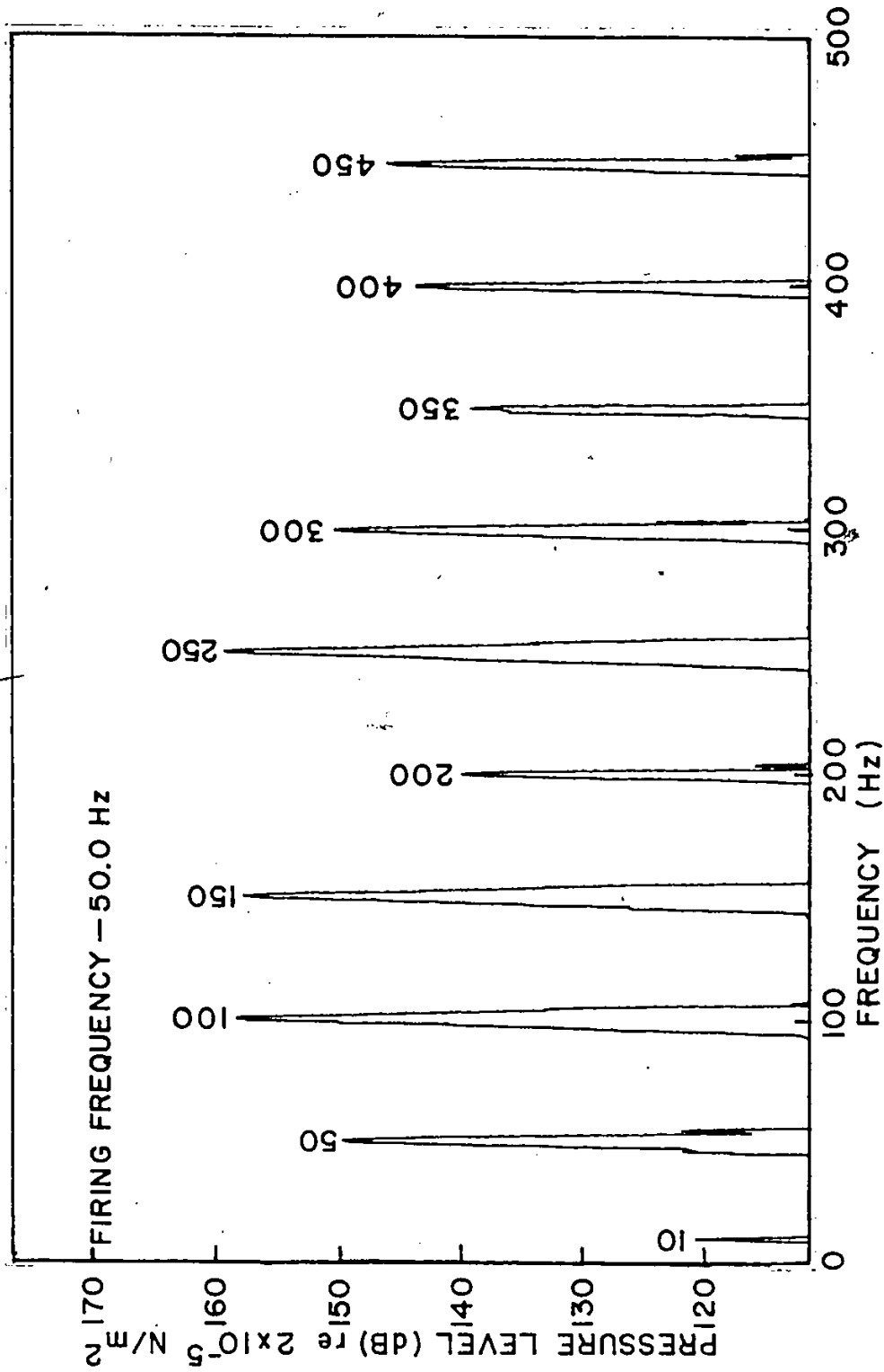


FIGURE 17. GRAPH OF THE EXHAUST GAS PRESSURE LEVEL SPECTRUM, NEAR THE EXHAUST PORT, AT AN ENGINE SPEED OF 3000 RPM

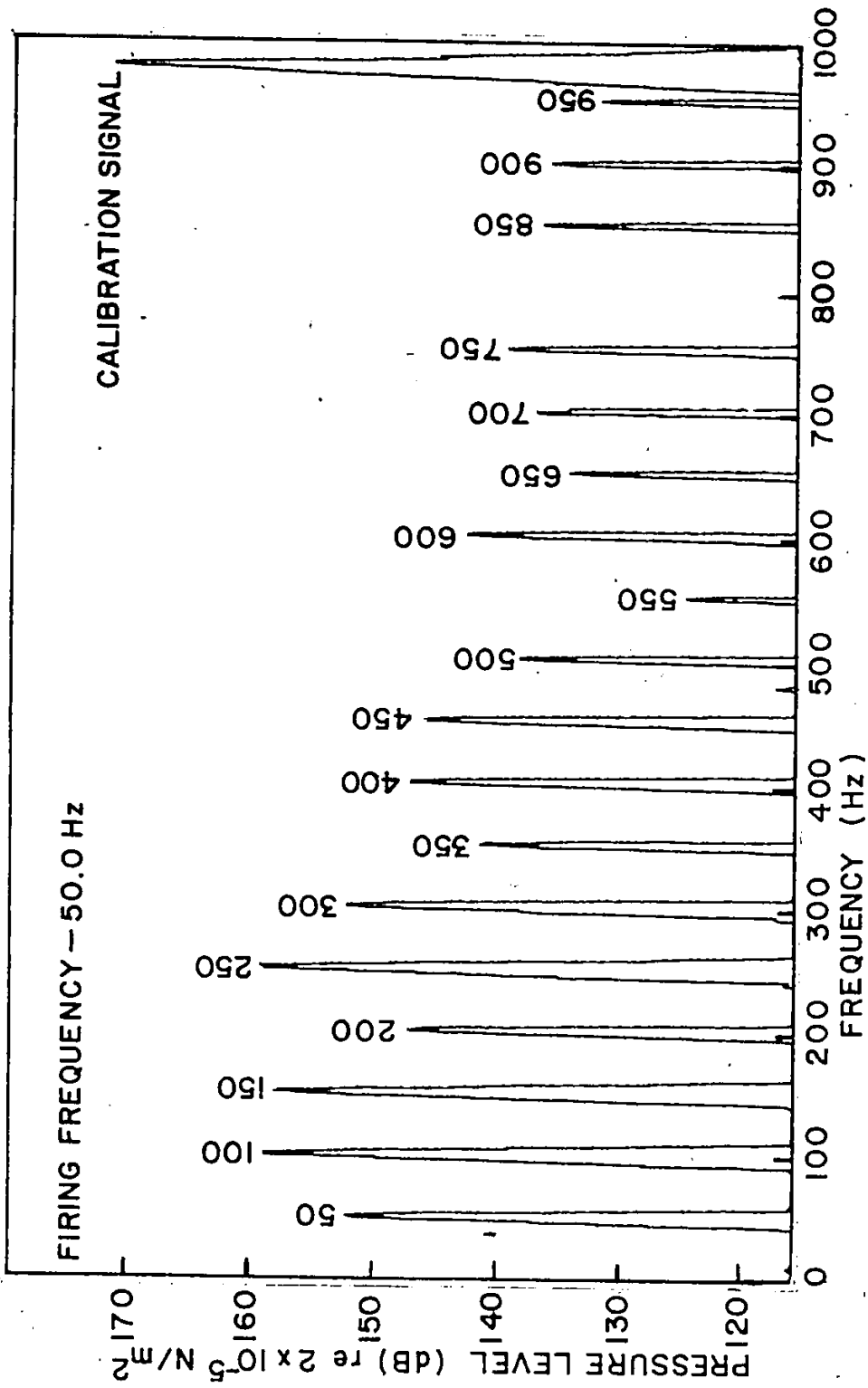


FIGURE 18. GRAPH OF THE EXHAUST GAS PRESSURE LEVEL SPECTRUM, NEAR THE EXHAUST PORT, AT AN ENGINE SPEED OF 3000 RPM

NEAR EXHAUST PORT 4000 RPM 108

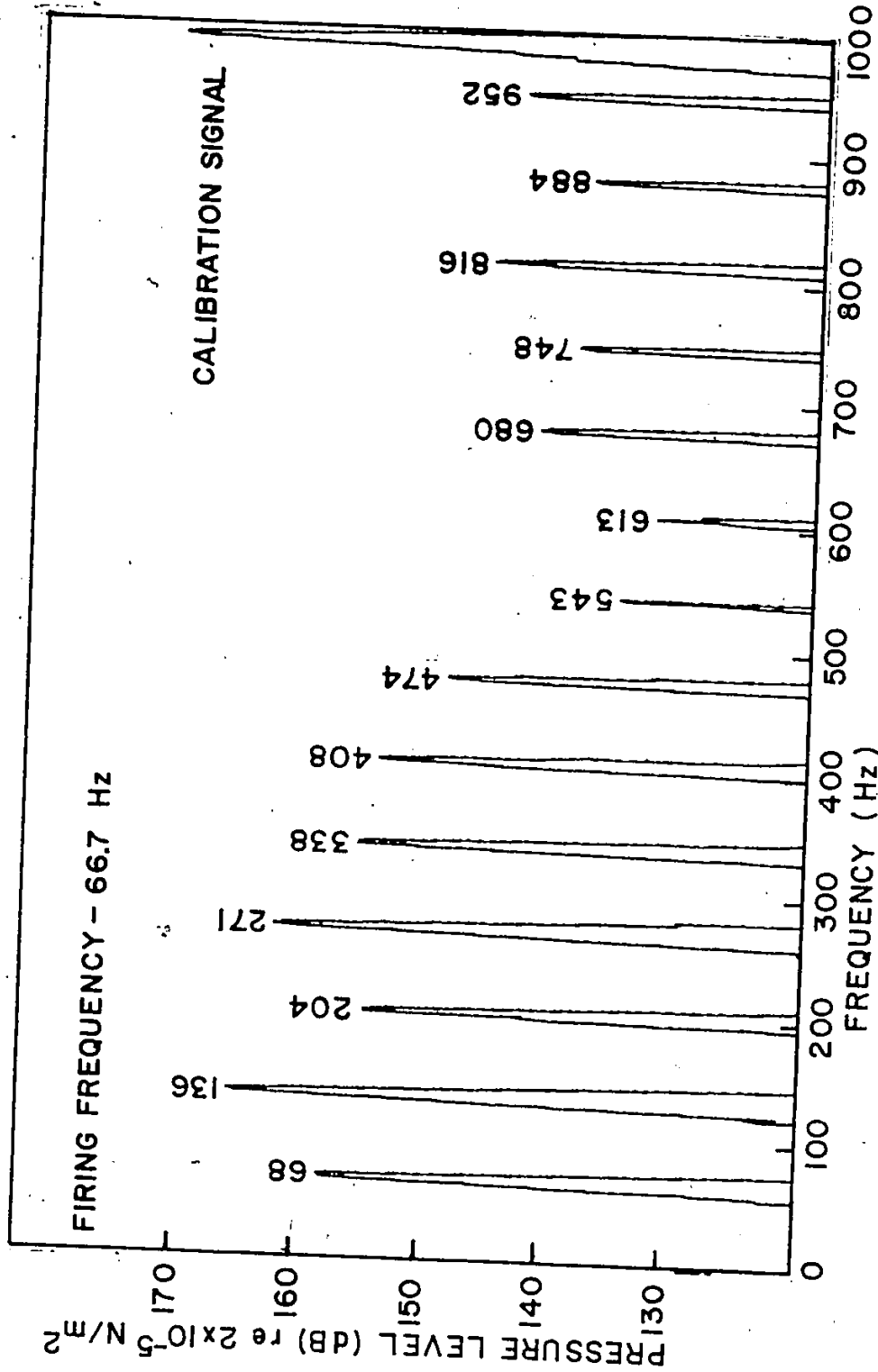


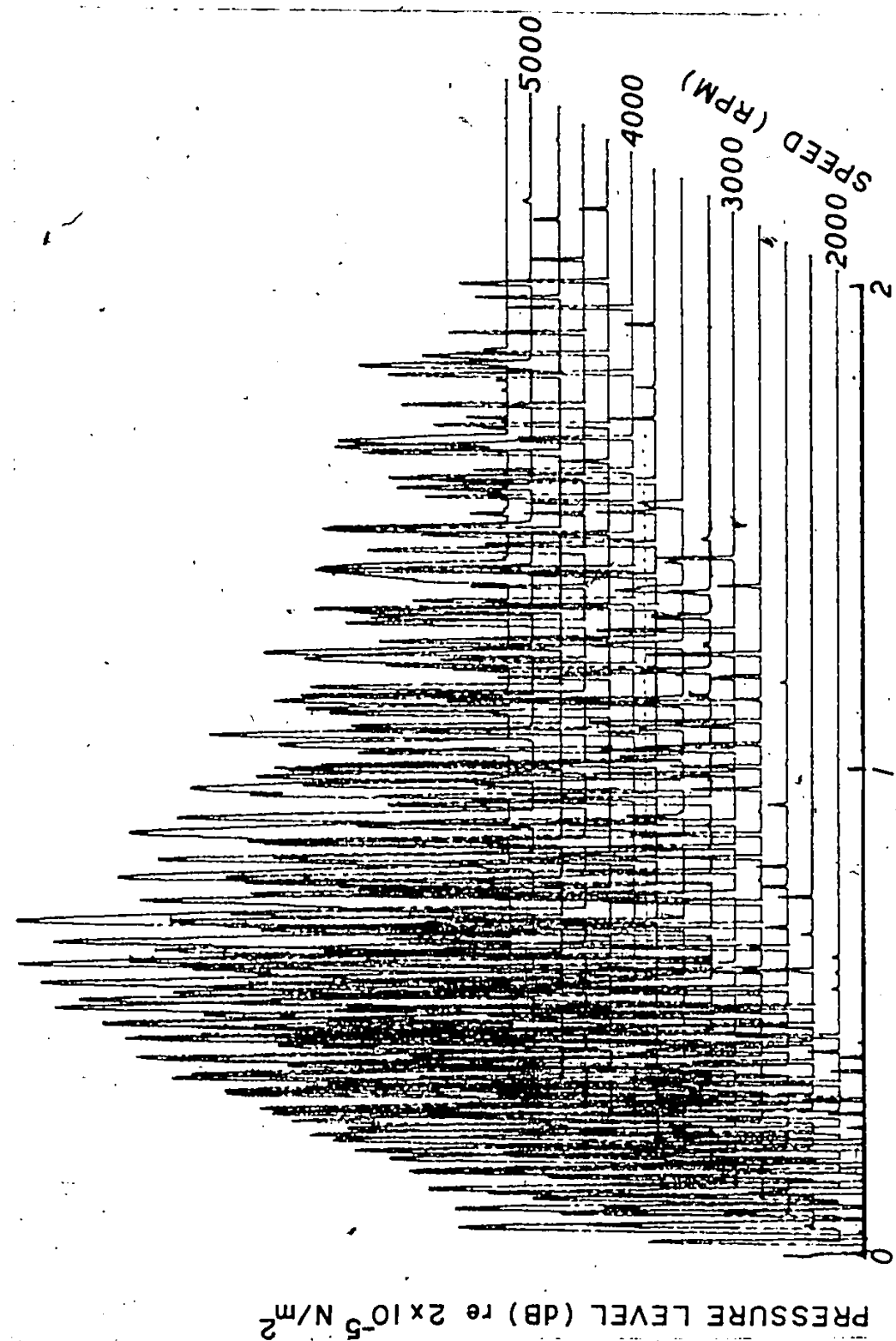
FIGURE 19. GRAPH OF THE EXHAUST GAS PRESSURE LEVEL SPECTRUM, NEAR THE EXHAUST PORT, AT AN ENGINE SPEED OF 4000 RPM

Figure 20 is a 'waterfall' diagram of the pressure spectra for a frequency range of 0 to 2 kHz and for engine speeds ranging from 1750 to 5250 rpm. The figure shows that the important portion of all spectra occurs in the range from 0 to 1 kHz. As the range was not changed on the spectrum analyser, when this figure was created, all amplitudes shown fall within a 70 db range with the highest levels occurring between 170 and 180 dB. In addition, it can be seen that the amplitude of the harmonics occurring near 2 kHz are very small and that there are less than 23 harmonics which are present in any of the engine spectra.

To gain a better understanding of the pressure variation which were occurring in the exhaust gas, samples of the pressure versus time behaviour were plotted. Figures 21, 22 and 23 are examples of the results of this investigation. The engine speeds, for which the results were plotted, are the same as those used to generate the spectra of figures 16 to 20. An inspection of the lower curve of Figure 21 reveals the reason that so many harmonics of the firing frequency were present in the corresponding spectrum. This curve represents the pressure variation with time at the measuring location closest to the exhaust port opening.

The pressure variation is quite complex as it is not only controlled by the direct exhaust pressure pulses but also by the reflections of these pressure pulses at both ends of the exhaust pipe. If the two pressure pulses are examined closely, it is evident that there are distinguishable differences in their shape. This adds an additional degree of complexity to the problem. In addition, it is almost impossible to determine if the sample plotted provides a true representation of the pressure pulses, produced by the engine, at the given engine speed. By inspection of the upper curve shown in the figure, it can be seen that there is a further complication involved with the pressure pulse behaviour. It is observed that the shape of the pressure pulse has changed in the time it has taken to propagate one metre in the exhaust

Close to Exhaust Port



FREQUENCY (kHz)

FIGURE 20. GRAPH OF THE EXHAUST GAS PRESSURE LEVEL SPECTRA FOR ENGINE SPEEDS RANGING FROM 1750 TO 5250 RPM IN 250 RPM INCREMENTS, MEASURED NEAR THE EXHAUST PORT

2000 RPM

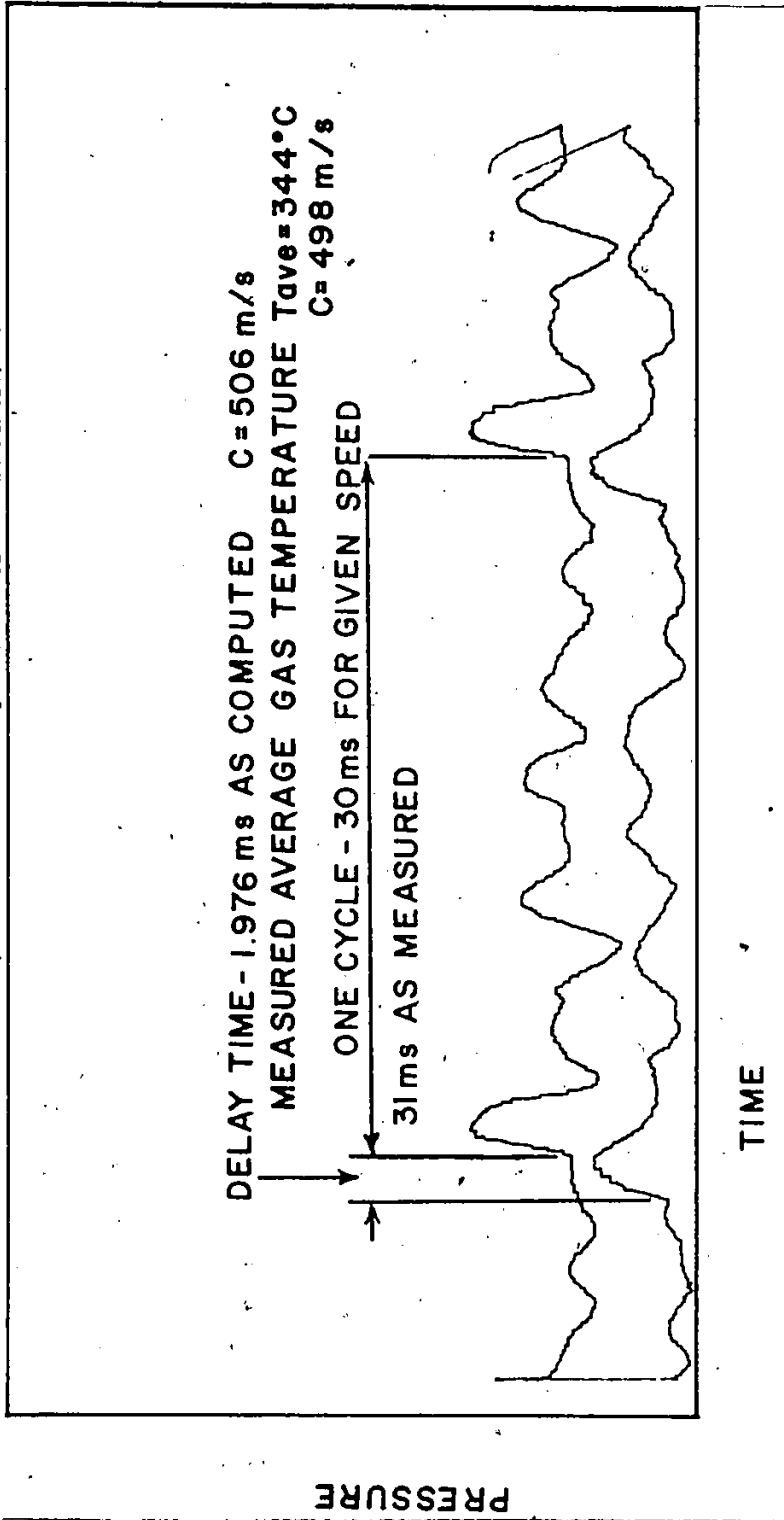


FIGURE 21. GRAPH OF EXHAUST GAS PRESSURE VERSUS TIME WITH A ONE METRE SEPARATION DISTANCE BETWEEN MEASURING LOCATIONS, AT AN ENGINE SPEED OF 2000 RPM

pipe.

By using the engine speed as a reference, it is possible to calculate the period required for one engine cycle which is also the time interval between pressure pulses. The time interval for an engine speed of 2000 rpm is 30 milliseconds. By using a magnified scale, whose smallest division is 0.2 mm, and by measuring the interval between pulses on the screen of a digital storage oscilloscope, it was determined that the interval was 31 milliseconds. The use of this measurement and Figure 21, yielded a delay time of 1.976 milliseconds for the pulse to travel one metre. This resulted in a computed speed of sound in the exhaust gas of 506 m/s. This measurement compares favourably with the speed of sound in the gas of 498 m/s which was determined from ideal gas theory and using the average of the two exhaust gas temperature measurements. The difference between the two velocities is 8 m/s or 1.6%.

Similar calculations were performed using the information provided in Figures 22 and 23. In the case of Figure 22, the results indicated a much wider variation between the two calculated values of the speed of sound. At the engine speed of 3000 rpm, of Figure 22, the difference was 30 m/s or 5.5% which is the greatest difference of the three examples presented. In the case of Figure 23, the difference in the speed of sound for the two calculation methods used was 17 m/s or 2.9%. The percentage errors indicate that this crude method of measurement provides very good results; however, it is possible that the accuracy of these measurements could be improved if the entire process could be handled in digital form by interfacing the digital storage oscilloscope with a computer. In that way the information could be extracted easily and the time base measurements would be more precise.

There are several interesting features which are present in Figures 22 and 23. In Figure 22, the amplitudes have increased. A change in the pressure pulse shape

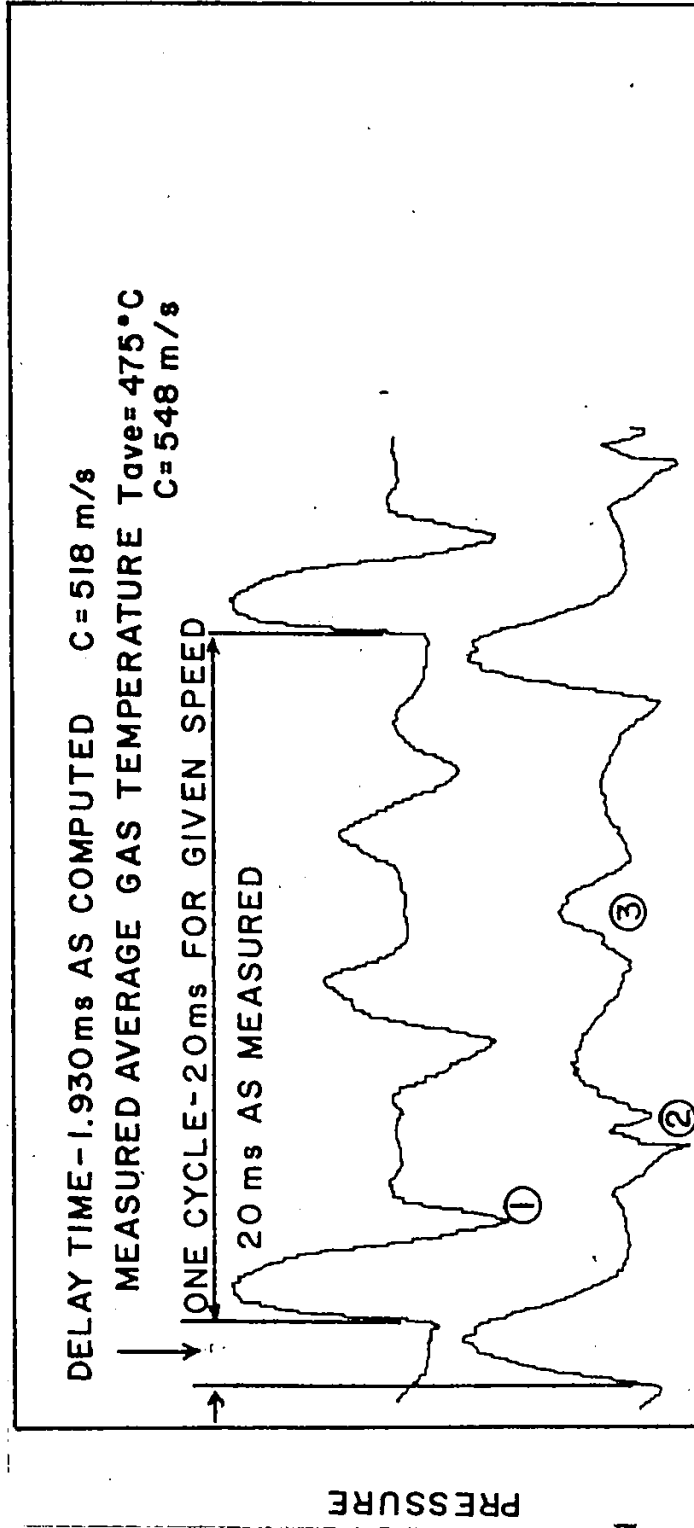


FIGURE 22. GRAPH OF EXHAUST GAS PRESSURE VERSUS TIME WITH A ONE METRE SEPARATION DISTANCE BETWEEN MEASURING LOCATIONS, AT AN ENGINE SPEED OF 3000 RPM

4000 RPM 114

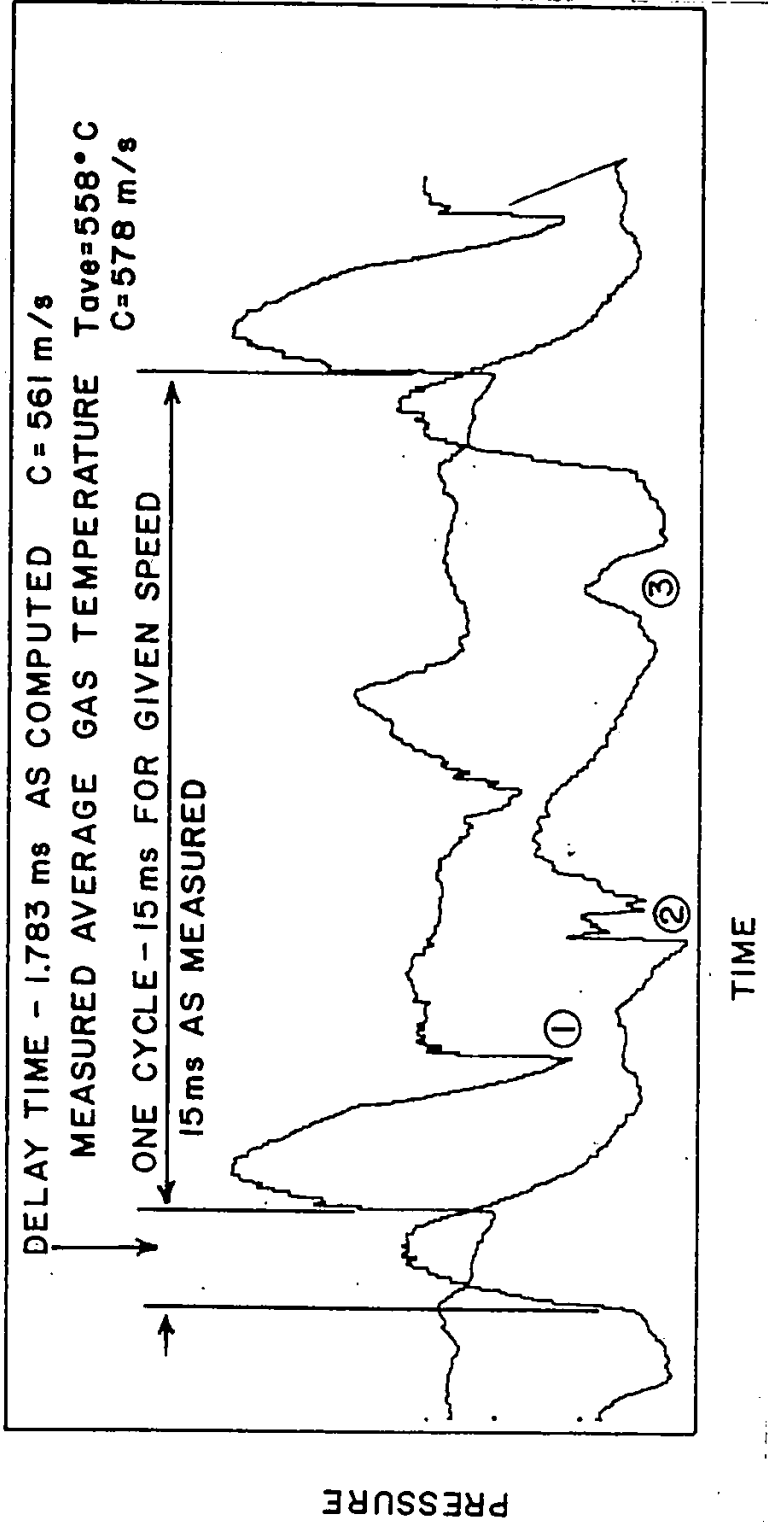


FIGURE 23. GRAPH OF EXHAUST GAS PRESSURE VERSUS TIME WITH A ONE METRE SEPARATION DISTANCE BETWEEN MEASURING LOCATIONS, AT AN ENGINE SPEED OF 4000 RPM

which is immediately evident is the steepening of its leading edge. This occurs in the 1.93 millisecond propagation time during which the pulse travels from the first to the second measuring location. It is also possible to distinguish pressure variations in the expansion wave which was created when the pressure pulse reached the open end of the exhaust pipe. The variation in the shape of the expansion wave, which has been marked by the circled number one on the upper curve, can be seen as it travels toward the engine. In the lower curve, it has been marked by the circled number 2 and it can be seen that it has steepened into a discrete jump in pressure. This discontinuity in the reflected wave is important as it has occurred first in the reflected wave. The formation of a small shock is evidence of nonlinear acoustic behaviour. It must also be noted that there have been some general changes in the pressure variations between each rotor chamber blow-down; however, if Figures 21 and 22 are compared, there are similarities in the pressure variations. This helps to explain why there were similarities in the predominant harmonics of their corresponding spectra.

Figure 23 presents a good example of how quickly a pressure pulse can be distorted into a shock wave. It was the observation of this phenomena which suggested use of a nonlinear model for the pressure pulse. It is also possible to note the considerable changes which have taken place in the interval between pressure pulses. As the period for each cycle decreases, the periods of the individual reflected waves do not decrease proportionally. Thus the intermediate pressure variations tend to shift within the firing period. The shift can be observed by comparing the change in position of the wave shapes marked by the circled numbers 2 and 3. The movement of position 3 is the more noticeable of the two shifts. As can be seen, in Figure 23, position 3 has come very close to interacting with the next pressure pulse. In the case of Figure 22, location 3 is almost in the middle of the period between the two

pressure pulses.

A comparison of the spectra, measured at both pressure transducers, was made to determine if significant differences in harmonic amplitudes were present. An example of this comparison has been presented in Figure 24 for an engine speed of 4000 rpm. This engine speed was chosen for comparison because of the marked differences between the two pressure pulse shapes. As can be seen, there is an increase in the amplitudes of the higher harmonics; however, only the amplitude of the second harmonic shows a significant decrease. It is observed that spectrum analysis does not provide evidence of significant distortions of the pressure pulse. A cautionary note must be directed to those investigators who would rely solely on spectrum analysis for exhaust system evaluation. It is evident from the preceding discussion that the use of spectrum analysis does not always yield all of the information necessary for optimizing the exhaust system design.

Figures 25 and 26 are plots of the single cycle pressure variation at engine speeds ranging from 1750 to 5250 rpm. Figure 25 is a presentation of the pressure variations which were measured at the transducer location closest to the exhaust port. Figure 26 is a presentation of the pressure variations which were measured at the transducer location one metre further down stream. As can be seen by inspection of either of the two figures, there are distinct shifts in the pressure variation. These shifts are important as they can be responsible for changes in engine performance. These effects which were created by the pressure variation will be referred to in a later discussion.

The results of the transient exhaust pressure measurements, made 12.6 cm from the engine exhaust port, have been presented in Figures 27, 28 and 29. The data presented in these figures was the result of using the analog to digital conversion

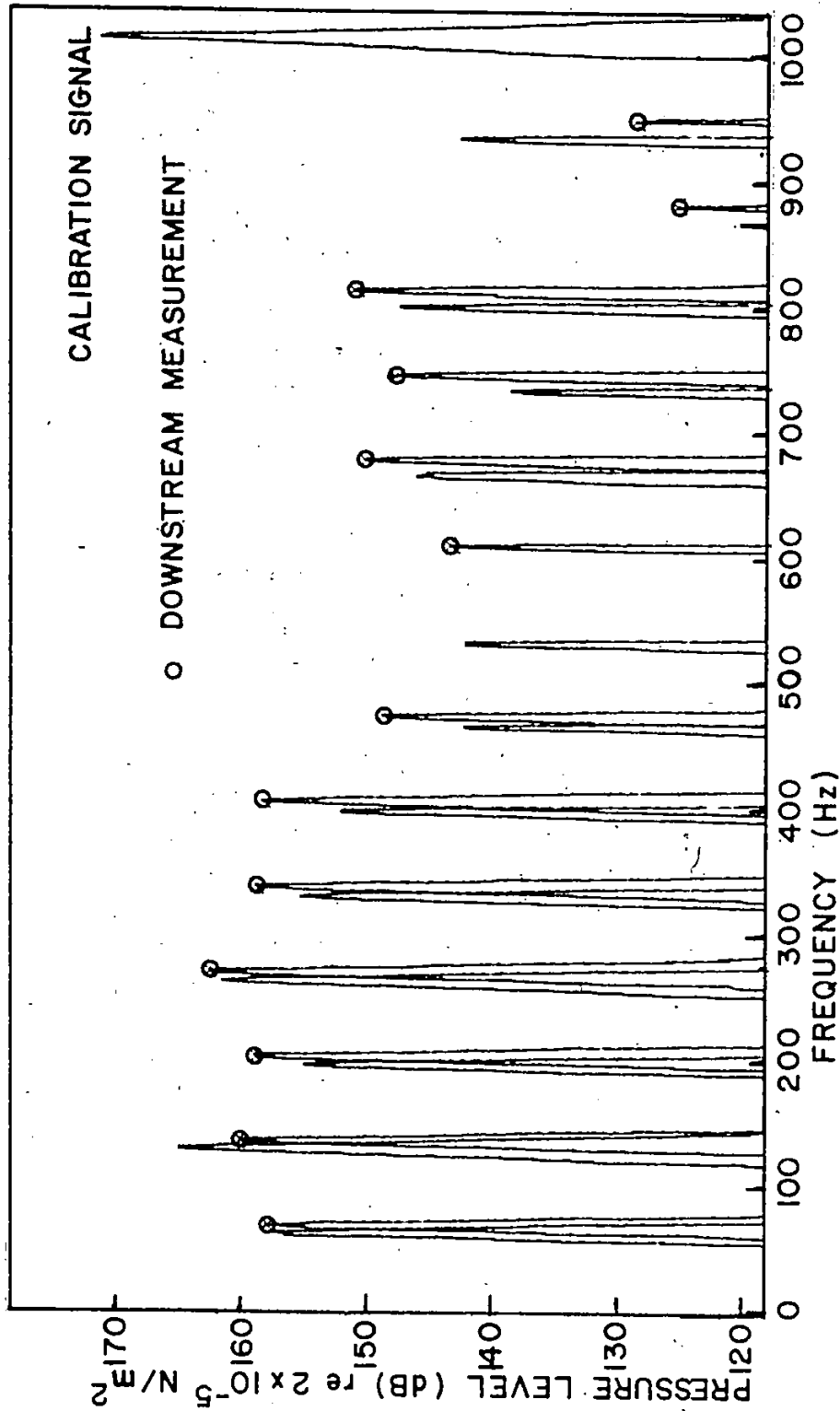


FIGURE 24. GRAPH OF EXHAUST GAS PRESSURE LEVEL SPECTRA AT A LOCATION NEAR THE EXHAUST PORT AND AT ANOTHER LOCATION ONE METRE DOWNSTREAM, FOR AN ENGINE SPEED OF 4000 RPM

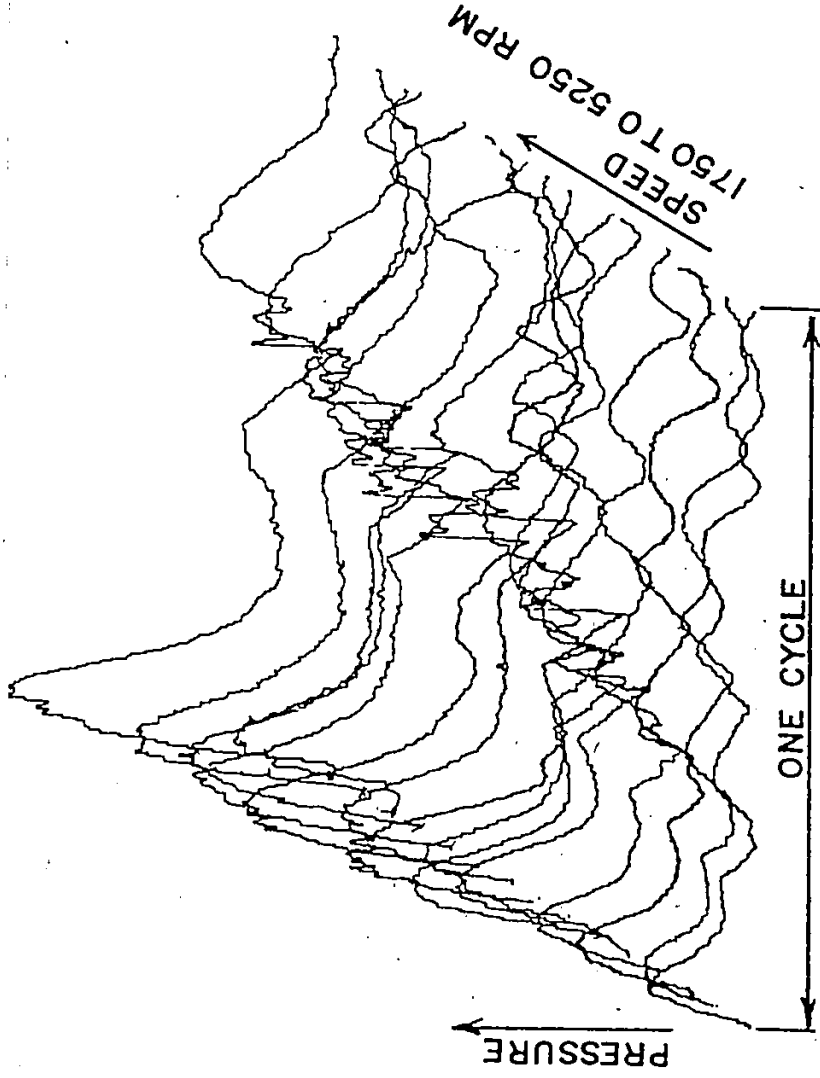


FIGURE 25. GRAPH OF ONE CYCLE OF THE EXHAUST PRESSURE SIGNALS NEAR THE EXHAUST PORT, FOR ENGINE SPEEDS RANGING FROM 1750 TO 5250 RPM IN INCREMENTS OF 250 RPM

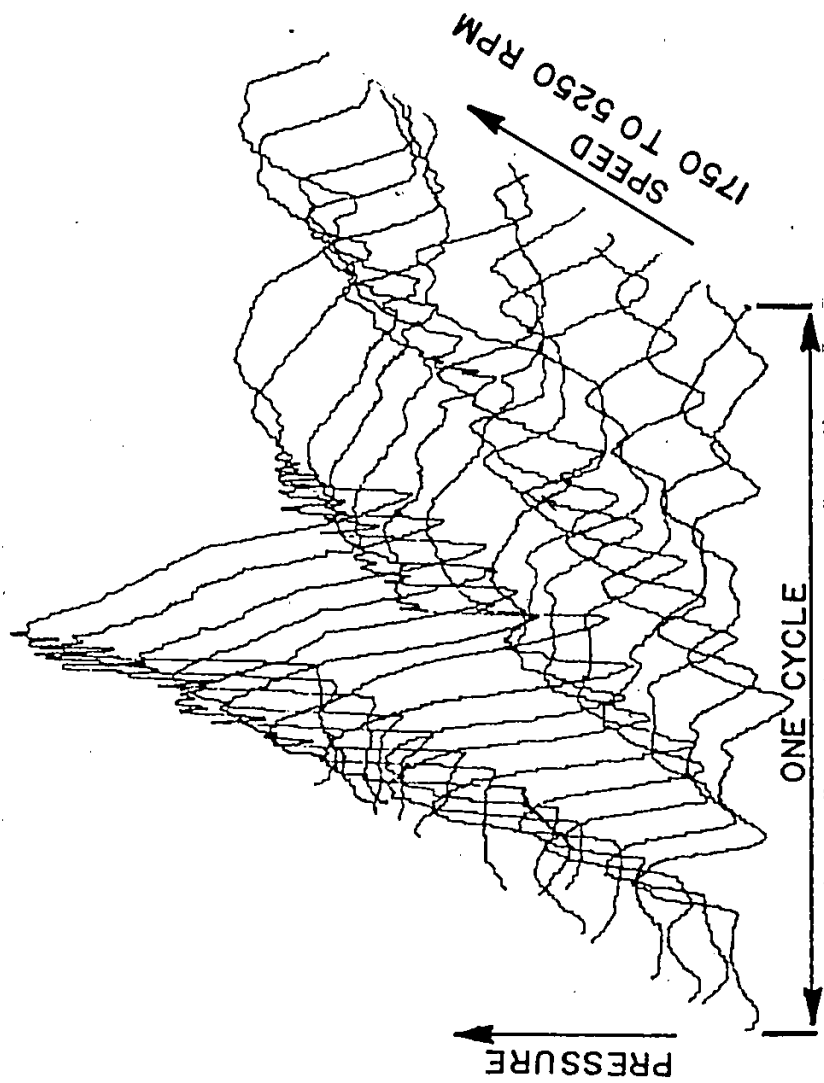


FIGURE 26. GRAPH OF ONE CYCLE OF THE EXHAUST PRESSURE SIGNALS, ONE METRE DOWNSTREAM OF THE FIRST MEASURING LOCATION, FOR ENGINE SPEEDS RANGING FROM 1750 TO 5250 RPM IN INCREMENTS OF 250 RPM

peripheral board and the program KLAATU.DC as previously described in Section 5.1 and Appendix I. It should also be noted that the data presented in each figure represents in excess of 900 measurements. Figure 27 illustrates the variation in the maximum pressure pulse amplitude as a function of engine speed. It can be seen that there is considerable variation in these measurements and little possibility of determining a curve of best fit for this situation. However, it is important to note that the peak pulse pressures exceed the 3.447 kPa that Blair [28] suggested was the upper limit for linear acoustic behaviour in an exhaust system. The results also prove the point that Eriksson [64] made concerning internal sound levels being as high as 190 dB since this level translates into an acoustic pressure of approximately 63 kPa. In all cases the pressures measured exceed the 140 dB (200 Pa) lower bound on nonlinear behaviour mentioned by Rowley [109].

If the values of Figure 27 are divided by the absolute mean static pressure, the result is the variation as a function of engine speed as shown in Figure 28. It can be seen that a pattern is beginning to emerge from this information; however, the scatter of data is still quite high. A much clearer picture of the transient exhaust pressure behaviour can be seen by inspecting Figure 29. The average pressure amplitudes which were measured were divided by the absolute mean static pressure at the measuring location. In this case, the lower portion of the results in the range from 2000 rpm to 4000 rpm appear to be linear. The solid correlation line, shown in the figure, was computed using this data. The correlation appears to also pass through the data at the highest engine speeds. The dotted curve, shown in the figure, is only an estimate of the curve of best fit as no correlation equation could be found which would adequately fit the points.

The reason for this demonstrated behaviour can be explained in terms of the pressure pulse propagation. The decrease in the pulse amplitude is due to an expansion

V MAX. PK. PRESSURE VS RPM REF 58 121

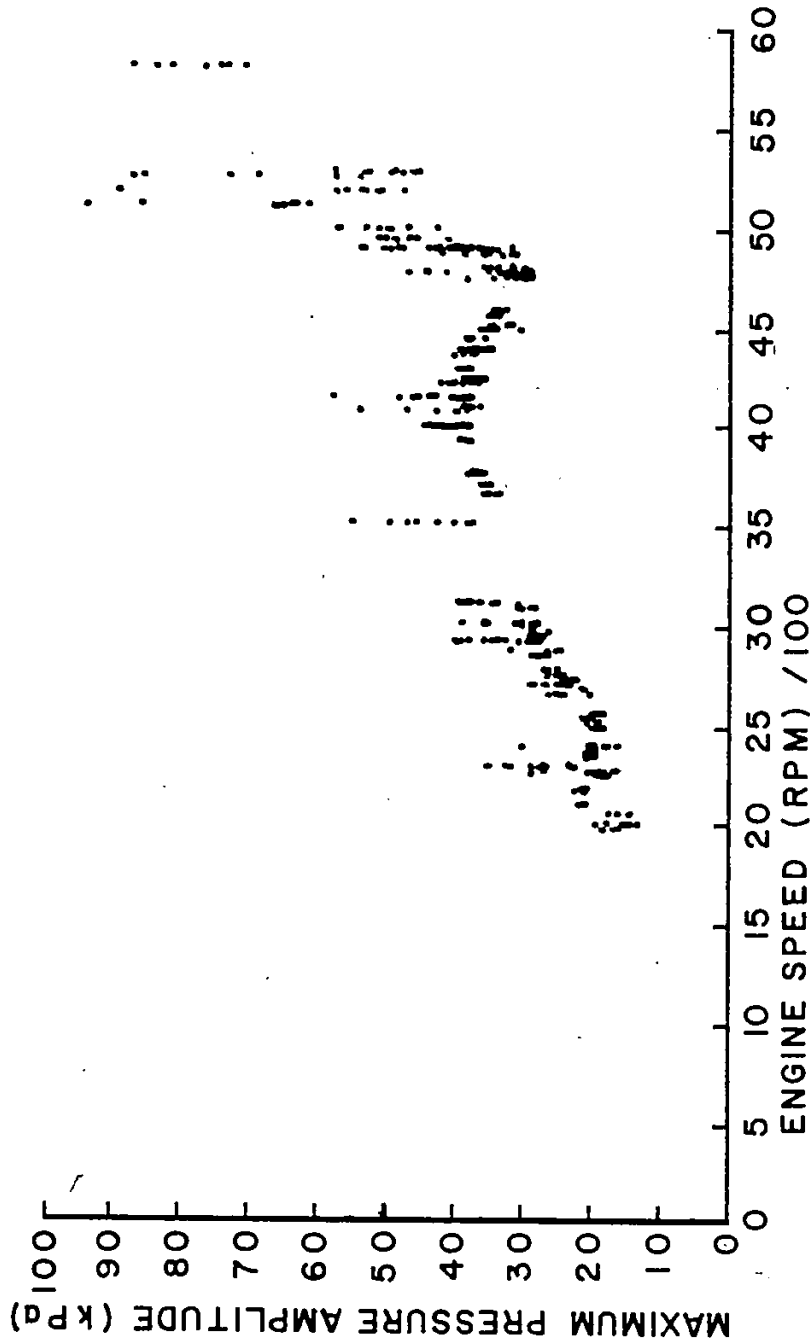


FIGURE 27. GRAPH OF MAXIMUM AMPLITUDE OF THE EXHAUST GAS PRESSURE PULSE VERSUS ENGINE SPEED

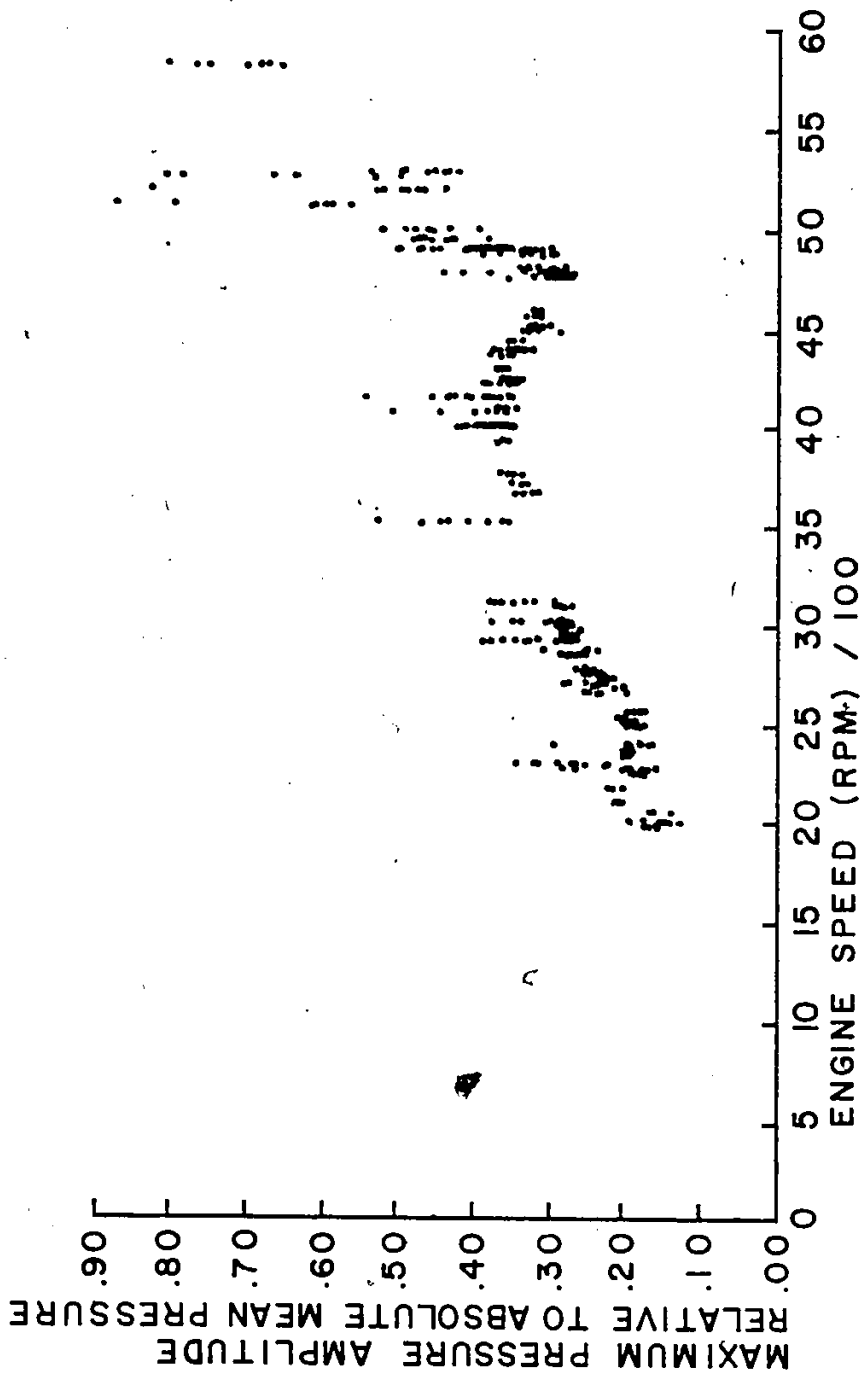


FIGURE 28. GRAPH OF THE RELATIVE, MAXIMUM PRESSURE PULSE AMPLITUDE VERSUS ENGINE SPEED.

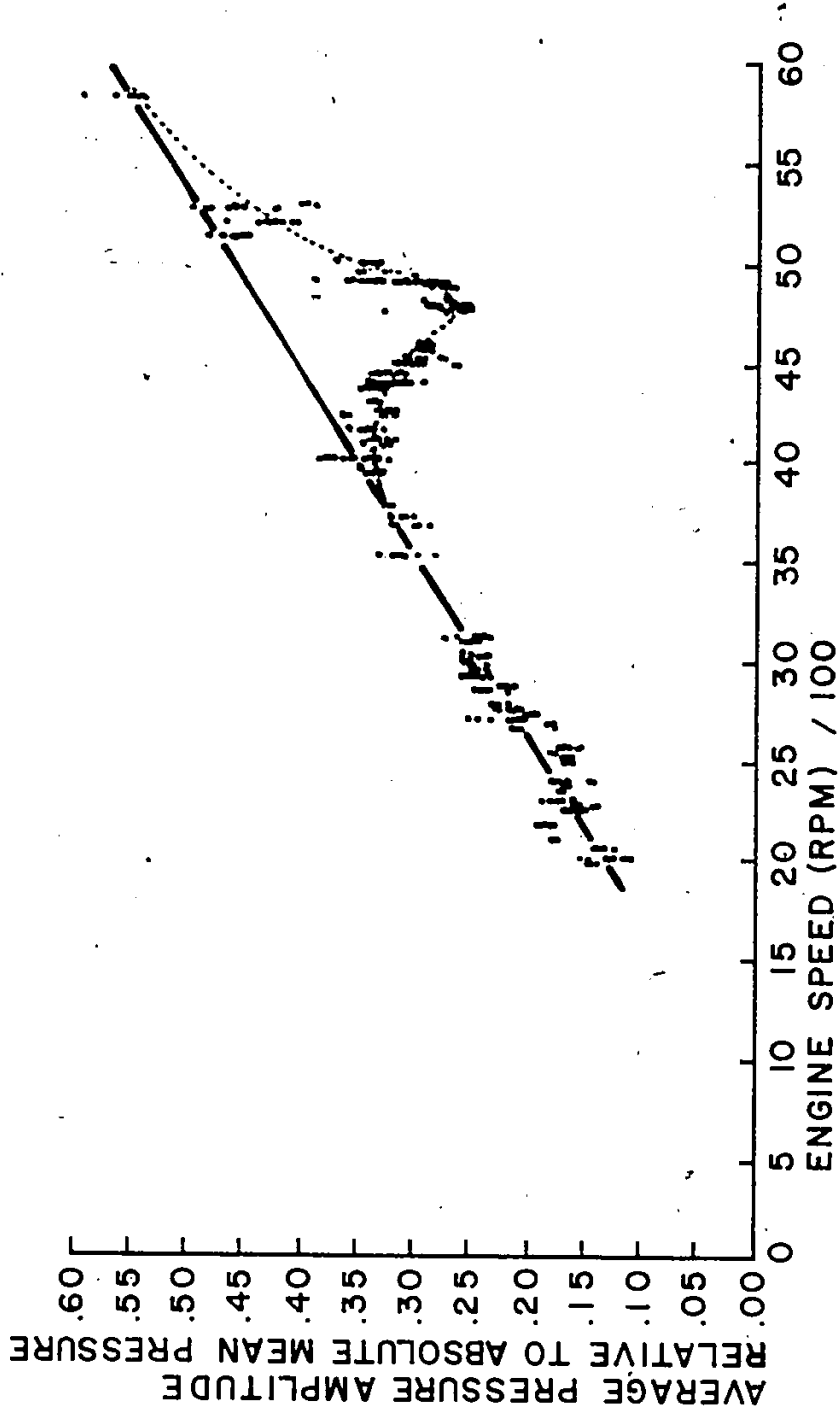


FIGURE 29. GRAPH OF THE RELATIVE, AVERAGE PRESSURE PULSE AMPLITUDE VERSUS ENGINE SPEED

wave arriving at the measuring location at approximately the same time as the pressure pulse, created by the rotor chamber blow-down, reaches the same location. The expansion wave which is responsible for this behaviour can be seen through a close inspection of Figure 25 and also by referring back to Figure 23. It can be seen that the expansion wave to the right of the pulse, identified by the circled number 3 in Figure 23, begins to interact with the exhaust pressure pulse. This results in a reduction in the average pressure pulse amplitude which was measured. This reduction can also be seen by carefully observing the pressure pulse amplitudes shown in Figure 25. The results of this interaction also carry over into the volumetric flow rate of air into the engine. As the expansion wave reaches the engine just prior to the opening of the exhaust port, it interacts with the rotor chamber which is being charged with a fresh mixture of air and fuel. Thus the expansion wave assists in the induction of the new charge and consequently, the flow rate into the engine is improved.

6.4 The Pressure Pulse Correlation

The results of running the sequence of programs KLAATU, BARADA, NICTO and BARANGA have been presented in Figures 30 to 43. In all figures, each square dot represents one data point as digitally sampled from the analog pressure signal. The solid curve represents the computed line of best fit when the nonlinear pressure pulse model was correlated with the data. Figures 30, 31, 32 and 33 illustrate the data which resulted from sampling sections 1.1, 1.2, 1.3 and 1.4 of the tape recording of the analog pressure signal when the engine was operating at 2000 rpm under a light load. The correlation results for these figures are included in Appendix V and are listed as Files 1, 2, 3 and 4 respectively. As can be seen, the minimum correlation coefficient for this data is 0.984. In addition, the variation about the average values of pseudofrequency (149.2 Hz) and distortion coefficient (0.205) are less than 1 Hz

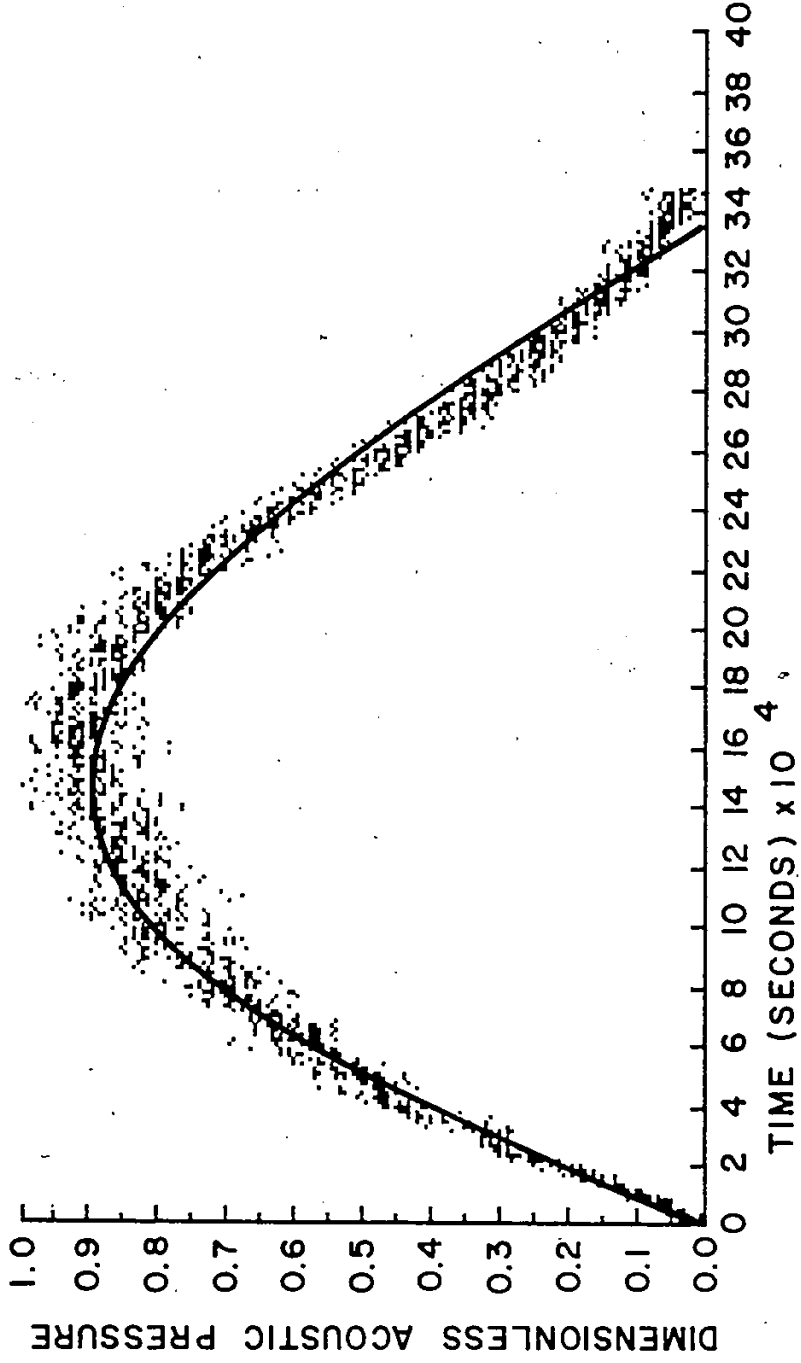


FIGURE 30. GRAPH OF DIMENSIONLESS ACOUSTIC PRESSURE VERSUS TIME, SAMPLED AT LOCATION 1 NEAR THE EXHAUST PORT FOR AN ENGINE SPEED OF 2000 RPM, TAPE SECTION 1.1

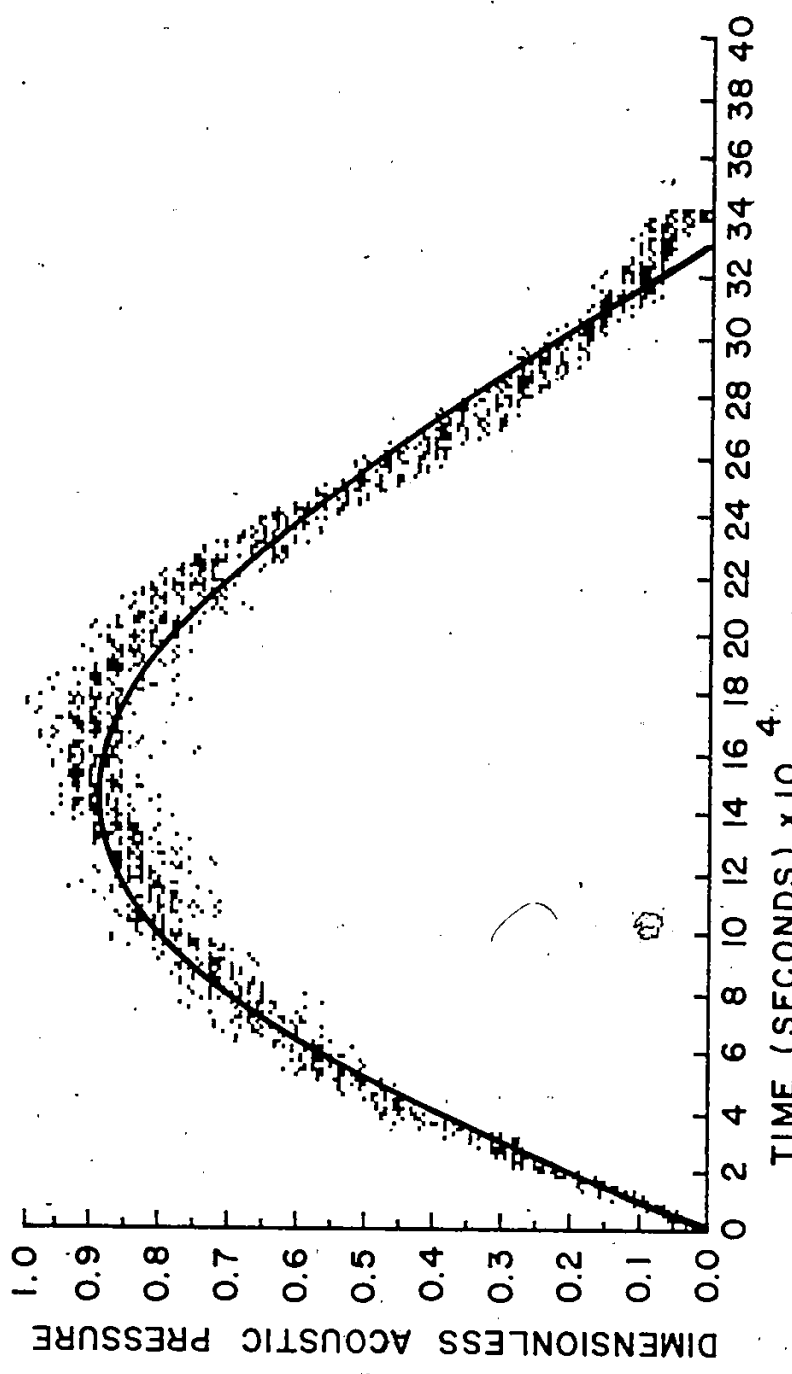


FIGURE 31. GRAPH OF DIMENSIONLESS ACOUSTIC PRESSURE VERSUS TIME, SAMPLED AT LOCATION 1 NEAR THE EXHAUST PORT FOR AN ENGINE SPEED OF 2000 RPM, TAPE SECTION 12

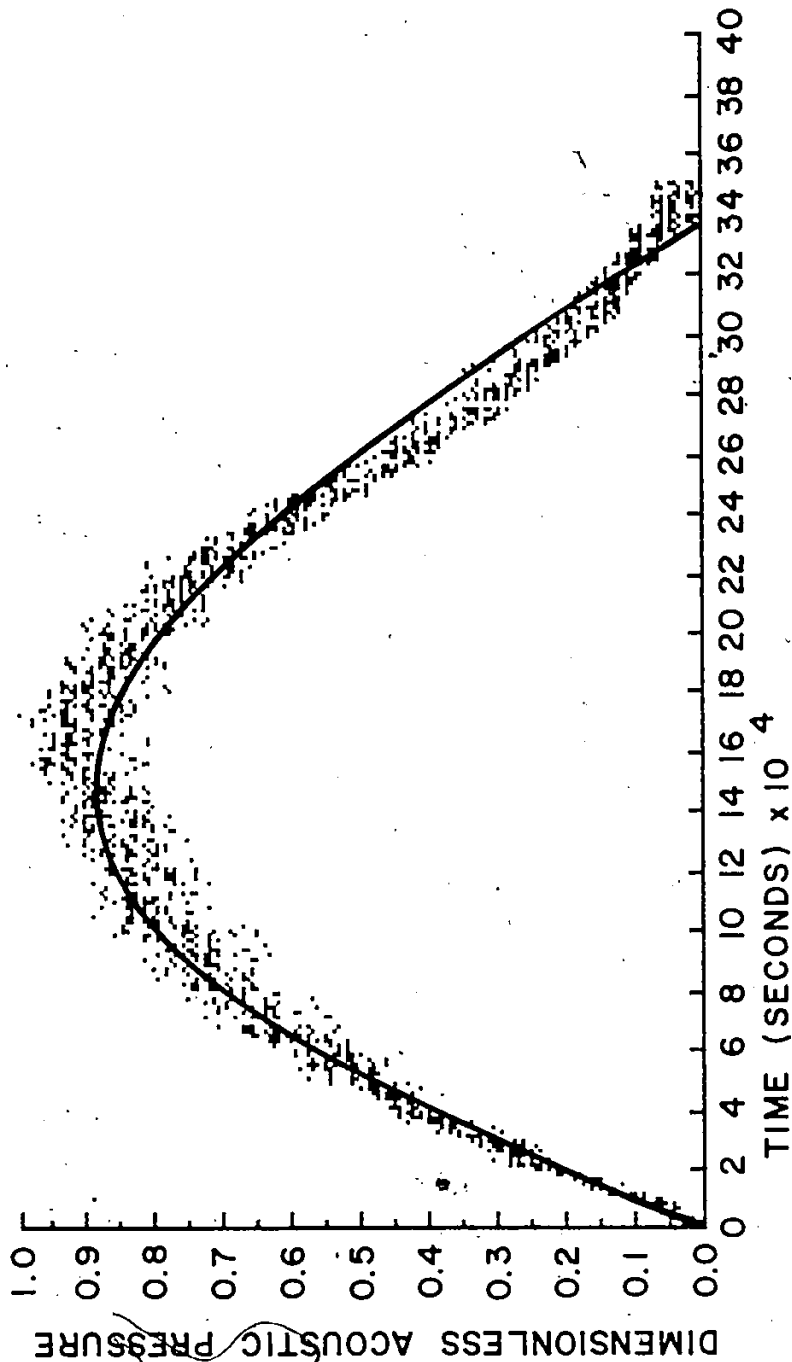


FIGURE 32. GRAPH OF DIMENSIONLESS ACOUSTIC PRESSURE VERSUS TIME, SAMPLED AT LOCATION 1 NEAR THE EXHAUST PORT FOR AN ENGINE SPEED OF 2000 RPM, TAPE SECTION 1.3

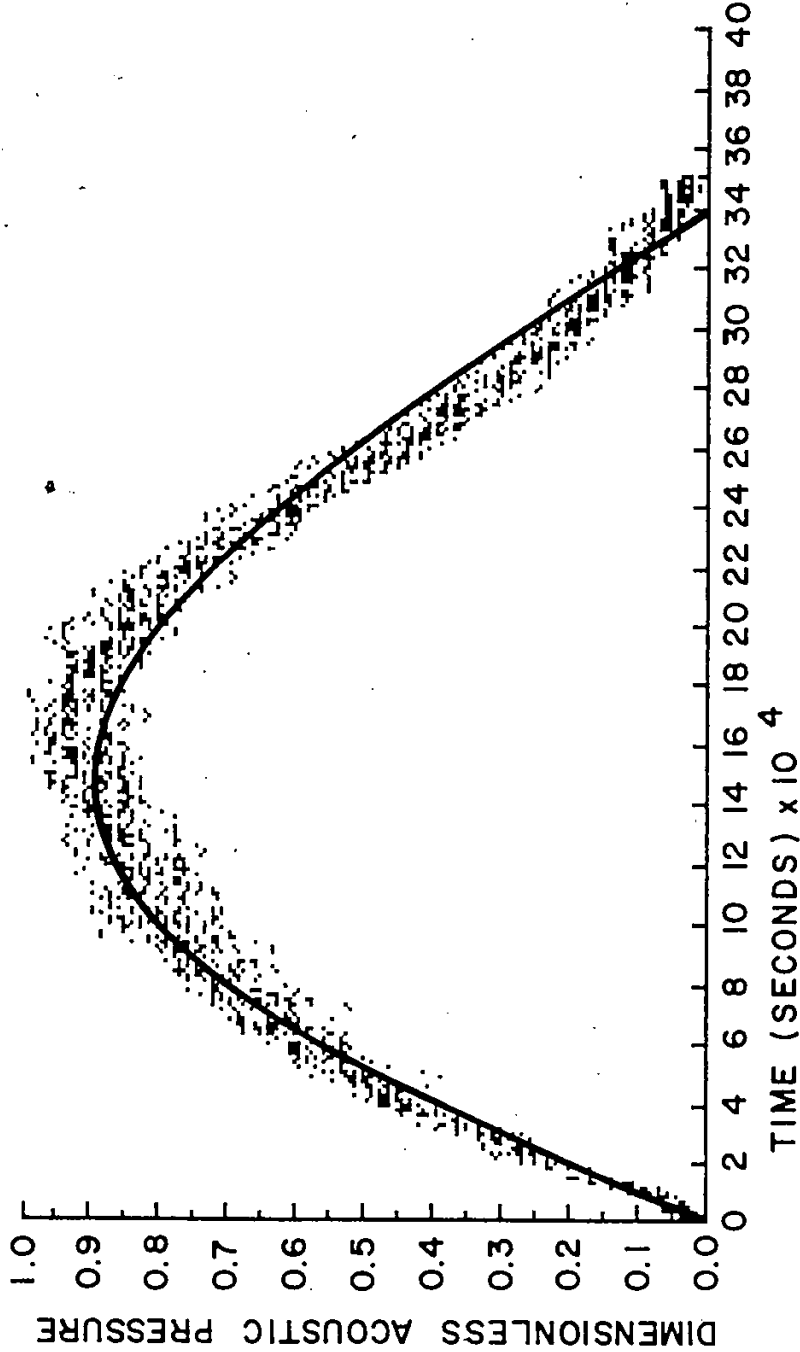


FIGURE 33. GRAPH OF DIMENSIONLESS ACOUSTIC PRESSURE VERSUS TIME, SAMPLED AT LOCATION 1 NEAR THE EXHAUST PORT FOR AN ENGINE SPEED OF 2000 RPM, TAPE SECTION 1.4

and 0.003 respectively. The four figures were included to illustrate a point in opposition to the observations on light load performance of rotary engines discussed by Kohno et al. The authors have observed that this operating range exhibits a consistent miss-fire sequence; however, by inspection of all of the data presented, no great variation in data scatter can be observed even when the results of one engine speed are compared with any other.

It is evident, from an inspection of Figures 30, 31, 32 and 33, that there is considerable scatter in the data. This is particularly true near the peak of the pressure pulse. That is, each individual pressure pulse shows a marked variation in its pressure versus time behaviour when it was approaching its maximum value. It should be noted that the correlation curve fits best in the rising portion of the pressure data but that it does not fit as well in the falling pressure portion. In the last third of the pressure data, the shape can best be described as concave which is the opposite to that of the correlation curve which could best be described as convex. There are two possible reasons for the 'concave' nature of the pressure data. One possible reason is related to the rotor chamber blow-down when the flow is no longer choked; that is, after the peak of the pressure pulse has occurred. The decrease in pressure appears to follow a relationship of the form: $p \cdot t^n = \text{constant}$. Where n is a constant which is greater than one. This is similar to the polytropic equation of state for a tank emptying process.

The second explanation of the falling pressure behaviour is that there is an interaction with an expansion wave which is passing the measuring location at the same time. Although this does not appear to be as strong a possibility as the first suggestion, Figure 21 illustrates a change in the falling portion of the pressure pulse from the first to the second measuring location. As it happens, Figure 21 is the pressure versus time diagram for an engine speed of 2000 rpm. The lower curve

of Figure 21 illustrates the concave behaviour of the falling portion of the pressure pulse. However, the upper curve shows the same pressure pulse, one metre down the exhaust pipe, with a definite convex shape to the falling pressure portion of the curve. It must be noted here that, even with nonlinear wave propagation, although the rising pressure portion of a sinusoidal wave will distort, the shape of the falling pressure portion of the wave will always remain convex.

Figures 34, 35 and 36 present the results of three separate samples of the pressure pulse data at an engine speed of 2250. These samples were taken from analog recordings at tape sections 2.1, 2.2 and 2.3. In this case, there are noticeable differences in the scatter of the data. An inspection of Figure 34 reveals that the correlation curve does not fit through the centre of the rising portion of the data. Similar situations cannot be seen in Figures 35 and 36; however, it appears that the data scatter is progressively reduced from Figure 34 which visually appears to have the greatest scatter to Figure 36 which appears to have the least scatter. The variances computed for these three cases do not indicate full agreement with the visual appearance of the data. It is Figure 35 which has the greatest variance while Figure 36 has the least. Files 5, 6 and 7, which present the correlation results for Figures 34, 35 and 36 respectively, indicate that the maximum variation from the average value of the pseudofrequency (166.9 Hz) is only 2.1 Hz, the variation about the average value of the distortion coefficient (0.234) is 0.038 which is very large in comparison to that calculated for the previous samples. A possible explanation for this variation is that there is an interaction of the pressure pulse with a reflected wave form. A comparison of the computer calculated engine speeds shown in Files 5, 6 and 7 indicates that there is a variation in engine speed. However, with the present information, it is not possible to determine if this speed variation and subsequent changes in the wave interactions are responsible for the deviations noted.

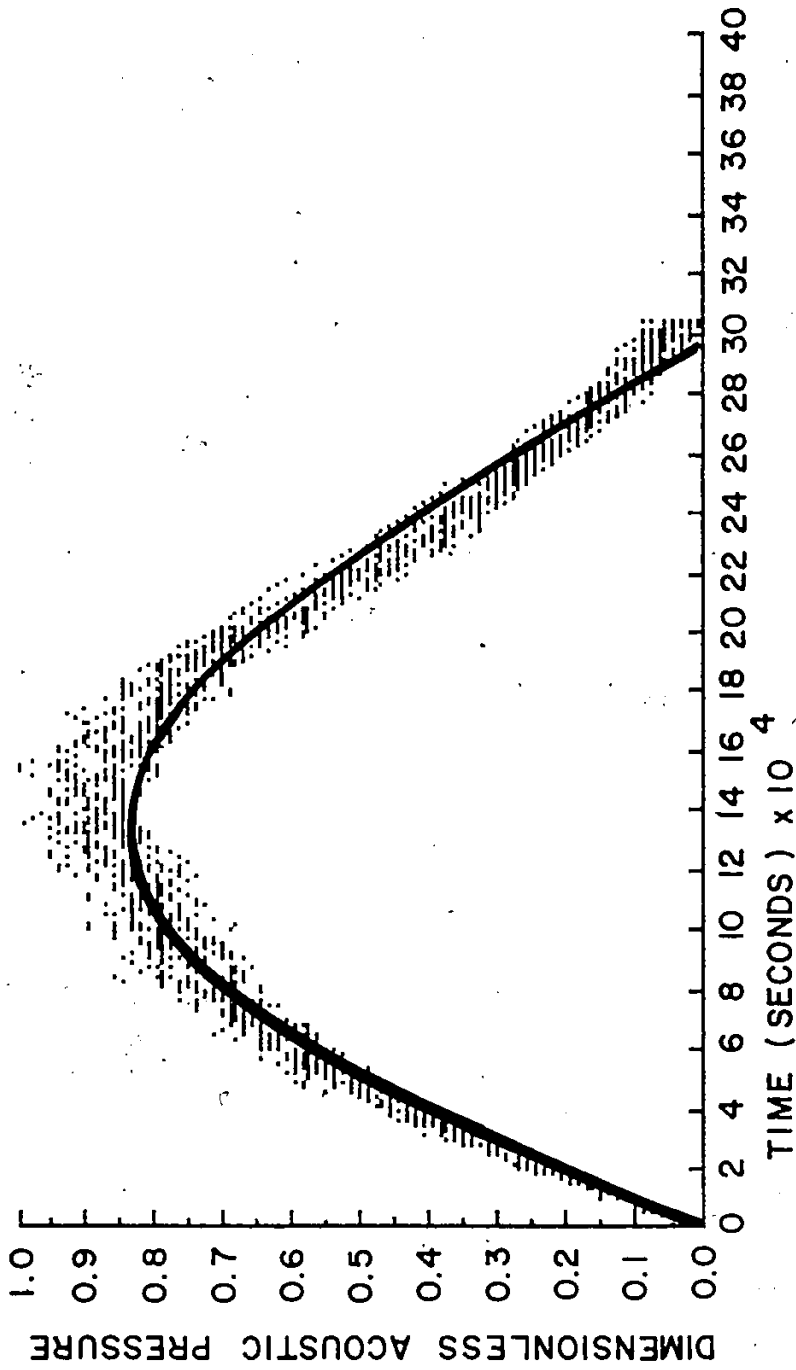


FIGURE 34. GRAPH OF DIMENSIONLESS ACOUSTIC PRESSURE VERSUS TIME, SAMPLED AT LOCATION 1 NEAR THE EXHAUST PORT FOR AN ENGINE SPEED OF 2250 RPM, TAPE SECTION 2.1

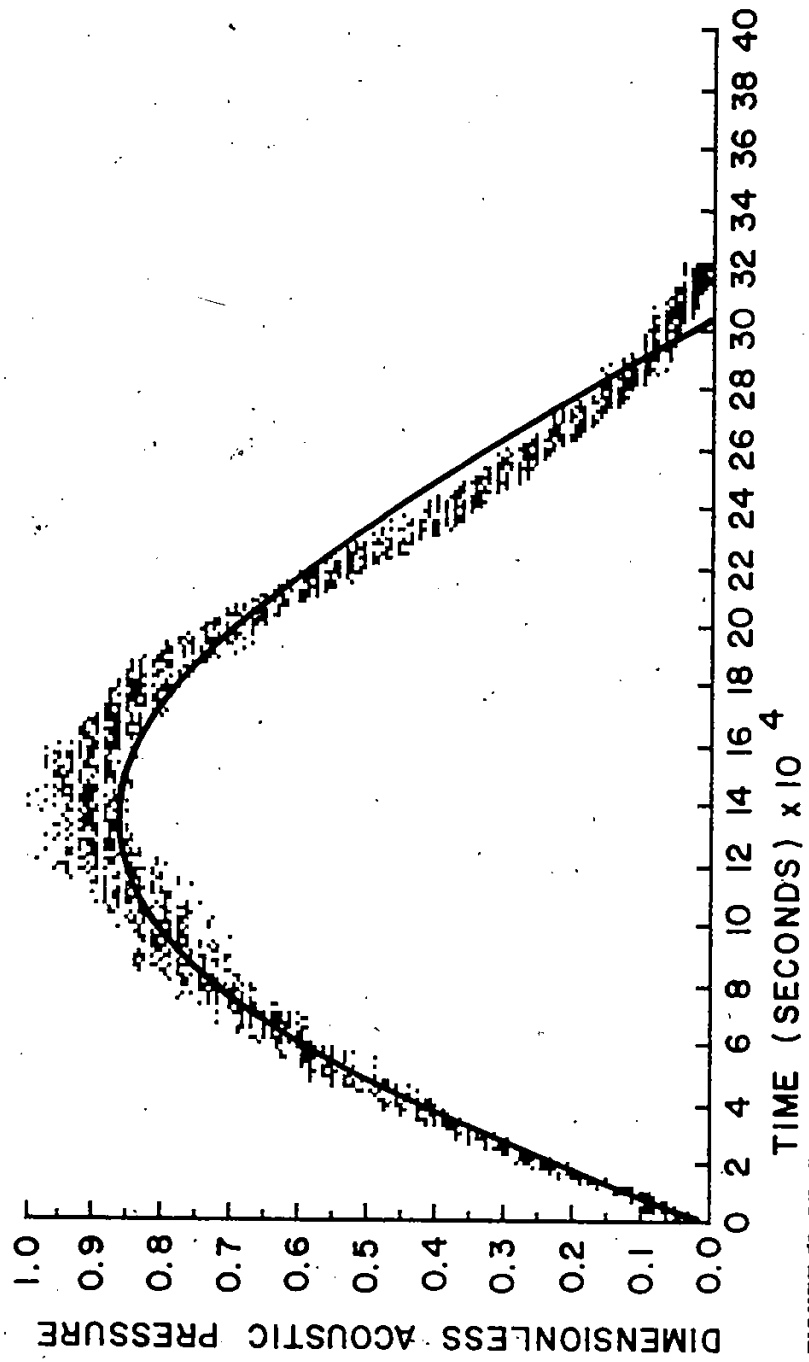


FIGURE 35. GRAPH OF DIMENSIONLESS ACOUSTIC PRESSURE VERSUS TIME, SAMPLED AT LOCATION 1 NEAR THE EXHAUST PORT FOR AN ENGINE SPEED OF 2250 RPM, TAPE SECTION 2.2

134

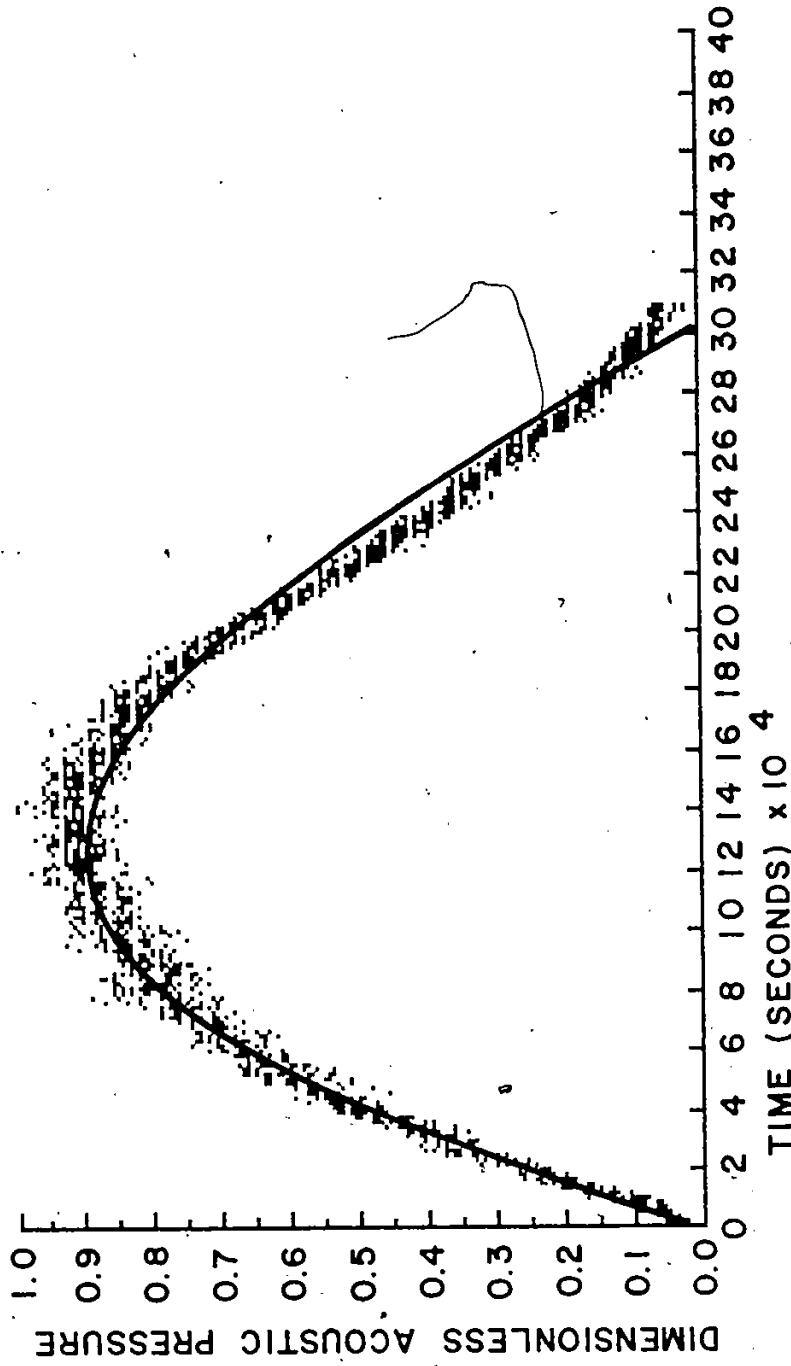


FIGURE 36. GRAPH OF DIMENSIONLESS ACOUSTIC PRESSURE VERSUS TIME, SAMPLED AT LOCATION 1 NEAR THE EXHAUST PORT FOR AN ENGINE SPEED OF 2250 RPM, TAPE SECTION 2.3

Figures 37 and 38 have been included to demonstrate that the problems that have just been discussed do not appear at an engine speed which is slightly higher. These samples were taken from the analog record at tape sections 3.1 and 3.2. Files 8 and 9 which are listed in Appendix V indicate that the correlation of both sets of data with the pressure pulse model is 0.990. The computed pseudofrequencies are within 1.7 Hz of each other; however, the difference between the two distortion coefficients is 0.033. As difference between the distortion coefficients is high, there should be some observable differences in the pressure data. To facilitate this study, one figure was laid on top of the other and inspected with the aid of rear illumination. The information revealed by this inspection was that there were no visually observable differences in the rising portion of the pressure data. The correlation curves in this section of data appear to be indistinguishable. It is only at the peak of the pressure curve and in the falling pressure portion of the data that the correlation curves differ. A possible explanation of the difference in distortion coefficients is that any deviation in the falling pressure data may have a large influence on the calculated value of the distortion coefficient. A possible solution to this problem is to increase the number of waves sampled while proportionally reducing the number of individual data points.

The Figures 39, 40, 41, 42 and 43 have been included to demonstrate that the nonlinear pressure pulse model correlates well with arbitrary samples of data taken at various engine speeds. The best correlation of the samples presented is shown in Figure 39. It is not surprising that the correlation coefficient is 0.994, which was the highest correlation coefficient obtained. Other correlation data for this curve can be found in File 10 of Appendix V. Figures 40 and 41 are included in the sample as they are for engine speeds near 3000 and 4000 rpm. Thus Figure 40 is complimentary to Figures 17, 18 and 22. Figure 41 is complimentary to Figures 19 and 23. Figures 42

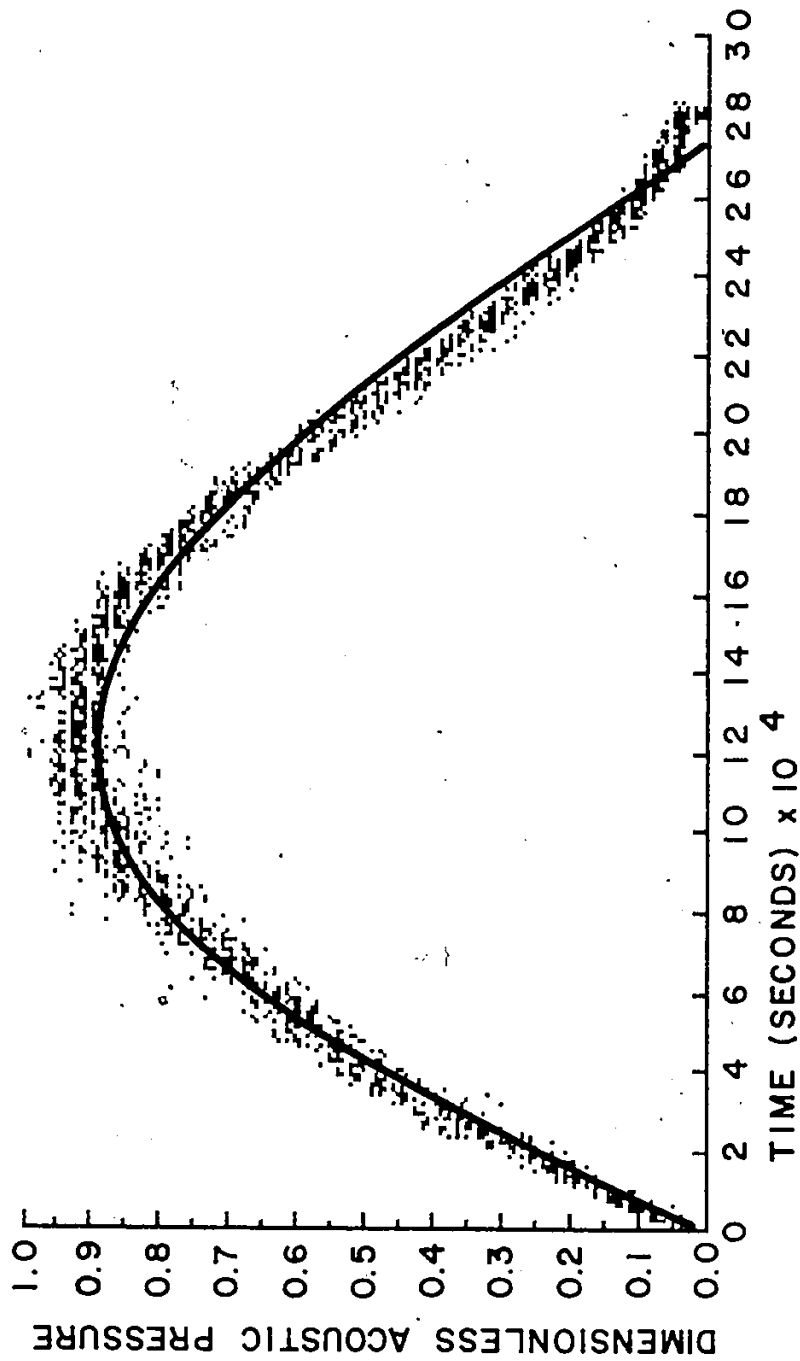


FIGURE 37. GRAPH OF DIMENSIONLESS ACOUSTIC PRESSURE VERSUS TIME, SAMPLED AT LOCATION 1 NEAR THE EXHAUST PORT FOR AN ENGINE SPEED OF 2510 RPM, TAPE SECTION 3.1

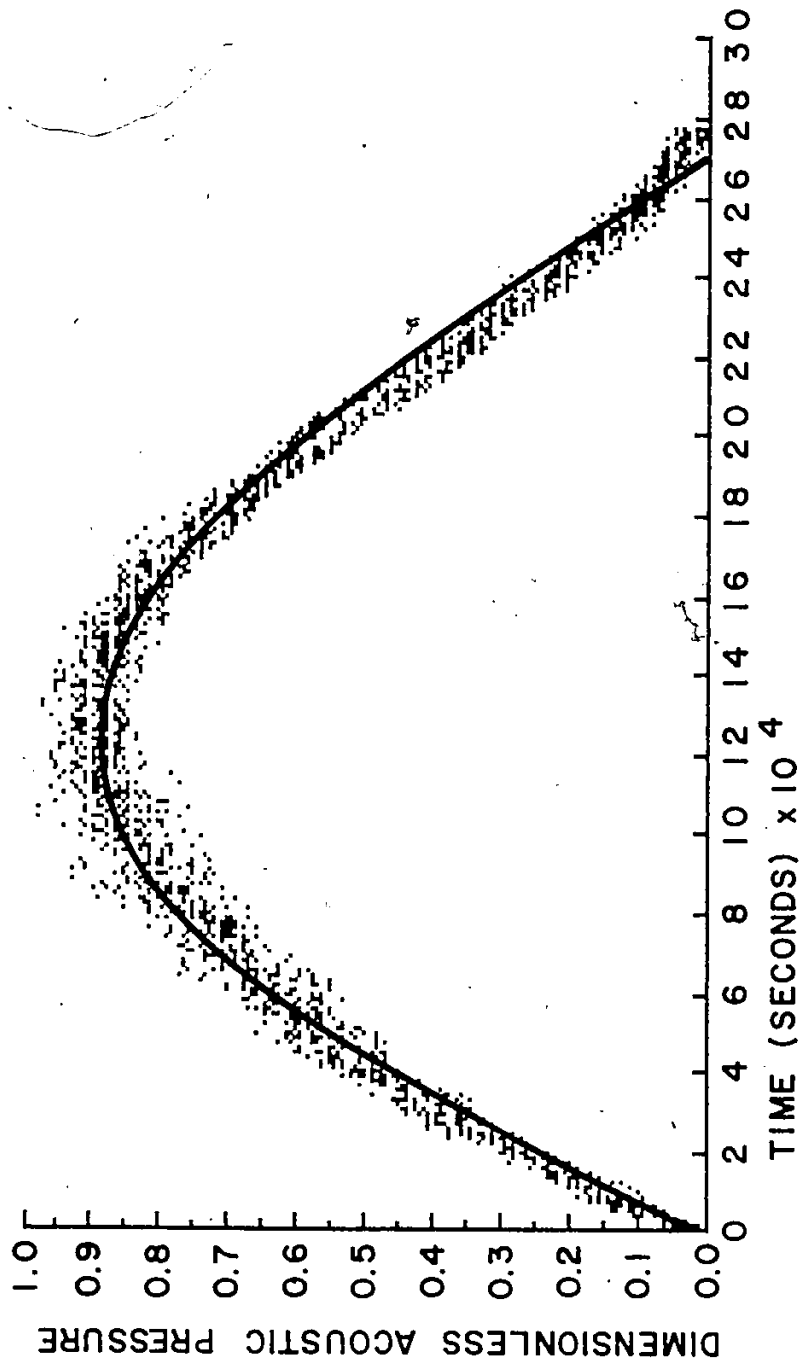


FIGURE 38. GRAPH OF DIMENSIONLESS ACOUSTIC PRESSURE VERSUS TIME, SAMPLED AT LOCATION 1 NEAR THE EXHAUST PORT FOR AN ENGINE SPEED OF 2510 RPM, TAPE SECTION 3.2

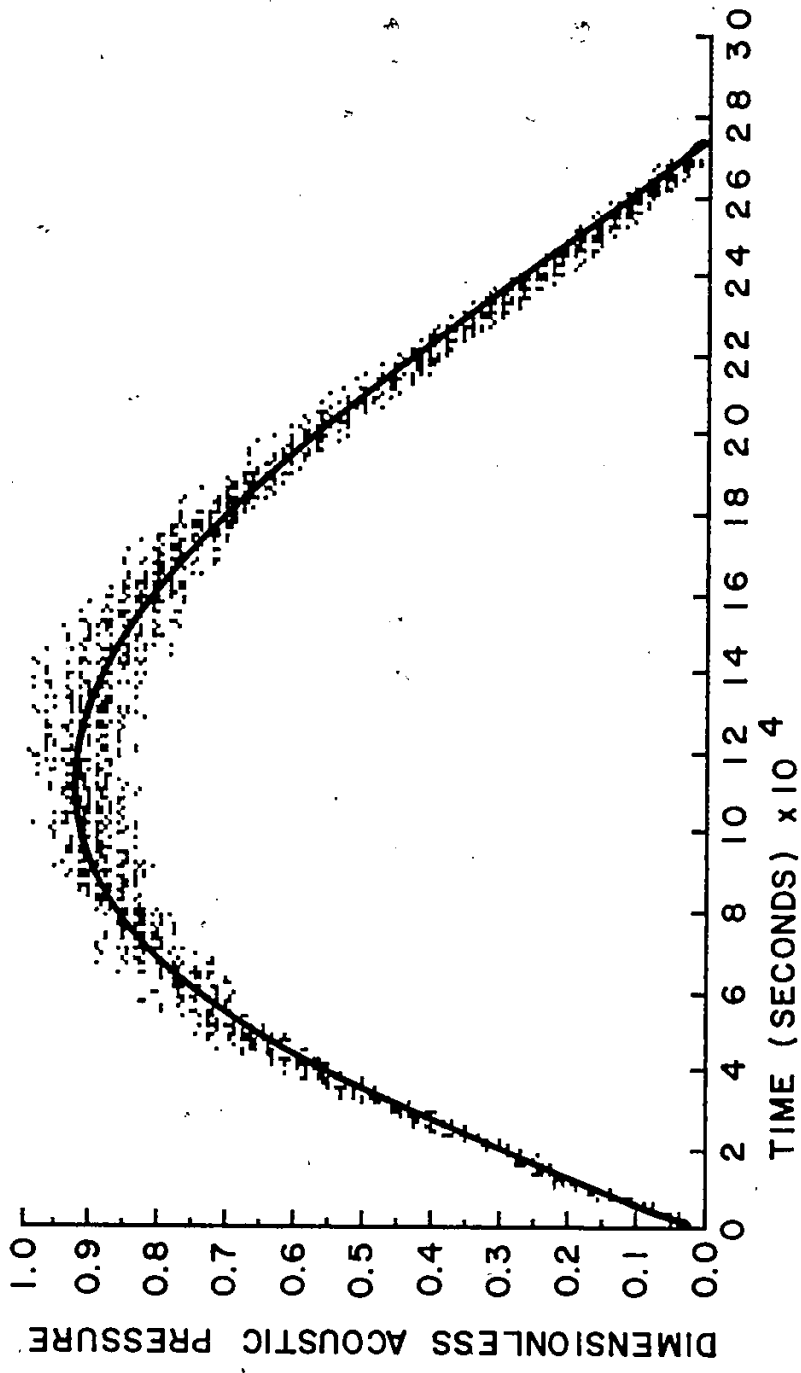


FIGURE 39. GRAPH OF DIMENSIONLESS ACOUSTIC PRESSURE VERSUS TIME, SAMPLED AT LOCATION 1 NEAR THE EXHAUST PORT FOR AN ENGINE SPEED OF 2730 RPM

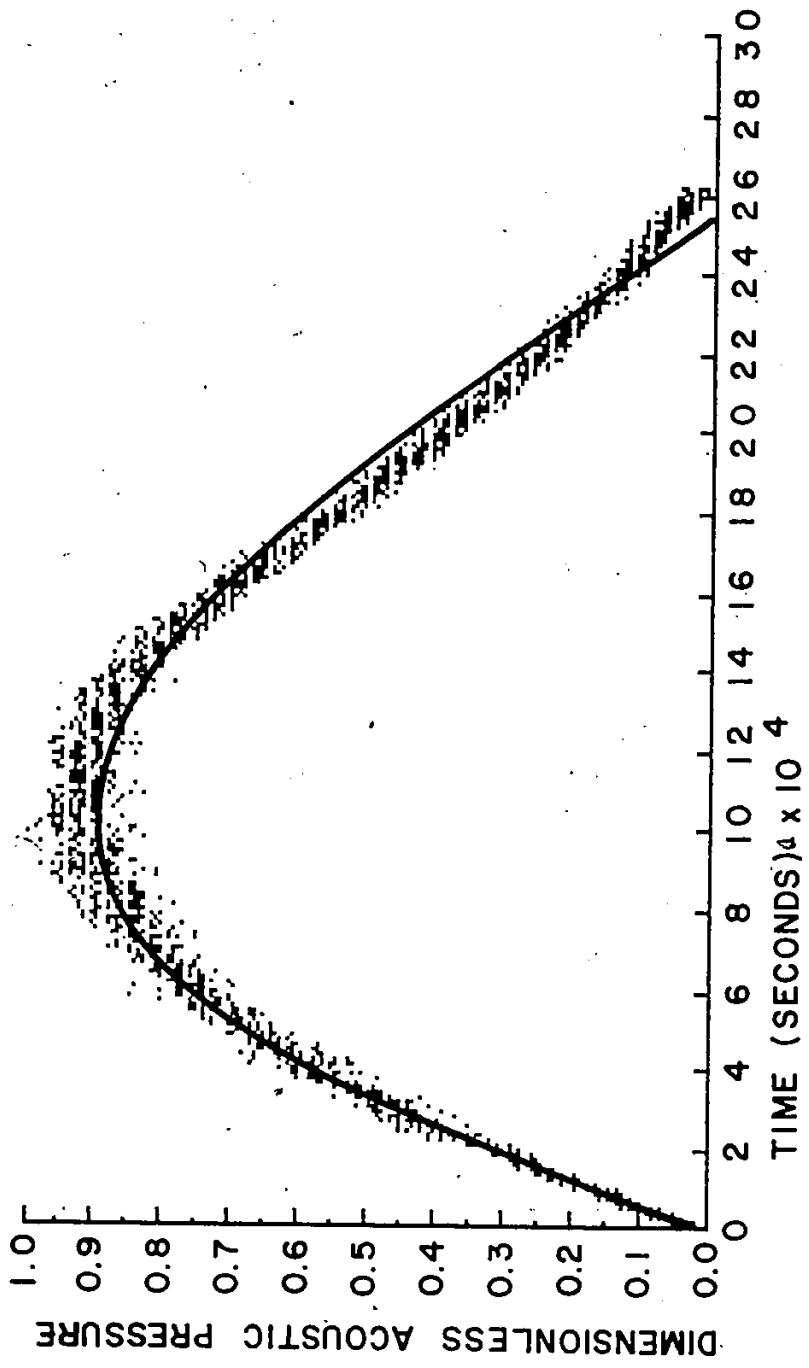


FIGURE 40. GRAPH OF DIMENSIONLESS ACOUSTIC PRESSURE VERSUS TIME, SAMPLED AT LOCATION 1 NEAR THE EXHAUST PORT FOR AN ENGINE SPEED OF 2980 RPM

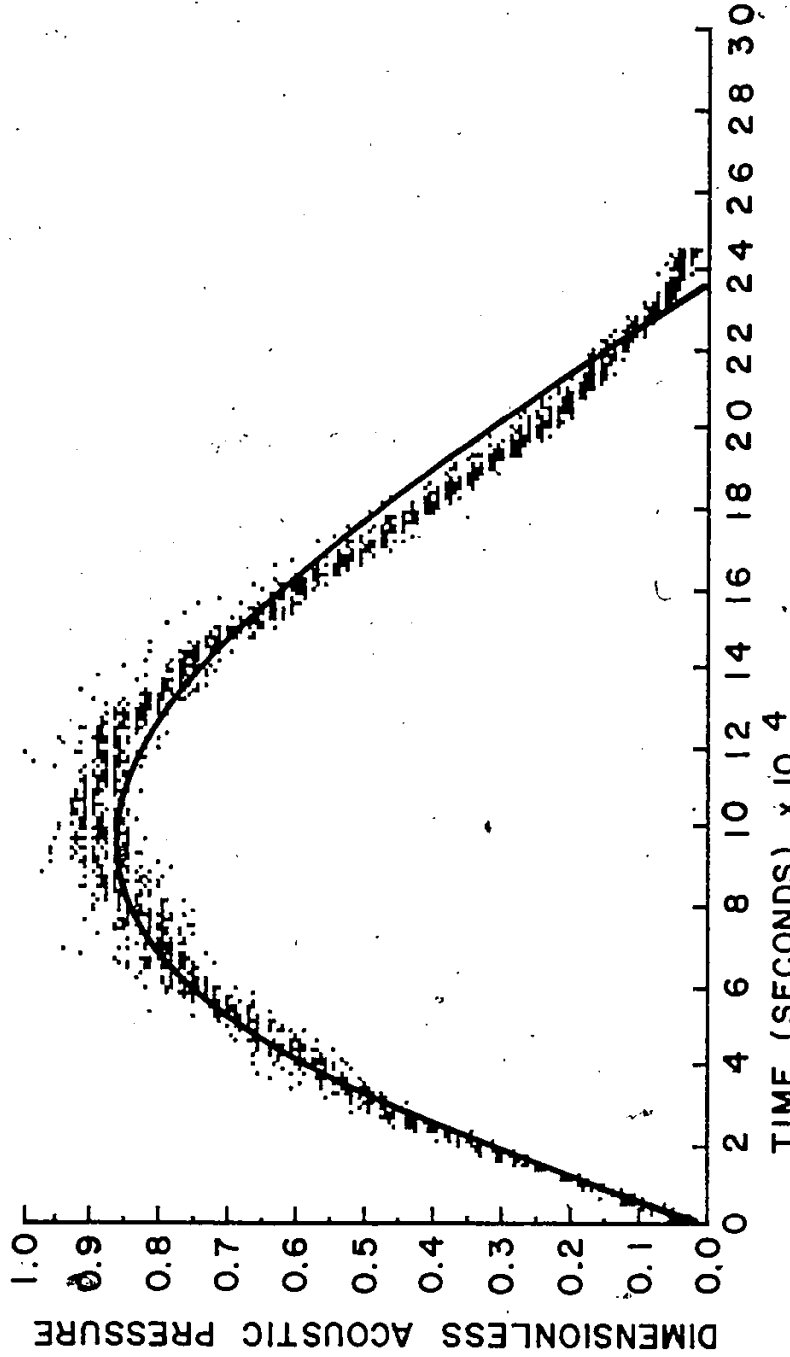


FIGURE 41. GRAPH OF DIMENSIONLESS ACOUSTIC PRESSURE VERSUS TIME, SAMPLED AT LOCATION 1 NEAR THE EXHAUST PORT FOR AN ENGINE SPEED OF 4020 RPM

87 KERC 134

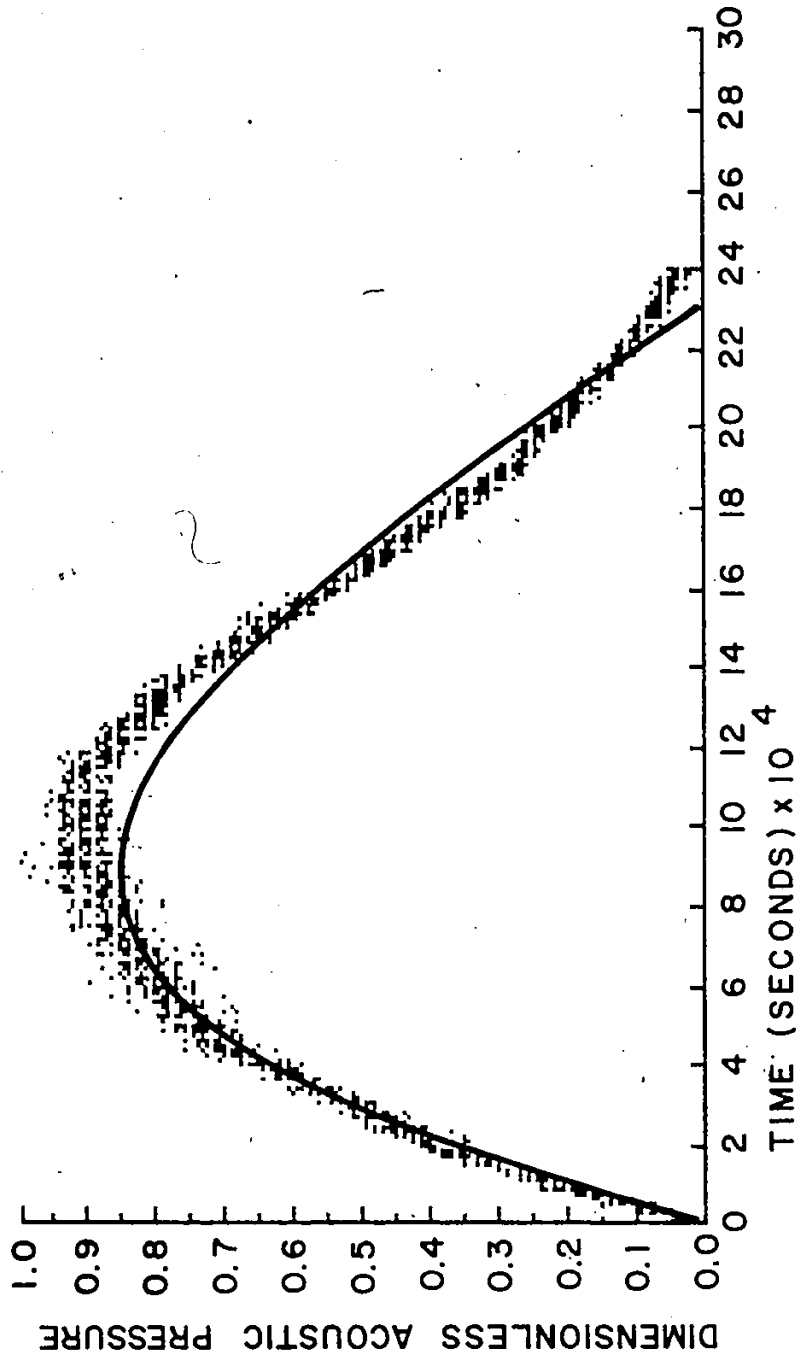


FIGURE 42. GRAPH OF DIMENSIONLESS ACOUSTIC PRESSURE VERSUS TIME, SAMPLED AT LOCATION 1 NEAR THE EXHAUST PORT FOR AN ENGINE SPEED OF 4250 RPM

and 43 illustrate the correlation of pressure data which has been taken at the start of peak amplitude variation, as is the case in Figure 42, and at the approximate point of greatest pulse amplitude deviation (see Figure 29). In each of these cases, the correlation coefficient is 0.988 which indicates that the model also works in this region.

The results of these correlations have been condensed for presentation in the next two figures. Figure 44 illustrates the variation of the calculated pseudofrequency with engine speed. An inspection of Figure 44 indicates that the data falls on a correlation curve which reaches a maximum of approximately 218 Hz. It is interesting to note that, if the pseudofrequencies at engine speeds of 2000, 3000, and 4000 rpm are compared with the results of the spectrum analyses for the same engine speeds, there is a pattern in the data. In the case of the 2000 rpm data, the average pseudofrequency of 149.2 Hz falls between the fourth harmonic at 131 Hz and fifth harmonic at 164 Hz. In the case of the 3000 rpm data, the pseudofrequency of 196.5 Hz is very close to the fourth harmonic at 200 Hz. Finally, in the case of the 4000 rpm data, the pseudofrequency of 212.4 Hz is also very close to the third harmonic at 204 Hz. In each case, the amplitudes in the spectra are less than the amplitude at the fundamental frequency.

The distortion coefficients were plotted against engine speed and have been presented in Figure 45. It can be seen that the data points are somewhat scattered; however, the straight line shown in the figure was determined to be the curve of best fit. The correlation indicates that the distortion coefficient increases with increasing engine speed. This suggests that the pressure pulse issuing from the exhaust port is increasingly distorted as the engine speed increases. Thus the distance through which the pulse must travel before it becomes a discontinuity will decrease.

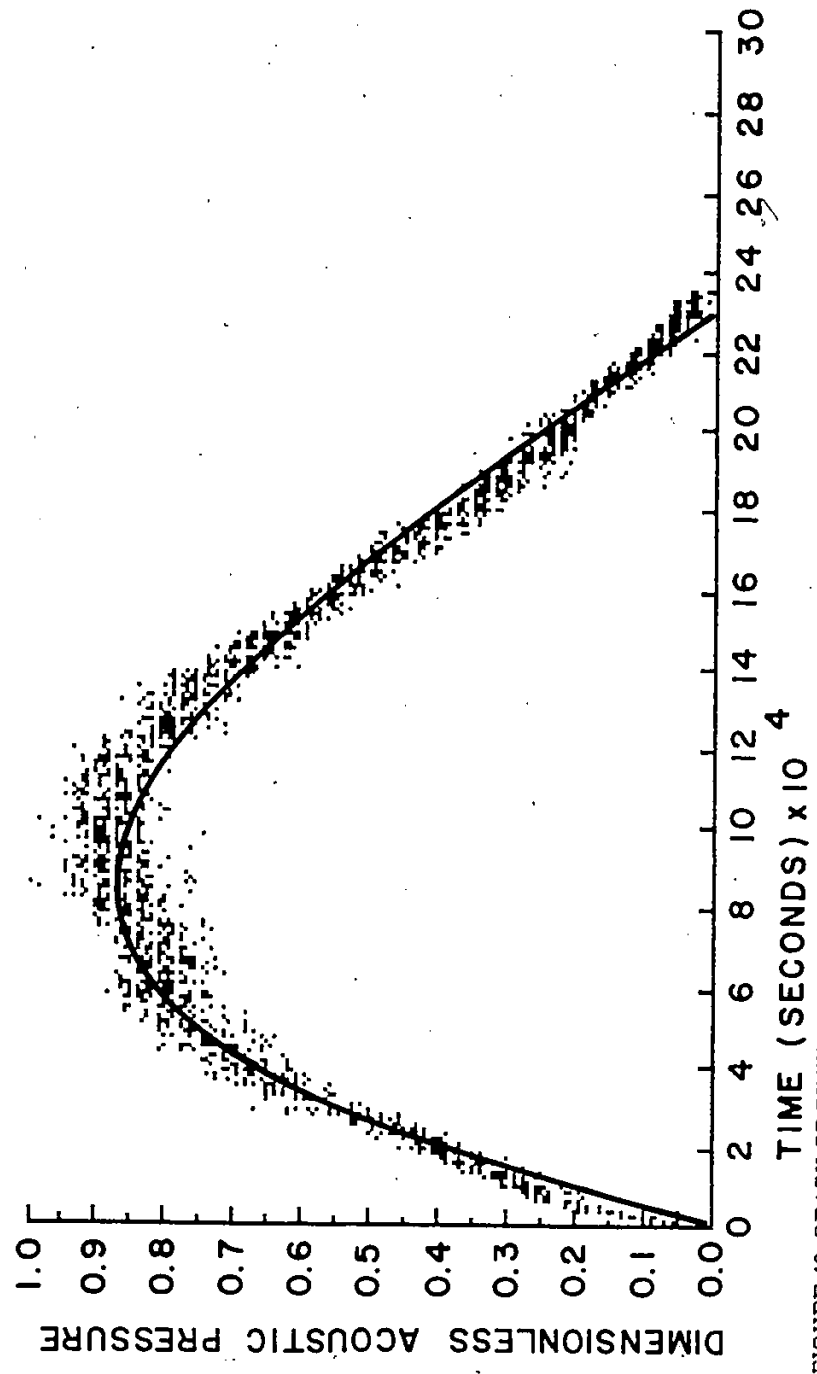


FIGURE 43. GRAPH OF DIMENSIONLESS ACOUSTIC PRESSURE VERSUS TIME, SAMPLED AT LOCATION 1 NEAR THE EXHAUST PORT FOR AN ENGINE SPEED OF 4760 RPM

131-REV 24

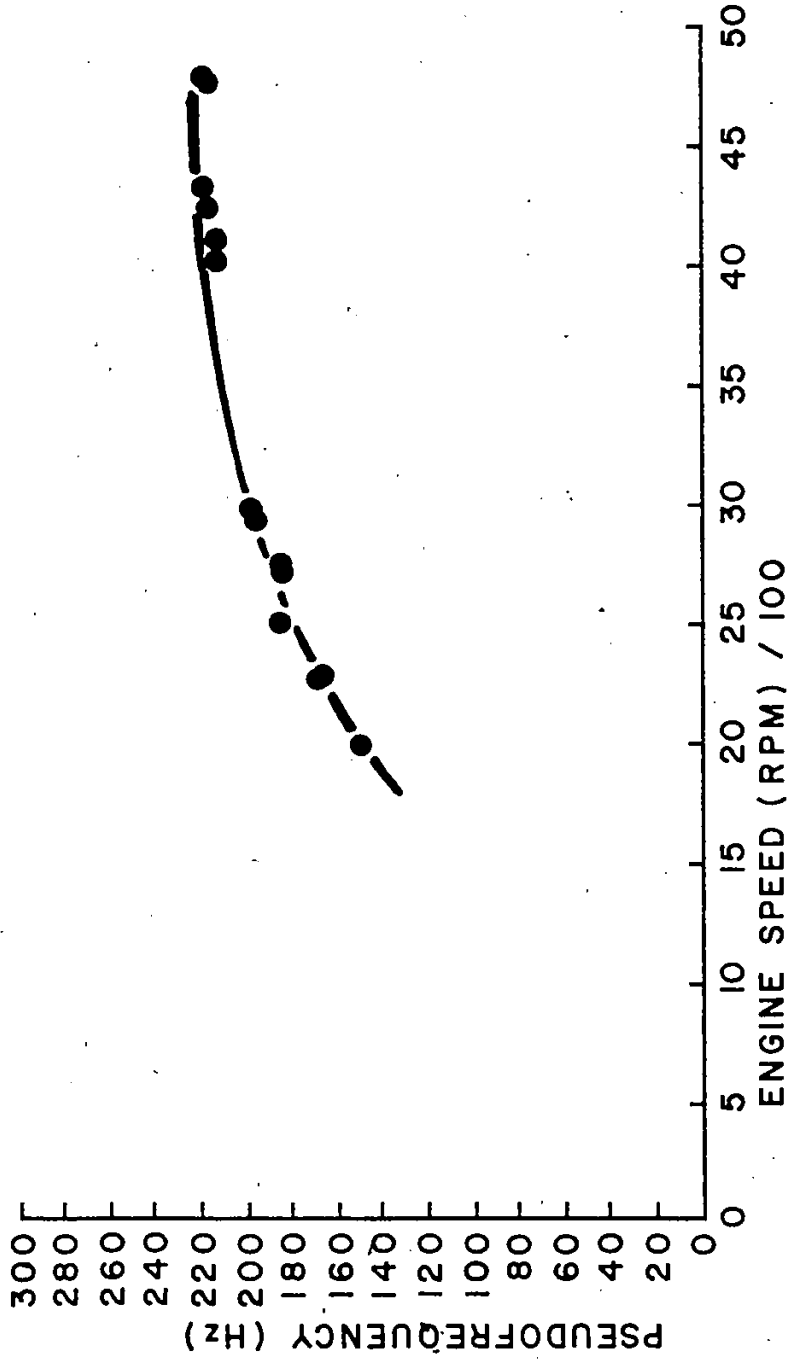


FIGURE 44. GRAPH OF PRESSURE PULSE PSEUDOFREQUENCY VERSUS ENGINE SPEED

PIST COEF. VS RPM REF #2 1-7-41

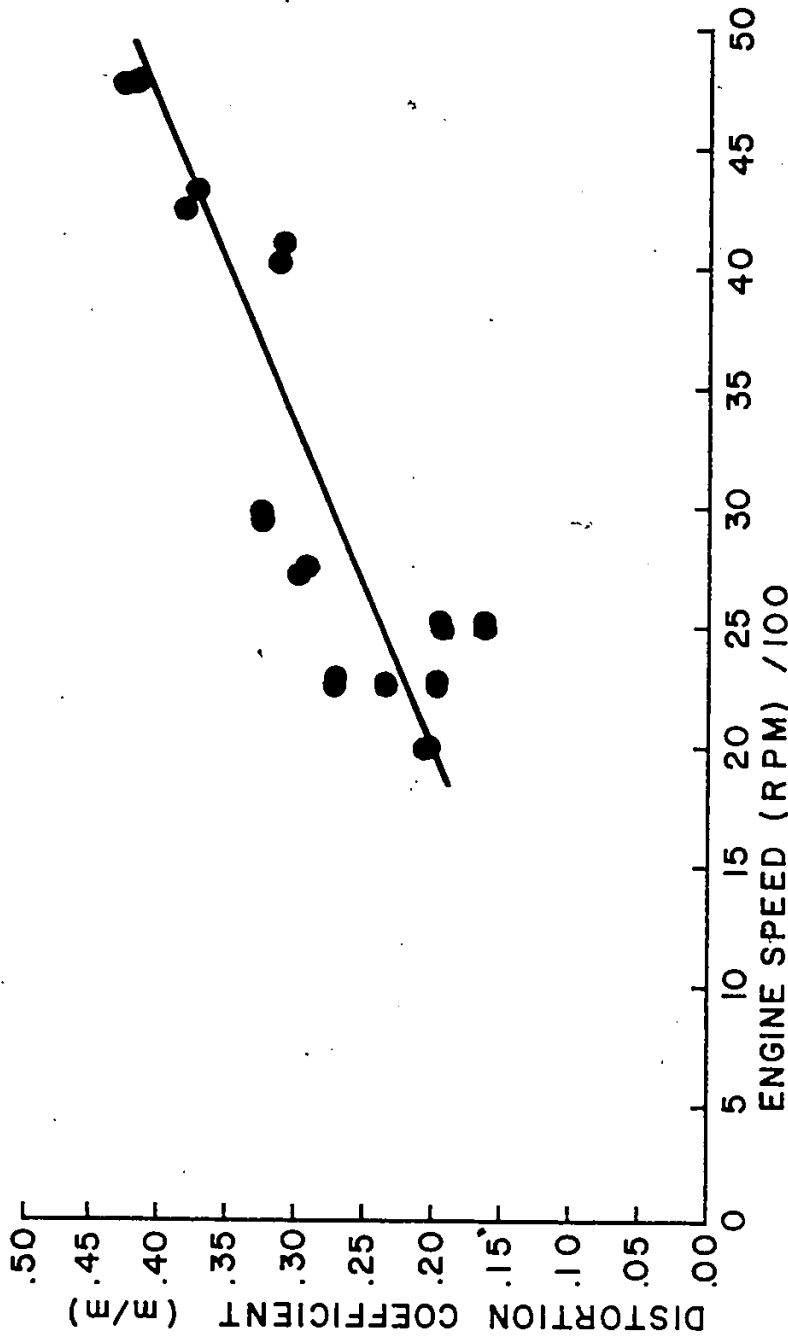


FIGURE 45. GRAPH OF DISTORTION COEFFICIENT VERSUS ENGINE SPEED

6.5 Predicting the Discontinuity Distance

It is possible to determine the discontinuity distance or the distance for a sinusoidal pulse to distort into a shock by making use of Equation 50. To make use of this equation it is necessary to determine the ratio of specific heats, γ , for the gas, the peak particle velocity of the wave, u_p , the angular frequency of the wave, ω , and the mean speed of sound in the gas, c_0 . In the case of the specific heat ratio, the value used was that of 1.4 which is for air. In the case of the peak particle velocity, Equation 73 was rearranged to solve for the particle velocity in terms of the acoustic pressure, the mean density of the gas and the mean speed of sound in the gas. The relationship for the isentropic speed of sound as a function of absolute temperature was substituted for the speed of sound. The ideal gas equation of state was used to substitute for the mean gas density and the angular velocity was replaced by the product of $2\pi f$. Simplification yielded the following equation:

$$l = [\gamma/(\gamma+1)] * 20.04 * T^{1/2}/(\pi f * P_{relative}) \quad \text{Eqn. 96}$$

The value of the discontinuity length was then determined as a function of engine speed, s , by substituting the correlation equations for the average absolute gas temperature, which was determined to be:

$$T = 300.6 * \ln(s) - 1951.9 \text{ } ^\circ\text{C} \quad \text{Eqn. 97}$$

the pseudofrequency, which was determined to be:

$$f = c_0 - c_1*s + c_2*s^2 - c_3*s^3 + c_4*s^4 - c_5*s^5 \quad \text{Eqn. 98}$$

where: $c_0 = 773.5$, $c_1 = -1.459$, $c_2 = 1.1598\text{E-}03$, $c_3 = -4.1472\text{E-}07$,

$c_4 = 6.9718\text{E-}11$, $c_5 = -4.4822\text{E-}15$.

and the relative average peak pressure in the exhaust pipe, which was found to be:

$$P_{\text{relative}} = 1.1005E-05 * s - 0.09099 \quad \text{Eqn. 99}$$

The results of these calculations are shown in Figure 46. The graph shows that a shock should not be present in the exhaust pipe for engine speeds up to at least 5000 rpm. At this point it should be remembered that the relative average peak pressure is not the same as the relative peak pressure. To correct for this difference, a cumulative average of the average peak pressures determined by the correlation program, were used. The results of this correction were plotted in Figure 47. It can be seen that this correction has very little effect on the position of the curve.

There is one more correction which must be made. It has already been noted that the exhaust pressure pulse is distorted when it leaves the exhaust port. Therefore, it is necessary to also take this into account when a determination of the location in the exhaust pipe where a shock should occur is desired. To determine this length as a function of engine speed, all that is necessary is to multiply the values of Figure 47 by the value of one minus the distortion coefficient. The correlation relationship for the distortion coefficient as a function of engine speed, s , was:

$$x/l = 7.476E-05 * s + 0.5207 \quad \text{Eqn. 100}$$

These values have been plotted in Figure 48. An inspection of this graph indicates that a shock should be detected at the second measuring location at an engine speed of approximately 3600 rpm. A careful inspection of Figure 26 indicates that this is possible.

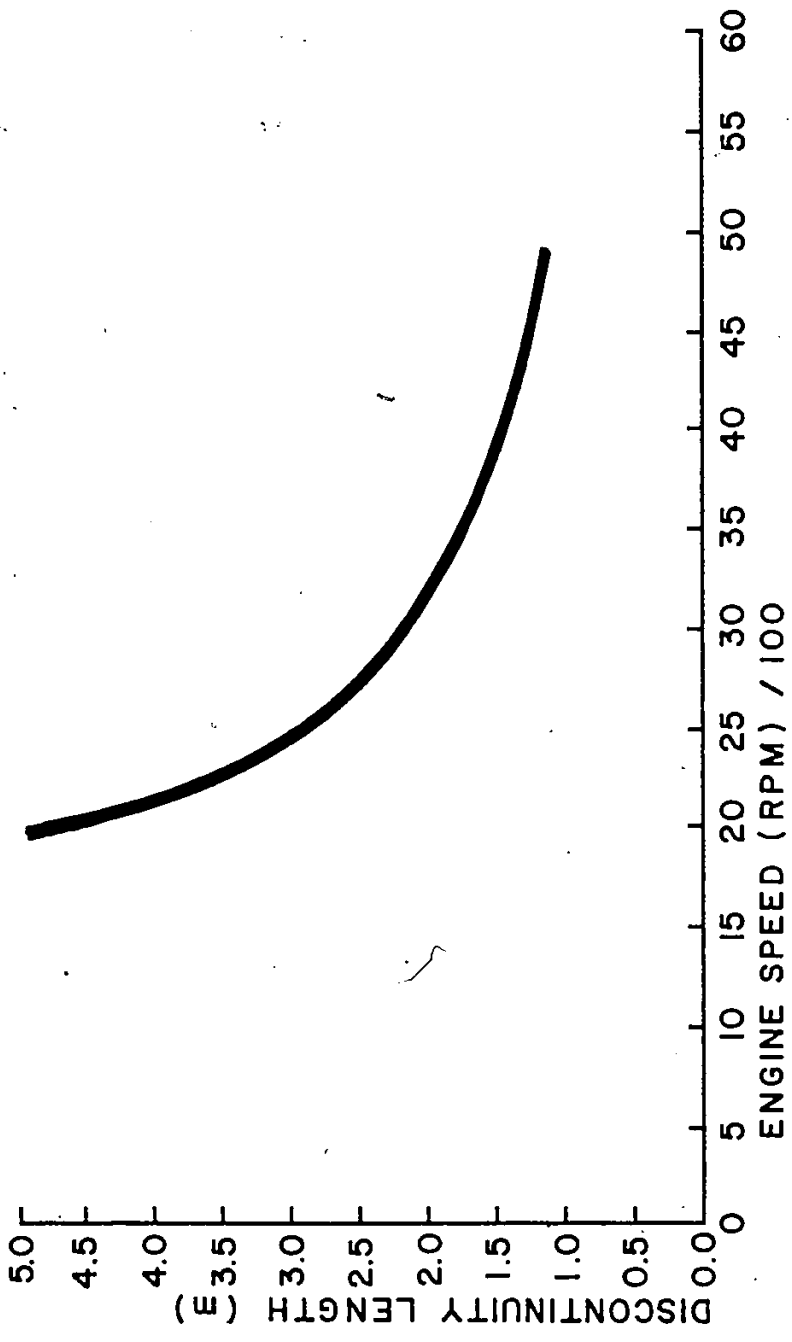


FIGURE 46. GRAPH OF PREDICTED DISCONTINUITY LENGTH VERSUS ENGINE SPEED, USING AVERAGE PRESSURE PULSE AMPLITUDE

DISCONTINUITY LENGTH (m) 117

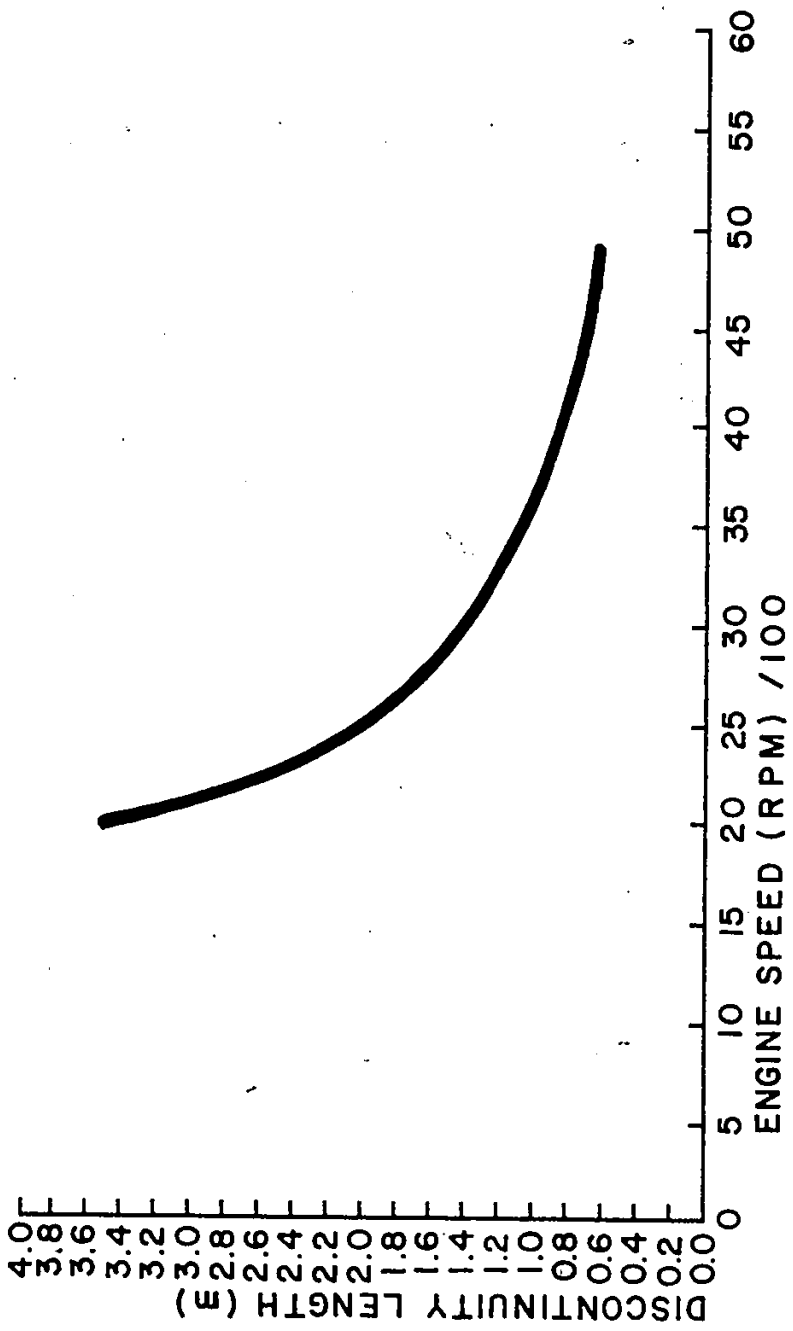


FIGURE 48. GRAPH OF PREDICTED DISCONTINUITY LENGTH VERSUS ENGINE SPEED, WHEN CORRECTED FOR INITIAL PRESSURE PULSE DISTORTION AND PEAK PULSE PRESSURE

VII. CONCLUSIONS

The following conclusions have been reached after studying the results of the experiments, the computer correlations and the predictive curves which were generated by the application of the nonlinear pressure pulse model:

1. The pressure relationship, which is an extension of the Fubini-Ghiron theoretical solution for particle velocity, has been proven to correlate very highly with the experimentally measured data.
2. By using the discontinuity length equation and the regression equations which fit the experimental data, it is possible to predict the position where a shock should occur in a straight exhaust pipe.
3. The study of pressure pulse behaviour in the exhaust gas requires exhaust systems with the instrumentation at locations where the greatest information may be gathered. The most likely locations, for these measurements can now be estimated by applying the procedures used to produce the graph of Figure 48. In cases where there may be a number of exhaust pipe configurations to test, the best approach is to start with a straight exhaust pipe having a flow area which is comparable to that of the engine exhaust port.

VIII. RECOMMENDATIONS

The following recommendations are presented to provide a direction of study for future work:

1. A study should be made of the effect of exhaust pipe diameter and shape on shock development in exhaust gases.
2. A parallel study should be performed using a motored engine or a rotary valve and compressed air. This would reduce the effects of temperature variations in the gas. It should be noted that Blair [26] used this technique as a starting point in his investigations.
3. The possibility of increasing the memory area of the Apple computer should be investigated. The benefit of the increased memory would be the ability to sample more successive exhaust cycles of the engine.
4. The possibility of developing a two channel sampling method with a variable sampling interval should be investigated. This would allow the development of programs which could compare the pressure pulse behaviour between the two measuring locations. If this is possible, it would allow accurate measurements of the propagation time from one measuring location to another and it would no longer be necessary to determine time delays using a magnified measuring scale as was done in Figures 21, 22 and 23.

APPENDIX I
SAMPLING PROGRAMS

APPENDIX I
MAIN SAMPLING PROGRAM

The following program identified by the name "KLAATU" was used for the analog to digital sampling. It was written in APPLESOFT BASIC for implementation on an APPLE II+ computer which is a product of Apple Computer Inc.

```
1000 REM PROGRAM KLAATU ALLOWS MONITORING OF WAVEFORMS USING THE ANALOG  
TO DIGITAL CONVERSION OPTION  
1010 REM THE FOLLOWING ROUTINES BLOAD THE MACHINE LANGUAGE PROGRAMS  
FOR THE ANALOG TO DIGITAL SAMPLING PROCEDURE  
1020 D$ = CHR$(4)  
1050 PRINT D$;"BLOAD BIGSAMPLE"  
1060 PRINT D$;"BLOAD MAXGR"  
1070 PRINT D$;"BLOAD ADD7$345"  
1080 HIMEM: 8080  
1090 DIM A%(300)  
1100 DIM M(40),P(40)  
1110 INPUT "HIT RETURN TO SAMPLE FROM TAPERECORDER";B$  
1120 BEG = 16384:FINISH = 38400  
1130 POKE 8083,81  
1140 POKE 8084,00  
1150 POKE 8085,64
```

1160 CALL 8080
1170 POKE 251,00: POKE 252,64: POKE 253,00: POKE 254,150
1180 CALL 773
1190 PLACE = PEEK (769) * 256 + PEEK (768)
1200 MAZ = PEEK (770)
1210 PRINT MAZ,PLACE
1220 POKE 251,00: POKE 252,64: POKE 253,00: POKE 254,150
1230 IF (FINISH - PLACE) IS LESS THAN 270 GOTO 1120
1240 IF (PLACE - BEG) IS LESS THAN 270 GOTO 1120
1250 CALL 837
1260 SUM = PEEK (836) * 256 * 256 + PEEK (835) * 256 + PEEK (834)
1270 SAMPLES = PEEK (832) + PEEK (833) * 256
1280 AVG = SUM / SAMPLES
1290 PRINT "DO YOU WANT TO REPEAT SAMPLING RUN ? Y/N"
1300 KX = PEEK (- 16384): POKE - 16368,0
1310 IF KX IS GREATER THAN 127 GOTO 1330
1320 GOTO 1300
1330 IF KX IS EQUAL TO 217 GOTO 1120
1340 PRINT "AVG ";AVG: PRINT "SUM ";SUM
1350 PRINT "SAMPLE NO. ";SAM
1360 INPUT "ENGINE RPM = ";RP
1370 RQ = INT (60 / RP / 19.55E - 6)
1380 INPUT "% OF LEADING WAVE ";W%
1385 INPUT "DRIVE NUMBER FOR DATA STORAGE ";DR
1390 FRQ = RP
1400 FOR I = PLACE TO BEG STEP - 1
1410 IF PEEK (I) IS LESS THAN AVG THEN ZERO = I: GOTO 1430


```
1420 NEXT I
1430 DOUBLE = 2 * (PLACE - ZERO)
1440 DF = PLACE - DOUBLE
1450 MIZ = PEEK (DF):P2 = DF
1460 FOR I = DF TO PLACE
1470 IF PEEK (I) IS LESS THAN MIZ THEN MIZ = PEEK (I):P2 = I
1480 NEXT I
1490 IF ZZ IS NOT EQUAL TO 2 THEN CD = P2 .
1500 NUM = PLACE - P2
1510 MO% = (279 - NUM) / 2
1520 ST = INT (P2 - MO% * W% / 100)
1530 FOR I = ST TO ST + 279
1540 A%(CT) = PEEK (I)
1550 CT = CT + 1
1560 NEXT
1570 HGR
1580 HCOLOR 3 .
1590 CT = 279
1600 FOR I = 0 TO CT
1610 HPLOT I,159 - A%(I) / 2
1620 NEXT
1630 FOR I = 0 TO 279 STEP 3
1640 HPLOT I,159 - MIZ / 2: HPLOT I,159 - MAZ / 2
1650 NEXT
1660 FOR I = 159 - MIZ / 2 - 5 TO 159 - MIZ / 2 + 5
1670 HPLOT MO% * W% / 100,I
1680 NEXT
```

```
1700 VTAB 21: CALL - 958
1710 HTAB 18
1720 VTAB 21: CALL - 958
1730 IF ZZ IS EQUAL TO 2 THEN PRINT "WAVE ";W
1740 HTAB 10
1750 VTAB 22
1760 IF ZZ IS EQUAL TO 2 THEN PRINT "ADDRESS ";P(W);" MAX. ";M(W)
1770 FOR I = 0 TO 279
1780 H PLOT I,159 - AVG / 2: NEXT
1790 VTAB 3: HTAB 10: PRINT "EXHAUST PRESSURE WAVE"
1800 IF ZZ IS NOT EQUAL TO 2 THEN VTAB 2: HTAB 17: PRINT "MAXIMUM"
1810 IF ZZ IS NOT EQUAL TO 2 THEN HTAB 10: VTAB 20: PRINT "ADDRESS ";PLACE;"
MAX ";MAZ
1820 FOR I = 0 TO 10:OP = INT (I * 25.575)
1830 FOR J = - 3 TO 3: H PLOT OP,(159 - AVG / 2) + J: NEXT J,I
1850 HTAB 7: VTAB 23: PRINT "ESTIMATED ENGINE SPEED = ";RP
1860 IF ZZ IS NOT EQUAL TO 2 GOTO 2050
1870 MX = A%(0):MN = A%(0)
1880 PX = 0:PN = 0
1890 FOR I = 0 TO 279
1900 IF A%(I) IS GREATER THAN MX THEN PX = I + 1:MX = A%(I)
1910 IF I IS EQUAL TO 279 GOTO 1930
1920 IF A%(I) IS LESS THAN MN AND A%(I + 1) IS GREATER THAN A%(I) THEN PN
= I + 1:MN = A%(I)
1930 IF I IS EQUAL TO 0 GOTO 1960
1940 IF I IS GREATER THAN PX GOTO 1960
1950 IF A%(I - 1) IS LESS THAN AVG AND A%(I) IS EQUAL TO OR IS GREATER THAN
```

```
AVG THEN ZE = I + 1
1960 NEXT
1961 D$ = CHR$ (4)
1970 PRINT D$;"OPEN FREQ(";FRQ;"")/";W;"",D";DR
1980 PRINT D$;"DELETE FREQ(";FRQ;"")/";W
1990 PRINT D$;"OPEN FREQ(";FRQ;"")/";W
2000 PRINT D$;"WRITE FREQ(";FRQ;"")/";W
2010 PRINT PX: PRINT ZE: PRINT PN
2020 PRINT MAZ: PRINT MX: PRINT AVG: PRINT MN
2030 FOR I = 0 TO 279: PRINT A%(I): NEXT
2040 PRINT D$;"CLOSE FREQ(";FRQ;"")/";W
2045 FW = W
2050 IF ZZ IS EQUAL TO 2 THEN RETURN
2060 TEMP = BEG
2070 FOR W = 1 TO 40
2080 M(W) = PEEK (TEMP):P(W) = TEMP
2090 FOR I = TEMP TO TEMP + RQ
2100 IF PEEK (I) IS GREATER THAN M(W) THEN M(W) = PEEK (I):P(W) = I
2110 NEXT I
2120 IF W IS EQUAL TO OR IS GREATER THAN 2 THEN RP = INT (60 / ((P(W) - P(W
- 1)) * 19.55E - 06))
2130 TEMP = P(W) + INT (RQ / 2)
2140 PLACE = P(W): IF (PLACE - BEG) IS LESS THAN 270 THEN TEMP = TEMP + RQ:
GOTO 2070
2145 IF TEMP + RQ IS GREATER THAN FINISH THEN VTAB 21: CALL - 958
2150 IF TEMP + RQ IS GREATER THAN FINISH THEN VTAB 23: HTAB 13: PRINT "END
OF SAMPLES"
```

```
2160 IF TEMP + RQ IS GREATER THAN FINISH THEN RP = INT (60 * (W - 1) / ((P(W)
- P(1)) * 19.55E - 06)): VTAB 20: HTAB 4: PRINT "AVERAGE ENGINE SPEED ";RP
2170 IF TEMP + RQ IS GREATER THAN FINISH THEN PRINT D$;"OPEN RPM";FRQ: PRINT
D$;"DELETE RPM";FRQ: PRINT D$;"OPEN RPM";FRQ: PRINT D$;"WRITE RPM";FRQ
2180 IF TEMP + RQ IS GREATER THAN FINISH THEN PRINT RP: PRINT FRQ: PRINT
D$;"CLOSE RPM";FRQ
2190 CT = 0
2200 ZZ = 2
2210 IF TEMP + RQ IS GREATER THAN FINISH GOTO 2250
2220 ZZ = 2:CT = 0
2230 GOSUB 1400
2240 NEXT W
2250 TEXT : HOME
2260 PRINT "SAMPLING COMPLETED"
2270 PRINT D$;"PR#1"
2280 PRINT "KLAATU.V3"
2290 PRINT FW;" WAVES WERE SAMPLED "
2300 PRINT "ENGINE TEST SPEED WAS ";FRQ;" RPM"
2310 PRINT "COMPUTER ESTIMATE WAS ";RP;" RPM"
2320 PRINT D$;"PR#0"
2330 END
```

APPENDIX I
AUXILIARY SAMPLING PROGRAM

The following program identified by the name "KLAATU.DC" was used for the analog to digital sampling of the peak value of the pressure pulse. It was written in APPLESOFT BASIC for implementation on an APPLE II+ computer which is a product of Apple Computer Inc.

```
1000 REM PROGRAM KLAATU.DC ALLOWS MONITORING OF WAVEFORMS USING THE
ANALOG TO DIGITAL CONVERSION OPTION
1002 HIMEM: 8080
1004 J = 0
1006 REM DC VERSION FOR PEAK PRESSURE SAMPLING
1010 DIM TE(280),MZ(280),AV(280)
1020 D$ = CHR$(4)
1050 PRINT D$;"BLOAD BIGSAMPLE"
1060 PRINT D$;"BLOAD MAXGR"
1070 PRINT D$;"BLOAD ADD7$345"
1105 INPUT "TAPE # ";TN
1110 INPUT "HIT RETURN TO SAMPLE FROM TAPERECORDER";B$
1120 BEG = 16384:FINISH = 38400
1130 POKE 8083,B1
1140 POKE 8084,00
```

1150 POKE 8085,64
1160 CALL 8080
1170 POKE 251,00: POKE 252,64: POKE 253,00: POKE 254,150
1180 CALL 773
1190 PLACE = PEEK (769) * 256 + PEEK (768)
1200 MAZ = PEEK (770)
1210 PRINT MAZ,PLACE
1220 POKE 251,00: POKE 252,64: POKE 253,00: POKE 254,150
1250 CALL 837
1260 SUM = PEEK (836) * 256 * 256 + PEEK (835) * 256 + PEEK (834)
1270 SAMPLES = PEEK (832) + PEEK (833) * 256
1280 AVG = SUM / SAMPLES
1290 PRINT "DO YOU WANT TO REPEAT SAMPLING RUN ? Y/N"
1300 GET B\$: PRINT :KX = 128 + ASC (B\$): IF KX IS EQUAL TO 217 THEN 1120
1332 INPUT "TAPE COUNT ";TF
1334 PRINT
1335 PRINT "MAX PEAK ";MAZ
1340 PRINT "AVG ";AVG: PRINT "SUM ";SUM
1350 PRINT "SAMPLE NO. ";SAM
1360 PRINT "TAPE NUMBER ";TN
1361 PRINT "LOCATION ON TAPE ";TF
1370 IF TF IS LESS THAN 50 THEN CMZ = MAZ:CAV = AVG: GOTO 1410
1380 PRINT "DO YOU WANT TO SAVE THIS DATA? Y/N "; GET I\$: PRINT I\$: IF NOT
(I\$ IS NOT EQUAL TO "Y" OR I\$ IS NOT EQUAL TO "N") THEN 1380
1390 IF I\$ IS EQUAL TO "N" THEN 1410
1400 J = J + 1:TF(J) = TF:MZ(J) = MAZ:AV(J) = AVG
1410 PRINT "DO YOU WANT TO STOP? Y/N "; GET I\$: PRINT I\$: IF NOT (I\$ IS NOT

```
EQUAL TO "Y" OR I$ IS NOT EQUAL TO "N") THEN 1410
1420 IF I$ IS EQUAL TO "Y" THEN 1440
1430 GOTO 1290
1440 PRINT "DO YOU WANT TO SAVE THIS DATA TO FILE? Y/N "; GET I$: PRINT
I$: IF NOT (I$ IS NOT EQUAL TO "Y" OR I$ IS NOT EQUAL TO "N") THEN 1440
1450 IF I$ IS EQUAL TO "N" THEN END
1455 ONERR GOTO 1540
1460 PRINT D$;"OPEN TAPE:FILE*";TN
1470 PRINT D$;"DELETE TAPE:FILE*";TN
1480 PRINT D$;"OPEN TAPE:FILE*";TN
1490 PRINT D$;"WRITE TAPE:FILE*";TN
1500 PRINT J: PRINT CMZ: PRINT CAV
1510 FOR I = 1 TO J
1520 PRINT TF(I): PRINT MZ(I): PRINT AV(I): NEXT
1530 PRINT D$;"CLOSE TAPE:FILE*";TN
1531 END
1540 POKE 216,0
1560 PRINT D$;"CLOSE TAPE:FILE*";TN
1570 INPUT "READY?";I$
1580 GOTO 1455
```

APPENDIX I
MACHINE LANGUAGE PROGRAM — BIGSAMPLE

The source code for this program was assembled using the LISA 2.0 assembler
by Programma International Inc.

```

0000          1          ;MOUNTAIN COMPUTER A/D PROGRAM.
0000          2          ;MODIFIED BY G. RAY AND E. SCOTT
0000          3          ;*****
0000          4          ;THIS SUBROUTINE OPERATES THE D/A
0000          5          ;CONVERTER, THE STARTING ADDRESS
0000          6          ;IS 1F90, 1F93-1F95 ARE RESERVED
0000          7          ;FOR INFORMATION TRANSFER FROM
0000          8          ;THE MAIN PROGRAM
0000          9          ;*****
1F90          10  ORG $1F90 ;INTENDED LOCATION OF PROGRAM
1F90          11  OBJ $000  ;ASSEMBLER LOCATION OF OBJECT CODE
1F90 4C 96 1F  12  JMP $1F96 ;JUMP TO START OF ROUTINE
1F93 00          13  BRK      ;LEAVE LINE BLANK
1F94 00          14  BRK      ;LEAVE LINE BLANK
1F95 00          15  BRK      ;LEAVE LINE BLANK
1F96 78          16  SEI      ;SET INTERRUPT DISABLE
1F97 48          17  PHA      ;PUSH ACCUMULATOR ON STACK

```


1F98 8A	18	TXA	;TRANSFER INDEX X TO ACCUMULATOR
1F99 48	19	PHA	;PUSH ACCUMULATOR ON STACK
1F9A 98	20	TYA	;TRANSFER INDEX Y TO ACCUMULATOR
1F9B 48	21	PHA	;PUSH ACCUMULATOR ON STACK
1F9C AD 94 1F	22	LDA \$1F94	;LOAD ACCUMULATOR FROM 1F94
1F9F 85 FE	23	STA \$FE	;STORE ACCUMULATOR VALUE AT FE ON ZERO PAGE
1FA1 AD 95 1F	24	LDA \$1F95	;LOAD ACCUMULATOR FROM 1F95
1FA4 85 FF	25	STA \$FF	;STORE ACCUMULATOR VALUE AT FF ON ZERO PAGE
1FA6 AE 93 1F	26	LDX \$1F93	;LOAD INDEX X FROM 1F93
1FA9 8D 88 C8	27	LDA \$C888,X	;LOAD ACCUMULATOR FROM THE LOCATION C888+VALUE IN X
1FAC	28		;THIS TAKES A SAMPLE FROM THE A/D CONVERTER
1FAC A8 88	29	LDY #88	;LOAD INDEX Y WITH 88
1FAE EA	30	NOP	;NO OPERATION (TIMING OF CYCLE)
1FAF EA	31	NOP	
1FB0 EA	32	NOP	
1FB1 EA	33	NOP	
1FB2 8D 88 C8	34	LDA \$C888,X	;LOAD ACCUMULATOR FROM THE A/D
1FB5	35		;A/D MUST BE SAMPLED TWICE TO TURN IT ON FOR INPUT
1FB5 91 FE	36	STA (\$FE),Y	;STORE ACCUMULATOR AT LOCATION INDICATED BY VALUE AT FE+VALUE IN INDEX Y
1FB7 C8	37	INY	;INCREMENT INDEX Y BY ONE
1FB8 85 FD	38	STA \$FD	;STORE ACCUMULATOR VALUE AT FD ON ZERO PAGE
1FBA C8 FF	39	CPY #FF	;COMPARE Y INDEX WITH THE VALUE FF
1FBC D8 F4	40	BNE \$1FB2	;BRANCH TO LOCATION 1FB2 IF COMPARISON IS NOT ZERO
1FBE 8D 88 C8	41	LDA \$C888,X	;SAMPLE A/D AGAIN

1FC1 91 FE	42	STA (\$FE),Y	;STORE VALUE AT LOCATION VALUE GIVEN BY FE+Y
1FC3 C8	43	INY	;INCREMENT Y AGAIN
1FC4 EA	44	NOP	;TIMING CONTROL
1FC5 E6 FF	45	INC \$FF	;INCREMENT THE VALUE IN FF ON ZERO PAGE BY ONE
1FC7 BD 88 C8	46	LDA \$C888,X	;SAMPLE A/D AGAIN
1FCA 91 FE	47	STA (\$FE),Y	;STORE VALUE AT LOCATION VALUE GIVEN BY FE+Y
1FCC C8	48	INY	;INCREMENT Y AGAIN
1FCD A5 FF	49	LDA \$FF	;LOAD THE ACCUMULATOR FROM LOCATION FF ON ZERO PAGE
1FCF C9 96	50	CMP #96	;COMPARE WITH THE VALUE 96
1FD1	51		;THIS IS THE UPPER MEMORY LIMIT FOR DATA
1FD1 D8 DF	52	BNE \$1FB2	;IF THE RESULT IS NOT ZERO GO BACK TO 1FB2
1FD3 68	53	PLA	;PULL ACCUMULATOR FROM STACK
1FD4 A8	54	TAY	;TRANSFER ACCUMULATOR TO Y INDEX
1FD5 68	55	PLA	;PULL ACCUMULATOR FROM STACK
1FD6 AA	56	TAX	;TRANSFER ACCUMULATOR TO X INDEX
1FD7 68	57	PLA	;PULL ACCUMULATOR FROM STACK
1FD8 58	58	CLI	;CLEAR INTERRUPT DISABLE
1FD9 68	59	RTS	;RETURN FROM SUBROUTINE

APPENDIX I
MACHINE LANGUAGE PROGRAM - MAXGR.

The source code for this program was assembled using the LISA 2.0 assembler
by Programma International Inc.

```
0800          1          ;PROGRAM WRITTEN BY E. SCOTT AND G. RAY
0800          2          ;1982
0800          3          ;*****
0800          4          ;THIS SUBROUTINE FINDS THE MAXIMUM
0800          5          ;VALUE OF THE SAMPLED DATA FROM THE
0800          6          ;A/D CONVERTER, STORES ITS VALUE
0800          7          ;AND ITS LOCATION IN ADDRESS
0800          8          ;LOCATIONS 300-304
0800          9          ;LOCATION 305 IS THE STARTING
0800         10          ;ADDRESS OF THE SUBROUTINE
0800         11          ;*****
0300         12  ORG $300  ;LOCATION OF ROUTINE START
0300         13  OBJ $000  ;ASSEMBLER LOCATION OF OBJECT CODE
0300 00       14  BRK      ;LEAVE LINE BLANK
0301 00       15  BRK      ;LEAVE LINE BLANK
0302 00       16  BRK      ;LEAVE LINE BLANK
0303 00       17  BRK      ;LEAVE LINE BLANK
```

0304 00	18	BRK	;LEAVE LINE BLANK
0305 38	19	SEC	;SET CARRY FLAG
0306 A5 FD	20	LDA \$FD	;LOAD THE ACCUMULATOR FROM
0308	21		;ZERO PAGE LOCATION FD
0308 E5 FB	22	SBC \$FB	;SUBTRACT VALUE AT ZERO PAGE
030A	23		;LOCATION FB FROM ACCUMULATOR
030A	24		;WITH BORROW
030A 8D 03 03	25	STA \$0303	;STORE ACCUMULATOR IN MEMORY LOCATION 0303
030D A5 FE	26	LDA \$FE	;LOAD THE ACCUMULATOR FROM
030F	27		;ZERO PAGE LOCATION FE
030F E5 FC	28	SBC \$FC	;SUBTRACT VALUE AT ZERO PAGE
0311	29		;LOCATION FC FROM ACCUMULATOR
0311	30		;WITH BORROW
0311 8D 04 03	31	STA \$0304	;STORE ACCUMULATOR IN MEMORY LOCATION 0304
0314 AE 04 03	32	LDX \$0304	;LOAD INDEX X FROM 0304
0317 A9 00	33	LDA #\$00	;LOAD ACCUMULATOR WITH 00
0319 8D 00 03	34	STA \$0300	;STORE ACCUMULATOR AT
031C	35		;MEMORY LOCATION 0300
031C D1 FB	36	CMP (\$FB),Y	;COMPARE ACCUMULATOR WITH
031E	37		;THE VALUE AT ZERO PAGE LOCATION FB
031E	38		;+THE VALUE OF THE INDEX Y
031E 80 0D	39	BCS \$032D	;BRANCH ON CARRY SET TO
0320	40		;LOCATION 032D
0320 A5 FC	41	LDA \$FC	;LOAD THE ACCUMULATOR FROM
0322	42		;LOCATION FC ON ZERO PAGE

0322 8D 01 03	43	STA \$0301	;STORE ACCUMULATOR AT
0325	44		;LOCATION 0301
0325 8C 00 03	45	STY \$0300	;STORE THE INDEX Y AT
0328	46		;LOCATION 0300
0328 B1 FB	47	LDA (\$FB),Y	;LOAD THE ACCUMULATOR
032A	48		;FROM THE LOCATION GIVEN BY THE
032A	49		;VALUE AT ZERO PAGE LOCATION FB+
032A	50		;THE VALUE OF THE INDEX Y
032A 8D 02 03	51	STA \$0302	;STORE THE ACCUMULATOR
032D	52		;AT LOCATION 0302
032D 88	53	DEY	;DECREMENT INDEX Y BY ONE
032E D0 EC	54	BNE \$031C	;BRANCH ON RESULT NOT
0330	55		;ZERO TO LOCATION \$031C
0330 E6 FC	56	INC \$FC	;INCREMENT THE VALUE AT
0332	57		;MEMORY LOCATION FC ON ZERO PAGE
0332	58		;BY ONE
0332 CA	59	DEX	;DECREMENT INDEX X BY ONE
0333 D0 E7	60	BNE \$031C	;BRANCH ON RESULT NOT
0335	61		;ZERO TO LOCATION 031C
0335 60	62	RTS	;RETURN FROM SUBROUTINE

APPENDIX I
MACHINE LANGUAGE PROGRAM — ADD7#345

The source code for this program was assembled using the LISA 2.0 assembler
by Programma International Inc.

```

0000          1          ;PROGRAM WRITTEN BY G. RAY AND E. SCOTT
0000          2          ;1982
0000          3          ;*****
0000          4          ;THIS SUBROUTINE DETERMINES THE SUM
0000          5          ;OF ALL SAMPLES TAKEN AND THE NUMBER
0000          6          ;OF SAMPLES WHEN IT IS CALLED
0000          7          ;LOCATIONS 340-344 ARE USED FOR DATA
0000          8          ;STORAGE WHICH IS CALLED FROM THE
0000          9          ;MAIN PROGRAM
0000         10         ;LOCATION 345 IS THE STARTING
0000         11         ;ADDRESS OF THE SUBROUTINE
0000         12         ;*****
0340         13  ORG $340 ;LOCATION OF ROUTINE START
0340         14  OBJ $800 ;ASSEMBLER LOCATION OF OBJECT CODE
0340 00      15  BRK      ;LEAVE LINE BLANK
0341 00      16  BRK      ;LEAVE LINE BLANK
0342 00      17  BRK      ;LEAVE LINE BLANK

```

0343 00	18	BRK	;LEAVE LINE BLANK
0344 00	19	BRK	;LEAVE LINE BLANK
0345 A9 00	20	LDA #00	;LOAD THE ACCUMULATOR WITH 00
0347 8D 42 03	21	STA #0342	;STORE THE ACCUMULATOR AT
034A	22		;LOCATION 342
034A 8D 43 03 23		STA #0343	;STORE THE ACCUMULATOR AT
034D	24		;LOCATION 343
034D 8D 44 03	25	STA #0344	;STORE THE ACCUMULATOR AT
0350	26		;LOCATION 344
0350 A8	27	TAY	;TRANSFER THE ACCUMULATOR VALUE
0351	28		;TO INDEX Y
0351 38	29	SEC	;SET CARRY FLAG
0352 A5 FD	30	LDA \$FD	;LOAD THE ACCUMULATOR WITH
0354	31		;THE VALUE IN MEMORY LOCATION FD ON
0354	32		;ZERO PAGE
0354 E5 FB	33	SBC \$FB	;SUBTRACT THE VALUE IN MEMORY
0356	34		;LOCATION FB FROM THE ACCUMULATOR
0356	35		;WITH BORROW
0356 8D 40 03	36	STA #0340	;STORE THE ACCUMULATOR
0359	37		;AT LOCATION 0340
0359 A5 FE	38	LDA \$FE	;LOAD THE ACCUMULATOR WITH
035B	39		;THE VALUE IN MEMORY LOCATION FE ON
035B	40		;PAGE ZERO
035B E5 FC	41	SBC \$FC	;SUBTRACT THE VALUE IN MEMORY
035D	42		;LOCATION FC FROM THE ACCUMULATOR

035D	43		;WITH BORROW
035D 8D 41 03	44	STA \$0341	;STORE THE ACCUMULATOR
0360	45		;AT LOCATION 0341
0360 AE 41 03	46	LDX \$0341	;LOAD THE X INDEX WITH
0363	47		;THE VALUE AT LOCATION 0341
0363 18	48	CLC	;CLEAR CARRY FLAG
0364 B1 FB	49	LDA (\$FB),Y	;LOAD THE ACCUMULATOR
0366	50		;WITH THE VALUE IN MEMORY LOCATION
0366	51		;FB ON ZERO PAGE + THE VALUE IN
0366	52		;INDEX Y
0366 6D 42 03	53	ADC \$0342	;ADD THE VALUE AT LOCATION
0369	54		;0342 TO THE VALUE IN THE ACCUMULATOR
0369	55		;WITH CARRY
0369 8D 42 03	56	STA \$0342	;STORE THE ACCUMULATOR
036C	57		;AT LOCATION 0342
036C 98 09	58	BCC \$0377	;BRANCH ON CARRY CLEAR TO
036E	59		;LOCATION 0377
036E EE 43 03	60	INC \$0343	;INCREMENT THE VALUE AT
0371	61		;LOCATION 0343 BY ONE
0371 D0 04	62	BNE \$0377	;BRANCH ON THE RESULT
0373	63		;NOT EQUAL TO ZERO TO LOCATION 0377
0373 EE 44 03	64	INC \$0344	;INCREMENT THE VALUE AT
0376	65		;LOCATION 0344 BY ONE
0376 18	66	CLC	;CLEAR CARRY FLAG
0377 88	67	DEY	;DECREMENT THE VALUE IN THE Y

0378	68		;INDEX BY ONE
0378 D8 EA	69	BNE #0364	;BRANCH ON THE RESULT
037A	70		;NOT EQUAL TO ZERO TO LOCATION 0364
037A E6 FC	71	INC #FC	;INCREMENT THE VALUE IN
037C	72		;MEMORY LOCATION FC ON ZERO PAGE
037C	73		;BY ONE
037C CA	74	DEX	;DECREMENT THE VALUE IN THE X
037D	75		;INDEX BY ONE
037D F8 06	76	BEG #0385	;BRANCH ON THE RESULT
037F	77		;EQUAL TO ZERO TO LOCATION 0385
037F D8 E3	78	BNE #0364	;BRANCH ON THE RESULT
0381	79		;NOT EQUAL TO ZERO TO LOCATION 0364
0381 A0 40	80	LDY #40	;LOAD THE Y INDEX WITH
0383	81		;THE VALUE 40
0383 D8 DF	82	BNE #0364	;BRANCH ON THE RESULT
0385	83		;NOT EQUAL TO ZERO TO LOCATION 0364
0385 60	84	RTS	;RETURN FROM SUBROUTINE TO MAIN PROGRAM

APPENDIX II
WAVE CONFIGURATION PROGRAM . .

APPENDIX II
WAVE CONFIGURATION PROGRAM

The following program identified by the name "BARADA" was used to select the starting point for saving the pressure pulse data points. It was also used calculate a relative delay time for the first data point that was equal to or greater than the average value of all data points sampled. This delay time was calculated using linear interpolation. It was written in APPLESOFT BASIC for implementation on an APPLE II+ computer which is a product of Apple Computer Inc.

```
100 TEXT : CALL - 936
110 PRINT "INSERT DISKETTE CONTAINING SOURCE DATA IN DRIVE 1"
120 REM BARADA.V3
130 INPUT "DESTINATION DRIVE FOR EDITED DATA ";DR
140 VTAB 10: HTAB 8: INPUT "PRESS RETURN WHEN READY";WQ$
150 D$ = CHR$ (4)
160 DIM A%(279),B(279),I(279)
170 PRINT : PRINT
180 PRINT "THIS PROGRAM (BARADA.V3) RETRIEVES FREQUENCY TEXT FILES AND
EDITS THEM TO POSITIVE WAVES"
190 PRINT
200 INPUT " REFERENCE FREQUENCY , NUMBER OF WAVES ";FRQ,NW
205 PRINT D$;"NOMON I,O"
```

```
210 FOR KW = 1 TO NW
220 WA = KW
230 PRINT D$;"OPEN FREQ(";FRQ;")/";WA;" ,D1"
240 PRINT D$;"READ FREQ(";FRQ;")/";WA
250 INPUT PX: INPUT ZE: INPUT PN
260 INPUT PEAKMAX
270 INPUT MAXLOCAL
280 INPUT AVG
290 INPUT MINLOCAL
300 FOR J = 0 TO 279
310 INPUT A%(J)
320 NEXT J
330 PRINT D$;"CLOSE FREQ(";FRQ;")/";WA
340 PRINT "PX ";PX;" ZE ";ZE;" PN ";PN
350 PRINT "MAZ ";PEAKMAX;" MX ";MAXLOCAL;" AVG ";AVG;" MN ";MINLOCAL
360 PRINT "WAVE(";KW;")"
370 OZ = ZE - 1
380 ZE = OZ
390 GVA = AVG
400 HGR
410 HCOLOR 3
420 QR = AVG
430 FOR I = 0 TO 279
440 HPLOT I,159 - A%(I) / 2
450 NEXT I
460 FOR I = 0 TO 279 STEP 2
470 HPLOT I,159 - AVG / 2
```

```
480 NEXT I
490 FOR I = ZE TO 279
500 IF A%(I - 1) IS EQUAL TO OR IS GREATER THAN AVG AND A%(I) IS LESS THAN
AVG THEN Z2 = I - 1: GOTO 520
510 Z2 = I: NEXT I
520 NC = (A%(ZE) - AVG) / (A%(ZE) - A%(ZE - 1))
530 VTAB 19: CALL - 958
540 PRINT PRINT
550 PRINT "Y(",ZE,")= ",A%(ZE);" Y(",ZE - 1,")= ",A%(ZE - 1);" AVG ";AVG;" Y(",ZE -
2,")= ",A%(ZE - 2)
560 PRINT "NC ";NC
570 PRINT "Z2= ";Z2
580 FL = Z2 - ZE
590 FOR J = 0 TO FL
600 A%(J) = A%(J + ZE)
610 NEXT J
620 TEXT
630 PRINT D$;"OPEN WORK";KW;"D";DR
640 PRINT D$;"DELETE WORK";KW
650 PRINT D$;"OPEN WORK";KW
660 PRINT D$;"WRITE WORK";KW
670 PRINT NC
680 PRINT FL
690 PRINT PEAKMAX
700 PRINT AVG
710 FOR I = 0 TO FL
720 PRINT A%(I)
```

```
730 NEXT I
740 PRINT D$;"CLOSE WORK";KW
750 NEXT KW
760 PRINT D$;"OPEN RPM";FRQ;"D1"
770 PRINT D$;"READ RPM";FRQ
780 INPUT RP: INPUT FRQ
790 PRINT D$;"CLOSE RPM";FRQ
800 PRINT D$;"OPEN WORK";KW;"D";DR
810 PRINT D$;"DELETE WORK";KW
815 PRINT D$;"OPEN WORK";KW
820 PRINT D$;"WRITE WORK";KW
830 PRINT FRQ: PRINT RP
840 PRINT D$;"CLOSE WORK";KW
850 PRINT "END OF PROCESSING"
855 PRINT D$;"PR#1"
860 PRINT KW;" WORK FILES WERE CREATED"
865 PRINT "END OF BARADA.V3": PRINT D$;"PR#0"
870 END
```

APPENDIX III
WAVE CONCATENATION PROGRAM

APPENDIX III
WAVE CONCATENATION PROGRAM

The following program identified by the name "NICTO" was used to reorganize the individual pressure pulse shapes into a single overlapping shape. This was done by organizing the data against increasing time relative to a reference zero time. That is, the starting point for saving the pressure pulse data points. It did this by using the relative delay time for the first data point that was equal to or greater than the average value of all data points sampled. This delay time was calculated using linear interpolation in the previous program BARADA. It was written in APPLESOFT BASIC for implementation on an APPLE II+ computer which is a product of Apple Computer Inc.

```
100 REM PROGRAM NAME NICTO.V3: THIS PROGRAM TAKES INDIVIDUAL WAVE FILES
110 REM AND RE-ORDERS THE DATA AGAINST INCREASING TIME
120 REM USING THE MACHINE LANGUAGE PROGRAM MERGE TO ASSEMBLE.
130 REM AND MOVE THE DATA
140 HIMEM: 8192
150 D$ = CHR$(4)
160 INPUT "WHAT IS THE BASE NAME OF THE FILE ";NA$
170 INPUT "HOW MANY FILES ARE THERE BY THAT NAME ";NO
175 NO = NO - 1
180 INPUT "DRIVE NUMBER FOR DATA ";DR
185 INPUT "NAME OF MERGED FILE ";GT$ 178
```



```
190 DIM NC(NO),FL(NO)
200 DIM P(NO)
210 FOR I = 1 TO NO
220 PRINT D$;"OPEN ";NA$;I;"D";DR
230 PRINT D$;"READ ";NA$;I
240 INPUT NCD
250 INPUT FLD
260 INPUT PEAKMAX
270 INPUT AVG
280 PRINT D$;"CLOSE ";NA$;I
290 NEXT I
300 PRINT D$;"OPEN ";NA$;I
310 PRINT D$;"READ ";NA$;I
320 INPUT FRQ: INPUT RP
330 PRINT D$;"CLOSE ";NA$;I
340 MINNC = NC(1)
350 LEAST = FL(1)
360 FOR J = 1 TO NO
370 FOR I = 1 TO NO
380 IF NC(I) IS LESS THAN OR IS EQUAL TO MINNC THEN MINNC = NC(I):P(J) = I
390 NEXT I
400 NC(P(J)) = NC(P(J)) * 1000
410 MINNC = NC(1)
420 NEXT J
430 FOR I = 1 TO NO
440 IF FL(I) IS LESS THAN LEAST THEN LEAST = FL(I)
450 NEXT I
```

```
460 DIM Z(LE)
465 IF DR IS EQUAL TO 2 GOTO 480
470 INPUT "INSERT PROGRAM DISK IN DRIVE 1 AND PRESS RETURN TO CONTINUE
";W$
480 PRINT D$;"BLOAD MERGE,D1"
485 IF DR IS EQUAL TO 2 GOTO 510
490 PRINT "INSERT DATA FILE DISKETTE IN DRIVE ";DR
500 INPUT "PRESS RETURN TO CONTINUE ";W$
510 FOR Y = 1 TO NO
520 PRINT D$;"OPEN ";NA$;P(Y);",D";DR
530 PRINT D$;"READ ";NA$;P(Y)
540 INPUT NQ(Y)
550 FOR U = 1 TO 3
560 INPUT WQ: NEXT U
570 FOR H = 0 TO LEAST
580 INPUT Z(H): NEXT H
590 PRINT D$;"CLOSE ";NA$;P(Y)
600 FOR Q = 0 TO LEAST
610 POKE 8192 + MOVE + JK,Z(Q)
620 JK = JK + 1
630 NEXT Q
640 JK = 0
650 MOVE = MOVE + 256
660 NEXT Y
670 POKE 768,32: POKE 769,32 + NO - 1
680 POKE 253,00: POKE 254,32 + NO
690 POKE 808,LEAST + 1
```

```
700 CALL 773
710 V = 0
730 FOR I = 1 TO NO
740 PRINT D$;"OPEN ";GT$;I
750 PRINT D$;"DELETE ";GT$;I
760 PRINT D$;"OPEN ";GT$;I
770 PRINT D$;"WRITE ";GT$;I
780 PRINT LEAST
790 FOR U = V TO LEAST + V
800 SW = PEEK ((32 + NO) * 256 + U)
810 RZ = (SW - AVG) / (PEAKMAX - AVG)
820 PRINT RZ
830 NEXT U
840 PRINT D$;"CLOSE ";GT$;I
850 V = V + LEAST + 1
860 NEXT I
870 PRINT D$;"OPEN ";GT$;I
880 PRINT D$;"DELETE ";GT$;I
890 PRINT D$;"OPEN ";GT$;I
900 PRINT D$;"WRITE ";GT$;I
910 FOR J = 1 TO NO
920 PRINT NCC(J)
930 NEXT J
940 PRINT FRQ: PRINT RP
950 PRINT D$;"CLOSE ";GT$;I
960 PRINT " END OF NICTO.V3 "
970 PRINT D$;"PR#1"
```

980 PRINT "THE LAST FILE NAME WAS ";GT\$;I

990 PRINT D\$;"PR#0": END

APPENDIX III
MACHINE LANGUAGE PROGRAM — MERGE

The source code for this program was assembled using the LISA 2.0 assembler
by Programma International Inc.

```

0800      1      ;PROGRAM WRITTEN BY E. SCOTT AND G. RAY
0800      2      ;1982
0800      3      ;*****
0800      4      ;THIS SUBROUTINE REORDERS DATA AGAINST
0800      5      ;A SPECIFIED INCREASING VALUE
0800      6      ;EACH DATA SET OCCUPIES AT THE MOST
0800      7      ;ONE PAGE OF MEMORY
0800      8      ;THESE VALUES ARE SEQUENTIALY
0800      9      ;TRANSFERED TO A HIGHER PAGE IN
0800     10      ;MEMORY THAN THE LAST USED DATA PAGE
0800     11      ;MEMORY LOCATIONS 0300 AND 0301 ARE
0800     12      ;USED FOR INFORMATION TRANSFER
0800     13      ;THE SUBROUTINE STARTS AT LOCATION
0800     14      ;0305
0800     15      ;*****
0300     16  ORG $0300 ;LOCATION OF ROUTINE START
0300     17  OBJ $0800 ;ASSEMBLER LOCATION OF OBJECT CODE

```

0300 00	18	BRK	;LEAVE LINE BLANK
0301 00	19	BRK	;LEAVE LINE BLANK
0302 00	20	BRK	;LEAVE LINE BLANK
0303 00	21	BRK	;LEAVE LINE BLANK
0304 00	22	BRK	;LEAVE LINE BLANK
0305 A9 00	23	LDA #000	;LOAD THE ACCUMULATOR WITH 00
0307 A8	24	TAY	;TRANSFER THE ACCUMULATOR TO
0308	25		;THE Y INDEX
0308 AA	26	TAX	;TRANSFER THE ACCUMULATOR TO
0309	27		;THE X INDEX
0309 05 FB	28	STA \$FB	;STORE THE ACCUMULATOR IN
030B	29		;MEMORY LOCATION FB ON ZERO PAGE
030B AD 00 03	30	LDA \$030B	;LOAD THE ACCUMULATOR FROM
030E	31		;MEMORY LOCATION 030B
030E	32		;INFORMATION TRANSFER FROM MAIN
030E	33		;PROGRAM
030E 05 FC	34	STA \$FC	;STORE THE ACCUMULATOR IN
0310	35		;MEMORY LOCATION FC ON ZERO PAGE
0310 01 FB	36	LDA (\$FB),Y	;LOAD THE ACCUMULATOR
0312	37		;WITH THE VALUE AT MEMORY LOCATION
0312	38		;FB ON ZERO PAGE + THE VALUE IN Y
0312	39		;INDEX
0312 01 FD	40	STA (\$FD,X)	;STORE THE ACCUMULATOR
0314	41		;AT MEMORY LOCATION FD + X INDEX ON
0314	42		;ZERO PAGE

0314 E6 FD	43	INC \$FD	;INCREMENT THE VALUE STORED
0316	44		;AT MEMORY LOCATION FD BY ONE
0316 D8 02	45	BNE \$031A	;BRANCH ON RESULT NOT ZERO
0318	46		;TO LOCATION 031A
0318 E6 FE	47	INC \$FE	;INCREMENT THE VALUE STORED
031A	48		;AT MEMORY LOCATION FE BY ONE
031A E6 FC	49	INC \$FC	;INCREMENT THE VALUE STORED*
031C	50		;AT MEMORY LOCATION FC BY ONE
031C A5 FC	51	LDA \$FC	;LOAD THE ACCUMULATOR FROM
031E	52		;MEMORY LOCATION FC ON ZERO PAGE
031E CD 01 03	53	CMP \$0301	;COMPARE WITH THE VALUE AT
0321	54		;LOCATION 0301
0321 98 ED	55	BCC \$0310	;BRANCH ON CARRY CLEAR TO LOCATION 0310
0323 F0 EB	56	BEQ \$0310	;BRANCH ON RESULT EQUAL
0325	57		;TO ZERO TO LOCATION 0310
0325 C8	58	INY	;INCREMENT Y INDEX BY ONE
0326 98	59	TYA	;TRANSFER Y INDEX TO ACCUMULATOR
0327 C9 00	60	CMP #00	;COMPARE WITH THE VALUE 00
0329 F0 00	61	BEQ \$0333	;BRANCH ON RESULT EQUAL TO ZERO TO LOCATION 0333
032B AD 00 03	62	LDA \$0300	;LOAD THE ACCUMULATOR FROM MEMORY LOCATION 0300
032E 85 FC	63	STA \$FC	;STORE THE ACCUMULATOR AT
0330	64		;MEMORY LOCATION FC ON ZERO PAGE
0330 4C 10 03	65	JMP \$0310	;JUMP TO LOCATION 0310
0333 60	66	RTS	;RETURN FROM SUBROUTINE TO MAIN PROGRAM

APPENDIX IV
WAVE CORRELATION PROGRAM

APPENDIX IV
WAVE CORRELATION PROGRAM

The following program identified by the name "BARANGA1" is the first part of a two-part program which was used to calculate the values of pseudo frequency, distortion coefficient and optionally, the relative peak acoustic pressure by minimizing the squared error between the model and the data. The program has been provided with the capability of doing a faster correlation on a small number of data points. This was included so that it could yield a set of initial values of the variables to be iterated. This program reads in the concatenated data from the previous program "NICTO". If there is more data than memory space available, the program switches to a random discard routine after determining the fraction of data to be discarded. This was done to ensure that samples would be taken from all portions of the wave. It was written in APPLESOFT BASIC for implementation on an APPLE II+ computer which is a product of Apple Computer Inc. Additionally, the program was set up for compilation using TASC (The AppleSoft Compiler) which is a product of Microsoft Inc.

```
1000 REM !INTEGER MJ,KJ,KW,WN,DR,J,N,IJ,K,P,IX,M,CM,PZ,BP,T1,A3,BA,I1,A8,A9
1010 REM !DEFCOMMON MJ,KJ,KW,WN,DR,J,N,IJ,K,P,IX,M,CM,PZ,BP,T1,A3,BA,I1,A8,A9
1020 REM !DEFCOMMON T(2500),WE(2500)
1030 REM !DEFCOMMON N$,ZO,HO,UPO,ER,FRQ,RP,A5
1040 D$ = CHR$(4): PRINT D$;"MON C": VTAB PEEK(37): CALL - 868:PI = ATN(1.0)
```

```
* 4:VO = 1:BP = 0:AS = 0

1050 PRINT "DO YOU WANT SUPERFAST BARANGA, Y / N ? "; GET YN$: PRINT YN$:
IF NOT (YN$ IS EQUAL TO "N" OR YN$ IS EQUAL TO "Y") GOTO 1050

1060 IF YN$ IS EQUAL TO "N" GOTO 1080

1070 BP = PEEK (78) + 128 * PEEK (79): IF BP IS EQUAL TO 0 THEN BP = 1

1080 PRINT "TYPE: 1. INVOLVES FREQ, DIST AND PRESS": PRINT "TYPE: 2. INVOLVES
FREQ. AND DIST."

1090 PRINT "PROGRAM BARANGA, TYPE 1 OR 2 ? "; GET BA: PRINT BA: IF NOT (BA
IS EQUAL TO 1 OR BA IS EQUAL TO 2) THEN PRINT "INVALID KEYSTROKE": GOTO
1090

1100 INPUT "INITIAL Z-VALUE ";ZO

1110 INPUT "INITIAL H-VALUE ";HO

1120 IF BA IS EQUAL TO 2 THEN UP0 = 1: GOTO 1140

1130 INPUT "INITIAL P-VALUE ";UP0

1140 INPUT "ERROR VALUE ";ER

1150 INPUT "BASE NAME OF DATA FILES ";N$

1160 INPUT "NUMBER OF FILES BY THAT NAME ";IJ

1170 DIM T(2500),WE(2500),NC(40)

1180 PRINT "DRIVE NUMBER FOR DATA "; GET R$: PRINT R$:DR = VAL (R$)

1190 IF DR EQUALS 1 THEN PRINT "PLACE DATA DISKETTE IN DRIVE 1 AND PRESS
ANY KEY TO CONTINUE "; GET R$: PRINT

1200 WN = IJ - 1

1210 PRINT D$;"OPEN ";N$;IJ;"D";DR

1220 PRINT D$;"READ ";N$;IJ

1230 FOR K = 1 TO WN: INPUT NC(K): NEXT K

1240 INPUT FRQ: INPUT RP: PRINT D$;"CLOSE ";N$;IJ

1250 IX = - 1: MJ = 1: KJ = 0
```

```
1260 FOR KW = 1 TO WN
1270 I1 = - 1
1280 PRINT D$;"OPEN ";N$;KW
1290 PRINT D$;"READ ";N$;KW
1300 INPUT N
1310 IF IX IS EQUAL TO OR GREATER THAN 0 THEN 1350
1320 IF BP IS GREATER THAN 0 THEN A4 = 1 - 400 / (WN * (N + 1)): GOSUB 1590
1330 IF BP IS GREATER THAN 0 GOTO 1350
1340 GOSUB 1560
1350 FOR I = 0 TO N
1360 A8 = I:IX = IX + 1
1370 INPUT WED(X)
1380 I1 = I1 + 1:T(IX) = (NC(MJ) + KJ) * 19.55E - 06
1390 IF MJ IS EQUAL TO WN THEN KJ = KJ + 1
1400 IF MJ IS EQUAL TO WN THEN MJ = 0
1410 MJ = MJ + 1
1420 IF BP IS EQUAL TO 0 GOTO 1480
1430 A3 = IX - T1 + I1
1440 IF A3 IS LESS THAN 0 THEN A3 = PEEK (78) + 128 * PEEK (79)
1450 IF RND (A3) IS GREATER THAN A4 GOTO 1480
1460 IF I1 IS EQUAL TO N GOTO 1480
1470 GOTO 1370
1480 IF IX IS EQUAL TO 2500 GOTO 1510
1490 IF I1 IS EQUAL TO N GOTO 1510
1500 NEXT
1510 PRINT D$;"CLOSE ";N$;KW
1520 A4 = A4 + A5 - (N - I) / N
```

1530 IF IX IS EQUAL TO 2500 GOTO 1550

1540 A9 = KW: NEXT KW

1550 GOTO 1620

1560 IF $WN * (N + 1) - 2501$ IS EQUAL TO IS LESS THAN 0 THEN RETURN

1570 $BP = INT ((N + 1) * WN / (.638025 * (WN * (N + 1) - 2501)))$

1580 $A4 = (WN * (N + 1) - 2501) / (WN * (N + 1))$

1590 A5 = A4

1600 $T1 = INT (RND (BP) * WN + .05)$

1610 RETURN

1620 REM !CLEAR CHAIN

1630 PRINT CHR\$(4);"BRUNBARANGA2.OBJ,D1"

REMARK: BARANGA1 ENDS HERE WITH THE PROGRAM NOW CALLING FOR THE
CORRELATION SECTION, WHICH IS PART 2.

REMARK: BARANGA2 STARTS HERE

1640 REM !INTEGER MJ,KJ,KW,WN,DR,J,N,IJ,K,P,IX,M,CM,PZ,BP,T1,A3,BA,I1,A8,A9

1650 REM !USECOMMON MJ,KJ,KW,WN,DR,J,N,IJ,K,P,IX,M,CM,PZ,BP,T1,A3,BA,I1,A8,A9

1660 REM !USECOMMON T(2500),WE(2500)

1670 REM !USECOMMON N\$,ZO,HO,UP0,ER,FRQ,RP,A5

1680 D\$ = CHR\$(4): PRINT D\$;"MON C": VTAB PEEK (37): CALL - 868:PI = ATN (1.0)

* 4

1690 PRINT "IS PRINTER AVAILABLE? "; GET YN\$: PRINT YN\$: IF NOT (YN\$ IS EQUAL
TO "N" OR YN\$ IS EQUAL TO "Y") GOTO 1690

1700 DIM T(2500),WE(2500),A1Y(33),A2Y(33),TMP(21),TNP(22)

1710 $A4 = N - AB:A4 = A9 * (N + 1) - A4:CR$ = ".DATA":A3 = 0$

1720 $A4 = (INT ((1000 * (1 - A4 / (WN * (N + 1)))) + 0.5) / 10)$

1730 $A5 = (INT (A5 * 1640)) / 10:A9 = WN * (N + 1): GOSUB 2560$

1740 A1Y(1) = 1:A2Y(1) = 1

```

1750 FOR I = 2 TO 33:A2Y(I) = A2Y(I - 1) * I:A1Y(I) = A2Y(I - 1): NEXT I
1760 FOR N = 1 TO 21:AA = N * ZO / 2:FUNC = 0
1770 FOR N = 1 TO 21:AA = N * ZO / 2:FUNC = 0
1780 FOR M = 1 TO 34 - N:P = M - 1:CM = P + N
1790 TOTAL = (AA ↑ N / A1Y(M)) * (AA ↑ P) * (AA ↑ P / A2Y(CM))
1800 PZ = INT (P / 2):PZ = PZ * 2: IF PZ IS NOT EQUAL TO P THEN TOTAL = - TOTAL
1810 FUNC = FUNC + TOTAL: NEXT M:TMP(N) = FUNC: NEXT N
1820 FOR N = 2 TO 22:AA = (N - 1) * ZO / 2:FUNC = 0
1830 FOR M = 1 TO 34 - N:P = M - 1:CM = P + N
1840 TOTAL = (AA ↑ N / A1Y(M)) * (AA ↑ P) * (AA ↑ P / A2Y(CM))
1850 PZ = INT (P / 2):PZ = PZ * 2: IF PZ IS NOT EQUAL TO P THEN TOTAL = - TOTAL
1860 FUNC = FUNC + TOTAL: NEXT M:TNP(N) = FUNC: NEXT N
1870 IF ZO IS GREATER THAN 1 THEN ZO = 2 - ZO
1880 IF ZO IS LESS THAN 0 THEN ZO = - ZO
1890 F1 = 0:F2 = 0:F3 = 0:F4 = 0:F5 = 0:F6 = 0:F7 = 0:F8 = 0:F9 = 0
1900 XS = 0:YS = 0:XY = 0:SX = 0:SY = 0:FV = 0
1910 PH = PEEK (36):PC = PEEK (37)
1920 FOR J = 0 TO IX
1930 VTAB 2: HTAB 30: PRINT J;" / ";IX
1940 CNST = 0:ZPRIME = 0:HPRIME = 0:OZ = ZO
1950 FOR N = 1 TO 21
1960 IF OZ IS EQUAL TO 0 AND N IS EQUAL TO 1 THEN TMP(N) = 1:ZO = 2
1970 IF OZ IS EQUAL TO 0 AND N IS GREATER THAN 1 THEN TMP(N) = 0:ZO = 1
1980 IF OZ IS EQUAL TO 0 THEN TNP(N + 1) = 0
1990 CNST = CNST + TMP(N) * SIN (N * 2 * PI * HO * T(J)) / (N * ZO)
2000 IF A3 IS EQUAL TO 1 THEN NEXT N
2010 IF A3 IS EQUAL TO 1 THEN WE(J) = CNST * 2 * UP0: GOTO 2120

```

```

2020 ZPRIME = ZPRIME + SIN (N * 2 * PI * HO * T(J)) * (((N - 1) / N) * (TMP(N)
/ (ZO ↑ 2)) - TNP(N + 1) / ZO)
2030 HPRIME = HPRIME + T(J) * TMP(N) * COS (2 * PI * HO * T(J)) / ZO
2040 NEXT N
2050 CNST = CNST * 2:ZPRIME = ZPRIME * 2:HPRIME = HPRIME * 4 * PI
2060 YS = YS + CNST * UP0:XS = XS + WE(J):XY = XY + WE(J) * CNST * UP0:SX =
SX + WE(J) * WE(J):SY = SY + CNST * CNST * UP0 * UP0
2070 DF = UP0 * CNST - WE(J):FV = FV + DF * DF
2080 F1 = F1 + DF * ZPRIME / UP0:F2 = F2 + ZPRIME * ZPRIME
2090 F3 = F3 + ZPRIME * HPRIME:F4 = F4 + DF * HPRIME / UP0
2100 F5 = F5 + HPRIME * HPRIME:F6 = F6 + ZPRIME * CNST / UP0
2110 F7 = F7 + HPRIME * CNST / UP0:F8 = F8 + CNST * CNST / (UP0 * UP0):F9 =
F9 + DF * CNST / (UP0 * UP0)
2120 VTAB 2: HTAB 30: CALL - 868: NEXT J: POKE 36,PH: POKE 37,PC: CALL - 922
2130 IF A3 IS EQUAL TO 1 GOTO 2540
2140 DET = F2 * (F5 * F8 - F7 * F7) - F3 * (F3 * F8 - F6 * F7) + F6 * (F3 * F7
- F6 * F5)
2150 Z2 = - (F1 * (F5 * F8 - F7 * F7) - F4 * (F3 * F8 - F6 * F7) + F9 * (F3 * F7
- F6 * F5)) / DET
2160 H2 = - (F2 * (F4 * F8 - F7 * F9) - F1 * (F3 * F8 - F6 * F7) + F6 * (F3 * F9
- F6 * F4)) / DET
2170 IF BA IS EQUAL TO 2 GOTO 2190
2180 U2 = - (F2 * (F5 * F9 - F4 * F7) - F3 * (F3 * F9 - F6 * F4) + F1 * (F3 * F7
- F5 * F6)) / DET
2190 VAR = FV / (IX + 1)
2200 PRINT " Z2 = ";Z2: PRINT " H2 = ";H2: IF BA IS EQUAL TO 1 THEN PRINT "
U2 = ";U2

```

```

2240 PRINT " VAR = ";VAR
2220 CALL - 922
2230 PRINT "Z(NEW)= ";Z0 + Z2: PRINT "H(NEW)= ";H0 + H2: IF BA IS EQUAL TO 1
THEN PRINT "P(NEW)= ";UP0 + U2
2240 IF VAR IS GREATER THAN V0 GOTO 2340
2250 V0 = VAR + 0.05 * ( ABS (V0 - VAR))
2260 IF BA IS EQUAL TO 2 GOTO 2280
2270 IF ABS (U2 / UP0) IS GREATER THAN ER GOTO 2320
2280 IF ABS (Z2) IS LESS THAN .0005 GOTO 2300
2290 IF ABS (Z2 / Z0) IS GREATER THAN ER GOTO 2320
2300 IF ABS (H2 / H0) IS GREATER THAN ER GOTO 2320
2310 GOTO 2370
2320 H0 = H0 + H2:Z0 = Z0 + Z2: IF BA IS EQUAL TO 1 THEN UP0 = UP0 + U2
2330 GOTO 1760
2340 IF YN$ IS EQUAL TO "Y" THEN PRINT D$;"PR#1"
2350 PRINT " RUN ENDED ON VARIANCE DEFAULT"
2360 PRINT " CHECK STARTING PARAMETERS FOR CAUSE OF DIVERGENCE "
2370 NP = IX + 1:S1 = NP * SX - XS * XS:S2 = NP * SY - YS * YS:S3 = NP * XY
- XS * YS:CR = S3 / SQR(S1 * S2)
2380 HOME
2390 IF YN$ IS EQUAL TO "Y" THEN PRINT D$;"PR#1": CALL - 922: GOTO 2420
2400 PRINT D$;"OPEN RESULTS ";N$;"D";DR: PRINT D$;"DELETE RESULTS ";N$
2410 PRINT D$;"OPEN RESULTS ";N$: PRINT D$;"WRITE RESULTS ";N$
2420 PRINT " RESULTS OF ";N$;" ", "WN;" FILES": PRINT " ENGINE TEST SPEED =
";FRQ
2430 PRINT " COMPUTER ESTIMATED SPEED = ";RP: IF BP IS GREATER THAN 0 THEN
PRINT " PERCENT RANDOM DELETIONS = ";A5

```

```
2440 IF BP IS GREATER THAN 0 THEN PRINT " PERCENT DATA NOT SAMPLED = ";A4
2450 IF BP IS GREATER THAN 0 THEN PRINT " DATA POINTS AVAILABLE = ";A9
2460 PRINT " CORRELATION COEFFICIENT = ";CR: PRINT " VARIANCE = ";VAR
2470 PRINT " DISTORTION COEFFICIENT = ";ZO: PRINT " PSEUDO FREQUENCY = ";HO
2480 IF BA IS EQUAL TO 1 THEN PRINT " AVERAGE PEAK PRESSURE = ";UP0
2490 PRINT " NUMBER OF DATA POINTS = ";NP
2500 IF YN$ IS EQUAL TO "N" THEN PRINT "END"
2510 IF YN$ IS EQUAL TO "N" THEN PRINT D$;"CLOSE RESULTS ";N$: CALL - 922
2520 IF YN$ IS EQUAL TO "Y" THEN PRINT D$;"PR#1": CALL - 922
2530 IF A3 IS NOT EQUAL TO 1 THEN A3 = 1: GOTO 1760
2540 CR$ = ".CURVE": GOSUB 2570: GOSUB 2600: REM !CLEAR COMMON
2550 PRINT "PROGRAMME DISKETTE READY IN DRIVE 1?": GET R$: PRINT R$: PRINT
CHR$(4);"BRUNBARANGA1.OBJ,D1"
2560 PRINT "DATA DISK READY, DRIVE 1 ? ": GET R$: PRINT R$
2570 PRINT D$;"OPEN CORREL";CR$;"D1": PRINT D$;"DELETE CORREL";CR$
2580 PRINT D$;"OPEN CORREL";CR$: PRINT D$;"WRITE CORREL";CR$
2590 P = IX + 1: PRINT P: PRINT P: FOR I = 0 TO IX: PRINT T(I): NEXT : FOR I =
0 TO IX: PRINT WEO: NEXT : PRINT D$;"CLOSE CORREL";CR$: RETURN
2600 PRINT D$;"OPEN";N$: PRINT D$;"DELETE";N$: PRINT D$;"OPEN";N$: PRINT
D$;"WRITE";N$: PRINT N$: PRINT D$;"CLOSE";N$: RETURN
```


APPENDIX V
SAMPLE RESULTS FROM THE CORRELATION PROGRAMME

APPENDIX V

SAMPLE RESULTS FROM THE CORRELATION PROGRAMME

1. RESULTS OF FILE 1

RESULTS OF TEST RUN NUMBER 3, 13 FILES

ENGINE TEST SPEED	= 2000 RPM
COMPUTER ESTIMATED SPEED	= 1996 RPM
CORRELATION COEFFICIENT	= 0.986
VARIANCE	= 2.436E-03
DISTORTION COEFFICIENT	= 0.206
PSEUDO FREQUENCY	= 149.1 Hz
DIMENSIONLESS AVERAGE PEAK PRESSURE	= 0.899
NUMBER OF DATA POINTS	= 2314

2. RESULTS OF FILE 2

RESULTS OF TEST RUN NUMBER 4, 11 FILES

ENGINE TEST SPEED	= 2000 RPM
COMPUTER ESTIMATED SPEED	= 1995 RPM
CORRELATION COEFFICIENT	= 0.986
VARIANCE	= 2.385E-03
DISTORTION COEFFICIENT	= 0.205
PSEUDO FREQUENCY	= 150.0 Hz
DIMENSIONLESS AVERAGE PEAK PRESSURE	= 0.888
NUMBER OF DATA POINTS	= 1936

3. RESULTS OF FILE 3


RESULTS OF TEST RUN NUMBER 5, 11 FILES

ENGINE TEST SPEED	= 2000 RPM
COMPUTER ESTIMATED SPEED	= 1990 RPM
CORRELATION COEFFICIENT	= 0.985
VARIANCE	= 2.687E-03
DISTORTION COEFFICIENT	= 0.202
PSEUDO FREQUENCY	= 149.2 Hz
DIMENSIONLESS AVERAGE PEAK PRESSURE	= 0.882
NUMBER OF DATA POINTS	= 1980

4. RESULTS OF FILE 4

RESULTS OF TEST RUN NUMBER 6, 13 FILES

ENGINE TEST SPEED	= 2000 RPM
COMPUTER ESTIMATED SPEED	= 1992 RPM
CORRELATION COEFFICIENT	= 0.984
VARIANCE	= 2.938E-03
DISTORTION COEFFICIENT	= 0.206
PSEUDO FREQUENCY	= 148.3 Hz
DIMENSIONLESS AVERAGE PEAK PRESSURE	= 0.897
NUMBER OF DATA POINTS	= 2340



5. RESULTS OF FILE 5

RESULTS OF TEST RUN NUMBER 7, 15 FILES

ENGINE TEST SPEED	= 2250 RPM
COMPUTER ESTIMATED SPEED	= 2282 RPM
CORRELATION COEFFICIENT	= 0.986
VARIANCE	= 2.193E-03
DISTORTION COEFFICIENT	= 0.198
PSEUDO FREQUENCY	= 169.0 Hz
DIMENSIONLESS AVERAGE PEAK PRESSURE	= 0.852
NUMBER OF DATA POINTS	= 2340

6. RESULTS OF FILE 6

RESULTS OF TEST RUN NUMBER 8, 15 FILES

ENGINE TEST SPEED	= 2250 RPM
COMPUTER ESTIMATED SPEED	= 2270 RPM
CORRELATION COEFFICIENT	= 0.985
VARIANCE	= 2.788E-03
DISTORTION COEFFICIENT	= 0.233
PSEUDO FREQUENCY	= 165.1 Hz
DIMENSIONLESS AVERAGE PEAK PRESSURE	= 0.877
NUMBER OF DATA POINTS	= 2475

7. RESULTS OF FILE 7

RESULTS OF TEST RUN NUMBER 9, 15 FILES

ENGINE TEST SPEED	= 2250 RPM
COMPUTER ESTIMATED SPEED	= 2306 RPM
CORRELATION COEFFICIENT	= 0.991
VARIANCE	= 1.592E-03
DISTORTION COEFFICIENT	= 0.272
PSEUDO FREQUENCY	= 166.5 Hz
DIMENSIONLESS AVERAGE PEAK PRESSURE	= 0.904
NUMBER OF DATA POINTS	= 2370

8. RESULTS OF FILE 8

RESULTS OF TEST RUN NUMBER 10, 16 FILES

ENGINE TEST SPEED	= 2510 RPM
COMPUTER ESTIMATED SPEED	= 2514 RPM
CORRELATION COEFFICIENT	= 0.990
VARIANCE	= 1.775E-03
DISTORTION COEFFICIENT	= 0.195
PSEUDO FREQUENCY	= 184.0 Hz
DIMENSIONLESS AVERAGE PEAK PRESSURE	= 0.899
NUMBER OF DATA POINTS	= 2320

9. RESULTS OF FILE 9

RESULTS OF TEST RUN NUMBER 11, 17 FILES

ENGINE TEST SPEED	= 2510 RPM
COMPUTER ESTIMATED SPEED	= 2530 RPM
CORRELATION COEFFICIENT	= 0.990
VARIANCE	= 1.608E-03
DISTORTION COEFFICIENT	= 0.162
PSEUDO FREQUENCY	= 185.7 Hz
DIMENSIONLESS AVERAGE PEAK PRESSURE	= 0.884
NUMBER OF DATA POINTS	= 2414

10. RESULTS OF FILE 10

RESULTS OF TEST RUN NUMBER 12, 17 FILES

ENGINE TEST SPEED	= 2730 RPM
COMPUTER ESTIMATED SPEED	= 2761 RPM
CORRELATION COEFFICIENT	= 0.994
VARIANCE	= 9.581E-04
DISTORTION COEFFICIENT	= 0.297
PSEUDO FREQUENCY	= 183.5 Hz
DIMENSIONLESS AVERAGE PEAK PRESSURE	= 0.927
NUMBER OF DATA POINTS	= 2346

11. RESULTS OF FILE 11

RESULTS OF TEST RUN NUMBER 13, 19 FILES

ENGINE TEST SPEED	= 2980 RPM
COMPUTER ESTIMATED SPEED	= 2937 RPM
PERCENT RANDOM DELETIONS	= 2.8
PERCENT DATA NOT SAMPLED	= 0.1
DATA POINTS AVAILABLE	= 2546
CORRELATION COEFFICIENT	= 0.992
VARIANCE	= 1.395E-03
DISTORTION COEFFICIENT	= 0.326
PSEUDO FREQUENCY	= 196.5 Hz
DIMENSIONLESS AVERAGE PEAK PRESSURE	= 0.896
NUMBER OF DATA POINTS	= 2500

12. RESULTS OF FILE 12

RESULTS OF TEST RUN NUMBER 14, 26 FILES

ENGINE TEST SPEED	= 4020 RPM
COMPUTER ESTIMATED SPEED	= 4101 RPM
PERCENT RANDOM DELETIONS	= 38.7
PERCENT DATA NOT SAMPLED	= 5.2
DATA POINTS AVAILABLE	= 3276
CORRELATION COEFFICIENT	= 0.990
VARIANCE	= 1.737E-03
DISTORTION COEFFICIENT	= 0.314
PSEUDO FREQUENCY	= 212.4 Hz
DIMENSIONLESS AVERAGE PEAK PRESSURE	= 0.869
NUMBER OF DATA POINTS	= 2501

13. RESULTS OF FILE 13

RESULTS OF TEST RUN NUMBER 1, 29 FILES

ENGINE TEST SPEED	= 4250 RPM
COMPUTER ESTIMATED SPEED	= 4334 RPM
PERCENT RANDOM DELETIONS	= 49
PERCENT DATA NOT SAMPLED	= 4.7
DATA POINTS AVAILABLE	= 3567
CORRELATION COEFFICIENT	= 0.988
VARIANCE	= 2.5485E-03
DISTORTION COEFFICIENT	= 0.382
PSEUDO FREQUENCY	= 216.4 Hz
DIMENSIONLESS AVERAGE PEAK PRESSURE	= 0.851
NUMBER OF DATA POINTS	= 2501

14. RESULTS OF FILE 14

RESULTS OF TEST RUN NUMBER 2, 33 FILES

ENGINE TEST SPEED	= 4760 RPM
COMPUTER ESTIMATED SPEED	= 4796 RPM
PERCENT RANDOM DELETIONS	= 61.2
PERCENT DATA NOT SAMPLED	= 4.4
DATA POINTS AVAILABLE	= 3993
CORRELATION COEFFICIENT	= 0.988
VARIANCE	= 1.942E-03
DISTORTION COEFFICIENT	= 0.425
PSEUDO FREQUENCY	= 216.7 Hz
DIMENSIONLESS AVERAGE PEAK PRESSURE	= 0.877
NUMBER OF DATA POINTS	= 2501

APPENDIX VI
RESULTS OF ENGINE TESTING

APPENDIX VI
RESULTS OF ENGINE TESTING

The results of the engine testing are presented in Tables 1, 2, 3, 4, 5 and 6. The data presented was processed, reordered against increasing engine speed and is presented in Table 7. The ambient sound pressure levels measured inside the engine room and the engine room wall transmission loss measurements have been presented in Tables 8 and 9 respectively. The digitally sampled pressure values have been presented in Table 10. The minimum divisions on all measuring scales used during the engine testing are as follows:

1. Scale on angular position of tilting bank manometer: 1° (0.0349 radians)
2. Measuring scale of tilting bank manometer: 0.1 inches. The measurements are presented in columns two and three, titled SL. MANOMETER, of Tables 1. through 6.
3. The minimum division of the vertical manometer was: 0.1 inches. The measurements are presented in columns six and seven, titled V. MANOMETER, of Tables 1. through 6.
4. The minimum division on the potentiometer connected to the thermocouples was: 0.01 millivolts.
5. The minimum detectible engine speed variation, using the digital tachometer, was: 5 rpm.

TABLE 1. RAW ENGINE DATA
 SLOPING MANOMETER: 12°, MANOMETER COLUMN HEIGHTS ARE IN INCHES
 THERMOCOUPLE READINGS ARE IN MILLIVOLTS

TAPE 1	BAROMETRIC PRESSURE 100.4 kPa		V. MANOMETER		THERMOCOUPLES		ROOM TEMPERATURE 23 °C	LOAD	FUEL	TIME
RUN #	SL. MANOMETER	TAPE COUNT	HIGH	LEFT	RIGHT	NO. 1	NO. 2	RPM	LBF	MIN
1	0.25	120	180	2.9	2.7	19.58	11.48	2400	6.45	X--X 3.97
2	0.25	180	229	4.2	4.1	21.35	13.65	2740	8.45	X-X- 1.70
3	0.25	229	303	6.1	6.2	22.60	17.00	3060	8.90	X--X 1.80
4	0.25	303	361	5.5	5.4	21.67	15.96	2950	9.50	X--X 1.91
5	0.25	361	493	11.0	11.3	25.91	19.80	4000	10.40	X--X 1.48
6	0.25	494	550	12.2	12.4	27.29	21.30	4870	10.20	X--X 1.24
7	0.25	550	610	12.8	12.8	27.16	21.29	4810	10.10	X--X 1.34
8	0.25	610	673	10.7	10.9	27.33	20.64	4370	10.30	X--X 1.76
9	0.70	700	760	11.3	11.5	27.42	20.61	4370	10.95	X--X 1.35
10	0.70	760	822	14.3	14.4	27.72	21.75	5280	10.20	X--X 1.08
11	0.70	822	880	10.3	10.4	26.27	19.90	4000	10.15	X--X 1.56
12	0.70	880	940	9.0	9.1	24.30	18.05	3680	9.25	-X-X 1.25
13	0.70	940	1000	4.4	4.4	21.84	14.03	2790	8.55	X--X 2.49
14	0.70	1000	1060	2.2	2.0	18.62	10.30	2060	5.70	-X-X 3.44
15	0.70	1060	1120	2.2	2.0	19.40	11.17	2400	4.65	X--X 4.12

TABLE 2. RAW ENGINE DATA

SLOPING MANOMETER: 12°, MANOMETER COLUMN HEIGHTS ARE IN INCHES

THERMOCOUPLE READINGS ARE IN MILLIVOLTS

TAPE 2 RUN #	BAROMETRIC PRESSURE 101.0 kPa		V. MANOMETER		THERMOCOUPLES		SPEED RPM	LOAD LBF	FUEL	TIME MIN		
	SL. MANOMETER LEFT	SL. MANOMETER RIGHT	TAPE COUNT LOW	TAPE COUNT HIGH	LEFT	RIGHT					NO. 1	NO. 2
1	0.65	13.90	50	100	15.2	15.7	19.315	12.39	5830	2.95	X--X	0.98
2	0.65	12.65	100	150	14.2	14.7	27.29	21.33	5190	10.20	X--X	1.03
3	0.65	10.70	150	200	12.5	12.8	26.77	20.84	4900	10.55	X--X	1.21
4	0.65	8.40	200	250	10.6	10.9	27.50	20.74	4450	10.40	X--X	1.48
5	0.65	6.90	250	300	10.4	10.7	26.33	19.35	4150	10.10	X--X	1.60
6	0.60	3.25	351	418	4.8	4.8	20.97	13.74	2710	8.50	X--X	2.48
7	0.60	3.15	418	454	4.7	4.7	20.85	13.66	2850	8.15	X--X	2.38
8	0.60	2.60	454	500	3.7	3.5	20.07	12.54	2550	7.63	X-X-	1.41
9	0.80	1.65	600	650	1.7	1.5	20.03	10.48	1980	6.20	--XX	2.66
10	0.80	2.15	650	700	3.0	2.9	20.64	12.37	2490	6.47	X--X	3.22
11	0.80	3.00	700	750	4.5	4.5	22.69	14.69	2930	6.65	X--X	2.49
12	0.80	3.93	750	801	5.8	5.9	23.70	16.70	3130	7.00	X--X	2.34
13	0.78	5.70	801	850	8.0	8.0	25.21	18.37	3520	7.75	X--X	1.61
14	0.75	7.70	850	929	10.4	10.6	26.75	20.37	4160	9.20	X--X	1.45
15	0.75	8.15	929	965	10.6	10.8	27.40	21.00	4400	9.60	X--X	1.35
16	0.75	9.15	965	1010	11.1	11.4	28.48	21.85	4530	10.15	X--X	1.29

TABLE 2. RAW ENGINE DATA CONTINUED

RUN #	SL. MANOMETER		TAPE COUNT			V. MANOMETER		THERMOCOUPLES		SPEED RPM	LOAD LBF	FUEL	TIME MIN
	LEFT	RIGHT	LOW	HIGH	LEFT	RIGHT	NO. 1	NO. 2					
17	0.75	11.30	1010	1052	12.5	12.7	29.22	22.75	4770	10.20	X--X	1.17	
18	0.75	12.10	1052	1100	13.6	13.9	30.10	23.10	5000	9.10	X--X	1.09	
19	0.73	13.10	1100	1150	15.1	15.2	27.65	20.65	5270	5.40	X--X	1.05	
20	0.75	11.75	1150	1200	12.8	13.1	28.34	22.02	4790	10.25	X--X	1.13	
21	0.75	8.40	1250	1300	10.8	10.9	29.35	22.41	4300	10.15	X--X	1.38	
22	0.75	6.90	1300	1350	9.9	10.1	28.05	21.30	4000	9.45	X--X	1.54	
23	0.75	5.85	1350	1400	8.0	8.1	26.00	19.76	3730	8.95	X--X	1.81	
24	0.80	3.80	1400	1450	5.3	5.3	23.23	15.90	3000	8.70	X--X	2.28	
25	0.80	2.63	1450	1500	3.4	3.3	21.65	13.75	2500	7.10	-X-X	2.05	
26	0.80	1.80	1500	1550	2.5	2.3	20.00	11.73	2250	6.15	-X-X	2.23	

TABLE 3. RAW ENGINE DATA

SLOPING MANOMETER: 12°, MANOMETER COLUMN HEIGHTS ARE IN INCHES

THERMOCOUPLE READINGS ARE IN MILLIVOLTS

TAPE 3A	BAROMETRIC PRESSURE 101.1 kPa		ROOM TEMPERATURE 25.3 °C		DATE 76/04/12							
RUN #	SL. MANOMETER		TAPE COUNT V. MANOMETER		THERMOCOUPLES SPEED		LOAD	FUEL	TIME			
	LEFT	RIGHT	LOW	HIGH	LEFT	RIGHT	NO. 1	NO. 2	RPM	LBF		MIN
1	0.80	1.55	50	100	2.0	1.8	19.10	10.82	2270	4.10	X-X-	2.25
2	0.80	1.45	100	150	1.8	1.6	17.95	10.09	2000	4.90	XX--	1.34
3	0.80	2.75	200	250	3.9	3.9	21.47	14.00	2890	6.80	X--X	2.56
4	0.80	3.55	250	300	4.5	4.5	21.40	14.13	2860	8.35	X--X	1.67
5	0.80	4.20	300	350	5.7	5.8	22.47	16.45	3100	8.65	X--X	1.88
6	0.80	9.25	350	400	10.9	11.2	26.82	20.66	4230	10.20	X--X	1.38
7	0.75	9.15	400	450	10.6	10.8	27.51	21.11	4400	10.10	X--X	1.41
8	0.75	11.75	450	500	12.6	12.9	27.51	21.80	4900	9.95	X--X	1.11
9	0.75	12.70	500	550	14.1	14.8	27.04	20.85	5110	7.40	X--X	1.06

TABLE 4. RAW ENGINE DATA

SLOPING MANOMETER: 12°, MANOMETER COLUMN HEIGHTS ARE IN INCHES

THERMOCOUPLE READINGS ARE IN MILLIVOLTS

TAPE 3B	BAROMETRIC PRESSURE 100.4 kPa		ROOM TEMPERATURE 25.3 °C		DATE 76/04/13							
RUN #	SL. MANOMETER		TAPE COUNT V. MANOMETER		ROOM TEMPERATURE 25.3 °C	DATE 76/04/13						
	LEFT	RIGHT	LOW	HIGH	LEFT	RIGHT	NO. 1	NO. 2	RPM	LBF	FUEL	TIME
1	0.80	1.65	600	650	2.5	2.3	19.00	10.74	2300	3.55	X-X-	1.99
2	0.80	1.65	650	700	2.4	2.3	18.81	10.85	2270	5.40	X-X-	2.07
3	0.80	3.35	700	750	4.6	4.5	21.91	14.82	2930	8.25	X--X	2.23
4	0.80	3.35	750	800	4.4	4.4	21.95	13.69	2670	9.10	X--X	2.57
5	0.75	8.45	800	850	10.4	10.7	26.20	20.11	4260	10.15	X--X	1.38
6	0.75	7.40	850	900	10.3	10.4	25.47	19.47	4100	9.85	X--X	1.45
7	0.75	10.10	900	950	11.6	11.6	27.18	21.02	4570	10.65	X--X	1.28
8	0.75	7.35	1000	1050	10.5	10.8	25.01	19.75	3930	10.55	X--X	1.48
9	0.80	1.95	1050	1100	2.5	2.5	18.90	11.18	2180	6.80	-X-X	2.73

TABLE 4. RAW ENGINE DATA CONTINUED

RUN #	SL. MANOMETER		TAPE COUNT			V. MANOMETER		THERMOCOUPLES		SPEED	LOAD	FUEL	TIME
	LEFT	RIGHT	LOW	HIGH	LEFT	RIGHT	NO. 1	NO. 2	RPM				
10	0.80	2.00	1100	1150	2.9	2.8	19.16	11.52	2370	6.65	X-X-	1.72	
11	0.80	2.50	1150	1200	3.3	3.2	20.42	12.61	2680	7.25	X-X-	1.41	
12	0.80	3.25	1200	1250	4.6	4.6	21.04	14.70	3030	7.65	X-X-	1.16	
13	0.75	6.95	1250	1300	10.2	10.3	25.39	19.47	4090	9.40	X--X	1.47	
14	0.75	8.10	1300	1350	10.5	10.8	25.68	19.88	4250	10.20	X--X	1.41	
15	0.75	8.95	1350	1400	10.8	11.0	26.72	20.53	4400	10.55	X--X	1.37	
16	0.75	9.75	1400	1450	11.4	11.5	27.37	21.24	4600	10.45	X--X	1.31	
17	0.75	10.70	1450	1500	12.4	12.8	27.17	21.27	4760	10.30	X--X	1.18	
18	0.75	11.60	1500	1550	13.2	13.5	27.34	21.58	4910	9.80	X--X	1.12	

TABLE 5. RAW ENGINE DATA

SLOPING MANOMETER: 12", MANOMETER COLUMN HEIGHTS ARE IN INCHES

THERMOCOUPLE READINGS ARE IN MILLIVOLTS

TAPE #	SL. MANOMETER	BAROMETRIC PRESSURE 100.2 kPa	ROOM TEMPERATURE 22.2 °C	DATE 76/04/14								
RUN #	SL. MANOMETER	TAPE COUNT	V. MANOMETER	THERMOCOUPLES	SPEED	LOAD	FUEL	TIME				
	LEFT	RIGHT	LOW	HIGH	LEFT	RIGHT	NO. 1	NO. 2	RPM	LBF		MIN
1	0.80	1.55	50	100	1.8	1.7	17.55	10.09	2000	5.55	-X-X	3.46
2	0.80	1.70	100	150	2.3	2.2	18.56	10.75	2250	5.70	X-X-	2.09
3	0.80	2.10	150	200	3.0	2.9	19.83	12.18	2510	6.65	X-X-	1.62
4	0.80	2.50	200	250	3.4	3.4	20.60	13.00	2730	7.00	X-X-	1.37
5	0.80	3.15	250	300	4.4	4.5	21.55	14.28	2980	7.90	X-X-	1.17
6	0.78	7.10	300	350	10.2	10.4	25.10	19.28	4020	9.60	X-X-	0.97
7	0.75	8.10	350	400	10.8	11.0	25.86	20.00	4250	10.15	X-X	1.39
8	0.75	9.05	400	450	11.0	11.3	26.91	20.67	4390	10.55	X--X	1.38
9	0.75	11.00	450	500	12.5	12.7	27.10	21.27	4760	10.40	X--X	1.20
10	0.80	1.70	500	550	2.5	2.3	18.66	10.81	2250	5.80	X-X-	2.04
11	0.80	2.25	550	600	3.1	3.0	20.22	12.35	2570	6.60	XX--	0.76
12	0.80	3.13	600	650	4.4	4.5	22.32	14.08	2950	7.75	X--X	2.30
13	0.80	3.05	650	700	4.3	4.3	20.89	13.42	2750	8.15	X-X-	1.25
14	0.80	6.30	700	750	8.9	8.9	24.60	18.58	3780	9.55	-X-X	1.17
15	0.78	7.55	750	800	10.5	10.8	25.75	19.78	4100	10.10	X-X-	0.75
16	0.75	8.60	800	850	11.0	11.2	27.04	20.84	4300	10.65	-XX-	0.37

TABLE 5. RAW ENGINE DATA CONTINUED

RUN #	SL. MANOMETER		TAPE COUNT			V. MANOMETER		THERMOCOUPLES		SPEED	LOAD	FUEL	TIME
	LEFT	RIGHT	LOW	HIGH	LEFT	RIGHT	NO. 1	NO. 2	RPM				
17	0.75	9.40	850	900	11.3	11.5	27.53	21.40	4500	10.50	X--X	1.36	
18	0.75	10.80	900	950	12.2	12.4	27.15	21.29	4780	10.40	X--X	1.21	
19	0.70	12.20	950	1000	14.0	14.2	27.57	21.70	4950	9.35	X--X	1.10	
20	0.80	1.60	1000	1050	2.0	1.8	17.70	10.00	2100	5.50	XX--	1.05	
21	0.80	2.05	1050	1100	3.0	2.9	19.22	11.74	2360	6.57	X-X-	1.70	
22	0.80	2.40	1100	1150	3.3	3.2	20.04	12.51	2570	7.23	X-X-	1.46	
23	0.80	2.97	1150	1200	4.3	4.2	21.01	13.66	2850	7.75	X-X-	1.24	
24	0.80	3.30	1200	1250	4.5	4.6	21.94	14.55	2930	7.95	X-X-	1.19	
25	0.78	7.00	1250	1300	10.1	10.3	25.17	19.36	4000	9.50	-X-X	1.14	
26	0.78	8.00	1300	1350	10.5	10.7	25.87	19.90	4240	10.10	X-X-	0.72	
27	0.78	9.75	1350	1400	11.5	11.7	27.31	21.24	4500	10.65	X--X	1.37	
28	0.75	11.10	1400	1450	12.7	13.0	27.08	21.29	4780	10.40	X--X	1.15	
29	0.75	11.85	1450	1500	13.3	13.4	27.20	21.61	4900	9.85	--XX	0.32	

TABLE 6. RAW ENGINE DATA.

SLOPING MANOMETER: 12", MANOMETER COLUMN HEIGHTS ARE IN INCHES
THERMOCOUPLE READINGS ARE IN MILLIVOLTS

TAPE 5	BAROMETRIC PRESSURE 99.8 kPa		ROOM TEMPERATURE 24.5 °C		DATE 76/04/15							
RUN #	SL. MANOMETER	TAPE COUNT	V. MANOMETER	THERMOCOUPLES	SPEED	LOAD	FUEL	TIME				
	LEFT	RIGHT	LOW	HIGH	LEFT	RIGHT	NO.1	NO.2	RPM	LBF	MIN	
1	0.80	1.70	50	100	2.3	2.2	17.74	9.85	2100	5.45	X-X-	2.30
2	0.80	1.65	100	150	2.4	2.3	18.23	10.59	2240	5.60	X-X-	2.78
3	0.80	2.25	150	200	3.2	3.2	19.31	11.99	2460	6.90	X--X	3.15
4	0.80	2.80	200	250	4.0	3.9	20.16	12.79	2660	7.85	X-X-	1.49
5	0.80	3.15	250	300	4.6	4.6	21.27	13.79	2850	8.15	X--X	1.78

Fuel measurements were calibrated as follows:

1. X--X corresponds to 0.1195 lbm
2. -X-X corresponds to 0.0899 lbm
3. --XX corresponds to 0.0589 lbm
4. X-X- corresponds to 0.0606 lbm
5. XX-- corresponds to 0.0305 lbm
6. -XX- corresponds to 0.0310 lbm

TABLE 7. RESULTS OF ENGINE DATA REDUCTION

RUN #	SPEED RPM	AIR FLOW RATE		STATIC PRESSURE kPa	TEMPERATURE		POWER kW	FUEL FLOW kg/hr. kg/kW. hr	BSFC
		ACTUAL m ³ /min	THEORETICAL m ³ /min		NO. 1 °C	NO.2 °C			
1	1980	0.155	0.214	0.795	485.6	260.6	0.915	0.602	0.658
2	2000	0.137	0.216	0.844	436.5	251.4	0.731	0.620	0.849
3	2000	0.147	0.216	0.870	427.1	251.4	0.828	0.707	0.854
4	2060	0.165	0.222	1.044	452.3	256.3	0.876	0.711	0.812
5	2100	0.162	0.227	1.118	431.6	245.7	0.853	0.718	0.841
6	2100	0.152	0.227	0.944	430.7	249.3	0.861	0.791	0.919
7	2180	0.183	0.235	1.242	458.9	277.1	1.105	0.896	0.811
8	2240	0.157	0.242	1.167	443.1	263.2	0.935	0.594	0.635
9	2250	0.161	0.243	1.118	450.9	266.9	0.956	0.790	0.826
10	2250	0.169	0.243	1.193	484.8	290.0	1.032	1.097	1.063
11	2250	0.161	0.243	1.193	453.3	268.3	0.973	0.809	0.831
12	2270	0.157	0.245	1.167	456.8	269.3	0.914	0.797	0.872
13	2270	0.147	0.245	0.944	463.6	268.6	0.694	0.735	1.059
14	2300	0.157	0.248	1.192	461.3	266.7	0.609	0.829	1.362
15	2360	0.190	0.255	1.466	466.5	290.2	1.156	0.971	0.840
16	2370	0.187	0.256	1.415	465.1	285.1	1.175	0.960	0.817
17	2400	0.161	0.259	1.044	470.7	276.8	0.832	0.790	0.949
18	2400	0.197	0.259	1.391	475.0	284.1	1.154	0.819	0.710

TABLE 7. RESULTS OF ENGINE DATA REDUCTION CONTINUED

RUN #	SPEED RPM	AIR FLOW RATE		STATIC PRESSURE kPa	TEMPERATURE		POWER kW	FUEL FLOW kg/hr	BSFC kg/kWh hr
		ACTUAL m ³ /min	THEORETICAL m ³ /min		NO.1 °C	NO.2 °C			
19	2460	0.206	0.266	1.590	468.6	296.1	1.266	1.033	0.816
20	2490	0.196	0.269	1.466	499.8	305.1	1.201	1.010	0.841
21	2500	0.228	0.270	1.665	523.7	337.6	1.324	1.193	0.902
22	2510	0.194	0.271	1.466	480.8	300.6	1.245	1.019	0.819
23	2550	0.239	0.275	1.776	486.5	309.1	1.451	1.175	0.810
24	2570	0.204	0.278	1.516	490.0	304.6	1.265	1.093	0.864
25	2570	0.215	0.278	1.615	485.8	308.4	1.386	1.134	0.819
26	2660	0.241	0.287	1.962	488.6	315.0	1.557	1.108	0.711
27	2670	0.272	0.288	2.185	530.8	336.2	1.812	1.266	0.699
28	2680	0.222	0.289	1.614	494.7	310.7	1.449	1.171	0.808
29	2710	0.273	0.293	2.385	507.7	337.4	1.718	1.312	0.764
30	2730	0.221	0.295	1.690	499.0	319.9	1.425	1.205	0.845
31	2740	0.186	0.296	2.062	516.7	335.1	1.727	0.971	0.562
32	2750	0.255	0.297	2.137	505.8	329.8	1.671	1.310	0.784
33	2790	0.276	0.301	2.186	528.1	344.2	1.779	1.306	0.734
34	2850	0.270	0.308	2.335	504.9	335.5	1.732	1.367	0.789
35	2850	0.250	0.308	2.112	508.6	335.5	1.647	1.331	0.808
36	2850	0.262	0.308	2.285	514.8	338.5	1.732	1.827	1.055

TABLE 7. RESULTS OF ENGINE DATA REDUCTION CONTINUED

RUN #	SPEED RPM	AIR FLOW RATE		STATIC PRESSURE kPa	TEMPERATURE		POWER kW	FUEL FLOW kg/hr	BSFC kg/kWh hr
		ACTUAL m ³ /min	THEORETICAL m ³ /min		NO.1 °C	NO.2 °C			
37	2860	0.282	0.309	2.235	517.8	346.6	1.781	1.948	1.094
38	2890	0.237	0.312	1.937	519.5	343.5	1.465	1.271	0.867
39	2930	0.268	0.316	2.261	530.6	356.4	1.737	1.387	0.799
40	2930	0.250	0.316	2.236	548.2	359.7	1.453	1.309	0.901
41	2930	0.272	0.316	2.260	529.8	362.8	1.803	1.459	0.809
42	2950	0.231	0.319	2.708	524.2	389.7	2.090	1.703	0.815
43	2950	0.259	0.319	2.212	539.5	345.4	1.705	1.414	0.830
44	2980	0.260	0.322	2.212	521.4	350.1	1.756	1.417	0.807
45	3000	0.292	0.324	2.633	560.9	388.3	1.946	1.427	0.733
46	3030	0.267	0.327	2.285	509.3	360.0	1.728	1.423	0.823
47	3060	0.249	0.330	3.056	546.1	414.2	2.031	1.807	0.890
48	3100	0.313	0.335	2.856	543.0	401.2	2.000	1.735	0.868
49	3130	0.298	0.338	2.907	572.0	407.1	1.634	1.390	0.851
50	3520	0.374	0.380	3.975	607.6	446.4	2.034	2.020	0.993
51	3680	0.370	0.397	4.497	586.2	438.9	2.538	1.957	0.771
52	3730	0.381	0.403	4.000	626.2	479.2	2.489	1.797	0.722
53	3780	0.398	0.408	4.423	593.2	451.4	2.692	2.091	0.777
54	3930	0.438	0.424	5.289	602.9	479.0	3.092	2.198	0.711

TABLE 7. RESULTS OF ENGINE DATA REDUCTION CONTINUED

RUN #	SPEED RPM	AIR FLOW RATE		STATIC PRESSURE kPa	TEMPERATURE		POWER kW	FUEL FLOW kg/hr	BSFC kg/kWh hr
		ACTUAL m ³ /min	THEORETICAL m ³ /min		NO. 1 °C	NO. 2 °C			
55	4000	0.418	0.432	4.969	674.5	515.5	2.819	2.112	0.749
56	4000	0.423	0.432	5.070	606.6	469.8	2.834	2.146	0.757
57	4000	0.411	0.432	5.541	624.1	480.1	3.102	2.198	0.708
58	4000	0.426	0.432	5.143	632.6	482.5	3.028	2.085	0.689
59	4020	0.427	0.434	5.119	605.0	467.9	2.878	1.702	0.591
60	4090	0.424	0.442	5.091	611.8	472.4	2.867	2.213	0.772
61	4100	0.439	0.443	5.140	613.7	472.4	3.012	2.243	0.745
62	4100	0.442	0.443	5.293	620.3	479.7	3.088	2.201	0.713
63	4150	0.423	0.448	5.242	634.0	469.5	3.126	2.039	0.652
64	4160	0.444	0.449	5.217	643.9	493.6	2.854	2.251	0.789
65	4230	0.494	0.457	5.488	645.5	500.4	3.217	2.357	0.733
66	4240	0.456	0.458	5.268	623.1	482.5	3.193	2.292	0.718
67	4250	0.460	0.459	5.417	622.9	484.8	3.217	2.340	0.727
68	4250	0.462	0.459	5.289	618.5	482.0	3.233	2.307	0.714
69	4260	0.473	0.460	5.240	630.9	487.4	3.224	2.357	0.731
70	4300	0.466	0.464	5.391	705.1	541.6	3.255	2.357	0.724
71	4300	0.476	0.464	5.517	650.7	504.6	3.415	2.281	0.668
72	4370	0.454	0.472	5.367	657.4	499.9	3.356	1.848	0.551

TABLE 7. RESULTS OF ENGINE DATA REDUCTION CONTINUED

RUN #	SPEED RPM	AIR FLOW RATE		STATIC PRESSURE kPa	TEMPERATURE		POWER kW	FUEL FLOW kg/hr	BSFC kg/kWh. hr
		ACTUAL m ³ /min	THEORETICAL m ³ /min		NO.1 °C	NO.2 °C			
73	4370	0.480	0.472	5.665	659.7	499.1	3.568	2.409	0.675
74	4390	0.489	0.474	5.542	647.6	500.6	3.454	2.357	0.682
75	4400	0.488	0.475	5.413	643.2	497.3	3.462	2.374	0.686
76	4400	0.492	0.475	5.314	661.8	511.0	3.314	2.315	0.699
77	4400	0.459	0.475	5.317	659.2	508.4	3.150	2.409	0.765
78	4450	0.471	0.481	5.342	661.5	502.3	3.451	2.205	0.639
79	4500	0.499	0.486	5.666	662.2	517.8	3.523	2.392	0.679
80	4500	0.508	0.486	5.765	657.1	514.1	3.574	2.374	0.664
81	4530	0.489	0.489	5.590	684.6	528.4	3.429	2.531	0.738
82	4570	0.521	0.494	5.761	654.0	508.9	3.629	2.541	0.700
83	4600	0.511	0.497	5.686	658.4	513.9	3.585	2.483	0.693
84	4760	0.537	0.514	6.258	653.8	514.8	3.656	2.757	0.754
85	4760	0.543	0.514	6.262	652.1	514.8	3.692	2.711	0.734
86	4770	0.548	0.515	6.261	702.1	549.6	3.628	2.780	0.766
87	4780	0.538	0.516	6.113	653.3	515.2	3.707	2.688	0.725
88	4780	0.546	0.516	6.387	651.6	515.2	3.707	2.828	0.763
89	4790	0.559	0.517	6.435	681.3	532.4	3.661	2.879	0.786
90	4810	0.508	0.519	6.361	653.5	515.2	3.623	2.427	0.670

TABLE 7. RESULTS OF ENGINE DATA REDUCTION CONTINUED

RUN #	SPEED RPM	AIR FLOW RATE		STATIC PRESSURE kPa	TEMPERATURE		POWER kW	FUEL FLOW kg/hr	BSFC kg/kWh. hr
		ACTUAL m ³ /min	THEORETICAL m ³ /min		NO.1 °C	NO.2 °C			
91	4870	0.444	0.526	6.112	656.5	515.5	3.704	2.623	0.708
92	4900	0.565	0.529	6.635	654.5	522.8	3.599	5.007	1.391
93	4900	0.537	0.529	6.286	644.2	504.6	3.855	2.688	0.697
94	4900	0.563	0.529	6.332	661.8	527.3	3.636	2.944	0.810
95	4910	0.561	0.530	6.630	657.8	522.1	3.588	2.904	0.809
96	4950	0.576	0.535	7.008	663.2	524.9	3.451	2.957	0.857
97	5000	0.568	0.540	6.832	722.8	557.9	3.393	2.984	0.880
98	5110	0.587	0.552	7.176	650.7	504.9	2.820	3.083	1.093
99	5190	0.587	0.561	7.180	656.6	516.2	3.948	3.173	0.804
100	5270	0.593	0.569	7.528	665.1	500.2	2.122	3.098	1.460
101	5280	0.581	0.570	7.131	666.7	526.1	4.016	3.012	0.750
102	5830	0.616	0.630	7.677	468.7	305.4	1.282	3.319	2.588

TABLE 8. AMBIENT SOUND PRESSURE LEVELS MEASURED
INSIDE THE ENGINE ROOM.

FREQUENCY	SOUND PRESSURE LEVEL
Hertz	dB re. 20 μ Pa.
20	58
25	50
32	49
40	44
50	51
63	48
80	41
100	37
125	42
160	41
200	34
250	30
315	34
400	28
500	27
630	20
800	22
1000	22

TABLE 9. ENGINE ROOM WALL TRANSMISSION LOSS

FREQUENCY	SOUND PRESSURE LEVEL
Hertz	dB re 20 μ Pa.
100	20.0
100	24.0
150	22.0
150	23.5
200	25.0
200	21.0
200	23.5
250	32.0
250	24.0
300	27.0
300	26.5
315	28.5
350	29.0
400	35.0
400	33.0
400	34.0
500	38.0
500	35.5
500	36.0
600	38.0
700	37.0
800	51.0
800	44.0
1000	55.5
1000	50.0
1250	51.5
1250	51.5
1600	52.0
2000	58.0
2500	68.0
3150	61.0

TABLE 10. SAMPLED VALUES OF PEAK PRESSURE AND RELATIVE PRESSURE

SPEED	AVE PR	PEAK	SPEED	AVE PR	PEAK	SPEED	AVE PR	PEAK
1980	0.138	16.12	2060	0.135	16.15	2250	0.162	18.37
1980	0.140	17.62	2060	0.142	17.12	2250	0.158	18.07
1980	0.138	16.87	2060	0.134	16.15	2250	0.162	18.37
1980	0.138	16.12	2060	0.121	14.19	2250	0.151	17.65
1980	0.138	16.87	2060	0.139	16.15	2250	0.158	18.90
1980	0.139	16.12	2060	0.130	16.10	2250	0.154	17.65
1980	0.139	16.87	2100	0.178	20.98	2250	0.151	17.65
1980	0.145	17.62	2100	0.181	21.39	2250	0.160	18.37
1980	0.138	16.12	2100	0.178	20.98	2250	0.157	19.31
2000	0.121	14.62	2100	0.178	20.56	2250	0.168	19.31
2000	0.130	15.58	2100	0.180	20.98	2250	0.155	17.65
2000	0.126	15.16	2100	0.173	20.14	2250	0.167	19.31
2000	0.109	13.87	2100	0.181	20.56	2250	0.152	17.62
2000	0.124	14.74	2100	0.176	20.56	2250	0.162	19.31
2000	0.125	15.16	2100	0.178	20.56	2250	0.153	18.37
2000	0.154	18.90	2180	0.183	21.37	2250	0.153	18.07
2000	0.144	17.24	2180	0.183	22.12	2250	0.150	17.24
2000	0.111	13.87	2180	0.188	22.12	2250	0.155	18.07
2000	0.125	14.74	2180	0.186	22.12	2250	0.160	18.48
2000	0.127	15.16	2180	0.186	22.12	2250	0.158	18.37
2000	0.108	13.12	2180	0.175	20.62	2250	0.159	18.48
2000	0.113	13.87	2180	0.189	22.12	2270	0.161	28.87
2000	0.107	13.87	2180	0.179	20.62	2270	0.139	17.62
2000	0.109	13.12	2180	0.189	22.12	2270	0.139	16.87
2000	0.113	13.87	2250	0.162	18.37	2270	0.162	26.62
2000	0.117	13.87	2250	0.155	16.48	2270	0.137	16.12
2060	0.138	16.15	2250	0.164	19.12	2270	0.141	19.87
2060	0.137	16.15	2250	0.155	18.07	2270	0.142	20.62
2060	0.137	16.15	2250	0.148	17.62	2270	0.158	19.12
2060	0.138	16.15	2250	0.152	17.65	2270	0.154	17.62

TABLE 10. SAMPLED VALUES OF PEAK PRESSURE AND RELATIVE PRESSURE

CONTINUED

SPEED	AVE PR	PEAK	SPEED	AVE PR	PEAK	SPEED	AVE PR	PEAK
2270	0.138	18.37	2370	0.166	20.62	2490	0.169	19.12
2270	0.154	17.62	2370	0.168	19.87	2490	0.163	19.12
2270	0.137	16.12	2370	0.166	19.12	2490	0.164	19.12
2270	0.158	19.12	2370	0.165	19.12	2490	0.166	19.12
2270	0.156	18.37	2370	0.166	19.87	2490	0.165	19.12
2270	0.158	19.12	2370	0.165	19.87	2490	0.169	19.87
2270	0.155	17.62	2400	0.176	20.06	2500	0.159	18.37
2270	0.156	18.37	2400	0.140	16.15	2500	0.160	19.12
2270	0.157	19.87	2400	0.179	20.06	2500	0.161	18.37
2300	0.162	22.12	2400	0.170	19.08	2500	0.161	18.37
2300	0.167	25.87	2400	0.144	17.12	2500	0.162	19.87
2300	0.181	34.86	2400	0.180	20.06	2500	0.161	19.12
2300	0.179	28.87	2400	0.166	19.08	2500	0.160	18.37
2300	0.169	26.62	2400	0.177	20.06	2500	0.159	17.62
2300	0.160	22.87	2400	0.143	16.15	2510	0.159	18.48
2300	0.181	27.37	2400	0.174	20.06	2510	0.161	18.90
2300	0.185	31.87	2400	0.142	17.12	2510	0.159	18.48
2300	0.173	32.62	2400	0.178	20.06	2510	0.160	18.48
2360	0.171	19.73	2400	0.175	20.06	2510	0.168	20.14
2360	0.169	19.31	2400	0.175	20.06	2510	0.164	19.31
2360	0.172	20.56	2400	0.144	17.12	2510	0.161	18.48
2360	0.172	20.14	2400	0.178	20.06	2510	0.162	18.90
2360	0.170	19.31	2400	0.140	16.15	2510	0.164	18.90
2360	0.171	20.14	2400	0.141	16.15	2550	0.175	20.62
2360	0.173	20.14	2400	0.146	17.12	2550	0.175	19.87
2360	0.171	20.14	2400	0.163	29.85	2550	0.174	19.87
2360	0.171	20.56	2400	0.147	18.10	2550	0.176	19.87
2370	0.166	19.12	2490	0.164	19.12	2550	0.176	20.62
2370	0.165	19.12	2490	0.166	19.87	2550	0.179	21.37
2370	0.164	19.12	2490	0.165	19.12	2550	0.179	20.62

TABLE 10. SAMPLED VALUES OF PEAK PRESSURE AND RELATIVE PRESSURE

CONTINUED

SPEED	AVE PR	PEAK	SPEED	AVE PR	PEAK	SPEED	AVE PR	PEAK
2570	0.156	18.07	2680	0.177	20.62	2750	0.215	24.30
2570	0.168	19.31	2680	0.184	21.37	2750	0.206	23.47
2570	0.155	17.65	2680	0.183	21.37	2750	0.223	25.13
2570	0.155	17.65	2680	0.180	21.37	2750	0.218	24.30
2570	0.167	19.31	2680	0.181	21.37	2750	0.224	25.13
2570	0.163	18.48	2680	0.181	21.37	2750	0.211	23.88
2570	0.156	17.65	2680	0.177	20.62	2750	0.209	23.88
2570	0.167	19.31	2710	0.201	22.87	2750	0.228	25.96
2570	0.166	19.31	2710	0.232	25.87	2750	0.212	24.30
2570	0.156	17.65	2710	0.252	28.87	2790	0.224	24.95
2570	0.154	17.65	2710	0.207	24.37	2790	0.229	25.93
2570	0.156	17.65	2710	0.203	22.87	2790	0.226	26.91
2570	0.155	17.65	2710	0.214	24.37	2790	0.226	25.93
2570	0.168	18.90	2710	0.209	24.37	2790	0.231	25.93
2570	0.166	19.31	2710	0.243	28.12	2790	0.232	25.93
2570	0.156	18.07	2710	0.202	22.87	2790	0.226	25.93
2570	0.170	19.73	2710	0.202	24.37	2790	0.233	25.93
2570	0.166	19.31	2710	0.200	23.62	2790	0.217	25.93
2670	0.213	25.12	2710	0.216	25.12	2790	0.229	25.93
2670	0.206	23.62	2710	0.206	24.37	2850	0.242	28.04
2670	0.213	25.12	2730	0.192	22.22	2850	0.242	28.87
2670	0.214	25.87	2730	0.196	23.05	2850	0.238	27.37
2670	0.207	25.12	2730	0.195	22.64	2850	0.232	25.87
2670	0.208	24.37	2730	0.195	22.22	2850	0.245	28.04
2670	0.174	19.87	2730	0.195	22.64	2850	0.245	27.62
2670	0.207	25.12	2730	0.190	21.39	2850	0.245	27.37
2670	0.204	23.62	2730	0.193	22.22	2850	0.245	28.04
2670	0.208	25.12	2730	0.204	23.47	2850	0.244	28.04
2680	0.182	20.62	2730	0.194	22.64	2850	0.245	27.62
2680	0.181	21.37	2750	0.215	24.30	2850	0.216	25.87

TABLE 10. SAMPLED VALUES OF PEAK PRESSURE AND RELATIVE PRESSURE

CONTINUED

SPEED	AVE PR	PEAK	SPEED	AVE PR	PEAK	SPEED	AVE PR	PEAK
2850	0.238	28.12	2930	0.243	28.87	2980	0.235	26.37
2850	0.246	27.21	2930	0.257	35.61	2980	0.251	28.45
2850	0.246	27.62	2930	0.251	28.45	2980	0.251	28.04
2850	0.239	26.79	2930	0.248	28.04	2980	0.252	28.87
2850	0.233	26.62	2930	0.251	28.87	2980	0.248	28.04
2860	0.243	28.12	2930	0.249	28.45	2980	0.251	28.04
2860	0.239	27.37	2930	0.251	28.87	2980	0.251	28.45
2860	0.242	28.12	2930	0.238	27.37	2980	0.247	28.04
2860	0.243	27.37	2930	0.250	28.12	3000	0.256	28.87
2860	0.242	27.37	2930	0.255	37.11	3000	0.254	29.62
2860	0.245	28.12	2930	0.250	29.28	3000	0.257	28.87
2860	0.241	26.62	2930	0.251	32.62	3000	0.255	28.87
2860	0.245	27.37	2930	0.251	38.61	3000	0.255	29.62
2860	0.240	28.12	2930	0.251	34.12	3000	0.251	28.12
2890	0.211	25.12	2930	0.256	40.11	3000	0.258	29.62
2890	0.217	25.87	2930	0.251	28.12	3000	0.257	29.62
2890	0.216	24.37	2930	0.243	33.37	3030	0.245	29.62
2890	0.225	31.87	2930	0.248	28.12	3030	0.232	27.37
2890	0.219	25.87	2930	0.238	30.37	3030	0.259	35.61
2890	0.219	25.12	2930	0.233	27.37	3030	0.251	38.61
2890	0.218	25.12	2950	0.247	28.45	3030	0.249	31.12
2890	0.215	24.37	2950	0.251	28.45	3030	0.241	34.86
2890	0.212	25.12	2950	0.249	28.04	3030	0.231	28.12
2930	0.247	27.62	2950	0.237	26.79	3030	0.237	28.87
2930	0.251	28.04	2950	0.247	27.62	3030	0.237	30.37
2930	0.251	28.87	2950	0.244	28.04	3100	0.260	30.37
2930	0.241	27.37	2950	0.249	28.04	3100	0.242	28.12
2930	0.242	28.12	2950	0.246	27.62	3100	0.249	28.87
2930	0.247	28.45	2950	0.249	27.62	3100	0.257	29.62
2930	0.249	28.04	2980	0.251	28.04	3100	0.246	28.87

TABLE 10. SAMPLED VALUES OF PEAK PRESSURE AND RELATIVE PRESSURE

CONTINUED

SPEED	AVE PR	PEAK	SPEED	AVE PR	PEAK	SPEED	AVE PR	PEAK
3100	0.254	30.37	3680	0.319	35.72	4000	0.336	37.86
3100	0.242	28.12	3680	0.314	34.74	4000	0.332	37.59
3100	0.252	28.87	3730	0.311	35.61	4000	0.336	37.86
3100	0.247	28.87	3730	0.308	35.61	4000	0.365	41.59
3130	0.233	33.37	3730	0.308	35.61	4000	0.324	37.59
3130	0.243	34.12	3730	0.312	34.86	4000	0.338	38.61
3130	0.260	37.86	3730	0.300	34.86	4000	0.371	41.59
3130	0.236	36.36	3730	0.309	35.61	4000	0.339	42.99
3130	0.238	37.11	3730	0.312	36.36	4000	0.339	37.67
3130	0.273	39.36	3730	0.307	35.61	4000	0.342	38.65
3130	0.248	38.61	3780	0.320	36.76	4000	0.379	42.57
3130	0.231	37.11	3780	0.320	37.17	4000	0.335	37.86
3130	0.233	30.37	3780	0.321	36.76	4000	0.380	42.57
3520	0.315	37.86	3780	0.322	37.17	4000	0.333	37.67
3520	0.280	37.11	3780	0.321	36.34	4000	0.337	37.67
3520	0.309	40.11	3780	0.322	38.00	4000	0.371	41.59
3520	0.330	42.36	3780	0.323	36.34	4000	0.336	40.5
3520	0.312	46.86	3780	0.319	36.34	4000	0.379	43.54
3520	0.296	49.11	3780	0.321	35.51	4000	0.334	38.42
3520	0.311	37.86	3780	0.322	36.34	4000	0.335	38.42
3520	0.318	55.11	3930	0.336	39.36	4000	0.337	37.67
3520	0.318	45.36	3930	0.335	37.86	4000	0.332	37.86
3680	0.320	35.72	3930	0.335	37.86	4000	0.333	37.86
3680	0.285	32.78	3930	0.333	37.86	4000	0.334	37.86
3680	0.319	35.72	3930	0.342	39.36	4000	0.354	39.63
3680	0.300	33.76	3930	0.343	38.61	4000	0.334	37.67
3680	0.320	35.72	3930	0.330	37.11	4000	0.340	38.65
3680	0.298	33.76	3930	0.336	37.86	4000	0.354	39.63
3680	0.315	34.74	3930	0.326	37.86	4000	0.358	39.63
3680	0.300	33.76	4000	0.333	40.91	4000	0.365	40.61

116

TABLE 10. SAMPLED VALUES OF PEAK PRESSURE AND RELATIVE PRESSURE

CONTINUED

SPEED	AVE PR	PEAK	SPEED	AVE PR	PEAK	SPEED	AVE PR	PEAK
4000	0.334	38.00	4090	0.328	46.86	4150	0.340	38.61
4000	0.374	41.59	4090	0.327	37.86	4150	0.347	39.36
4000	0.334	38.83	4090	0.326	37.86	4150	0.340	39.36
4000	0.329	37.11	4090	0.330	37.86	4150	0.346	39.36
4000	0.362	41.59	4090	0.331	42.36	4150	0.348	39.36
4000	0.366	41.59	4090	0.331	39.36	4150	0.345	39.36
4000	0.334	37.67	4090	0.346	53.61	4150	0.347	40.11
4000	0.341	37.67	4090	0.325	40.11	4160	0.344	43.86
4000	0.361	40.61	4090	0.323	40.11	4160	0.338	43.11
4000	0.361	40.61	4100	0.338	37.59	4160	0.344	45.36
4000	0.361	40.61	4100	0.321	36.36	4160	0.334	37.86
4000	0.380	42.57	4100	0.340	38.42	4160	0.356	57.36
4000	0.341	37.67	4100	0.324	37.86	4160	0.344	45.36
4000	0.378	41.59	4100	0.319	37.11	4160	0.334	39.36
4000	0.364	39.63	4100	0.341	38.00	4160	0.341	48.36
4000	0.383	43.54	4100	0.315	36.36	4160	0.348	46.11
4000	0.340	37.67	4100	0.340	38.00	4160	0.337	40.86
4000	0.383	43.54	4100	0.320	37.11	4160	0.325	37.11
4000	0.373	41.59	4100	0.318	36.36	4160	0.338	40.11
4000	0.384	41.59	4100	0.337	37.59	4160	0.338	40.86
4000	0.379	42.57	4100	0.338	37.59	4160	0.328	37.86
4020	0.340	38.00	4100	0.316	36.36	4160	0.338	38.61
4020	0.339	38.42	4100	0.340	38.83	4230	0.361	40.86
4020	0.342	39.25	4100	0.322	37.11	4230	0.356	40.11
4020	0.347	44.23	4100	0.318	37.11	4230	0.361	40.86
4020	0.341	38.83	4100	0.334	37.59	4230	0.360	40.86
4020	0.380	43.82	4100	0.336	38.00	4230	0.358	40.11
4020	0.341	38.42	4100	0.337	38.42	4230	0.361	41.61
4020	0.342	38.83	4150	0.350	40.86	4230	0.364	41.61
4020	0.343	39.67	4150	0.340	37.86	4230	0.360	40.86

TABLE 10. SAMPLED VALUES OF PEAK PRESSURE AND RELATIVE PRESSURE

CONTINUED

SPEED	AVE PR	PEAK	SPEED	AVE PR	PEAK	SPEED	AVE PR	PEAK
4230	0.364	41.61	4260	0.325	37.86	4370	0.349	38.65
4240	0.325	36.34	4260	0.328	38.61	4370	0.343	38.65
4240	0.325	36.76	4260	0.326	37.11	4370	0.337	37.67
4240	0.328	37.17	4260	0.323	37.11	4370	0.342	38.65
4240	0.326	36.34	4260	0.325	37.11	4370	0.347	39.63
4240	0.327	37.17	4260	0.326	37.11	4370	0.346	38.65
4240	0.325	36.76	4260	0.323	36.36	4370	0.343	38.65
4240	0.325	38.42	4300	0.336	37.86	4370	0.336	38.65
4240	0.328	37.59	4300	0.338	38.42	4370	0.336	37.67
4240	0.320	36.34	4300	0.341	38.00	4370	0.325	36.69
4250	0.329	37.17	4300	0.341	39.25	4370	0.330	37.67
4250	0.333	36.76	4300	0.340	38.61	4370	0.342	38.65
4250	0.320	36.36	4300	0.339	38.61	4370	0.333	37.67
4250	0.326	37.86	4300	0.336	38.42	4370	0.346	38.65
4250	0.320	37.11	4300	0.340	38.00	4370	0.331	36.69
4250	0.331	38.00	4300	0.340	38.00	4370	0.343	37.67
4250	0.314	35.51	4300	0.339	38.61	4370	0.330	36.69
4250	0.330	36.76	4300	0.341	38.61	4390	0.332	37.59
4250	0.321	37.86	4300	0.338	38.42	4390	0.333	37.59
4250	0.328	36.76	4300	0.339	37.86	4390	0.318	36.76
4250	0.318	37.11	4300	0.333	37.17	4390	0.329	36.76
4250	0.319	36.36	4300	0.341	37.86	4390	0.334	37.59
4250	0.325	37.17	4300	0.338	37.59	4390	0.331	37.17
4250	0.331	37.59	4300	0.337	38.61	4390	0.329	36.76
4250	0.321	37.11	4370	0.345	39.63	4390	0.329	37.17
4250	0.331	38.00	4370	0.329	36.69	4390	0.330	37.17
4250	0.322	37.11	4370	0.340	37.67	4400	0.337	37.86
4250	0.322	38.61	4370	0.331	36.69	4400	0.291	34.12
4260	0.322	37.86	4370	0.342	39.63	4400	0.318	37.11
4260	0.325	37.11	4370	0.339	37.67	4400	0.307	35.61

TABLE 10. SAMPLED VALUES OF PEAK PRESSURE AND RELATIVE PRESSURE

CONTINUED

SPEED	AVE PR	PEAK	SPEED	AVE PR	PEAK	SPEED	AVE PR	PEAK
4400	0.322	37.11	4500	0.316	35.51	4570	0.297	33.37
4400	0.309	34.86	4500	0.307	35.10	4570	0.285	33.37
4400	0.324	37.11	4500	0.297	34.27	4570	0.296	34.12
4400	0.317	37.86	4500	0.292	33.44	4570	0.290	34.12
4400	0.305	34.86	4500	0.264	30.11	4570	0.295	33.37
4400	0.307	35.61	4500	0.303	34.27	4600	0.295	33.37
4400	0.311	35.61	4500	0.311	35.10	4600	0.291	33.37
4400	0.309	34.86	4500	0.311	35.10	4600	0.284	32.62
4400	0.341	38.61	4500	0.297	34.27	4600	0.295	34.12
4400	0.324	36.36	4500	0.308	34.68	4600	0.290	32.62
4400	0.317	36.36	4500	0.301	34.68	4600	0.288	32.62
4400	0.311	35.61	4500	0.268	30.11	4600	0.289	32.62
4400	0.334	38.61	4500	0.309	34.68	4600	0.288	32.62
4400	0.342	39.36	4500	0.308	34.68	4600	0.291	32.62
4400	0.342	39.36	4500	0.311	35.10	4760	0.264	31.36
4400	0.314	36.36	4500	0.311	35.51	4760	0.258	29.28
4400	0.338	38.61	4500	0.317	35.93	4760	0.328	37.86
4400	0.341	39.36	4500	0.314	35.51	4760	0.259	29.28
4400	0.335	37.86	4530	0.304	34.86	4760	0.253	28.87
4400	0.324	37.11	4530	0.298	34.12	4760	0.257	30.37
4400	0.326	37.86	4530	0.294	32.62	4760	0.254	28.87
4450	0.322	37.11	4530	0.273	31.87	4760	0.257	31.12
4450	0.312	35.61	4530	0.302	34.86	4760	0.260	29.70
4450	0.313	37.11	4530	0.305	34.12	4760	0.273	32.19
4450	0.330	37.11	4530	0.307	34.12	4760	0.269	30.94
4450	0.334	37.86	4530	0.276	34.12	4760	0.255	34.12
4450	0.331	37.86	4570	0.297	34.12	4760	0.254	29.70
4450	0.332	37.11	4570	0.292	33.37	4760	0.260	29.70
4450	0.316	35.61	4570	0.300	34.86	4760	0.264	30.37
4450	0.337	37.86	4570	0.298	34.12	4760	0.260	30.94

TABLE 10. SAMPLED VALUES OF PEAK PRESSURE AND RELATIVE PRESSURE

CONTINUED

SPEED	AVE PR	PEAK	SPEED	AVE PR	PEAK	SPEED	AVE PR	PEAK
4760	0.251	28.87	4790	0.262	30.37	4900	0.343	41.61
4760	0.250	28.87	4790	0.266	31.12	4900	0.338	43.86
4770	0.253	31.12	4790	0.268	31.87	4900	0.330	38.61
4770	0.257	29.62	4790	0.262	29.62	4900	0.334	41.61
4770	0.257	28.87	4790	0.271	32.62	4900	0.350	40.11
4770	0.258	29.62	4790	0.279	44.61	4900	0.344	42.36
4770	0.255	29.62	4810	0.264	30.82	4900	0.330	49.63
4770	0.254	28.87	4810	0.273	31.80	4900	0.274	31.87
4770	0.254	30.37	4810	0.268	31.80	4900	0.337	39.36
4770	0.254	29.62	4810	0.293	33.76	4900	0.283	34.68
4780	0.252	28.87	4810	0.273	35.72	4900	0.301	48.39
4780	0.270	31.77	4810	0.264	30.82	4900	0.359	41.61
4780	0.254	30.11	4810	0.273	33.76	4900	0.308	42.99
4780	0.265	30.53	4810	0.269	30.82	4900	0.288	33.37
4780	0.255	28.87	4810	0.271	34.74	4900	0.334	39.36
4780	0.255	29.70	4810	0.272	31.80	4900	0.312	37.86
4780	0.278	40.91	4810	0.265	29.85	4900	0.318	37.86
4780	0.263	30.53	4870	0.275	31.80	4900	0.312	42.57
4780	0.251	28.45	4870	0.276	41.59	4900	0.321	48.39
4780	0.265	33.02	4870	0.273	31.80	4900	0.347	39.36
4780	0.263	30.94	4870	0.268	32.78	4900	0.316	47.56
4780	0.288	33.44	4870	0.287	35.72	4900	0.314	36.36
4780	0.280	33.44	4870	0.276	38.65	4900	0.355	40.86
4780	0.254	28.87	4870	0.267	30.82	4900	0.307	38.42
4780	0.264	35.10	4870	0.270	34.74	4900	0.320	48.39
4780	0.250	29.28	4870	0.273	30.82	4910	0.292	50.61
4780	0.255	29.70	4870	0.278	41.59	4910	0.304	53.61
4780	0.257	29.70	4870	0.264	32.78	4910	0.288	39.36
4790	0.268	33.37	4900	0.331	39.36	4910	0.272	43.11
4790	0.281	46.86	4900	0.335	40.11	4910	0.276	38.61

TABLE 10. SAMPLED VALUES OF PEAK PRESSURE AND RELATIVE PRESSURE

CONTINUED

SPEED	AVE PR	PEAK	SPEED	AVE PR	PEAK	SPEED	AVE PR	PEAK
4910	0.283	35.61	5110	0.453	64.86	5270	0.484	85.10
4910	0.299	52.86	5110	0.453	66.36	5280	0.403	57.24
4910	0.290	37.11	5110	0.458	64.11	5280	0.397	47.46
4910	0.276	34.12	5110	0.449	61.11	5280	0.396	48.44
4950	0.345	51.30	5110	0.450	63.36	5280	0.400	45.50
4950	0.326	40.91	5110	0.461	85.85	5280	0.401	52.35
4950	0.344	48.80	5110	0.482	85.85	5280	0.395	45.50
4950	0.351	45.90	5190	0.411	47.61	5280	0.401	49.42
4950	0.328	47.14	5190	0.430	50.61	5280	0.386	46.48
4950	0.350	51.30	5190	0.425	53.61	5280	0.399	53.33
4950	0.344	50.88	5190	0.467	88.85	5280	0.401	49.42
4950	0.328	46.31	5190	0.417	55.86	5280	0.399	49.42
4950	0.346	50.05	5190	0.428	51.36	5830	0.589	83.60
5000	0.335	49.11	5190	0.405	52.86	5830	0.542	70.85
5000	0.344	49.11	5190	0.431	52.86	5830	0.547	73.85
5000	0.344	51.36	5190	0.439	57.36	5830	0.541	81.35
5000	0.331	42.36	5270	0.453	72.35	5830	0.564	87.35
5000	0.343	46.86	5270	0.466	85.10	5830	0.544	76.10
5000	0.348	56.61	5270	0.482	87.35	5830	0.538	73.10
5000	0.337	49.86	5270	0.422	57.36	5830	0.566	83.60
5000	0.369	52.86	5270	0.460	68.6	5830	0.546	73.10
5110	0.471	94.33	5270	0.476	85.10			
5110	0.453	65.61	5270	0.426	53.61			

6. The minimum division on the calibrated load cell was: 0.1 lbf.
7. The minimum measurement for the plint gauge calibration was: 0.01 oz (avoirdupois).
8. The minimum division available on the timer, used for determining the fuel flow was: 0.01 minutes.
9. All sound pressure levels were measured to: ± 0.2 dB.
10. The factory calibrated pressure transducers are linear to less than 1% of Full Scale. The calibration curves provided by the factory show no detectable deviation from a linear response to an input signal.
11. The pressure transducer was connected to the input stage of the analog to digital converter through a calibrated measuring amplifier. The amplifier has its own internal reference voltage of 50 mV at 1000 Hz. The amplitude stability is quoted by the manufacturer as being better than ± 0.01 dB for $\pm 10\%$ line voltage variation, and ± 0.005 dB/ $^{\circ}$ C. The change is rms voltage due to line voltage variations would be: 0.115%. The voltage change per degree Celsius would be: 28.8 microvolts.
12. The minimum detectible change in input voltage level would create a change in one bit in the output of the analog to digital converter. This represents a minimum measurement of one part in 256. As the voltage levels were scaled to give a peak bit value in the range of 240 to 250 and the voltages were measured relative to zero which is represented by a bit count of 128, the conversions are good to 1 part in 100. This would be a very conservative estimate.

13. The minimum division on the thermometer, used to measure the air temperature, was: 0.1 °C.
14. The minimum division on the barometer, used to measure the barometric pressure, was 0.1 mm of Mercury or 13.3 Pa.
15. The minimum division for the measurement of the orifice plate diameter was 0.001 inches.

A7.1 Uncertainty Analysis

The uncertainty in a measurement of a variable, X, is denoted by the symbol W_X . Thus, the measurement of the variable X is bounded by an estimate of the uncertainty as shown:

$$X \pm W_X \text{ units of } X$$

A more useful measure is to determine the relative uncertainty which can be multiplied by 100 to yield the percent relative uncertainty. For the variable X, the relative uncertainty is given by:

$$W_X/X$$

The percent relative uncertainty for the actual air flow rate, Q_a ; the gauge static pressure, P_s ; the exhaust gas temperature, T; the engine shaft power output, P_s ; the fuel flow rate, Q_f ; the brake specific fuel consumption, B_{sfc} ; the average relative pressure, P_r and the peak pressure P_p were calculated using the method suggested by Kline and McClintock † with 20 to 1 odds.

† Kline, S.J. and McClintock, F.A., Describing Uncertainties in Single-Sample Experiments, Mechanical Engineering, pp. 3-8, (January 1953).

An example calculation is presented for the determination of the percent relative uncertainty in the measurement of the actual air flow rate. The raw engine data, used for the calculations, is taken from Table 2., run number 9. The values derived from the raw data have been presented in Table 7 and are identified by sequence run number 1.

1. The actual air flow rate, Q_a .

The air flow rate is calculated from the relation:

$$Q_a = C * A * (2 * g * R' * \sin \theta * [(S1/S0) - 1])^{1/2}$$

where:

C is the discharge coefficient for the intake orifice and has the value 0.6

A is the cross-sectional flow area in square metres and is calculated from the relation:

$$A = \pi D^2 / 4$$

where D is the measured diameter of the orifice in metres.

g is the local acceleration due to gravity and has the value 9.806 m/s²

R' is the difference in the fluid column heights and is calculated from the relation:

$$R' = R_R - R_L$$

where R_R and R_L are respectively, the right and left manometer readings.

θ is the angle of inclination of the manometer in radians

$S1$ is the density of the manometer fluid (water). It is calculated from the linear regression for the density of water. In the range from 22 to 24 °C, the relation is:

$$S_1 = 1003.02 - 0.238 T_r$$

where T_r is the control room temperature in degrees Celsius

S_0 is the air density in the manometer. The density is calculated from the ideal gas relation:

$$S_0 = P_B/R * (T_r + 273)$$

where P_B is the barometric pressure in kPa and R is the gas constant for air, $R = 0.287 \text{ kJ/kg}^\circ\text{K}$

The relative uncertainty in the density of the manometer fluid is given by:

$$W_{S_1}/S_1 = \{[(\partial S_1/\partial T) * (W_T/S_1)]^2\}^{1/2}$$

where

$$\partial S_1/\partial T = -0.238 \text{ and } W_T = 0.05$$

(the uncertainty for any basic measurement is taken to be one-half of the smallest division of the measurement)

$$\text{For } T = 23.3 \text{ }^\circ\text{C}, S_1 = 997.47 \text{ kg/m}^3$$

and

$$W_{S_1}/S_1 = \pm 11.93 \times 10^{-6} \text{ or } \pm 1.19 \times 10^{-3}\%$$

The relative uncertainty in the density of the air is given by:

$$W_{S_0}/S_0 = \{[(\partial S_0/\partial P_B) * (W_{P_B}/S_0)]^2 + [(\partial S_0/\partial T_r) * (W_{T_r}/S_0)]^2\}^{1/2}$$

where

$$\partial S_0/\partial P_B = 1/R * (T_r + 273)$$

$$\partial S_0/\partial T_r = P_B/R$$

and

$$(\partial S_0/\partial P_B)/S_0 = 1/P_B$$

$$(\partial S_0/\partial T_r)/S_0 = 1/(T_r + 273)$$

$$\text{also: } S_0 = 1.188 \text{ kg/m}^3$$

Then:

$$W_{S_0}/S_0 = \{[W_{P_B}/P_B]^2 + [W_{T_r}/(T_r + 273)]^2\}^{1/2}$$

$$W_{S_0}/S_0 = \{[6.65/101000]^2 + [0.5/(23.3 + 273)]^2\}^{1/2}$$

$$W_{S_0}/S_0 = \pm 0.181 \times 10^{-3} \text{ or } \pm 0.0181\%$$

The relative uncertainty in the measurement of the difference in manometer column heights is given by:

$$W_R'/R' = \{[(\partial R'/\partial R_L) \cdot (W_{R_L}/R')]^2 + [(\partial R'/\partial R_R) \cdot (W_{R_R}/R')]^2\}^{1/2}$$

where

$$\partial R'/\partial R_L = 1 \text{ and } \partial R'/\partial R_R = 1$$

Then:

$$W_R'/R' = \{[0.05/3.2]^2 + [0.05/3.2]^2\}^{1/2}$$

$$W_R'/R' = \pm 0.022 \text{ or } \pm 2.2\%$$

The relative uncertainty in the measurement of the cross-sectional flow area of the orifice plate is given by:

$$W_A/A = \{[(\partial A/\partial D) \cdot (W_D/A)]^2\}^{1/2}$$

where

$$\partial A/\partial D = \pi D/2 \text{ and } (\partial A/\partial D)/A = 2/D$$

$$W_A/A = \{[2 \cdot (W_D/D)]^2\}^{1/2}$$

$$W_A/A = \{[2 \cdot (0.0005)/0.998]^2\}^{1/2}$$

Then

$$W_A/A = \pm 0.001 \text{ or } (\pm 0.1\%)$$

The relative uncertainty in the flow rate of air is given by:

$$W_{Q_a}/Q_a = \{[(\partial Q_a/\partial A) \cdot (W_A/Q_a)]^2 + [(\partial Q_a/\partial R') \cdot (W_{R'}/Q_a)]^2 + [(\partial Q_a/\partial \theta) \cdot (W_\theta/Q_a)]^2 + [(\partial Q_a/\partial S_1) \cdot (W_{S_1}/Q_a)]^2 + [(\partial Q_a/\partial S_0) \cdot (W_{S_0}/Q_a)]^2\}^{1/2}$$

where

$$(\partial Q_a/\partial A)/Q_a = 1/A$$

$$(\partial Q_a/\partial R')/Q_a = 1/2 \cdot R'$$

$$(\partial Q_a/\partial \theta)/Q_a = 1/2 \cdot \tan \theta$$

$$(\partial Q_a/\partial S_1)/Q_a = 1/2 \cdot (S_1 - S_0)$$

$$(\partial Q_a/\partial S_0)/Q_a = -S_1/2 \cdot S_0 \cdot (S_1 - S_0)$$

Then:

$$W_{Q_a}/Q_a = \left\{ [W_A/A]^2 + [W_R/2*R]^2 + [W_\theta/2*\tan \theta]^2 + [W_{S1}/2*(S1 - S0)]^2 + [-S1*W_{S0}/2*S0*(S1 - S0)]^2 \right\}^{1/2}$$

Then

$$W_{Q_a}/Q_a = \left\{ [0.001]^2 + [0.022/2]^2 + [0.0175/2*\tan (0.419)]^2 + [0.0119/2*(997.47 - 1.188)]^2 + [-997.47*0.000215/2*1.188*(997.47 - 1.188)]^2 \right\}^{1/2}$$

and

$$W_{Q_a}/Q_a = \pm 0.0426 \text{ or } \pm 4.3\%$$

It should be noted that it is the uncertainty in the measurement of the angle of inclination of the manometer which has the greatest influence on the uncertainty in the measurement of the actual air flow rate.

By similar procedures, it can be shown that the percent relative uncertainty in the measurement of:

2. The static pressure is:

$$W_{P_s}/P_s = \pm 2.2\%$$

3. The exhaust gas temperature is:

$$W_T/T = \pm 0.75\%$$

4. The engine shaft power is:

$$W_{P_e}/P_e = \pm 0.85\%$$

5. The fuel flow rate is:

$$W_{Q_f}/Q_f = \pm 0.56\%$$

6. The brake specific fuel consumption is:

$$W_{B_{sfc}}/B_{sfc} = \pm 1.02\%$$

7. The relative average pressure is:

$$W_{P_r}/P_r = \pm 1.42\%$$

8. The peak pressure is:

$$w_{Pp}/P_p = \pm 1.42\%$$

Table 11 is a presentation of one-third of the sampled data and its correlation values for File 10. Table 12 is a tabulation of the results of pseudofrequency and distortion coefficient correlations.

TABLE 11. SAMPLED VALUES OF DIMENSIONLESS PRESSURE AND THE
CORRESPONDING CORRELATION VALUE

TIME	PRESS	CORR	TIME	PRESS	CORR	TIME	PRESS	CORR
msec			msec			msec		
0.02	4.0E-03	4.0E-03	9.02	0.901	0.901	18.01	0.737	0.694
0.02	4.0E-03	4.0E-03	9.02	0.885	0.901	18.01	0.712	0.694
0.02	4.0E-03	4.0E-03	9.02	0.885	0.901	18.01	0.704	0.694
0.03	4.0E-03	5.0E-03	9.03	0.926	0.902	18.02	0.720	0.693
0.05	4.0E-03	7.0E-03	9.04	0.827	0.902	18.03	0.712	0.692
0.16	0.021	0.025	9.16	0.827	0.905	18.15	0.663	0.685
0.22	0.021	0.033	9.21	0.852	0.906	18.21	0.671	0.682
0.22	0.021	0.033	9.21	0.909	0.906	18.21	0.704	0.682
0.23	0.021	0.035	9.22	0.877	0.907	18.21	0.687	0.682
0.24	0.037	0.037	9.24	0.819	0.907	18.23	0.695	0.681
0.29	0.045	0.045	9.29	0.877	0.908	18.28	0.704	0.678
0.36	0.045	0.054	9.35	0.909	0.910	18.34	0.695	0.674
0.42	0.053	0.063	9.41	0.844	0.911	18.40	0.679	0.670
0.42	0.070	0.063	9.41	0.918	0.911	18.40	0.671	0.670
0.42	0.070	0.064	9.42	0.926	0.911	18.41	0.687	0.670
0.44	0.070	0.067	9.43	0.926	0.912	18.43	0.761	0.669
0.51	0.070	0.078	9.51	0.901	0.913	18.50	0.663	0.664
0.61	0.086	0.093	9.60	0.934	0.915	18.60	0.704	0.658
0.61	0.086	0.093	9.60	0.934	0.915	18.60	0.704	0.658
0.61	0.103	0.093	9.60	0.918	0.915	18.60	0.638	0.658
0.62	0.111	0.094	9.61	0.909	0.915	18.60	0.695	0.657
0.64	0.095	0.096	9.63	0.885	0.916	18.62	0.638	0.656
0.75	0.128	0.114	9.74	0.893	0.918	18.74	0.621	0.649
0.81	0.103	0.122	9.80	0.835	0.919	18.79	0.630	0.646
0.81	0.103	0.122	9.80	0.901	0.919	18.79	0.671	0.646
0.81	0.103	0.123	9.81	0.868	0.919	18.80	0.646	0.645
0.83	0.111	0.126	9.82	0.901	0.919	18.82	0.663	0.644
0.88	0.144	0.133	9.87	0.893	0.920	18.87	0.679	0.641
0.94	0.160	0.143	9.94	0.918	0.921	18.93	0.646	0.637
1.00	0.136	0.152	9.99	0.909	0.922	18.99	0.671	0.633

TABLE 11. SAMPLED VALUES OF DIMENSIONLESS PRESSURE AND THE
CORRESPONDING CORRELATION VALUE CONTINUED

TIME	PRESS	CORR	TIME	PRESS	CORR	TIME	PRESS	CORR
msec			msec			msec		
1.00	0.169	0.152	9.99	0.893	0.922	18.99	0.613	0.633
1.01	0.169	0.153	10.00	0.835	0.922	19.00	0.654	0.633
1.03	0.169	0.155	10.02	0.959	0.922	19.01	0.679	0.632
1.10	0.185	0.166	10.09	0.844	0.923	19.09	0.630	0.627
1.20	0.218	0.181	10.19	0.951	0.924	19.18	0.638	0.620
1.20	0.193	0.181	10.19	0.868	0.924	19.18	0.621	0.620
1.20	0.218	0.181	10.19	0.909	0.924	19.18	0.605	0.620
1.21	0.218	0.182	10.20	0.934	0.924	19.19	0.638	0.620
1.22	0.218	0.184	10.21	0.901	0.924	19.21	0.605	0.619
1.34	0.218	0.201	10.33	0.934	0.925	19.32	0.588	0.611
1.39	0.226	0.209	10.39	0.909	0.926	19.38	0.613	0.608
1.39	0.218	0.209	10.39	0.909	0.926	19.38	0.621	0.608
1.40	0.226	0.211	10.39	0.901	0.926	19.39	0.588	0.607
1.42	0.235	0.213	10.41	0.868	0.926	19.40	0.630	0.606
1.47	0.226	0.220	10.46	0.926	0.926	19.45	0.621	0.603
1.53	0.235	0.230	10.52	0.901	0.927	19.52	0.613	0.598
1.59	0.251	0.238	10.58	0.868	0.927	19.57	0.580	0.595
1.59	0.235	0.238	10.58	0.893	0.927	19.57	0.597	0.595
1.60	0.259	0.239	10.59	0.893	0.927	19.58	0.605	0.594
1.61	0.267	0.241	10.61	0.901	0.927	19.60	0.671	0.593
1.69	0.259	0.252	10.68	0.860	0.928	19.67	0.613	0.588
1.78	0.259	0.266	10.78	0.877	0.928	19.77	0.605	0.581
1.78	0.267	0.266	10.78	0.934	0.928	19.77	0.572	0.581
1.78	0.267	0.266	10.78	0.885	0.928	19.77	0.564	0.581
1.79	0.276	0.267	10.78	0.918	0.928	19.78	0.605	0.581
1.81	0.284	0.270	10.80	0.901	0.928	19.79	0.572	0.580
1.92	0.276	0.286	10.92	0.835	0.929	19.91	0.556	0.572
1.98	0.267	0.294	10.97	0.827	0.929	19.97	0.564	0.568
1.98	0.300	0.294	10.97	0.877	0.929	19.97	0.572	0.568
1.99	0.284	0.295	10.98	0.852	0.929	19.97	0.523	0.568

TABLE 11. SAMPLED VALUES OF DIMENSIONLESS PRESSURE AND THE
CORRESPONDING CORRELATION VALUE CONTINUED

TIME	PRESS	CORR	TIME	PRESS	CORR	TIME	PRESS	CORR
msec			msec			msec		
2.00	0.317	0.297	11.00	0.959	0.929	19.99	0.588	0.566
2.05	0.284	0.304	11.05	0.877	0.929	20.04	0.580	0.563
2.12	0.325	0.313	11.11	0.934	0.929	20.10	0.564	0.559
2.17	0.325	0.321	11.17	0.877	0.929	20.16	0.564	0.555
2.17	0.333	0.321	11.17	0.909	0.929	20.16	0.556	0.555
2.18	0.317	0.323	11.18	0.934	0.929	20.17	0.564	0.554
2.20	0.333	0.325	11.19	0.959	0.929	20.19	0.605	0.553
2.27	0.325	0.335	11.27	0.918	0.928	20.26	0.564	0.548
2.37	0.374	0.348	11.36	0.909	0.928	20.36	0.580	0.541
2.37	0.350	0.348	11.36	0.909	0.928	20.36	0.556	0.541
2.37	0.350	0.348	11.36	0.934	0.928	20.36	0.547	0.541
2.38	0.366	0.350	11.37	0.934	0.928	20.36	0.539	0.540
2.39	0.333	0.352	11.39	0.909	0.928	20.38	0.547	0.539
2.51	0.391	0.367	11.50	0.901	0.927	20.49	0.498	0.531
2.57	0.366	0.375	11.56	0.885	0.927	20.55	0.523	0.527
2.57	0.366	0.375	11.56	0.951	0.927	20.55	0.539	0.527
2.57	0.350	0.376	11.57	0.893	0.927	20.56	0.523	0.527
2.59	0.399	0.378	11.58	0.893	0.927	20.58	0.523	0.525
2.64	0.424	0.385	11.63	0.926	0.927	20.63	0.547	0.522
2.70	0.399	0.393	11.70	0.942	0.926	20.69	0.498	0.517
2.76	0.416	0.401	11.75	0.918	0.926	20.75	0.514	0.513
2.76	0.383	0.401	11.75	0.918	0.926	20.75	0.523	0.513
2.77	0.383	0.402	11.76	0.868	0.926	20.76	0.539	0.513
2.79	0.432	0.404	11.78	0.967	0.926	20.77	0.564	0.512
2.86	0.416	0.414	11.85	0.860	0.925	20.85	0.490	0.506
2.96	0.440	0.426	11.95	0.942	0.924	20.94	0.523	0.499
2.96	0.432	0.426	11.95	0.926	0.924	20.94	0.490	0.499
2.96	0.457	0.426	11.95	0.918	0.924	20.94	0.481	0.499
2.96	0.432	0.428	11.96	0.926	0.924	20.95	0.498	0.499
2.98	0.449	0.430	11.97	0.934	0.924	20.97	0.473	0.497

TABLE 11. SAMPLED VALUES OF DIMENSIONLESS PRESSURE AND THE
CORRESPONDING CORRELATION VALUE CONTINUED

TIME	PRESS	CORR	TIME	PRESS	CORR	TIME	PRESS	CORR
msec			msec			msec		
3.10	0.457	0.444	12.09	0.877	0.922	21.08	0.449	0.489
3.15	0.432	0.451	12.15	0.877	0.922	21.14	0.465	0.485
3.15	0.449	0.451	12.15	0.877	0.922	21.14	0.481	0.485
3.16	0.432	0.452	12.15	0.895	0.921	21.15	0.457	0.484
3.18	0.457	0.455	12.17	0.901	0.921	21.16	0.498	0.483
3.23	0.465	0.461	12.22	0.967	0.921	21.21	0.481	0.480
3.29	0.490	0.469	12.28	0.951	0.920	21.28	0.457	0.475
3.35	0.490	0.476	12.34	0.877	0.919	21.33	0.465	0.471
3.35	0.531	0.476	12.34	0.901	0.919	21.33	0.457	0.471
3.36	0.490	0.477	12.35	0.901	0.919	21.34	0.481	0.470
3.37	0.514	0.479	12.37	0.959	0.919	21.36	0.514	0.469
3.45	0.490	0.488	12.44	0.918	0.917	21.43	0.457	0.464
3.54	0.523	0.500	12.54	0.934	0.916	21.53	0.457	0.456
3.54	0.531	0.500	12.54	0.967	0.916	21.53	0.473	0.456
3.54	0.506	0.500	12.54	0.901	0.916	21.53	0.416	0.456
3.55	0.547	0.501	12.54	0.909	0.916	21.54	0.457	0.456
3.57	0.514	0.503	12.56	0.959	0.915	21.55	0.432	0.455
3.68	0.547	0.516	12.67	0.860	0.913	21.67	0.416	0.446
3.74	0.531	0.523	12.73	0.868	0.912	21.72	0.416	0.442
3.74	0.539	0.523	12.73	0.909	0.912	21.72	0.449	0.442
3.75	0.498	0.524	12.74	0.885	0.912	21.73	0.399	0.441
3.76	0.547	0.526	12.76	0.909	0.912	21.75	0.449	0.440
3.81	0.588	0.531	12.81	0.819	0.911	21.80	0.424	0.436
3.88	0.556	0.539	12.87	0.901	0.910	21.86	0.416	0.431
3.93	0.580	0.545	12.93	0.975	0.908	21.92	0.440	0.427
3.93	0.539	0.545	12.93	0.901	0.908	21.92	0.416	0.427
3.94	0.556	0.546	12.94	0.893	0.908	21.93	0.432	0.427
3.96	0.564	0.548	12.95	0.901	0.908	21.94	0.449	0.425
4.03	0.564	0.557	13.03	0.885	0.906	22.02	0.407	0.420
4.13	0.597	0.567	13.12	0.877	0.904	22.12	0.416	0.412

TABLE 11. SAMPLED VALUES OF DIMENSIONLESS PRESSURE AND THE
CORRESPONDING CORRELATION VALUE CONTINUED

TIME	PRESS	CORR	TIME	PRESS	CORR	TIME	PRESS	CORR
msec			msec			msec		
4.13	0.613	0.567	13.12	0.951	0.904	22.12	0.424	0.412
4.13	0.588	0.567	13.12	0.918	0.904	22.12	0.383	0.412
4.14	0.564	0.568	13.13	0.926	0.904	22.12	0.407	0.412
4.15	0.588	0.570	13.15	0.868	0.903	22.14	0.374	0.411
4.27	0.597	0.583	13.26	0.877	0.901	22.25	0.383	0.402
4.33	0.564	0.589	13.32	0.868	0.899	22.31	0.374	0.397
4.33	0.580	0.589	13.32	0.893	0.899	22.31	0.383	0.397
4.33	0.572	0.590	13.33	0.835	0.899	22.32	0.358	0.397
4.35	0.679	0.591	13.34	0.934	0.899	22.34	0.399	0.396
4.40	0.630	0.597	13.39	0.926	0.898	22.38	0.383	0.392
4.46	0.679	0.604	13.46	0.926	0.896	22.45	0.383	0.387
4.52	0.630	0.609	13.51	0.885	0.894	22.51	0.391	0.383
4.52	0.630	0.609	13.51	0.934	0.894	22.51	0.391	0.383
4.53	0.630	0.610	13.52	0.885	0.894	22.51	0.399	0.382
4.55	0.638	0.612	13.54	0.959	0.894	22.53	0.399	0.381
4.62	0.654	0.620	13.61	0.918	0.892	22.60	0.342	0.375
4.72	0.663	0.629	13.71	0.909	0.889	22.70	0.366	0.367
4.72	0.630	0.629	13.71	0.877	0.889	22.70	0.391	0.367
4.72	0.671	0.629	13.71	0.901	0.889	22.70	0.317	0.367
4.72	0.728	0.630	13.72	0.967	0.889	22.71	0.366	0.367
4.74	0.663	0.632	13.73	0.909	0.888	22.73	0.342	0.366
4.85	0.679	0.643	13.85	0.893	0.885	22.84	0.309	0.357
4.91	0.630	0.649	13.90	0.885	0.883	22.90	0.317	0.352
4.91	0.720	0.649	13.90	0.868	0.883	22.90	0.333	0.352
4.92	0.663	0.650	13.91	0.835	0.883	22.91	0.317	0.352
4.94	0.728	0.651	13.93	0.868	0.882	22.92	0.342	0.350
4.99	0.646	0.656	13.98	0.877	0.881	22.97	0.325	0.347
5.05	0.679	0.662	14.04	0.967	0.879	23.04	0.317	0.342
5.11	0.646	0.668	14.10	0.844	0.877	23.09	0.325	0.337
5.11	0.671	0.668	14.10	0.868	0.877	23.09	0.325	0.337

TABLE 11. SAMPLED VALUES OF DIMENSIONLESS PRESSURE AND THE
CORRESPONDING CORRELATION VALUE CONTINUED

TIME	PRESS	CORR	TIME	PRESS	CORR	TIME	PRESS	CORR
msec			msec			msec		
5.12	0.695	0.668	14.11	0.852	0.877	23.10	0.325	0.336
5.13	0.737	0.670	14.12	0.975	0.876	23.12	0.358	0.335
5.21	0.728	0.677	14.20	0.852	0.874	23.19	0.317	0.329
5.30	0.728	0.686	14.30	0.918	0.871	23.29	0.317	0.322
5.30	0.720	0.686	14.30	0.860	0.871	23.29	0.342	0.322
5.30	0.695	0.686	14.30	0.835	0.871	23.29	0.284	0.322
5.31	0.687	0.686	14.30	0.885	0.870	23.30	0.317	0.321
5.33	0.695	0.688	14.32	0.918	0.870	23.31	0.276	0.320
5.44	0.695	0.698	14.43	0.786	0.866	23.43	0.259	0.311
5.50	0.695	0.703	14.49	0.844	0.864	23.48	0.267	0.306
5.50	0.720	0.703	14.49	0.926	0.864	23.48	0.284	0.306
5.51	0.745	0.704	14.50	0.819	0.864	23.49	0.276	0.306
5.52	0.704	0.705	14.52	0.860	0.863	23.51	0.300	0.304
5.57	0.794	0.709	14.56	0.885	0.861	23.56	0.292	0.301
5.64	0.770	0.715	14.63	0.811	0.859	23.62	0.276	0.295
5.69	0.720	0.719	14.69	0.852	0.857	23.68	0.284	0.291
5.69	0.728	0.719	14.69	0.868	0.857	23.68	0.284	0.291
5.70	0.728	0.720	14.69	0.844	0.856	23.69	0.300	0.290
5.72	0.819	0.721	14.71	0.934	0.856	23.70	0.300	0.289
5.79	0.695	0.728	14.78	0.860	0.853	23.78	0.276	0.283
5.89	0.753	0.735	14.88	0.868	0.849	23.88	0.276	0.275
5.89	0.728	0.735	14.88	0.893	0.849	23.88	0.284	0.275
5.89	0.728	0.735	14.88	0.893	0.849	23.88	0.235	0.275
5.90	0.761	0.736	14.89	0.868	0.849	23.88	0.276	0.275
5.91	0.770	0.737	14.91	0.794	0.848	23.90	0.243	0.273
6.03	0.778	0.746	15.02	0.827	0.844	24.01	0.210	0.264
6.08	0.770	0.751	15.08	0.802	0.842	24.07	0.235	0.260
6.08	0.712	0.751	15.08	0.868	0.842	24.07	0.243	0.260
6.09	0.761	0.751	15.09	0.802	0.841	24.08	0.218	0.259
6.11	0.745	0.753	15.10	0.942	0.841	24.10	0.259	0.258

TABLE 11. SAMPLED VALUES OF DIMENSIONLESS PRESSURE AND THE
CORRESPONDING CORRELATION VALUE CONTINUED

TIME	PRESS	CORR	TIME	PRESS	CORR	TIME	PRESS	CORR
msec			msec			msec		
6.16	0.778	0.756	15.15	0.877	0.839	24.14	0.251	0.254
6.22	0.704	0.761	15.22	0.835	0.836	24.21	0.251	0.249
6.28	0.778	0.765	15.27	0.835	0.834	24.27	0.243	0.244
6.28	0.770	0.765	15.27	0.811	0.834	24.27	0.226	0.244
6.29	0.770	0.766	15.28	0.844	0.833	24.27	0.243	0.243
6.30	0.745	0.767	15.30	0.909	0.833	24.29	0.251	0.242
6.38	0.728	0.772	15.37	0.860	0.830	24.36	0.210	0.236
6.48	0.720	0.779	15.47	0.844	0.825	24.46	0.235	0.228
6.48	0.819	0.779	15.47	0.860	0.825	24.46	0.235	0.228
6.48	0.794	0.779	15.47	0.835	0.825	24.46	0.169	0.228
6.48	0.728	0.780	15.48	0.868	0.825	24.47	0.218	0.228
6.50	0.770	0.781	15.49	0.811	0.824	24.49	0.193	0.226
6.61	0.745	0.789	15.61	0.811	0.819	24.60	0.169	0.217
6.67	0.720	0.792	15.66	0.794	0.817	24.66	0.185	0.213
6.67	0.819	0.792	15.66	0.811	0.817	24.66	0.193	0.213
6.68	0.728	0.793	15.67	0.761	0.816	24.67	0.177	0.212
6.70	0.893	0.794	15.69	0.852	0.816	24.68	0.210	0.211
6.74	0.827	0.797	15.74	0.827	0.813	24.73	0.202	0.207
6.81	0.852	0.801	15.80	0.868	0.810	24.80	0.193	0.201
6.87	0.852	0.805	15.86	0.877	0.808	24.85	0.185	0.197
6.87	0.835	0.805	15.86	0.802	0.808	24.85	0.185	0.197
6.87	0.811	0.806	15.87	0.786	0.808	24.86	0.202	0.196
6.89	0.844	0.807	15.88	0.877	0.807	24.88	0.202	0.195
6.96	0.819	0.811	15.96	0.786	0.803	24.95	0.169	0.189
7.06	0.811	0.817	16.06	0.802	0.799	25.05	0.177	0.181
7.06	0.827	0.817	16.06	0.802	0.799	25.05	0.169	0.181
7.06	0.811	0.817	16.06	0.786	0.799	25.05	0.136	0.181
7.07	0.860	0.817	16.06	0.802	0.798	25.06	0.177	0.180
7.09	0.802	0.818	16.08	0.835	0.798	25.07	0.144	0.179
7.20	0.794	0.825	16.19	0.770	0.792	25.19	0.119	0.17

TABLE 11. SAMPLED VALUES OF DIMENSIONLESS PRESSURE AND THE
CORRESPONDING CORRELATION VALUE CONTINUED

TIME	PRESS	CORR	TIME	PRESS	CORR	TIME	PRESS	CORR
msec			msec			msec		
7.26	0.794	0.828	16.25	0.819	0.789	25.24	0.136	0.165
7.26	0.852	0.828	16.25	0.835	0.789	25.24	0.144	0.165
7.27	0.819	0.829	16.26	0.761	0.789	25.25	0.144	0.164
7.28	0.802	0.830	16.28	0.802	0.788	25.27	0.169	0.163
7.33	0.802	0.832	16.32	0.802	0.786	25.32	0.136	0.159
7.40	0.877	0.836	16.39	0.802	0.783	25.38	0.152	0.154
7.45	0.827	0.839	16.45	0.819	0.780	25.44	0.152	0.149
7.45	0.811	0.839	16.45	0.811	0.780	25.44	0.144	0.149
7.46	0.827	0.839	16.45	0.786	0.779	25.45	0.152	0.148
7.48	0.852	0.840	16.47	0.844	0.778	25.46	0.169	0.147
7.55	0.835	0.844	16.54	0.802	0.775	25.54	0.136	0.141
7.65	0.827	0.849	16.64	0.802	0.770	25.63	0.119	0.133
7.65	0.811	0.849	16.64	0.827	0.770	25.63	0.136	0.133
7.65	0.827	0.849	16.64	0.802	0.770	25.63	0.095	0.133
7.66	0.844	0.849	16.65	0.811	0.769	25.64	0.128	0.132
7.67	0.852	0.850	16.67	0.753	0.768	25.66	0.103	0.131
7.79	0.794	0.855	16.78	0.770	0.763	25.77	0.086	0.122
7.84	0.786	0.858	16.84	0.745	0.760	25.83	0.095	0.117
7.84	0.852	0.858	16.84	0.786	0.760	25.83	0.095	0.117
7.85	0.794	0.859	16.85	0.712	0.759	25.84	0.095	0.116
7.87	0.794	0.859	16.86	0.802	0.758	25.85	0.103	0.115
7.92	0.860	0.861	16.91	0.794	0.756	25.90	0.103	0.111
7.98	0.852	0.864	16.98	0.770	0.752	25.97	0.095	0.106
8.04	0.835	0.867	17.03	0.770	0.749	26.03	0.095	0.101
8.04	0.868	0.867	17.03	0.770	0.749	26.03	0.095	0.101
8.05	0.852	0.867	17.04	0.786	0.749	26.03	0.111	0.100
8.06	0.835	0.868	17.06	0.844	0.748	26.05	0.119	0.099
8.14	0.827	0.871	17.13	0.786	0.744	26.12	0.078	0.093
8.24	0.877	0.875	17.23	0.794	0.739	26.22	0.095	0.085
8.24	0.860	0.875	17.23	0.778	0.739	26.22	0.095	0.085

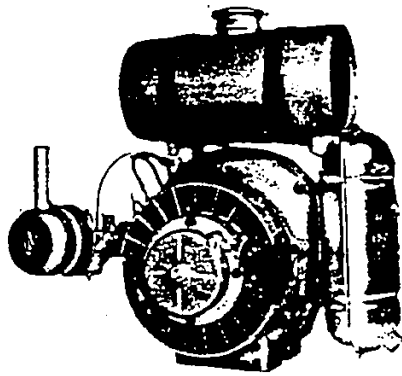
TABLE 11. SAMPLED VALUES OF DIMENSIONLESS PRESSURE AND THE
CORRESPONDING CORRELATION VALUE CONTINUED

TIME	PRESS	CORR	TIME	PRESS	CORR	TIME	PRESS	CORR
msec			msec			msec		
8.24	0.860	0.875	17.23	0.770	0.739	26.22	0.053	0.085
8.24	0.885	0.875	17.24	0.802	0.738	26.23	0.078	0.084
8.26	0.893	0.876	17.25	0.720	0.737	26.25	0.070	0.083
8.37	0.893	0.880	17.37	0.728	0.731	26.36	0.045	0.073
8.43	0.877	0.882	17.42	0.720	0.728	26.42	0.062	0.069
8.43	0.827	0.882	17.42	0.778	0.728	26.42	0.070	0.069
8.44	0.868	0.883	17.43	0.704	0.727	26.42	0.045	0.068
8.46	0.918	0.883	17.45	0.753	0.726	26.44	0.078	0.067
8.50	0.868	0.885	17.50	0.720	0.724	26.49	0.053	0.063
8.57	0.893	0.887	17.56	0.786	0.720	26.56	0.070	0.057
8.63	0.909	0.889	17.62	0.778	0.717	26.61	0.053	0.053
8.63	0.901	0.889	17.62	0.695	0.717	26.61	0.070	0.053
8.63	0.909	0.890	17.63	0.737	0.716	26.62	0.062	0.052
8.65	0.909	0.890	17.64	0.786	0.715	26.64	0.078	0.051
8.72	0.844	0.893	17.72	0.704	0.711	26.71	0.037	0.044
8.82	0.918	0.896	17.81	0.753	0.705	26.81	0.070	0.036
8.82	0.893	0.896	17.81	0.712	0.705	26.81	0.053	0.036
8.82	0.835	0.896	17.81	0.712	0.705	26.81	0.021	0.036
8.83	0.860	0.896	17.82	0.728	0.705	26.82	0.045	0.036
8.85	0.819	0.896	17.84	0.728	0.704	26.83	0.021	0.034

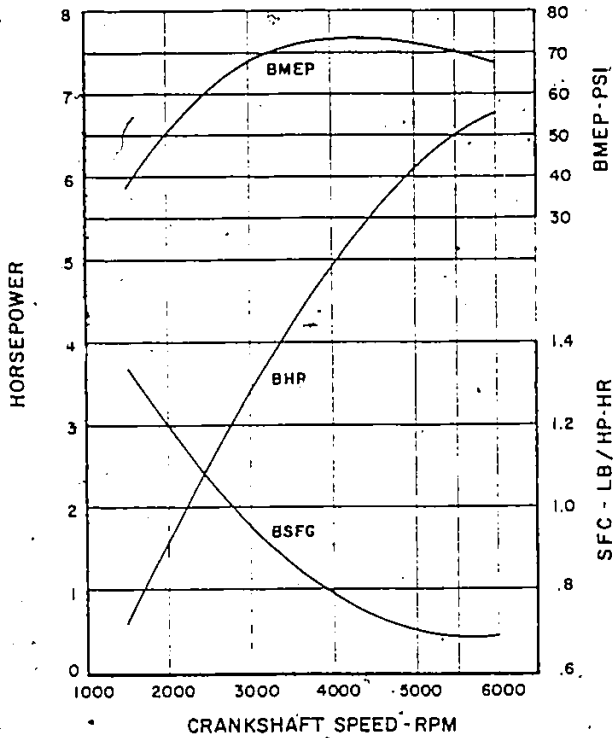
TABLE 12. COMPUTED PSEUDOFREQUENCY AND DISTORTION
COEFFICIENT FOR THE ENGINE SPEEDS SHOWN

SPEED	PSEUDOFREQUENCY	DISTORTION COEFFICIENT
RPM	Hertz	m/m
1990	149	0.202
1992	148	0.207
1995	149	0.205
1996	149	0.206
2000	149	0.206
2000	149	0.206
2000	149	0.202
2000	148	0.205
2250	166	0.272
2250	165	0.233
2250	169	0.198
2270	165	0.233
2282	169	0.198
2306	166	0.272
2510	184	0.162
2510	185	0.195
2514	184	0.195
2530	186	0.162
2730	183	0.297
2761	184	0.292
2937	196	0.327
2980	196	0.326
4020	212	0.314
4101	213	0.309
4250	216	0.382
4334	218	0.374
4760	216	0.425
4796	218	0.413

APPENDIX VII
ENGINE DATA SHEET

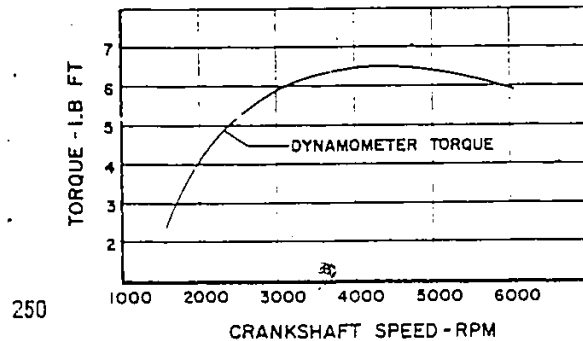
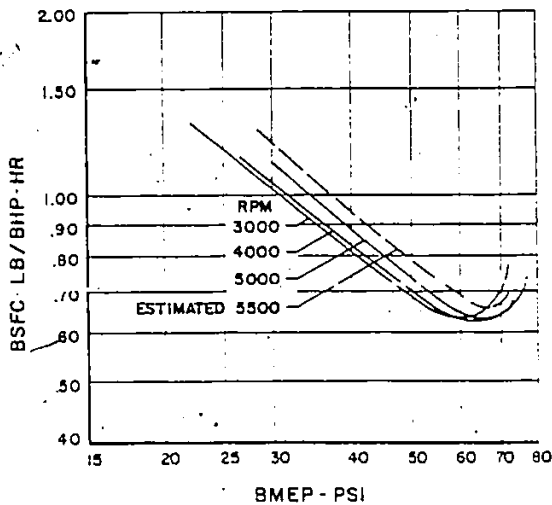


CURTISS-WRIGHT RC 1-6.6 ROTATING COMBUSTION ENGINE Base Mounted



SMALL AIR-COOLED-ROTATING COMBUSTION ENGINE

DIRECTION OF ROTATION	COUNTERCLOCKWISE (WHEN LOOKING AT DRIVE END)
DISPLACEMENT	6.6 CU. IN. (108 CC)
COOLING	AIR COOLED BLOWER
COMPRESSION RATIO	8.5 TO 1
PERFORMANCE	6.55 HP AT 5500 RPM (TOLERANCE RANGE ± 5%)
IGNITION	BOSCH FLYWHEEL MAGNETO 34Z/URB-1/116 R 2 OR BOSCH 157W
SPARK PLUG	CHAMPION L-85 OR BOSCH W 190 M 11 S
IGNITION TIMING	10 DEGREES BEFORE TDC
BREAKER GAP	0.014 - 0.018 IN.
CARBURETOR	BING 8/14/1
AIR FILTER	WET-TYPE
STARTING METHOD	HAND START
CONTROL	TOP SPEED LIMIT (GOVERNOR)
WEIGHT	34-LBS. ENGINE INCLUDING STARTER, GOVERNOR, CARBURETOR AND MUFFLER
LUBRICATION	
OIL	SHELL ROTELLA SAE 30 OR 40
PREMIX	50:1 FUEL TO OIL
FUEL	GASOLINE, REGULAR GRADE



CURTISS-WRIGHT CORPORATION ■ WRIGHT AERONAUTICAL DIVISION ■ WOOD-RIDGE, NEW JERSEY U.S.A.

REFERENCES

1. , Noise in the Human Environment, The Environment Council Of Alberta, Volumes 1 and 2, (1979).
2. Adams, T.G., Effect of Exhaust System Design on Engine Performance, SAE Paper No. 800319, (1980).
3. Adgey, J.M., A.B. Birks and G.P. Blair, The Development of a High Speed Dynamometer and Preliminary Results Obtained From a C.A.V. 01 Turbine, SAE Paper No. 690757, (1969).
4. Alfredson, R.J. and P.O.A.L. Davies, Performance of Exhaust Silencer Components, J. Sound Vib., 15, No. 2, pp. 175-196, (1971).
5. Alfredson, R.J., Performance Predictions of Resonator Mufflers, NASA Langley Research Center, Document L-7712, pp. 54-58, (1977).
6. Ansdale, R.F., Air-Cooled Wankel Engine, Automobile Engineer, pp. 354-356, (August, 1965).
7. Ansdale, R.F., The Wankel RC Engine (Design and Performance), Iliffe Books Ltd., London, (1968).
8. Apps, D.C., Automobile Noise, Handbook of Noise Control, (Editor, C.M. Harris), Chapter 31, pp. 1-50, McGraw-Hill Book Co., Inc., New York, (1957).
9. Texas, Automotive Engineering, Mazda's Rotary Engine Developments, 89, No. 12, pp. 79-80, (December, 1981).
10. Texas, Automotive Engineering, Rotary Engine Efficiency Improved, 90, No. 1, pp. 79-85, (January, 1982).

11. Texas, Automotive Engineering, A Worldwide Rotary Update, 86, No. 2, pp. 31-42, (February, 1978).
12. , Automotive Handbook, Robert Bosch GmbH, Stuttgart, Federal Republic of Germany, Distributed by SAE, Warrendale, Pennsylvania, pp. 5-36, (1978).
13. , Instruction Manual, Level Recorder Type 2307, Section 5.4, pp. 71-73, Brüel & Kjør, Nørum, Denmark, (Reprint August 1974).
14. Baker, A.J., Finite Element Computational Fluid Mechanics, Hemisphere Publishing Corporation and McGraw-Hill Book Company, New York, (1983).
15. Baumeister, K.J., Influence of Exit Impedance on Finite Difference Solutions of Transient Acoustic Mode Propagation in Ducts, ASME Paper No. 81-WA/NCA-13, (November, 1981).
16. Bender, E.K., Research Needs for Internal Combustion Engine Mufflers, The International Conference on Noise Control Engineering, pp. 153-157, Copenhagen, Denmark, (August 22-24, 1973).
17. Benson, R.S., Experiments on Two Stroke Engine Exhaust Ports Under Steady and Unsteady Flow Conditions, Proceedings of the Institution of Mechanical Engineers, 175, pp. 511-546, (1957).
18. Benson, R.S., R.D. Garg and D. Woollatt, A Numerical Solution of Unsteady Flow Problems, Int. J. Mech. Sci., 6, pp. 117-144, Pergamon Press Ltd., Great Britain, (1964).
19. Beranek, L.L. and S. Labate, Properties of Porous Acoustical Materials, Noise Reduction, (Editor, L.L. Beranek), Chapter 12, pp. 246-279, McGraw-Hill Book Company, New York, (1960).
20. Beyer, R.T., Nonlinear Acoustics, Physical Acoustics: Principles and Methods, (Editor, W.P. Mason), II-Part B, Chapter 10, pp. 231-264, Academic Press, New York, (1965).

21. Beyer, R.T., Nonlinear Acoustics, pp. 1-138, Written for the Naval Ship Systems Command, Department of Navy, Naval Sea Systems Command, Washington, (1974).
22. Blackstock, D.T., Propagation of Plane Sound Waves of Finite Amplitude in Nondissipative Fluids, 34, No. 1, Journal of the Acoustical Society of America, pp. 9-30, (January, 1962).
23. Blair, G.P., A Direct Evaluation of the Exhaust Lead of a Two-Stroke Cycle Diesel Engine, SAE Paper No. 650728, (1965).
24. Blair, G.P. and J.R. Goulburn, The Pressure-Time History in the Exhaust System of a High Speed Reciprocating Internal Combustion Engine, SAE Paper No. 670477, (1967).
25. Blair, G.P. and M.B. Johnston, Unsteady Flow Effects in Exhaust Systems of Naturally Aspirated Crankcase Compression Two-Cycle Internal Combustion Engines, SAE Paper No. 680594, (1968).
26. Blair, G.P. and J.R. Goulburn, An Unsteady Flow Analysis of Exhaust Systems for Multicylinder Engines, SAE Paper No. 690469, (1969).
27. Blair, G.P. and J.A. Arbuckle, Unsteady Flow in the Induction System of a Reciprocating Internal Combustion Engine, SAE Paper No. 700443, (1970).
28. Blair, G.P. and M.B. Johnston, Simplified Design Criteria for Expansion Chambers for Two-Cycle Gasoline Engines, SAE Paper No. 700123, (1970).
29. Blair, G.P. and W.L. Cahoon, Design and Initial Development of a High Specific Output 500 cc Single-Cylinder, Two-Stroke, Racing Motorcycle Engine, SAE Paper No. 710082, (1971).
30. Blair, G.P. and W.L. Cahoon, A More Complete Analysis of Unsteady Gas Flow Through a High-Specific-Output Two-Cycle Engine, SAE Paper No. 720156, (1972).
31. Blair, G.P. and J.A. Spechko, Sound Pressure Levels Generated by Internal Combustion Engine Exhaust Systems, SAE Paper No. 720155, (1972).

32. Blair, G.P. and S.W. Coates, Noise Produced by Unsteady Exhaust Efflux from an Internal Combustion Engine, SAE Paper No. 730160, (1973).
33. Blair, G.P. and J.H. McConnell, Unsteady Gas Flow Through High-Specific-Output 4-Stroke Cycle Engines, SAE Paper No. 740736, (1974).
34. Blair, G.P., Further Developments of a 500 cc Single Cylinder 2-Cycle Engine for Motorcycle Racing and Moto-Cross Applications, SAE Paper No. 740745, (1974).
35. Blair, G.P., Studying Scavenge Flow in a Two-Stroke Cycle Engine, SAE Paper No. 750752, (1975).
36. Blair, G.P. and M.C. Ashe, Unsteady Gas Exchange Characteristics of A Two-Cycle Engine, SAE Paper No. 760644, (1976).
37. Blair, G.P., Prediction of Two-Cycle Engine Performance Characteristics, SAE Paper No. 760645, (1976).
38. Blair, G.P. and R. Fleck, Unsteady Gas Flow Behaviour in a Charge Cooled Rotary Piston Engine, SAE Paper No. 770763, (1977).
39. Blair, G.P., A Theoretical Examination of the Relevant Parameters for Dynamometer Testing of 2-Cycle Engine Mufflers, pp. 449-495, Proceedings: Surface Transportation Exhaust System Noise Symposium, The United States Environmental Protection Agency, Office of Noise Abatement & Control, EPA 550/9-78-206, (October, 1977).
40. Blair, G.P., Computer-Aided Design of Small Two-Stroke Engines for both Performance Characteristics and Noise Levels, Instn of Mech Eng., pp. 77-86, London, England, (1978).
41. Blair, G.P. and R.G. Kenny, Further Developments in Scavenging Analysis For Two-Cycle Engines, SAE Paper No. 800038, (1980).
42. Brammer, A.J., N. Olson, J.E. Piercy and F.E. Toole, Non-Linear Effects in Helmholtz Resonator Mufflers for Internal Combustion Engines, Paper presented orally to the Buffalo meeting of the Acoustical Society of America, (April, 1972).

43. Brammer, A.J. and J.E. Piercy, Mufflers for Small Engines: Some Phenomena Revealed by Analysis of Waveforms, Paper presented orally to the Boston meeting of the Acoustical Society of America, (April, 1973).
44. Byrne, V.P. and J.B. Hart, Systems Approach for the Control of Intake and Exhaust Noise, SAE Paper No. 730429, (1973).
45. Coates, S.W. and G.P. Blair, Further Studies of Noise Characteristics of Internal Combustion Engine Exhaust Systems, SAE Paper No. 740713, (1974).
46. Craggs, A., The Application of the Finite Element Method to Studying the Performance of Reactive & Dissipative Mufflers With Zero Mean Flow, pp. 401-416, Proceedings: Surface Transportation Exhaust System Noise Symposium, The United States Environmental Protection Agency, Office of Noise Abatement & Control, EPA 550/9-78-206, (October, 1977).
47. Crocker, M.J., Review of Internal Combustion Engine Exhaust Muffling, pp. 295-357, Proceedings: Surface Transportation Exhaust System Noise Symposium, The United States Environmental Protection Agency, Office of Noise Abatement & Control, EPA 550/9-78-206, (October, 1977).
48. , Curtiss-Wright RC 1-6.6 Rotating Combustion Engine, Data Sheet SP 221A, Curtiss-Wright Corporation, Wright Aeronautical Division, Wood-Ridge, New Jersey, (1966).
49. Danieli, G.A.; J.C. Keck and J.B. Heywood, Experimental and Theoretical Analysis of Wankel Engine Performance, SAE Paper No. 780416, (1978).
50. Davies, P.O.A.L., and M.J. Dwyer, A Simple Theory for Pressure Pulses in Exhaust Systems, Proc Instn Mech Engrs, 179, Part 1, No. 10, pp. 365-394, (1964-65).
51. Davies, P.O.A.L. and R.J. Alfredson, Design of Silencers for Internal Combustion Engine Exhaust Systems, pp. 17-23, Instn Mech Engrs, 96, pp. 17-23, (1971).
52. Davies, P.O.A.L., Mufflers for Internal Combustion Engines, Proceedings of the International Conference for Noise Control Engineering, Copenhagen, Denmark, pp. 143-152, (August 22-24, 1973).

53. Davies, P.O.A.L., Bench Test Procedures and Exhaust System Performance Prediction, pp. 5-47, Proceedings: Surface Transportation Exhaust System Noise Symposium, The United States Environmental Protection Agency, Office of Noise Abatement & Control, EPA 550/9-78-206, (October, 1977).
54. Davis, D.D., Acoustical Filters and Mufflers, Handbook of Noise Control, (Editor, C.M. Harris), Chapter 21, pp. 1-44, McGraw-Hill Book Co., Inc., New York, (1957).
55. Diehl, G.M., Machinery Acoustics, pp. 168-172, John Wiley & Sons, New York, (1973).
56. Doelling, N., Dissipative Mufflers, Noise Reduction, (Editor, L.L. Beranek), Chapter 17, pp. 434-465, McGraw-Hill Book Company, New York, (1960).
57. , Guidelines for Noise Impact Analysis (DRAFT), The United States Environmental Protection Agency, Washington, (December, 1980).
58. Eberle, M.K. and E.D. Klomp, An Evaluation of the Potential Performance Gain from Leakage Reduction in Rotary Engines, SAE Paper No. 730117, (1979).
59. Eisenberg, J., Affordable Computers Limited, personal communication, Windsor, Ontario, (July, 1982).
60. Embleton, T.F.W., Mufflers, Noise and Vibration Control, (Editor, L.L. Beranek), Chapter 12, pp. 362-405, McGraw-Hill Book Co., Inc., New York, (1971).
61. Toronto, Engineering Digest, Industrial Rotary Engine Performs Well, 26, No. 4, pp. 36-38, (April, 1980).
62. Eriksson, L.J., Power or Pressure - A Discussion of Current Alternatives in Exhaust System Acoustic Evaluation, pp. 233-266, Proceedings: Surface Transportation Exhaust System Noise Symposium, The United States Environmental Protection Agency, Office of Noise Abatement & Control, EPA 550/9-78-206, (October, 1977).
63. Eriksson, L.J., An Analytical Model for Exhaust System Design, SAE Paper No. 780472, (1978).

64. Eriksson, L.J., Silencers, Noise Control In Internal Combustion Engines, (Editor, D.E. Baxa), Chapter 5, pp. 237-292, John Wiley & Sons, Inc., Toronto, (1982).
65. Ferguson, C.R., G.A. Danieli, J.B. Heywood and J.C. Keck, Time Resolved Measurements of Exhaust Composition and Flow Rate in a Wankel Engine, SAE Paper No. 750024, (1975).
66. Toronto, The Financial Post, Look, no Cylinders - That's Mazda's secret, Pg. 44, Perspective, (April, 1978).
67. Fox, F.E. and W.A. Wallace, Absorption of Finite Amplitude Sound Waves, 26, No. 6, Journal of the Acoustical Society of America, pp. 994-1006, (November, 1954).
68. Gajendra Babu, M.K., P.A. Janakiraman and B.S. Murthy, Measurement of Exhaust Gas Velocity in an Internal Combustion Engine, SAE Paper No. 750689, (1975).
69. Gaspar, R., Z. Reif and K. Sridhar, Frequency and Time Domain Analysis of Exhaust Pressure Pulses From a Small Rotary Engine, Proceedings of the 1980 International Conference on Noise Control Engineering, 1, pp. 223-238, Miami, Florida, (December 8-10, 1980).
70. Goyal, M., G. Scharpf and G. Borman, The Simulation of Single Cylinder Intake and Exhaust Systems, SAE Paper No. 670478, (1967).
71. Helmholtz, H., On the Sensations of Tone, Dover Publications, Inc., New York, (1954).
72. Hirata, Y. and T. Itow, Influence of Air Flow on the Attenuation Characteristics of Resonator Type Mufflers, Acustica, 28, pp. 115-120, (1973).
73. James J.H., Acoustic Finite Element Analysis of Axisymmetric Fluid Regions, ARL/R/R4, Admiralty Research Laboratory, Teddington, Middlesex, (1974).
74. Jante, A., Scavenging Flow Ducts of 3-Cyl 2-Stroke Cycle Engines, SAE Paper No. 680468, (1968).

75. John, J.E.A. and W.L. Haberman, Introduction to Fluid Mechanics, Second Edition, Pg. 487, Prentice-Hall, Inc., Englewood Cliffs, New Jersey, (1980).
76. Jones, C., A Progress Report on Curtis-Wright's Rotary Stratified Charge Engine Development, SAE Paper No. 741206, (1974).
77. Jones, A.D., Determination of 2-Stroke Engine Exhaust Noise by the Method of Characteristics, Hills Industries, Clarence Gardens, South Australia, Personal Communication, (1980).
78. Kamiya, S. and S. Shirasagi, Suzuki Production Rotary Engine, Model RE-5 for Powering Motorcycles, SAE Paper No. 770190, (1977).
79. Kelsay, R. and D. Margolis, An Experimental Investigation of Two Stroke Internal Combustion Engine Performance, SAE Paper No. 750859, (1975).
80. Kohno, T., R. Ito, M. Morita and N. Minzuno, Analysis of Light-Load Performance in Rotary Engines, SAE Paper No. 790435, (1979).
81. Lambert, R.F., Acoustic Filtering in a Moving Medium, JASA, 28, No. 6, pp. 1054-1058, (1956).
82. Lancaster, A., Modifying Snowmobiles to Produce Lower Noise Levels, SAE Paper No. 730813, (1973).
83. Levine, H. and J. Schwinger, On the Radiation of Sound from an Unflanged Circular Pipe, The Physical Review, 73, No. 4, Second Series, pp. 383-406, (1948).
84. Liepmann, H.W. and A.E. Puckett, Introduction to Aerodynamics of a Compressible Fluid, John Wiley and Sons, Inc., New York, (1947).
85. Lykkeberg, P., Design of Reflection Type Silencers Based on the Theory of Reactive Acoustic Filters, Proceedings of the 1973 International Conference on Noise Control Engineering, pp. 158-162, Copenhagen, Denmark, (August 22-24, 1973).
86. , Model Municipal Noise Control By-Law, The Province of Ontario, Ministry of the Environment, (August, 1978).

87. Malchow, G.L., S.C. Sorenson and R.O. Buckius, Heat Transfer in the Straight Section of an Exhaust Port of a Spark Ignition Engine, SAE Paper No. 790309, (1979).
88. Margolis, D., Modeling of Two-Stroke Internal Combustion Engine Dynamics Using the Bond Graph Techniques, SAE Paper No. 750860, (1975).
89. Margolis, D., D.C. Karnopp and H.A. Dwyer, Analytical and Experimental Testing Procedures for Quieting Two-Stroke Engines, pp. 203-231, Proceedings: Surface Transportation Exhaust System Noise Symposium, The United States Environmental Protection Agency, Office of Noise Abatement & Control, EPA 550/9-78-206, (October, 1977).
90. Martens, H.R. and A.C. Bell, A Logical Procedure for the Construction of Bond Graphs in Systems Modeling, pp. 183-188, Journal of Dynamic Systems, Measurement, and Control, Transactions of the ASME, (September, 1972).
91. Masuko, K. and T. Abe, On Factors of Noise Emitted by Small Vehicles and Noise Simulation of Pass-By Test, SAE Paper No. 770011, (1977).
92. McReynolds, L.A., Small Engines -- An Energy Perspective, SAE Paper No. 790477, (1979).
93. Mucklow, G.F. and A.J. Wilson, Wave Action in Gases -- The Attenuation and Reflection of Compression Waves Propagated in Pipes, Proceedings of the Institution of Mechanical Engineers, 169, pp. 69-82, (1955).
94. Mungur, P. and G.M.L. Gladwell, Acoustic Wave Propagation in a Sheared Fluid Contained in a Duct, J. Sound Vib., 9, No. 1, pp. 28-48, (1969).
95. Munjal, M.L., Velocity Ratio-Cum-Transfer Matrix Method for the Evaluation of a Muffler with Mean Flow, Journal of Sound and Vibration, 39, No. 1, pp. 105-119, (1975).
96. Mutyala, B.R.C. and W. Soedel, A Mathematical Model of Helmholtz Resonator Type Gas Oscillation Discharges of Two-Stroke Cycle Engines, 44, No. 4, pp. 479-491, (1976).

97. Nassif, M.H., Acoustical Analysis Applied to Internal Combustion engine Exhaust Systems of Conical Form, Journal Mechanical Engineering Science, 11, No. 4, (1969).
98. Nowak, K.F., Discussion of SAE Paper No. 700123, (Reference No. 28).
99. Nowak, K.F., Computer Design Calculations by Cosmocon Ltd., personal communication, (October, 1979).
100. Olver, F.W.J., Bessel Functions of Integer Order, Handbook of Mathematical Functions, (Edited by M. Abramowitz and I.A. Stegun), Chapter 9, pp. 355-478, Dover Publications, Inc., New York, (1972).
101. Ospring, M., D. Karnopp and D. Margolis, Comparison of Computer Predictions and Experimental Tests for Two-Stroke Engine Exhaust Systems, SAE Paper No. 760172, (1976).
102. Pierce, A.D., Acoustics: An Introduction to Its Physical Principles and Applications, McGraw-Hill Book Company, New York, (1981).
103. Prasuhn, A.L., Fundamentals of Fluid Mechanics, pp. 93-104, Prentice-Hall, Inc., Englewood Cliffs, New Jersey, (1980).
104. Priede, T., In Search of Origins of Engine Noise - an Historical Review, SAE Paper No. 800534, (1980).
105. Rayleigh, J.W.S., The Theory of Sound, Dover Publications, Inc., New York, (1954).
106. Roe, G.E., The Silencing of a High Performance Motorcycle, Journal of Sound and Vibration, 33, No. 1, pp. 29-39, (1973).
107. Roe, G.E., An Empirical Approach to Motorcycle Silencing, SAE Paper No. 770188, (1977).
108. Rosenberg, R.C. and D.C. Karnopp, A Definition of the Bond Graph Language, pp. 179-182, Journal of Dynamic Systems, Measurement, and Control, Transactions of the ASME, (September, 1972).

109. Rowley, D.W., Comments on Evaluation Techniques of Exhaust System Noise Control, pp. 161-180, Proceedings: Surface Transportation Exhaust System Noise Symposium, The United States Environmental Protection Agency, Office of Noise Abatement & Control, EPA 550/9-78-206, (October, 1977).
110. Rudenko, O.V. and S.I. Soluyan, Theoretical Foundations of Nonlinear Acoustics, (Translated by R.T. Beyer), pp. 1-29, Consultants Bureau, A Division of Plenum Publishing Corporation, New York, (1977).
111. Sachs rotary piston engine, Manual No. 4010.2 E/2, Fichtel & Sachs A.G., 8720 Schweinfurt, Federal Republic of Germany, (1967).
112. Sanborn, D.S., G.P. Blair, R.G. Kenny and A.H. Kingsbury, Experimental Assessment of Scavenging of Two-Stroke Cycle Engines, SAE Paper No. 800975, (1980).
113. Shepherd, C.D., Exhaust System Design - Art or Science?, SAE Paper No. 690006, (1969).
114. Sreenath, A.V. and M.L. Munjal, Evaluation of Noise Attenuation Due to Exhaust Mufflers, Journal of Sound and Vibration, 12, No. 1, pp. 1-19, (1970).
115. Sturtevant, B. and J.E. Craig, Shock-Tube Methods for Simulating Exhaust Pressure Pulses of Small High-Performance Engines, pp. 359-380, Proceedings: Surface Transportation Exhaust System Noise Symposium, The United States Environmental Protection Agency, Office of Noise Abatement & Control, EPA 550/9-78-206, (October, 1977).
116. Swanson, I.N., Air Intake Silencing for Small Engines, SAE Paper No. 750751, (1975).
117. Thawani, P.T. and A.G. Doige, Effect of Mean Flow and Damping on the Performance of Reactive Mufflers, Canadian Acoustics, 11, No. 1, pp. 29-47, (1983).
118. Thomas, D.G., Muffler Selection and Design for Internal Combustion Engines, SAE Paper No. 700537, (1970).

119. Tsao, K.C. and D. Losinger, Mass Burning Rate in a Rotary Combustion Engine, SAE Paper No. 741089, (1974).
120. Wald, B., Choosing the Right Material for Noise Control, ASME Paper No. 73-DE-40, (1973).
121. Wallace, F.J. and M.H. Nassif, Air Flow in a Naturally Aspirated Two-stroke Engine, Instn Mech Engrs, pp. 515-544, (1953).
122. Wallace, F.J. and G.P. Blair, The Pulsating Flow Performance of Inward-Radial Flow Turbines, ASME Gas Turbine Conference, (Feb. 28 - Mar. 4, 1965).
123. Wallace, F.J., J.M. Adgey and G.P. Blair, Performance of Inward Radial Flow Turbines Under Non-Steady Flow Conditions, Inst. Mech. Eng., Proceedings (Part 1), General Proceedings, 184, No. 10, pp. 183-195, (1969-1970).
124. Walter, G.A. and M. Chapman, Numerical Simulation of the Exhaust Flow From a Single Cylinder of a Two Cycle Engine, SAE Paper No. 790243, (1979).
125. Ward, H., M. Griffith, G. Miller and O. Stephenson, Outboard Marine Corp's Production Rotary Combustion Snowmobile Engine, SAE Paper No. 730119, (1973).
126. Welbourne, E.R., Regulation of Motor Vehicle Noise in Canada, SAE Paper No. 780385, (1978).
127. Wiener, F.M., The Measurement of Power Levels and Directivity Patterns of Noise Sources, Noise Reduction, (Editor, L.L. Beranek), Chapter 8, pp. 163-181, McGraw-Hill Book Company, New York, (1960).
128. Windsor, The Windsor Star, B. Shields, The rotary engine spins into its own, Pg. C6, (October 12, 1982).
129. Woollatt, D., An Approximate Theory for The Transmission and Reflection of Simple Waves at Area Changes and Junctions in Pipes, Int. J. Mech. Sci., 7, pp. 777-783, Pergamon Press Ltd., (1965).
130. Wylie, Jr., C.R., Advanced Engineering Mathematics, pp. 187-188, Second Edition, McGraw-Hill Book Company, Inc., New York, (1960).

131. Yun, H.J. and W. Mirsky, Schlieren-Streak Measurements of Instantaneous Exhaust Gas Velocities from a Spark-Ignition Engine, SAE Paper No. 741015, (1974).

VITA AUCTORIS

- 1946 Born in Windsor, Ontario, (April 15).
- 1965 Completed Secondary School Education at Merlin District High School in Merlin, Ontario, (August 20).
- 1969 Received the Degree of Bachelor of Applied Science in Mechanical Engineering from the University of Windsor, Windsor, Ontario, (May 31).
- 1973 Received the Degree of Master of Applied Science from the University of Windsor, Windsor, Ontario, (October 13).
- 1977 Joined the Faculty of Engineering, Department of Mechanical Engineering of the University of Windsor as a Sessional Instructor, Windsor, Ontario, (June).

Recent Publications

- 1983 Further Time Domain Analysis of Exhaust Pressure Pulses from a Small Rotary Engine, co-authors: Z.F. Reif and K. Sridhar, Proceedings Internoise '83, Edinburgh, Scotland.
- 1982 Evaluation of Ground Vibration from Forging Plants, co-author: T.N. Moore, Prepared for the Seminar on Vibration Sponsored by the Canadian Acoustical Association, Session Number 1, Excitation, Toronto, Ontario.
- 1981 Railway Noise and Vibration Monitoring Studies, for the Ontario Ministry of the Environment and funded by an Experience '81 Grant.
- 1980 Frequency and Time Domain Analysis of Exhaust Pressure Pulses from a Small Rotary Engine, co-authors: Z.F. Reif and K. Sridhar, Proceedings Internoise '80, Miami, Florida.

1978 Engine Noise Testing in an Economical 'Semi' Anechoic Room, co-authors: K. Sridhar and Z.F. Reif, The Society of Automotive Engineers, Detroit, Michigan.